THE PHYSICS OF FREE ELECTRON LASERS. AN INTRODUCTION

E.L. SALDIN[a], E.A. SCHNEIDMILLER[a], M.V. YURKOV[b]

[a] *Automatic Systems Corporation, 443050 Samara, Russia*
[b] *Joint Institute for Nuclear Research, Dubna, 141980 Moscow Region, Russia*

ELSEVIER

AMSTERDAM – LAUSANNE – NEW YORK – OXFORD – SHANNON TOKYO

ELSEVIER

Physics Reports 260 (1995) 187–327

PHYSICS REPORTS

The physics of free electron lasers. An introduction

E.L. Saldin [a], E.A. Schneidmiller [a], M.V. Yurkov [b]

[a] *Automatic Systems Corporation, 443050 Samara, Russia*

[b] *Joint Institute for Nuclear Research, Dubna, 141980 Moscow Region, Russia*

Received January 1995; editor: D.L. Mills

Contents:

SSDI 0370-1573(95)00004-6

Abstract

The present paper contains a systematic exposure of basic principles of free electron laser physics. FEL models are discussed wherein space charge fields, energy spread of the electrons in the beam and diffraction effects are taken into account. We present a detailed study of the one-dimensional theory of a FEL amplifier, FEL oscillator and FEL oscillator with multicomponent undulator. We present also an introduction to the analysis of the diffraction effects using the FEL amplifier model.

When exposing linear theory we use analytical techniques and the investigation of nonlinear modes in the operation of FEL devices is performed using the results of numerical simulations. The results of the linear theory serve as a primary standard to check the accuracy of numerical simulations. We perform a thorough analysis of the saturation effects in the FEL devices and of the methods to increase the FEL efficiency.

A theoretical study is performed with a wide use of similarity techniques, so the obtained results are simultaneously of high degree of generality and completely specified. Numerous universal graphs illustrating various modes of the FEL operation together with the reduced design formulae can help the reader to find FEL characteristics using simple dimensional analysis only. It may be useful also for FEL designers, especially at the design stage of an experiment.

This article is dedicated to our respected colleague and close friend Professor V.P. Sarantsev, whose recent death on January 31, 1995 will have an impact on all of us. Professor Sarantsev was an internationally known expert on plasma physics and accelerator design, responsible for numerous fundamental innovations in these fields. He authored over two hundreds research papers in these fields during his very active career.

1. Introduction

The progress in the FEL physics and technique during last decade was so rapid that there are only small groups of experts in each branch of the FEL science which possess the required knowledge of the problem. On the other hand, a large number of scientists working in the field of the FEL physics, FEL applications and another branches of science have significant interest in this subject. People who begin to study FEL physics face a severe problem, namely that there is no textbook or review where the different FEL devices are considered not as separate objects but in a common way. It is difficult to understand the principles of operation of one device without a knowledge of the principles of operation of another devices, because all the FEL devices are tightly connected with each other. So, there is an urgent need in a textbook on the FEL physics where all the existent FEL devices are treated in a uniform way. The present paper is an attempt to fill this gap and contains a systematic exposure of basic principles of free electron laser physics. It might be extremely useful for physicists specializing in the FEL physics as well as in the adjacent fields: laser physics, microwave electronics, particle accelerator physics etc. It will be of help also for those who use the FEL as a research or industrial tool in their work.

All the results presented in the paper are derived from the "first principles" and the reader can follow the whole derivation process from beginning to end. The present treatment requires from the reader only the knowledge of classical mechanics, electrodynamics and a moderate knowledge of higher mathematics (differential equations, Laplace transform and special functions). Both simplicity and strictness of exposure are explained by the features of the object under study (FELs are described rather well in the framework of classical physics) and by the simplicity of the accepted FEL models. In the present paper we study in details one-dimensional model of the FEL and present rather deep introduction to the analysis of diffraction effects using the FEL amplifier model. Despite their simplicity, such models describe rather well almost all main effects influencing the FEL operation. When presenting theoretical results, we have tried to include all significant results obtained by other authors. Of course, the aspiration to make the exposure uniform has led us to the necessity to obtain some well known results in a different way with respect to the original papers. On the other hand, significant fraction of the presented material is based on our previous publications.

1.1. The place of a FEL among the sources of coherent radiation

During last two decades free electron lasers have passed a long way from the first experimental demonstration [1] and occupied an appropriate place among another sources of coherent radiation. FEL devices possess many attractive features. FEL radiation is tunable and existent level of accelerator technique R&D provides a possibility to construct FEL devices operating in a wide range of

electromagnetic spectrum, from centimeters down to X-ray range. FEL radiation is always totally polarized and has ideal, i.e. diffraction dispersion. FELs are capable to provide a high efficiency of transformation of the electron beam power into the radiation power. It has been demonstrated experimentally, the efficiency of a FEL amplifier has reached the value of 34% [2]. Remembering that electron accelerators of driving beams for the FELs can provide high average and peak power at effective transformation of electric power into the electron beam power, one can expect to reach a high level of the total FEL efficiency, high peak and average power. Due to these unique features, the FELs are considered as perspective devices for a huge number of scientific and industrial applications.

When the first operating free electron laser has been constructed, it seemed that FELs will form only a small supplement to a long list of existent at that time quantum lasers. Actually, the appearance of the FELs formed a novel direction in the field of the sources of coherent radiation: they embodied the type of the coherent source to which all the experimenters aspired since the invention of the laser. The FELs have made to be a reality the dream to find such a laser which is capable to generate powerful coherent radiation at any wavelength from far infrared to ultraviolet part of the spectrum similarly to the vacuum-tube devices which are capable to generate coherent radiation at any wavelength, from kilometer to millimeter range.

It is relevant to notice that despite the FEL is named as a laser, when considering the principles of its operation, we find that it forms a separate class of vacuum-tube devices, the principle of which operation is based on interaction of electron beams with the radiation. From this point of view it is easy to realize the origin of the mentioned above advantages of the FEL against quantum lasers. The main advantage is tunability of the radiation. In quantum laser, the lasing wavelength is defined by discreet energy transitions between the quantum levels of atoms or molecules of an active medium. Despite the variety of the discovered types of the active medium, the number of quantum levels is and will remain to be finite. As for the FEL (or, in a more wide sense, for vacuum-tube devices), their operating frequency is defined by their design, namely by the electron beam parameters, characteristics of the electrodynamic structure (waveguide walls, resonator mirrors, etc.) and by characteristics of the electrical and magnetic fields in the interaction region. Due to these reasons, the FEL can be tuned, in principle, to any desired operating frequency.

Another important feature of the FEL is that its radiation is always coherent and has ideal, i.e. diffraction dispersion. In other words, the FEL radiation can always be focused to a spot which size is defined totally by diffraction effects. This feature of the FEL is the consequence of the fact that the process of the electromagnetic field amplification develops in vacuum. It reveals wide possibilities for the FEL applications in transportation of the radiation trough long distances and obtaining high intensity. Contrary to the FEL, the dispersion of radiation of powerful lasers usually exceeds by several tens of magnitude the value of diffraction limit. The main effects which determine the growth of the radiation dispersion are fluctuations of the active medium refractive index due to thermal effects and nonlinear effects in the active medium.

FEL predominates significantly conventional lasers in an ability to attain a high level of average output power. In the conventional laser, unused fraction of the pumping power (which significantly exceeds the output radiation power) is dissipated in the active medium. So, a possibility to increase average output power is limited by the heat elimination problem. Contrary to this, in the FEL amplifier the process of the electron beam energy conversion to the radiation one takes place in vacuum. Utilization of the used electron beam is rather routine problem in the accelerator technique.

The FEL, as a device converting the net electrical power to the radiation power, can provide, in

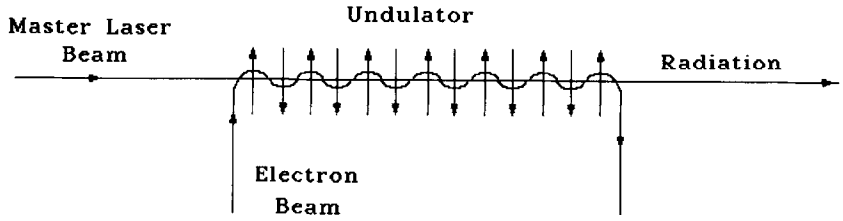

Fig. 1.1. Conceptual scheme of a FEL amplifier.

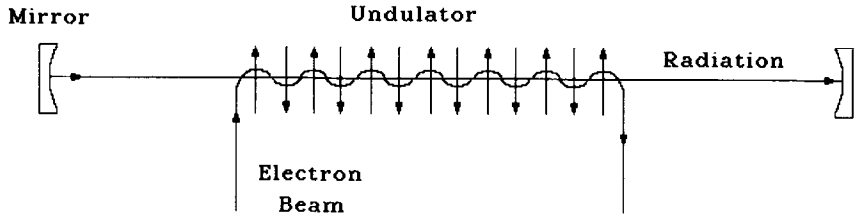

Fig. 1.2. Conceptual scheme of a FEL oscillator.

principle, a high efficiency close to 100%. There are no principal physical limitations which prohibit attaining such a high efficiency and it may be achieved at an appropriate development of the FEL technology. In this sense the situation with the FEL is similar to that with microwave electronic devices. Intensive development of the theory and technology of microwave devices during last fifty years has revealed a possibility to construct powerful devices with the efficiency of about 80%. The record value of the efficiency equal to 34% has been achieved in the millimeter wavelength range FEL amplifier at the peak radiation power equal to 1 GW [2].

The FEL technique is one of the youngest branches of the technology, it is only 20 years old and the main progress has been achieved during the last ten years. Nowadays there are several tens of the FEL devices operating in the wavelength range from 0.24 μm up to centimeter. Despite a strong competition from the side of conventional lasers, the FEL is recognized nowadays as a unique tool for scientific applications requiring tunable coherent radiation. Taking into account the future perspectives of the FEL, many industrial firms undertake intensive investigations in the FEL technology aiming a goal to construct powerful FELs for industrial applications such as material processing, microlithography, isotope separation, chemical applications, plasma heating, etc. Analysis of the dynamics of the FEL technology development indicates that within the next decades the FEL will be widely spread over the world as irreplaceable tool for a wide range of scientific and industrial applications [3–9].

1.2. Principle of a FEL operation

In the same way as vacuum-tube devices, the FEL devices can be divided into two classes, amplifiers and oscillators (see Figs. 1.1 and 1.2). The FEL amplifiers amplify the input electromagnetic wave from external master oscillator. There is no feedback between the output and input of the FEL amplifier. The FEL oscillator can be considered as the FEL amplifier with feedback. The radiation in the FEL oscillator grows from fluctuations of the electron beam density or from the spontaneous emission spectrum. For the FEL oscillator of optical wavelength range the feedback is carried out

by means of optical resonator which defines also the radiation modes which can be excited in the resonator. When the rate of electron beam power conversion into the radiation power exceeds the radiation losses in the resonator, the lasing process occurs.

The key element of the FEL is an undulator (or wiggler) which forces the electrons to move along curved periodical trajectories. There are two popular undulator configurations: a helical and a planar. The helical wiggler is formed by bifilar winding and produces rotating transverse magnetic field which forces the electrons to move along helical trajectories. The planar undulator is formed by a sequence of dipole magnets of the opposite polarity and produces linearly polarized transverse magnetic field which forces the electrons to move along sinusoidal trajectories.

To understand basic principles of the FEL operation, let us consider the helical undulator. Magnetic field at the axis of the helical undulator is given by

$$\boldsymbol{H}_w = \boldsymbol{e}_x H_w \cos(2\pi z/\lambda_w) - \boldsymbol{e}_y H_w \sin(2\pi z/\lambda_w), \tag{1.1}$$

where λ_w is the undulator period. In this helical field, the electrons move along the helical trajectories. The angle of the electron rotation in the undulator (i.e. the angle between the electron velocity and the undulator axis) is $\theta_s = K/\gamma$, where $K = \lambda_w e H_w/2\pi m_e c^2$ is the undulator parameter, $\gamma = \mathcal{E}/m_e c^2$ is relativistic factor, $(-e)$ and m_e are the charge and mass of the electron, respectively. As a rule, the electron rotation angle is small, $\theta_s^2 \ll 1$, and longitudinal velocity of the electron v_z is close to the velocity of light c (in other words, the longitudinal relativistic factor $\gamma_z = (1 - v_z^2)^{-1/2}$ is large, $\gamma_z^{-2} = \gamma^{-2} + \theta_s^2 = (1 + K^2)/\gamma^2 \ll 1$).

In the FEL the electromagnetic wave propagates in parallel with the electron beam. So as the field of the electromagnetic wave is transverse, the energy exchange between the electron and the wave is performed due to the transverse component of the electron velocity. The rate of the electron energy change is $d\mathcal{E}/dt = -e(\boldsymbol{v}_\perp \cdot \boldsymbol{E})$, where $\boldsymbol{v}_\perp$ is the vector of the transverse velocity of the electron and $\boldsymbol{E}$ is the electric field vector of the wave.

So as the longitudinal electron velocity v_z is less than the velocity of light c, the wave slips with respect to the electron beam with the relative velocity $(c - v_z)$. The FEL is a device with a prolonged beam-wave interaction, i.e. at the total undulator length, the wave slips with respect to the beam by the distance which is much more than the radiation wavelength. It means that the electric field vector $\boldsymbol{E}$ of the wave performs many turns at the undulator length. The vector $\boldsymbol{v}_\perp$ of the electron transverse velocity rotates, too, and performs one turn per undulator period. To provide effective energy exchange between the electron and the wave, the scalar product $(e\boldsymbol{v}_\perp \cdot \boldsymbol{E})$ should be maintained to be constant at the whole undulator length, i.e. a synchronism should be provided. Such a synchronism takes place when the wave slips against the electron beam by one wavelength at one undulator period:

$$\frac{\lambda_w}{v_z} = \frac{\lambda}{c - v_z}, \tag{1.2}$$

where $\lambda = 2\pi c/\omega$ is the radiation wavelength. So as $v_z \simeq c$, this resonance condition may be written as

$$\lambda \simeq \frac{\lambda_w}{2\gamma_z^2} = \lambda_w \frac{1 + K^2}{2\gamma^2}. \tag{1.3}$$

When the resonance condition takes place, the electrons with different relative phases with respect to the wave acquire different values of the energy increments (positive or negative, which results in

the modulation of the longitudinal velocity of the electrons v_z within the radiation wavelength λ). This velocity modulation is transformed into the density modulation of the electron beam. At some circumstances the electron bunches fall in a decelerating phase of the wave and average energy of the electrons is decreased while the field amplitude of the wave is increased due to coherent radiation of the evenly spaced electron bunches, and the process of the field amplification takes place.

In the present paper we describe this process in a classical way by simultaneous solution the equations of the electron motion and electrodynamic equations. Classical approach can be used while the energy of the radiated photon $\hbar\omega$ is much less than the electron energy $\mathcal{E}$ (i.e. $\hbar\omega/\mathcal{E} \ll 1$). As a rule, the energy range of the FEL photons is 0.01–10 eV and the energy of the electrons is $\mathcal{E} \simeq$ 10–100 MeV, parameter $\hbar\omega/\mathcal{E}$ is equal to 10^{-7} and quantum effects are negligible. On the other hand, many of the first papers on the FEL theory were based on a quantum approach. In these papers, for instance, the radiation process was considered as the scattering of virtual photons of the undulator wave in the electron frame of reference and the process of the interaction of the electron with the electromagnetic wave was described as the process of induced radiation and absorption of laser photons (see review paper [10] and references therein). In our opinion, the FEL description in terms of quantum physics is an artificial one. Indeed, the terms of spontaneous and induced radiation are necessary to describe quantum lasers, but this approach is not fruitful to describe vacuum-tube devices to which the FEL belongs. Nevertheless, giving no principally new results, the investigations based on quantum approach have influenced significantly on the terminology of the FEL physics and such essentially quantum notions as Compton regime and Raman regime are widely used now.

It became a tradition in many popular reviews and books to derive the FEL resonance condition using Lorentz transformation. Namely, the interaction of the electron with the combined electromagnetic field of the undulator and the wave is considered in the electron frame of reference. In this approach, factor $2\gamma_z^2$ appears in the resonance condition as a consequence of the Doppler effect. Our experience have shown that such an introduction to the FEL physics usually forces the readers to believe that description of the FEL operation is impossible without detailed knowledge of the special theory of relativity. We have shown above that the resonance condition can be simply derived in the laboratory frame of reference and there is no need to use the laws of relativistic kinematic. In connection with this we should note that the only relativistic formula necessary for the FEL description is [1]

$$d\boldsymbol{p}/dt = \boldsymbol{F} = -e\boldsymbol{E} - e\frac{\boldsymbol{v}}{c} \times \boldsymbol{H},$$

where $\boldsymbol{p} = m_e\gamma\boldsymbol{v}$. In other words, to describe the processes in the FEL it is necessary only to take into account the relativistic dependence of the electron momentum on the velocity. When the electron may be treated as a point particle, such an approach always gives a reliable way to describe the processes of the electron beam dynamics and radiation in the given electromagnetic fields. Such a situation, for instance, takes place in the theory of particle accelerators. [2]

[1] To be more strict, in the present paper we use Hamilton equations which are equivalent to $d\boldsymbol{p}/dt = \boldsymbol{F}$.

[2] Nevertheless, when the electron can not be treated as a point particle, for instance, to describe the spin motion of the electron, there is urgent need in the use of the Lorentz transformation.

1.3. The use of the similarity techniques in the FEL theory

In traditional microwave electronics similarity techniques have been widely used and served a good deal to clarify basic ideas of this science. But in physics of free electron lasers these techniques still did not get the popularity it might have due to variety and generality of their possible applications. At present, there is an urgent need for a handbook to effectively help the researchers in using the similarity techniques applied to FEL technology and present paper is an attempt to satisfy the need of specialists for such a tool.

The analysis by similarity techniques consists in transforming absolute variables into relative ones. Simultaneously, the problem parameters transform into dimensionless power complexes – similarity criteria. These latter are unique parameters of the problem under study reduced to its dimensionless form. Each factor influencing the FEL operation (space charge, energy spread etc.) is matched with its own dimensionless criterion. For a given effect the corresponding similarity criterion is a measure of its relative intensity. When some effect becomes less important for the FEL operation, this is reflected in the corresponding similarity criterion taking on small values and falling out of the number of problem arguments.

The advantages due to the application of similarity theory are evident. A dimensional analysis of any problem, performed prior to its analytic investigation, not only reduces the number of independent terms but also allows to classify the grouping of dimensional variables in a way to be most suitable for a subsequent study. Further on, the solution of the dimensionless equations produces final results in such a form that the information contained will be simultaneously of the high degree of generality and completely specified. The use of similarity techniques forms a style of physical mentality and leads to a deeper insight into the FEL physics.

To make the paper useful for calculations of practical devices, we have included numerous universal graphs illustrating various modes of FEL operation together with the reduced design formulae which will teach the reader to find FEL characteristics using the simple dimensional analysis only. It may be useful for FEL designers, especially at the design stage of an experiment.

1.4. Organization of the report

The paper proceeds as follows. Sections 2–4 are devoted to the one-dimensional theory of the FEL amplifier, Sections 5–8 present the one-dimensional theory of the FEL oscillator and Sections 9–11 present an introduction to the analysis of diffraction effects.

Section 2 deals with the linear theory of the FEL amplifier. In exposing the linear theory the main emphasis is put on finding analytic solutions of the self-consistent field equations with regard to the effects of the space charge and energy spread of particles in the beam. An interaction process of the electron beam with electromagnetic wave in an undulator in the linear mode of operation can be described by a unique integro-differential equation. The solution of the latter under stated initial conditions at the entrance into the interaction region allows to determine a relationship between wave field amplitude and undulator length and thus to calculate the output characteristics of the FEL amplifier. The solution of the initial problem has been performed by the Laplace transform technique. The rigorous results obtained in a reduced form furnish universal plots for calculating the output characteristics of the FEL amplifier in the linear mode of operation. Besides, these analytic solutions serve as a reliable basis for the development of numerical methods. The analysis of nonlinear

processes refers to the problems solvable only numerically by a computer. On the other hand, testing of the numerical simulation codes would be difficult without the use of rigorous results of the FEL amplifier linear theory as a primary standard.

The similarity techniques are known to play a dominant role in numerical simulation of processes observed in FEL. For instance, within the scope of the one-dimensional approximation the output characteristics of the FEL amplifier are controlled by 8 dimensional parameters of both the beam and undulator. The system of self-consistent field equations describing a phenomenon of the beam-wave interaction in the undulator may be formulated as a relation between dimensionless quantities. The equations show that a family of the similar modes of operation of the FEL amplifier is controlled by the values of 5 dimensionless parameters. In a high-gain mode, when the dimensionless undulator length is rather large, the field output amplitude in a saturation mode is independent of both undulator length and input signal amplitude. In this practically prominent case the maximum amplifier efficiency is a function of only 3 dimensionless parameters: detuning, space charge and energy spread.

The calculation scheme the FEL amplifier output saturation characteristics which is suitable for engineer's practice is presented in Section 3. This scheme stems from similarity techniques and numerical simulation results given as design formulae and universal plots. All stages of numerical experiment, i.e. the physical statement of the problem, the construction of a mathematical model, the realization of an algorithm and the computation process itself are consecutively exposed in the paper.

A promising means to increase the FEL amplifier efficiency up to about unity is the variation of undulator parameters along its axis. Further extensions of the similarity techniques for efficiency calculations of the amplifiers with variable undulator parameters are discussed in section 4. A procedure of the engineering calculations of the optimal undulator parameters and FEL amplifier output characteristics with an optimum undulator is given, too.

Sections 5–8 are devoted to the one-dimensional theory of the FEL oscillator. A simple FEL oscillator model is under consideration when the duration of the beam current pulse is infinitely long and the power gain per one undulator pass is small. The lasing frequency is assumed to correspond a maximum of the gain in a small-signal mode of operation and effects of the longitudinal mode competition are excluded from consideration. Despite of its relative simplicity, such a model is extremely fruitful to explain the main features of the FEL oscillator operation.

Section 5 deals with a linear theory of the FEL oscillator in the small signal approximation. In exposing the linear theory the main emphasis is put on finding analytic solutions of the self-consistent field equations with regard to the effects of space charge fields and energy spread of electrons in the beam. These rigorous solutions, written down in a reduced form, are of great practical significance. They are used to obtain the universal dependencies of the linear mode of the FEL oscillator operation, lasing conditions and serve as a reliable test base for numerical codes.

Section 6 deals with the description of the FEL oscillator operating in a saturation mode. The main emphasis is put on finding optimal conditions for the FEL operation to reach a maximal FEL efficiency. The present treatment is based on the results of numerical simulations and their subsequent generalization by similarity techniques. It is shown that the maximal FEL efficiency at the saturation and the maximal amplitude of radiation field in the resonator are universal functions of only three reduced parameters, namely the quality factor Q of a resonator, space charge and energy spread parameter.

In Section 7 we analyze a problem of the FEL oscillator efficiency enhancement by tapering the undulator parameters. Principal differences between the amplifier and oscillator cases are discussed.

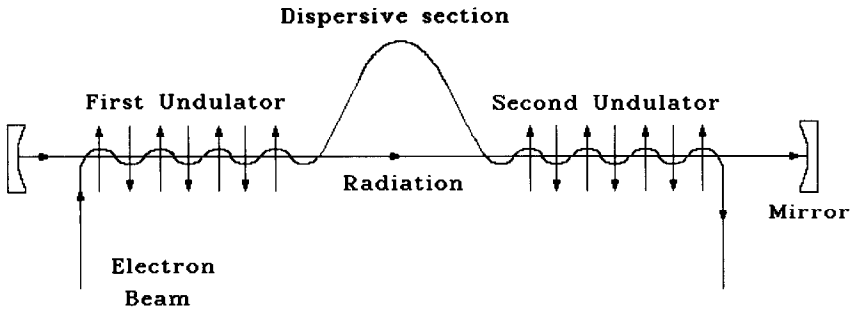

Fig. 1.3. Conceptual scheme of a FEL optical klystron.

In the FEL amplifier the frequency of amplified wave is determined by a master oscillator, the tapering of undulator parameters turns on near the saturation point and plays the only role to keep the beam-wave synchronism when particles lose energy. Contrary to this, in the FEL oscillator the undulator tapering strongly influences the small-signal mode of the FEL oscillator operation, the lasing frequency depends on the tapering depth and corresponds to the maximum gain in the small-signal mode of operation. We illustrate these features of the FEL oscillator with a specific case of the linear tapering law. Analytical formulae describing the small-signal mode of operation are obtained. The results of numerical simulations, presented by means of similarity techniques in the form of universal graphs and tables are used to find the optimal relations between the tapering depth and Q quality of the resonator.

Section 8 presents the theory of the FEL oscillator with a multicomponent undulator. The most popular case is considered when the undulator consists of two sections separated with a drift (or dispersion) section. Such a magnetic system is widely used in an optical klystron to increase the small signal amplification or in the FEL oscillator with a prebuncher to increase the efficiency at saturation (see Fig. 1.3). We describe thoroughly a practically prominent case when the first undulator section has fixed parameters and parameters of the second section are tapered by a linear law. A small-signal mode of operation is studied analytically. The obtained rigorous solutions describe lasing conditions taking into account the energy spread of electrons in the beam, relations between the length of undulator and drift section, wave phase shift in the drift section and the tapering depth. Nonlinear mode of operation is studied with the help of numerical simulation and application of similarity techniques. The universal reduced dependencies presented in the paper allow one to calculate all main characteristics of the FEL oscillator with a multicomponent undulator.

Sections 9–11 present an introduction to the three-dimensional FEL theory and reveal to the reader the applicability region of the one-dimensional theory. A basic approach to analyze diffraction effects in the FEL is formulated in section 9. The analyzed models are based on the Maxwell wave equation taken in a paraxial approximate form and on the description of particle motion by a kinetic equation expressed in "energy-phase" variables. It is anticipated that electrons move (averaged over constrained motion) only along trajectories parallel to the undulator axis. Such a models proved to be very fruitful to correctly explain the physical phenomena in the FEL. The general theory of beam-wave interaction is used for the analysis of the FEL taking into account diffraction effects, space charge and energy spread of particles in the beam.

To illustrate basic approach presented in Section 9, in Sections 10 and 11 we present selected

elements of the FEL amplifier theory wherein diffraction effects are taken into account. Particular features of this three-dimensional theory are illustrated by a model of the FEL amplifier with an axisymmetric electron beam. It is shown that in the linear high-gain limit the radiation of the electron beam in the undulator may be represented as a set of modes. In the amplification process the mode configuration in transverse plane remains unchanged while the amplitude grows with undulator length exponentially. Each mode is characterized by an increment eigenvalue and field distribution eigenfunction in terms of transverse coordinates. The mode with the highest gain has advantages over all other modes. By following the gain process along the undulator axis one can find that after all the field distribution is settled corresponding to the mode with a maximal increment (the so called "optical guiding" effect takes place here). The complete description of radiation modes is performed with the self-consistent field method to get from the kinetic equation and the Maxwell equation a unique equation for the field amplitude. The modes are calculated from the solution of the self-consistent field equations inside and outside of the beam. To define eigenvalues, the conditions of the quadratic integrability and the continuity of eigenfunction and its derivative at the beam boundary are used. The eigenvalue equation is derived and expressions for eigenfunctions and field distributions are found. The initial problem is solved for a practically important case when one has a nonmodulated electron beam and electromagnetic radiation from the master laser at the amplifier entrance. The asymptotic formulae for the high-gain mode are derived by taking into account space charge and energy spread of the beam electrons. The optimal conditions of the input radiation focusing on the electron beam are found for a Gaussian laser beam. Analytic results are compared with the results of the self-consistent field equations integration on a computer.

Section 11 is devoted to the analysis of a nonlinear mode of the FEL amplifier operation. The macroparticle method, developed in Sections 2–4, is extended to the three-dimensional case. Further extension of similarity techniques is discussed and the reduced self-consistent system of the FEL amplifier equations is formulated taking into account space charge fields, energy spread and diffraction effects. Then, using the results of numerical simulations presented in the reduced form, we analyze various features of the FEL amplifier in the nonlinear mode.

2. Linear mode of the FEL amplifier operation

As a rule, the following approximations are accepted in the one-dimensional theory of the FEL amplifier:

- the electron beam has a uniform density distribution in the direction perpendicular to the undulator axis;
- the electrons move along identical trajectories parallel to the undulator axis;
- the amplified wave is a plane wave;
- the slippage length of optical bunch with respect to the electron bunch is much less than the length of the electron bunch.

One-dimensional theory of the FEL amplifier has been studied thoroughly by many authors and the most essential results has been obtained in Refs. [11–14]. The authors of Ref. [11] carried out the first theoretical study of the linear mode of the FEL amplifier operation. They obtained the self-consistent field equations and derived from them the eigenvalue equation taking into account action of the space charge field and influence of the energy spread of the electrons in the beam. In

Ref. [12] the Laplace transform method was used to obtain the solution of the initial-value problem for the case of negligibly small energy spread of electrons in the beam. Ref. [13] contains the most comprehensive study of the initial value problem using Laplace transform technique. The authors of this paper obtained the Laplace transform of the self-consistent field equations, taking into account the effect of the energy spread of the beam particles and managed to derive from them an expression for the Laplace transform of the field amplitude. The field amplitude in this case may be found by means of inverse transform which requires the computation of an integral over complex plane. For a number of cases, for instance, for a Lorentzian energy spread, this integral can be transformed to an integral along the closed contour in the complex plane and calculated using the calculus of residue theory. This mathematical trick does not work for a Gaussian energy distribution, and in that case the authors of Ref. [13] solved the initial-value problem using numerical methods. However, it is important to note that in practice there is often no need for a complete solution of the initial-value problem, since it is sufficient to consider only the case of high gain. In the limit of high gain the Laplace method can be used to obtain an analytic solution of the initial-value problem even in the case of a Gaussian energy spread. The corresponding asymptotic expression for the gain has been derived in Ref. [14].

In the linear mode of the FEL amplifier operation, the output radiation power is proportional to input one. Physically it means that in the linear regime the first harmonic of the beam density modulation dominates significantly against the higher harmonics. So, when describing the linear mode, a linearized kinetic equation can be used for description of the particle motion. As a result, very powerful analytical technique can be used. In exposing the linear theory the main emphasis is put on finding analytic solutions of the self-consistent field equations with regard to the effects of space charge and energy spread of particles in the beam. An interaction process of electron beam with electromagnetic wave in an undulator in the linear mode of operation can be described by a unique integro-differential equation. The solution of the latter under stated initial conditions at the entrance into the interaction region allows to determine a relationship between wave field amplitude and undulator length and thus to calculate the output characteristics of the FEL amplifier. We solve the initial-value problem using the Laplace transform technique. The rigorous results obtained in a reduced form furnish universal plots for calculating the output characteristics of a FEL amplifier in the linear mode of operation. Besides, these analytic solutions serve as a reliable basis for the development of numerical methods. The analysis of nonlinear processes refers to the problems solvable only numerically by a computer. On the other hand, testing of the numerical simulation codes would be difficult without the use of rigorous results of the FEL amplifier linear theory as a primary standard.

2.1. *Effective Hamiltonian*

Let us consider a FEL amplifier with a helical undulator. The undulator magnetic field at the axis has the form

$$\boldsymbol{H}_w(z) = \boldsymbol{e}_x H_w \cos(\kappa_w z) - \boldsymbol{e}_y H_w \sin(\kappa_w z),$$

where $\kappa_w = 2\pi/\lambda_w$ is the undulator wavenumber and $\boldsymbol{e}_{x,y}$ are unit vectors directed along the x and y axes of the Cartesian coordinate system (x, y, z). One of the main characteristics of the undulator is the undulator parameter K:

$$K = eH_w/m_e c^2 \kappa_w,$$

where $(-e)$ and m_e are the charge and the mass of the electron, respectively, and c is the velocity of light. It is useful to present another form of this expression convenient for numerical calculations:

$$K = 0.0934 \times H_w[\mathrm{kG}] \times \lambda_w[\mathrm{cm}].$$

We neglect the transverse variation of the magnetic field and assume the electrons to move along the constrained helical trajectories parallel to the z axis:

$$\boldsymbol{v}_\perp(z) = c\theta_s[\boldsymbol{e}_x \cos(\kappa_w z) - \boldsymbol{e}_y \sin(\kappa_w z)].$$

The electron rotation angle $\theta_s = K/\gamma$ (where $\gamma = \mathcal{E}_0/m_e c^2$ is relativistic factor of the electron with nominal energy $\mathcal{E}_0$) is considered to be small and the longitudinal electron velocity v_z is close to the velocity of light c ($v_z \simeq c$).

The electric field of the amplified wave is presented in the complex form:

$$E_x + iE_y = \tilde{E}(z) \exp[i\omega(z/c - t)],$$

where ω is the frequency of the amplified wave. The complex amplitude of the field $\tilde{E}$ does not depend on time at any space point which corresponds to the standard formulation of the initial problem with the definite initial conditions at the undulator entrance at $z = 0$. We assume the complex amplitude $\tilde{E}(z)$ to be a slowly changing function, i.e. $|\partial\tilde{E}/\partial z| \ll \kappa_w|\tilde{E}|$.

Let us consider the Hamiltonian formalism for the equations of motion of the electrons in the total electromagnetic field of the undulator, the radiation and the space charge. The Hamiltonian is defined as

$$\mathcal{H}(p_z, z, t) = \left[(p_z c + eA_z)^2 + e^2(\boldsymbol{A} + \boldsymbol{A}_w)^2 + m_e^2 c^4\right]^{1/2} - e\phi. \tag{2.1}$$

Here p_z is the longitudinal component of the generalized particle momentum, $\boldsymbol{A}$ is the vector potential of the wave, ϕ and A_z are, respectively, the scalar potential and vector potential of the space charge field, and

$$\boldsymbol{A}_w(z) = -\boldsymbol{e}_z \times \int \boldsymbol{H}_w dz$$

is the vector potential of the undulator field. In the one-dimensional model the transverse generalized momentum of the particle is an integral of motion, and we take it to be zero. We transform the Hamiltonian $\mathcal{H}$ from the variables p_z, z and t to variables convenient for describing the amplification process. We shall use the extended Hamiltonian formalism where t is considered as a canonical variable (see Appendix A) and choose coordinate z as a new time. Phase

$$\psi = \kappa_w z + \omega(z/c - t) \tag{2.2}$$

is chosen as a new canonical coordinate. According to formula (A.7), transformation (2.2) is canonical when

$$\mathcal{P} = -p_0/\omega, \quad \mathcal{P}_0 = p_z + (p_0/\omega)(\kappa_w + \omega/c),$$

where (p_0, p_z) and $(\mathcal{P}_0, \mathcal{P})$ are the old and new canonical momentums conjugated to (t, z) and (z, ψ), respectively. Hence, the new Hamiltonian $\tilde{\mathcal{H}}(\mathcal{P}, \psi, z)$ is given by

$$\tilde{\mathcal{H}}(\mathcal{P},\psi,z) = (\kappa_w + \omega/c)\mathcal{P} - p_z(\mathcal{P},z,\psi) = (\kappa_w + \omega/c)\mathcal{P} + eA_z/c - c^{-1}[(\mathcal{P}\omega + e\phi)^2 - e^2(\boldsymbol{A}+\boldsymbol{A}_w)^2 - m_e^2c^4]^{1/2}, \tag{2.3}$$

and the canonical equations of motion have the form

$$d\psi/dz = \partial\tilde{\mathcal{H}}/\partial\mathcal{P}, \quad d\mathcal{P}/dz = -\partial\tilde{\mathcal{H}}/\partial\psi.$$

It is well known that the scalar potential ϕ and the longitudinal component of the vector potential A_z may be subjected to the following gauge transformation:

$$\phi \Rightarrow \phi' = \phi - c^{-1}\partial\tilde{\chi}/\partial t, \quad A_z \Rightarrow A_z' = A_z + \partial\tilde{\chi}/\partial z,$$

where $\tilde{\chi}$ is an arbitrary function of coordinate z and time t. In this case the longitudinal component of electric field

$$E_z = -\partial\phi/\partial z - c^{-1}\partial A_z/\partial t$$

remains unchanged[3]. We choose for the gauge transformation the following function

$$\tilde{\chi} = c\int dt\phi(z,t).$$

As a result, the space charge field is described with the only vector potential and we may write the following expression for Hamiltonian (2.3)

$$\tilde{\mathcal{H}} = (\kappa_w + \omega/c)\mathcal{E}/\omega - c^{-1}[\mathcal{E}^2 - e^2(\boldsymbol{A}+\boldsymbol{A}_w)^2 - m_e^2c^4]^{1/2} + \frac{e}{\omega}\int d\psi E_z(z,\psi).$$

Hence, the electron interaction with the space charge field is now described with the longitudinal component of electric field E_z. In the chosen gauge the canonical momentum $\mathcal{P}$ is equal to the electron kinetic energy $\mathcal{E}$ divided by ω.

It is convenient for the further consideration to simplify the expression for the Hamiltonian. First, we expand Hamiltonian $\tilde{\mathcal{H}}$ in the first order of the radiation field amplitude A. Such an approximation is valid when the electron transverse constrained motion is determined with the undulator field and not with the radiation field, i.e.

$$|\tilde{E}|(1 - v_z/c) \ll H_w,$$

where $|\tilde{E}| = c^{-1}|\partial\boldsymbol{A}/\partial t|$. So, we get

$$\tilde{\mathcal{H}} = \frac{\mathcal{E}}{\omega}(\kappa_w + \omega/c) - \frac{1}{c}[\mathcal{E}^2 - e^2|\boldsymbol{A}_w|^2 - m_e^2c^4]^{1/2} + \frac{e^2(\boldsymbol{A}\cdot\boldsymbol{A}_w)}{c}[\mathcal{E}^2 - e^2|\boldsymbol{A}_w|^2 - m_e^2c^4]^{-1/2} + \frac{e}{\omega}\int d\psi E_z. \tag{2.4}$$

Second, we expand Hamiltonian (2.4) up to the second order of the energy deviation $\mathcal{E}$ from the nominal value $\mathcal{E}_0$. Finally we get

[3] It should be noted that the value of canonical momentum $\mathcal{P}$ is not gauge invariant as well as potentials.

$$\tilde{\mathcal{H}}\omega = H(P,\psi,z) = CP + \frac{\omega}{2c\gamma_z^2\mathcal{E}_0}P^2 - (Ue^{i\psi} + U^*e^{-i\psi})(1 - P/\mathcal{E}_0) + \int d\psi e E_z, \tag{2.5}$$

where $P = \mathcal{E} - \mathcal{E}_0$, $C = \kappa_w - \omega/(2c\gamma_z^2)$ is the detuning of the electron with the nominal energy $\mathcal{E}_0$, $U = -e\theta_s\tilde{E}(z)/(2i)$ is the complex amplitude of the effective potential of the particle interaction with the electromagnetic wave, and

$$\theta_s = eH_w/(\mathcal{E}_0\kappa_w), \quad \gamma_z^{-2} = \gamma^{-2} + \theta_s^2, \quad \gamma = \mathcal{E}_0/(m_ec^2).$$

2.2. *Self-consistent field equations*

The evolution of the electron beam distribution function f is determined with the kinetic equation

$$\frac{\partial f}{\partial z} + \frac{\partial H}{\partial P}\frac{\partial f}{\partial \psi} - \frac{\partial H}{\partial \psi}\frac{\partial f}{\partial P} = 0. \tag{2.6}$$

In the linear approximation we shall seek the solutions for f and E_z in the form

$$f = f_0 + \tilde{f}_1 e^{i\psi} + \tilde{f}_1^* e^{-i\psi}, \quad E_z = \tilde{E}_z e^{i\psi} + \tilde{E}_z^* e^{-i\psi}.$$

Using Eqs. (2.5) and (2.6) we get

$$\frac{\partial \tilde{f}_1}{\partial z} + i(C + \omega P/(c\gamma_z^2\mathcal{E}_0))\tilde{f}_1 + (iU - e\tilde{E}_z)\frac{\partial f_0}{\partial P} = 0. \tag{2.7}$$

We assume that the electron beam at the entrance into the undulator is modulated neither in velocity nor in density, i.e.

$$\tilde{f}_1|_{z=0} = 0, \quad f_0|_{z=0} = n_0F(P), \quad \int F dP = 1, \tag{2.8}$$

where n_0 is the beam density. The beam current density is connected with the distribution function $\tilde{f}_1$ as follows (we assume here $v_z \simeq c$)

$$j_z = -j_0 + \tilde{j}_1 e^{i\psi} + \text{c.c.}, \quad \tilde{j}_1 \simeq -ec\int \tilde{f}_1 dP,$$

where $-j_0 \simeq -ecn_0$ is the longitudinal component of the beam current density at the undulator entrance.

In the framework of the one-dimensional model, from Maxwell's equation we have the following equation for E_z

$$\partial E_z/\partial t = -i\omega\tilde{E}_z e^{i\psi} + \text{c.c.} = -4\pi j_1\cos(\psi + \psi_1) = -4\pi\tilde{j}_1 e^{i\psi} + \text{c.c.} \tag{2.9}$$

Here j_1 and ψ_1 are the amplitude and phase of the first harmonic of the beam current density, respectively, which are connected with the complex amplitude $\tilde{j}_1(z)$ by relation: $\frac{1}{2}j_1\exp(i\psi_1) = |\tilde{j}_1|\exp(i\psi_1) = \tilde{j}_1$. As a result, we have

$$\tilde{E}_z = -i4\pi\tilde{j}_1(z)/\omega. \tag{2.10}$$

Substituting Eqs. (2.8) and (2.10) into the kinetic equation (2.7) and integrating over z and P we get the following integral equation for $\tilde{j}_1(z)$

$$\tilde{j}_1(z) = ij_0 \int_0^z dz' \left[U + \frac{4\pi e \tilde{j}_1(z')}{\omega} \right] \times \int dP \frac{dF(P)}{dP} \exp\left\{ i \left[C + \frac{\omega P}{c\gamma_z^2 \mathcal{E}_0} \right] (z' - z) \right\}. \tag{2.11}$$

One more relation between the amplitudes $\tilde{j}_1(z)$ and $\tilde{E}(z)$ must come from the solution of the electrodynamical problem. The vector potential of the radiation field can be found using the wave equation

$$\partial^2 \boldsymbol{A}/\partial z^2 - c^{-2}\partial^2 \boldsymbol{A}/\partial t^2 = -(4\pi/c)\boldsymbol{j}_\perp,$$

where the density of the transverse beam current is given by

$$j_x + ij_y = \theta_s \exp(-i\kappa_w z) j_1 \cos(\psi + \psi_1).$$

We shall seek a solution for $\boldsymbol{A}_\perp(z,t)$ in the form

$$A_{x,y} = \tilde{A}_{x,y}(z) \exp[i\omega(z/c - t)] + \text{c.c.}$$

in which we have explicitly isolated the strong z dependence of $\boldsymbol{A}_\perp$. From the wave equation we have

$$\exp[i\omega(z/c - t)] \left\{ \frac{2i\omega}{c} \frac{\partial}{\partial z} \begin{pmatrix} \tilde{A}_x \\ \tilde{A}_y \end{pmatrix} + \frac{\partial^2}{\partial z^2} \begin{pmatrix} \tilde{A}_x \\ \tilde{A}_y \end{pmatrix} \right\} + \text{c.c.} = \frac{-4\pi\theta_s}{c} \begin{pmatrix} \cos(\kappa_w z) \\ -\sin(\kappa_w z) \end{pmatrix} j_1 \cos(\psi + \psi_1). \tag{2.12}$$

Neglecting rapidly oscillating terms in Eq. (2.12), we transform it to the equation containing only slowly varying amplitudes:

$$d\tilde{E}/dz = -2\pi\theta_s c^{-1} \tilde{j}_1(z), \tag{2.13}$$

Here we have used the fact that in the one-dimensional approximation the vector potential and the electric field vector of the electromagnetic wave are related as $cE_{x,y} = -\partial(A_{x,y})/\partial t$. The characteristic scale of the complex amplitude $\tilde{E}$ change is much larger than the radiation wavelength, so in Eq. (2.13) we have omitted the second derivative of $\tilde{E}$ with respect to z. Substituting (2.11) into the right-hand side of Eq. (2.13), we easily obtain a single integro-differential equation for the field amplitude $\tilde{E}$. For the rest of our discussion it is convenient to transform to reduced parameters given by the relations:

$$\hat{z} = \Gamma z, \quad \hat{C} = C/\Gamma, \quad \hat{P} = \omega P/(c\gamma_z^2 \mathcal{E}_0 \Gamma).$$

The gain parameter Γ and longitudinal plasma wavenumber Λ_p are given by formulae

$$\Gamma = [\pi j_0 \theta_s^2 \omega/(c\gamma_z^2 \gamma I_A)]^{1/3}, \quad \Lambda_p = [4\pi j_0/(\gamma_z^2 \gamma I_A)]^{1/2},$$

where $I_A = m_e c^3/e \simeq 17$ kA. As a result, we obtain the following reduced equation:

$$\frac{d\tilde{E}}{d\hat{z}} = \int_0^{\hat{z}} d\hat{z}' \left\{ \tilde{E}(\hat{z}') + i\hat{\Lambda}_p^2 \frac{d\tilde{E}(\hat{z}')}{d\hat{z}'} \right\} \int_{-\infty}^{\infty} d\hat{P} \frac{d\hat{F}}{d\hat{P}} \exp\left\{ i\left(\hat{P} + \hat{C}\right)(\hat{z}' - \hat{z}) \right\}. \tag{2.14}$$

Here $\hat{\Lambda}_p^2 = \Lambda_p^2/\Gamma^2$ is the space charge parameter and $\hat{F}(\hat{P})$ is the distribution in the reduced momentum $\hat{P}$ satisfying the normalization condition $\int \hat{F}(\hat{P})d\hat{P} = 1$.

2.3. Solution of the initial-value problem by Laplace technique

Eq. (2.14) is an integro-differential equation for the field amplitude $\tilde{E}(\hat{z})$ and can be solved by a Laplace transform technique. Multiplying Eq. (2.14) by $\exp(-pz)$ with $\mathrm{Re}\, p > 0$ and integrating over z from 0 to ∞, we obtain for the integral of derivative of $\tilde{E}$ with respect to z the following expression

$$\int_0^{\infty} d\zeta \exp(-p\zeta)\partial\tilde{E}(\zeta)/\partial\zeta = p\bar{E}(p) - \tilde{E}_{\mathrm{ext}}.$$

Here $\bar{E}(p)$ is the Laplace transform of the field amplitude $\tilde{E}$

$$\bar{E}(p) = \int_0^{\infty} d\zeta \exp(-p\zeta)\tilde{E}(\zeta),$$

$\tilde{E}_{\mathrm{ext}}$ is the amplitude of the field at the undulator entrance at $z = 0$ (for definiteness, we assume its value to be real and positive, i.e. $\tilde{E}_{\mathrm{ext}} = E_{\mathrm{ext}} > 0$). The Laplace transform of Eq. (2.14) has the form

$$p\bar{E}(p) - E_{\mathrm{ext}} = [\bar{E}(p) + i\hat{\Lambda}_p^2\left(p\bar{E}(p) - E_{\mathrm{ext}}\right)] \int_{-\infty}^{\infty} d\xi \frac{\hat{F}'(\xi)}{p + i(\xi + \hat{C})}. \tag{2.15}$$

If we solve Eq. (2.15) for $\bar{E}(p)$, we obtain the expression

$$\bar{E}(p) = \frac{E_{\mathrm{ext}}}{p - \dfrac{\hat{D}}{1 - i\hat{\Lambda}_p^2\hat{D}}}, \tag{2.16}$$

where

$$\hat{D} = \int_{-\infty}^{\infty} d\xi \frac{\hat{F}'(\xi)}{p + i(\xi + \hat{C})}. \tag{2.17}$$

To find $\tilde{E}(z)$, we should take the inverse Laplace transform of (2.16). This transform is defined by the integral

$$\tilde{E}(z) = \frac{1}{2\pi i} \int_{\gamma'-i\infty}^{\gamma'+i\infty} d\lambda \bar{E}(\lambda)\exp(\lambda\hat{z}) = \frac{E_{\mathrm{ext}}}{2\pi i} \int_{\gamma'-i\infty}^{\gamma'+i\infty} d\lambda \frac{\exp(\lambda\hat{z})}{\lambda - \dfrac{\hat{D}}{1 - i\hat{\Lambda}_p^2\hat{D}}}. \tag{2.18}$$

Let the integration in the complex λ plane run parallel to the imaginary axis. The constant γ' is a real positive number, larger than the real parts of all the singularities of the integrand. The linear integral (2.18) obtained by the inverse transform is usually calculated by closing the integration contour by a semicircle at infinity in the left half-plane and using the residue theorem. For this trick to be applicable to the integral (2.18), it is necessary that the integrand in (2.18) have an analytic continuation into the left half-plane, and the coefficient of $\exp(\lambda\hat{z})$ in the integrand in (2.18) satisfies the conditions of Jordan's lemma.

According to Eq. (2.17), the function $\hat{D}$ is a complex integral and has a discontinuity on the imaginary λ axis. This integral becomes an analytic function if, following Landau's method [15], the function $\hat{D}$ is defined as

$$\hat{D} = \int_{-\infty}^{\infty} d\xi \frac{\hat{F}'(\xi)}{\lambda + i(\xi + \hat{C})}, \quad \mathrm{Re}(\lambda) > 0,$$

$$\hat{D} = P\int_{-\infty}^{\infty} d\xi \frac{\hat{F}'(\xi)}{\lambda + i(\xi + \hat{C})} + \pi\hat{F}'(i\lambda - \hat{C}), \quad \mathrm{Re}(\lambda) = 0,$$

$$\hat{D} = \int_{-\infty}^{\infty} d\xi \frac{\hat{F}'(\xi)}{\lambda + i(\xi + \hat{C})} + 2\pi\hat{F}'(i\lambda - \hat{C}), \quad \mathrm{Re}(\lambda) < 0 \tag{2.19}$$

Here $P(\ldots)$ denotes the principal value. If the distribution function $\hat{F}(\hat{P})$ is such that the coefficient

$$\frac{1}{\lambda - \dfrac{\hat{D}}{1 - i\hat{\Lambda}_p^2\hat{D}}}$$

of $\exp(\lambda\hat{z})$ in the integrand in (2.18) satisfies the conditions of Jordan's lemma, the complete wave field can be represented as a superposition of partial waves. Finally, using the residue theorem, we obtain the following expression for $\tilde{E}(z)$

$$\tilde{E}(z) = E_{\mathrm{ext}} \sum_j \frac{\exp(\lambda_j\hat{z})}{1 - \dfrac{\hat{D}'_j}{(1 - i\hat{\Lambda}_p^2\hat{D}_j)^2}}. \tag{2.20}$$

Here we have introduced the abbreviated notation

$$\hat{D}_j = \hat{D}|_{\lambda=\lambda_j}, \quad \hat{D}'_j = \left.\frac{d\hat{D}_j}{d\lambda}\right|_{\lambda=\lambda_j},$$

where λ_j is the j-th root of the equation

$$\lambda - \frac{\hat{D}}{1 - i\hat{\Lambda}_p^2\hat{D}} = 0, \tag{2.21}$$

and the function $\hat{D}$ is defined by expression (2.19).

2.3.1. "Cold" electron beam

In the limit of a small energy spread, the distribution function $\hat{F}$ can be replaced by the delta function $\hat{F} = \delta(\hat{P})$. In this case the function $\hat{D}$ is given in the entire complex λ plane by

$$\hat{D} = i(\lambda + i\hat{C})^{-2}.$$

Since the coefficient of $\exp(\lambda\hat{z})$ in (2.18)

$$\frac{1}{\lambda - \dfrac{\hat{D}}{1 - i\hat{\Lambda}_p^2\hat{D}}} = \frac{1}{\lambda - \dfrac{i}{\left(\lambda + i\hat{C}\right)^2 + \hat{\Lambda}_p^2}}$$

is of the order of $O(\lambda^{-1})$ for $|\lambda| \to \infty$, the condition of Jordan's lemma is satisfied. Therefore, Eq. (2.20) is applicable and the partial-wave expansion of the wave has the form

$$\tilde{E}(z) = E_{\text{ext}} \sum_j \frac{\exp(\lambda_j \hat{z})}{1 - 2i(\lambda_j + i\hat{C})\lambda_j^2},$$

where λ_j are the roots of the cubic equation

$$\lambda = i[(\lambda + i\hat{C})^2 + \hat{\Lambda}_p^2]^{-1}. \tag{2.22}$$

Using the relations between the roots of the cubic equation (2.22),

$$\lambda_1\lambda_2\lambda_3 = i, \quad \lambda_1\lambda_2 + \lambda_2\lambda_3 + \lambda_1\lambda_3 = -\hat{C}^2 + \hat{\Lambda}_p^2,$$
$$\lambda_1 + \lambda_2 + \lambda_3 = -2i\hat{C},$$

after simple algebra we obtain the familiar expression for the wave amplitude [12,13]:

$$\tilde{E}(z) = E_{\text{ext}}\left[\frac{\lambda_2\lambda_3\exp(\lambda_1\hat{z})}{(\lambda_1 - \lambda_2)(\lambda_1 - \lambda_3)} + \frac{\lambda_1\lambda_3\exp(\lambda_2\hat{z})}{(\lambda_2 - \lambda_3)(\lambda_2 - \lambda_1)} + \frac{\lambda_1\lambda_2\exp(\lambda_3\hat{z})}{(\lambda_3 - \lambda_1)(\lambda_3 - \lambda_2)}\right]. \tag{2.23}$$

Exactly on resonance ($\hat{C} = 0$) in the absence of the space charge field, the solution for $\tilde{E}(z)$ is written as

$$\tilde{E}(z) = \frac{E_{\text{ext}}}{3}\left[\exp\left(\frac{\sqrt{3}+i}{2}\hat{z}\right) + \exp\left(\frac{-\sqrt{3}+i}{2}\hat{z}\right) + \exp(-i\hat{z})\right]. \tag{2.24}$$

Fig. 2.1 illustrates the dependence of the field gain $|\tilde{E}|/E_{\text{ext}}$ on the reduced length $\hat{z}$. When the undulator length is sufficiently large, the contribution in Eq. (2.24) from the growing wave will exceed the other terms, and their contribution can be neglected. Then for $\tilde{E}(z)$ we can write the asymptotic expression:

$$\tilde{E}(z) = \frac{E_{\text{ext}}}{3}\exp\left(\frac{\sqrt{3}+i}{2}\hat{z}\right). \tag{2.25}$$

The power gain $G = |\tilde{E}|^2/E_{\text{ext}}^2$ is an important characteristic of the amplifier. According to Eq. (2.24), the value of G for $\hat{C} = 0$ is given by the expression

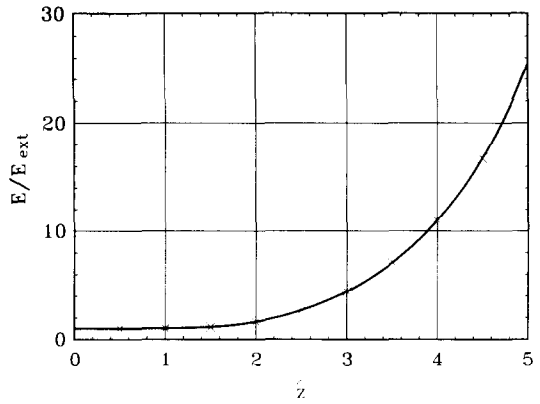

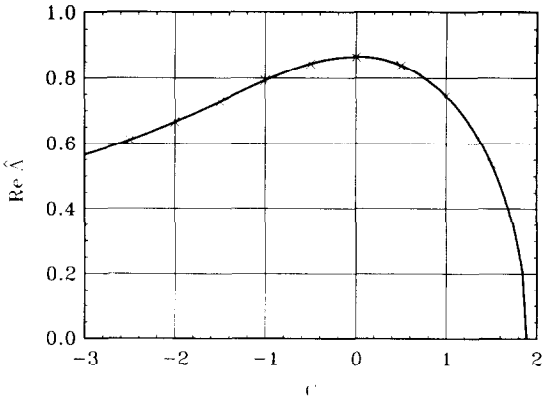

Fig. 2.1. Dependence of the field gain E/E_{ext} on the reduced length $\hat{z}$. Solid curve is calculated with analytical formula (2.24) and crosses are results of numerical simulations with Eqs. (3.5) and (3.6). Here $\hat{C} = 0$, $\hat{A}_p^2 = 0$ and $\hat{A}_T^2 = 0$.

Fig. 2.2. Dependence of the reduced increment $\mathrm{Re}(\hat{A})$ on the detuning parameter $\hat{C}$. Solid curve is calculated with exact solution of the eigenvalue Eq. (2.26) and crosses are results of numerical simulations with Eqs. (3.5) and (3.6). Here $\hat{A}_p^2 = 0$ and $\hat{A}_T^2 = 0$.

$$G = \frac{1}{9}\left[1 + \cosh\frac{\sqrt{3}}{2}\hat{z}\left(\cosh\frac{\sqrt{3}}{2}\hat{z} + \cos\frac{\sqrt{3}}{2}\hat{z}\right)\right].$$

In the high gain limit, according to Eq. (2.25), the power gain G in decibels is asymptotically equal to

$$G(\mathrm{dB}) = 10\lg\left(|\tilde{E}|^2/E_{ext}^2\right) = 7.5\hat{z} - 9.5.$$

It follows from Eq. (2.22) that for $\hat{A}_p^2 = 0$ the partial-wave propagation constants λ_1, λ_2 and λ_3 are universal functions of only the detuning parameter $\hat{C}$. Study of characteristic equation

$$\lambda\left(\lambda + i\hat{C}\right)^2 = i \tag{2.26}$$

shows that one of the partial waves is a growing wave in the detuning range $\hat{C} < 1.89$. We denote the propagation constant of the growing partial wave by $\hat{A}$. Then in the detuning range $\hat{C} < 1.89$ the power gain for a sufficiently long undulator can be written asymptotically as

$$G = A\exp\left(2\,\mathrm{Re}(\hat{A})\hat{z}\right), \tag{2.27}$$

where the increment $\mathrm{Re}(\hat{A})$ and the pre-exponential factor A are universal functions of the detuning parameter $\hat{C}$. Graphs of these functions are shown in Figs. 2.2 and 2.3. The maximal increment is reached exactly at resonance $\hat{C} = 0$. For small deviations from the resonance, when $\hat{C}^2 \ll 1$, the increment is given by

$$\mathrm{Re}(\hat{A}) = \frac{\sqrt{3}}{2}\left[1 - \frac{1}{9}\hat{C}^2\right]. \tag{2.28}$$

For large negative detuning, $|\hat{C}| \gg 1$, we asymptotically have

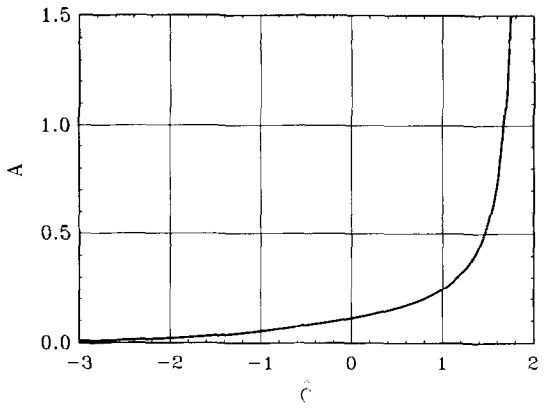

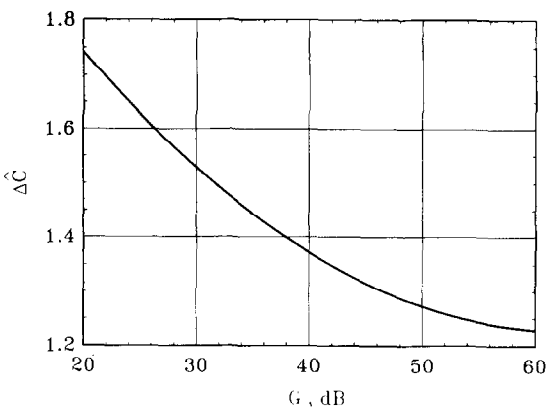

Fig. 2.3. Dependence of the preexponential factor A entering Eq. (2.27) on the detuning parameter $\hat{C}$. Here $\hat{\Lambda}_p^2 = 0$ and $\hat{\Lambda}_T^2 = 0$.

Fig. 2.4. The dependence of the amplification bandwidth $\Delta\hat{C}$ on the maximum power gain. Here $\hat{\Lambda}_p^2 = 0$ and $\hat{\Lambda}_T^2 = 0$.

$$\mathrm{Re}(\hat{\Lambda}) = |\hat{C}|^{-1/2}.$$

The electromagnetic wave amplification process in the undulator displays resonance behaviour which causes the gain factor to depend strongly on the detuning parameter $\hat{C}$. Usually the amplification bandwidth is defined as the difference of the input signal frequencies $\omega_1 - \omega_2 = \Delta\omega$ for which the output power is decreased by a factor of two. It is convenient to introduce the amplification bandwidth in the reduced detuning $\Delta\hat{C}$, which is related to the amplification bandwidth in the frequency of the input signal as $\Delta\omega/\omega_0 = (\Gamma/\kappa_w)\Delta\hat{C}$, where $\omega_0 = 2c\gamma_z^2\kappa_w$ is the resonance frequency. The amplification bandwidth can be found by solving the initial-value problem. In Fig. 2.4 we show a graph of the dependence of the amplification bandwidth $\Delta\hat{C}$ on the maximal power gain. This graph has been calculated using Eq. (2.23) and the roots of the characteristic equation (2.26). As an illustration, in Fig. 2.5 we give a graph of the amplitude-frequency characteristic for the maximal gain $G_{\max} = 40$ dB.

In the high gain limit, we may neglect the change of the pre-exponential factor A in Eq. (2.27), and the amplification bandwidth can be calculated using Eq. (2.28):

$$\Delta\hat{C} \simeq \frac{10.4}{\sqrt{G(\mathrm{dB}) + 9.5}}.$$

At $G > 40$ dB, this approximate expression for $\Delta\hat{C}$ provides an accuracy about of several per cent with respect to the exact solution of the initial-value problem (see Fig. 2.4).

Let us now consider the influence of the space charge field on the amplification process in the undulator. When the space charge parameter is small, $\hat{\Lambda}_p^2 \ll 1$, the space charge effects can be included using perturbation theory. After simple calculations using Eq. (2.22), we find that the maximal increment is attained for the detuning parameter $\hat{C}_m \simeq \hat{\Lambda}_p^2$ and is given by

$$\max(\mathrm{Re}(\hat{\Lambda})) \simeq \frac{\sqrt{3}}{2}\left(1 - \frac{\hat{\Lambda}_p^2}{3}\right).$$

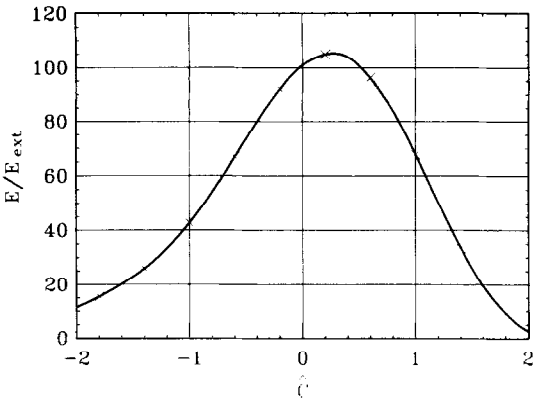

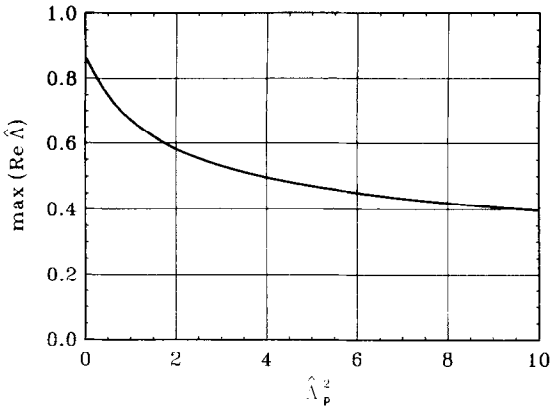

Fig. 2.5. Dependence of the field gain E/E_{ext} on the detuning parameter $\hat{C}$. Solid curve is calculated with analytical formula (2.23) and crosses are results of numerical simulations with Eqs. (3.5) and (3.6). Here the reduced length of the undulator is $z_f = 6.6$, $\hat{\Lambda}_p^2 = 0$ and $\hat{\Lambda}_T^2 = 0$.

Fig. 2.6. Dependence of the maximal reduced increment $\max \mathrm{Re}(\hat{\Lambda})$ on the space charge parameter $\hat{\Lambda}_p^2$. Here $\hat{\Lambda}_T^2 = 0$.

In the opposite case, $\hat{\Lambda}_p^2 \gg 1$, the space charge field significantly affects the increment, which at the maximum for $\hat{C}_m \simeq \hat{\Lambda}_p$ is equal to

$$\max(\mathrm{Re}(\hat{\Lambda})) \simeq \frac{1}{\sqrt{2\hat{\Lambda}_p}}.$$

When the space charge parameter $\hat{\Lambda}_p^2$ is of the order of unity, the increment can be found by solving the cubic characteristic equation (2.22). It should be noted that, according to Eq. (2.22), the maximal increment and the detuning parameter $\hat{C}_m$ for which this maximum is reached are universal functions of the space charge parameter $\hat{\Lambda}_p^2$. The pre-exponential factor A in the asymptotic expression (2.27) at tuning to the maximal increment (i.e. at $\hat{C} = \hat{C}_m$) is also a universal function of the space charge parameter $\hat{\Lambda}_p^2$. Graphs of these functions are shown in Figs. 2.6– 2.8. It is seen from Fig. 2.8 that preexponential factor A achieves the value of $1/4$ in the asymptotic of a large value of the space charge parameter. As an illustration, in Fig. 2.9 we show the curve describing the dependence of the increment on the detuning for several values of the space charge parameter $\hat{\Lambda}_p^2$.

The analysis of the initial-value problem presented in this section refers to the case when unmodulated electron beam and electromagnetic wave are fed to the FEL amplifier input. In Appendix B we present more general approach to the solution of the initial-value problem for the FEL amplifier with a "cold" electron beam.

2.3.2. *Lorentzian energy spread*

Let us consider the case of an electron beam whose energy distribution function is given by a Lorentzian distribution

$$F(\mathcal{E} - \mathcal{E}_0) = \frac{1}{\pi} \frac{q}{(\mathcal{E} - \mathcal{E}_0)^2 + q^2}.$$

The expression for the reduced distribution function $\hat{F}$ is of the form

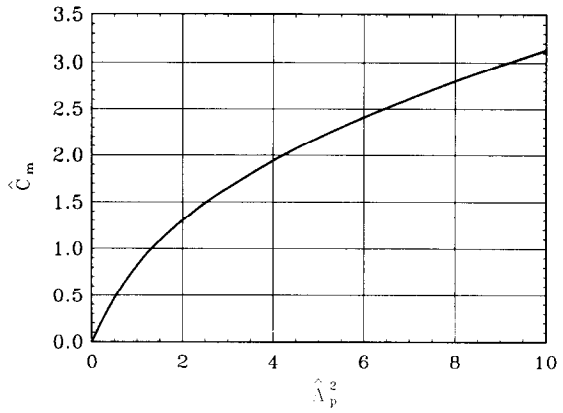

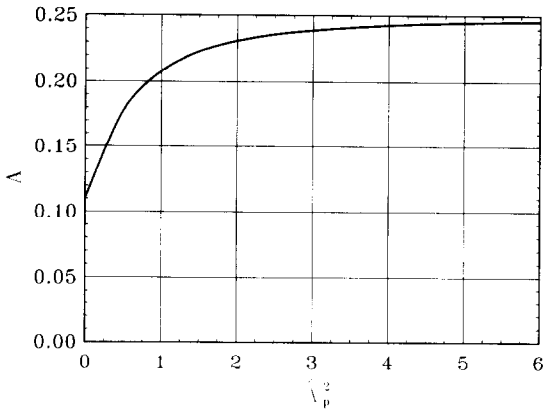

Fig. 2.7. Dependence of the optimal value of the detuning parameter $\hat{C}_m$ on the space charge parameter $\hat{\Lambda}_p^2$. Here $\hat{\Lambda}_T^2 = 0$.

Fig. 2.8. Dependence of the preexponential factor A entering Eq. (2.27) on the space charge parameter $\hat{\Lambda}_p^2$. Here $\hat{C} = \hat{C}_m$ and $\hat{\Lambda}_T^2 = 0$.

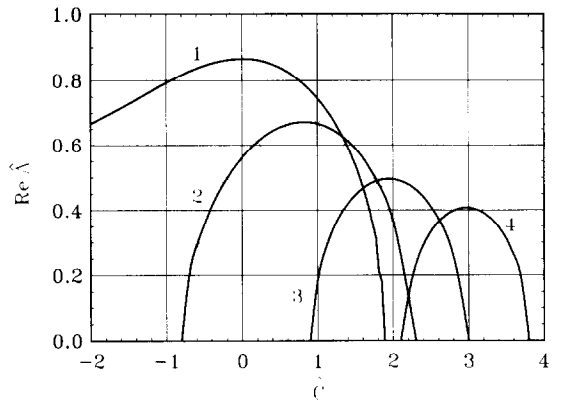

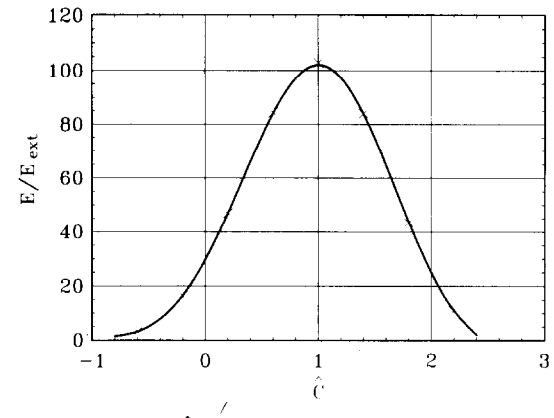

Fig. 2.9. Dependence of the reduced increment $\mathrm{Re}(\hat{\Lambda})$ on the detuning parameter $\hat{C}$ for several values of the space charge parameter $\hat{\Lambda}_p^2$. Curve (1): $\hat{\Lambda}_p^2 = 0$, curve (2): $\hat{\Lambda}_p^2 = 1$, curve (3): $\hat{\Lambda}_p^2 = 4$ and curve (4): $\hat{\Lambda}_p^2 = 9$. Solid curves are calculated with exact solution of the eigenvalue Eq. (2.22) and crosses are results of numerical simulations with Eqs. (3.6) and (3.16). Here $\hat{\Lambda}_T^2 = 0$.

Fig. 2.10. Dependence of the field gain E/E_{ext} on the detuning parameter $\hat{C}$. Solid curve is calculated with analytical formula (2.37) and crosses are results of numerical simulations with Eqs. (3.6) and (3.16). Here the reduced length of the undulator is $\hat{z}_f = 8.5$, $\hat{\Lambda}_p^2 = 1$ and $\hat{\Lambda}_T^2 = 0.1$.

$$\hat{F}(\hat{P}) = \frac{1}{\pi}\frac{\hat{q}}{\hat{P}^2 + \hat{q}^2}.$$

The relation between the parameters q and $\hat{q}$ is given by

$$\hat{q} = \omega q/(\gamma_z^2 c\mathcal{E}_0\Gamma).$$

Substituting Lorentzian distribution into Eq. (2.19), we find that the function $\hat{D}$ in the entire complex λ plane is given by

$$\hat{D} = i\left(\lambda + \hat{q} + i\hat{C}\right)^{-2}.$$

The coefficient of $\exp(\lambda\hat{z})$ in the integrand in Eq. (2.18) in this case is equal to

$$\frac{1}{\lambda - \dfrac{\hat{D}}{1 - i\hat{\Lambda}_p^2\hat{D}}} = \frac{1}{\lambda - \dfrac{i}{\left(\lambda + \hat{q} + i\hat{C}\right)^2 + \hat{\Lambda}_p^2}}$$

and obviously satisfies the conditions of Jordan's lemma. Therefore, Eq. (2.20) is applicable:

$$\tilde{E}(z) = E_{\text{ext}} \sum_j \frac{\exp(\lambda_j \hat{z})}{1 - 2i(\lambda + \hat{q} + i\hat{C})\lambda_j^2},$$

where λ_j are the roots of the cubic equation

$$\lambda = i[(\lambda + \hat{q} + i\hat{C})^2 + \hat{\Lambda}_p^2]^{-1}.$$

Therefore, in the case of the Lorentzian energy spread the electromagnetic wave in the undulator can be represented as the sum of three partial waves.

2.3.3. Gaussian energy spread

We conclude the analysis of the initial-value problem by considering the case of a Gaussian energy distribution

$$F(\mathcal{E} - \mathcal{E}_0) = \left(2\pi\langle(\Delta\mathcal{E})^2\rangle\right)^{-1/2} \exp\left(-\frac{(\mathcal{E} - \mathcal{E}_0)^2}{2\langle(\Delta\mathcal{E})^2\rangle}\right). \tag{2.29a}$$

The corresponding distribution in the reduced canonical momentum $\hat{P}$ has the form

$$F(\hat{P}) = (2\pi\hat{\Lambda}_T^2)^{-1/2} \exp(-\hat{P}^2/(2\hat{\Lambda}_T^2)). \tag{2.29b}$$

The energy spread parameter $\hat{\Lambda}_T^2$ is related to the rms energy spread $\langle(\Delta\mathcal{E})^2\rangle$ as

$$\hat{\Lambda}_T^2 = \omega^2\langle(\Delta\mathcal{E})^2\rangle/(\gamma_z^4 c^2 \Gamma^2 \mathcal{E}_0^2). \tag{2.29c}$$

We begin the calculation of the function $\hat{D}$ with the case $\mathrm{Re}(\lambda) > 0$. From Eq. (2.19) we have

$$\hat{D} = \int_{-\infty}^{\infty} d\xi \frac{\hat{F}'(\xi)}{\lambda + i(\xi + \hat{C})} = i\int_{-\infty}^{\infty} d\xi \frac{\hat{F}(\xi)}{\left(\lambda + i(\xi + \hat{C})\right)^2}, \quad \mathrm{Re}(\lambda) > 0. \tag{2.30}$$

Substituting the equation

$$\frac{1}{(\lambda + i(\xi + \hat{C}))^2} = \int_0^{\infty} \tau \exp\left\{-\left[\lambda + i(\xi + \hat{C})\right]\tau\right\} d\tau, \quad \mathrm{Re}(\lambda) > 0$$

into Eq. (2.30) and integrating over ξ, we obtain

$$\hat{D} = i\int_0^{\infty} \tau \exp\left\{-\frac{\hat{\Lambda}_T^2\tau^2}{2} - \left(\lambda + i\hat{C}\right)\tau\right\} d\tau, \quad \mathrm{Re}(\lambda) > 0 \tag{2.31}$$

In the left half-plane, using Eq. (2.19) and the expression

$$\frac{1}{(\lambda+i(\xi+\hat{C}))^2}=\int_0^\infty \tau\exp\{[\lambda+i(\xi+\hat{C})]\tau\}d\tau,\quad \mathrm{Re}(\lambda)<0,$$

the expression for the function $\hat{D}$ can be brought to the form

$$\hat{D}=i\int_0^\infty \tau\exp\left\{-\frac{\hat{\Lambda}_T^2\tau^2}{2}+\left(\lambda+i\hat{C}\right)\tau\right\}d\tau-i\frac{\sqrt{2\pi}}{\hat{\Lambda}_T^3}\left(\lambda+i\hat{C}\right)\exp\left\{\frac{\left(\lambda+i\hat{C}\right)^2}{2\hat{\Lambda}_T^2}\right\},$$
$$\mathrm{Re}(\lambda)<0 \tag{2.32}$$

We note that the expression for $\hat{D}$ in the left half-plane contains a term proportional to $\exp(\lambda^2)$. Therefore, the function $\hat{D}$ has a singularity at infinity. In this case, as follows from the Picard theorem, the integrand in Eq. (2.18)has an infinite number of poles in the left half-plane, which bunch up at infinity and are located near the lines $\arg(\lambda)=\pm 3\pi/4$. According to Jordan's lemma, the calculation of the linear integral (2.18) by closing the integration contour with an infinite semicircle in the left-hand plane is possible if the function $\bar{E}(\lambda)$ tends to zero for $|\lambda|\to\infty$ uniformly in the argument of λ. This condition is not satisfied for the Gaussian distribution function. In this case the Laplace transform method does not lead to an analytic solution of the initial-value problem in a closed form. However, it is important to note that there is often no need of a complete solution to the initial-value problem, since it is sufficient to consider only the case of high gain. Below we show that for the Gaussian distribution function the Laplace transform method can be used to obtain an asymptotic expression for the amplification of a FEL amplifier in a closed form.

We shall use the following mathematical trick. Shifting the integration path in (2.18) to the left half-plane, we use the residue theorem to transform the linear integral to the form

$$\int_{\gamma'-i\infty}^{\gamma'+i\infty} d\lambda\bar{E}(\lambda)\exp(\lambda\hat{z})=\int_{-\alpha'-i\infty}^{-\alpha'+i\infty} d\lambda\bar{E}(\lambda)\exp(\lambda\hat{z})+\sum_{-\alpha'<\mathrm{Re}\,\lambda}\mathrm{Res}\,\bar{E}(\lambda_j)\exp(\lambda_j\hat{z}), \tag{2.33}$$

where the summation runs over the roots of Eq. (2.21) lying to the right of the line $(-\alpha'-i\infty, -\alpha'+i\infty)$. Here α' is a real positive number, and Res $\bar{E}(\lambda_j)$ is the residue of the function $\bar{E}(\lambda)$ at the pole λ_j. Using equations (2.30) and (2.31), it can easily be checked that there is only one root of Eq. (2.21) in the right half-plane, and for any finite value of α' the number of roots in the interval $-\alpha'<\mathrm{Re}(\lambda)<0$ is always finite. If the undulator is sufficiently long, the contribution to Eq. (2.33) from the term proportional to $\exp(\lambda_s\hat{z})$ with $\mathrm{Re}(\lambda_s)>0$ will be greater than all the others, and the contribution of the latter can be neglected. Then for the amplitude $\tilde{E}(z)$ we can write down an asymptotic expression of the form

$$\tilde{E}(z)=E_{\mathrm{ext}}\frac{\exp(\hat{\Lambda}\hat{z})}{1-\dfrac{\hat{D}'}{(1-i\hat{\Lambda}_p^2\hat{D})^2}}, \tag{2.34}$$

where $\hat{\Lambda}$ is the growing root of Eq. (2.21) and the values of $\hat{D}$ and $\hat{D}'$ at $\lambda = \hat{\Lambda}$ can be found from Eq. (2.31). The next step is to write down expression (2.34) in the form convenient for numerical calculations.

We express the function $\hat{D}'(\lambda)$ in terms of the function $\hat{D}(\lambda)$. From integral tables we find the expression for $\mathrm{Re}(\lambda) > 0$

$$\hat{D} = i\int_0^\infty \tau \exp\left\{-\frac{\hat{\Lambda}_T^2\tau^2}{2} - \left(\lambda + i\hat{C}\right)\tau\right\} d\tau$$

$$= \frac{i}{\hat{\Lambda}_T^2} - \frac{i\sqrt{\pi/2}}{\hat{\Lambda}_T^3}\left(\lambda + i\hat{C}\right)\exp\left[\frac{\left(\lambda + i\hat{C}\right)^2}{2\hat{\Lambda}_T^2}\right]\left[1 - \mathrm{erf}\left(\frac{\lambda + i\hat{C}}{\sqrt{2}\hat{\Lambda}_T}\right)\right],$$

$$\hat{D}' = -i\int_0^\infty \tau^2 \exp\left\{-\frac{\hat{\Lambda}_T^2\tau^2}{2} - \left(\lambda + i\hat{C}\right)\tau\right\} d\tau$$

$$= \frac{i\left(\lambda + i\hat{C}\right)}{\hat{\Lambda}_T^4} - \frac{i\sqrt{2\pi}}{2\hat{\Lambda}_T^5}\left[(\lambda + i\hat{C})^2 + \hat{\Lambda}_T^2\right]\exp\left[\frac{\left(\lambda + i\hat{C}\right)^2}{2\hat{\Lambda}_T^2}\right]\left[1 - \mathrm{erf}\left(\frac{\lambda + i\hat{C}}{\sqrt{2}\hat{\Lambda}_T}\right)\right],$$

Here $\mathrm{erf}(\zeta)$ denotes the error function of complex argument:

$$\mathrm{erf}(\zeta) = 2\pi^{-1/2}\int_0^\zeta \exp(-u^2)\,du.$$

In the end we obtain

$$\hat{D}'(\lambda) = \frac{i\left(\lambda + i\hat{C}\right)}{\hat{\Lambda}_T^4} + \frac{\left(\lambda + i\hat{C}\right)^2 + \hat{\Lambda}_T^2}{\hat{\Lambda}_T^2\left(\lambda + i\hat{C}\right)}\left(\hat{D} - \frac{i}{\hat{\Lambda}_T^2}\right) \tag{2.35}$$

Using Eq. (2.21), the value of function $\hat{D}$ for $\lambda = \hat{\Lambda}$ can be expressed in terms of the root $\hat{\Lambda}$

$$\hat{D}(\hat{\Lambda}) = \hat{\Lambda}[1 + i\hat{\Lambda}_p^2\hat{\Lambda}]^{-1}. \tag{2.36}$$

Using Eqs. (2.34) - (2.36), we easily obtain an asymptotic expression for the gain in a form convenient for numerical calculations:

$$\tilde{E}(z) = E_{\mathrm{ext}}\exp(\hat{\Lambda}\hat{z})$$
$$\times\left\{1 + i\left(i - \hat{\Lambda}_p^2\hat{\Lambda}\right)^2\left[\left(\frac{\hat{\Lambda}}{i - \hat{\Lambda}_p^2\hat{\Lambda}} - \frac{1}{\hat{\Lambda}_T^2}\right)\left(\frac{1}{\hat{\Lambda} + i\hat{C}} + \frac{\hat{\Lambda} + i\hat{C}}{\hat{\Lambda}_T^2}\right) + \frac{\hat{\Lambda} + i\hat{C}}{\hat{\Lambda}_T^4}\right]\right\}^{-1}, \tag{2.37}$$

A particularly simple expression is obtained when the space charge effect is absent. In the limit $\hat{\Lambda}_p^2 \to 0$, form Eq. (2.37) we have

$$\tilde{E}(z) = \frac{\hat{\Lambda}_T^2[\hat{\Lambda} + i\hat{C}]}{i[\hat{C}\hat{\Lambda}_T^2 + 1] - \hat{\Lambda}[\hat{\Lambda} + i\hat{C}]^2}E_{\mathrm{ext}}\exp(\hat{\Lambda}\hat{z}), \tag{2.38}$$

where $\hat{\Lambda}$ is the growing root of the eigenvalue equation

$$\hat{\Lambda} = i \int_0^\infty \exp[-\hat{\Lambda}_T^2 \tau^2/2 - (\hat{\Lambda} + i\hat{C})\tau]\tau d\tau, \quad \mathrm{Re}(\hat{\Lambda}) > 0 \tag{2.39}$$

Let us illustrate the obtained results with calculations of the FEL amplifier characteristics. At a sufficiently long undulator, the power gain G can be written as

$$G = |\tilde{E}|^2/E_{\mathrm{ext}}^2 = A \exp[2\,\mathrm{Re}(\hat{\Lambda})\hat{z}],$$

where in the general case A and $\hat{\Lambda}$ are functions of the detuning $\hat{C}$, space charge parameter $\hat{\Lambda}_p^2$ and energy spread parameter $\hat{\Lambda}_T^2$. In Fig. 2.10 we show the dependence of the field amplitude gain on detuning $\hat{C}$ when there is a strong influence of the space charge field and energy spread ($\hat{z} = 8.5$, $\hat{\Lambda}_p^2 = 1$, $\hat{\Lambda}_T^2 = 0.1$, maximal field gain is equal to 40 dB). Calculations have been performed using asymptotic formula (2.37).

For the parameter region where the space charge effect can be neglected ($\hat{\Lambda}_p^2 \to 0$), the increment can be found by solving the eigenvalue equation (2.39). For a small energy spread, when $\hat{\Lambda}_T^2 \ll 1$, the maximal increment is attained for the detuning $\hat{C}_m \simeq 3\hat{\Lambda}_T^2$ and is equal to

$$\max(\mathrm{Re}(\hat{\Lambda})) \simeq \frac{\sqrt{3}}{2}(1 - \hat{\Lambda}_T^2).$$

In the opposite case, when $\hat{\Lambda}_T^2 \gg 1$, the energy spread significantly affects the increment, the maximum of which is attained at $\hat{C}_m \simeq \hat{\Lambda}_T$ and is equal to

$$\max(\mathrm{Re}(\hat{\Lambda})) \simeq \frac{0.76}{\hat{\Lambda}_T^2}.$$

The preexponential factor (see formula (2.27)) is close to the unity, $A \simeq 1$.

When the energy spread parameter $\hat{\Lambda}_T^2$ is of the order of unity, the increment can be found by solving the eigenvalue equation (2.39). It follows from this equation that the value of maximal increment and the value of the detuning parameter $\hat{C}_m$ at which it is achieved are universal functions of the energy spread parameter $\hat{\Lambda}_T^2$. The pre-exponential factor A at the value of $\hat{C} = \hat{C}_m$ is also universal function of $\hat{\Lambda}_T^2$. Graphs oh these functions are given in Figs. 2.11–2.13. For illustration, in Fig. 2.14 we show the curve describing the dependence of the increment on the detuning for several values of the energy spread parameter $\hat{\Lambda}_T^2$.

It is interesting to compare asymptotic analytical results with the results of numerical solution of integro-differential equation (2.14). This equation has been integrated with Runge Kutta method and in Fig. 2.13 we present the results of these calculations. It is seen that in the high gain limit analytical formulae provide sufficiently high accuracy.

2.4. Linear theory of the FEL amplifier with a planar undulator

We have considered above the operation of the FEL amplifier with the helical undulator. In the helical undulator the electrons move along helical trajectories and longitudinal component of the electron velocity is constant. Another popular undulator configuration is a planar one. Constrained

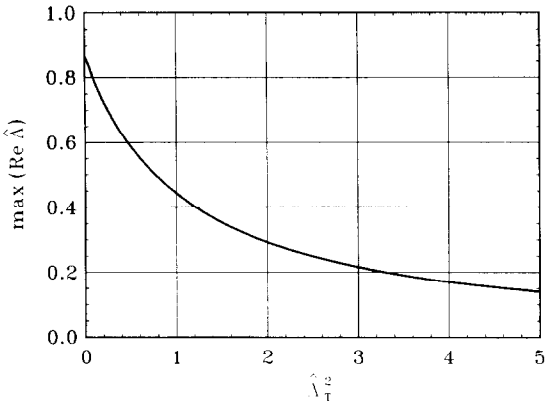

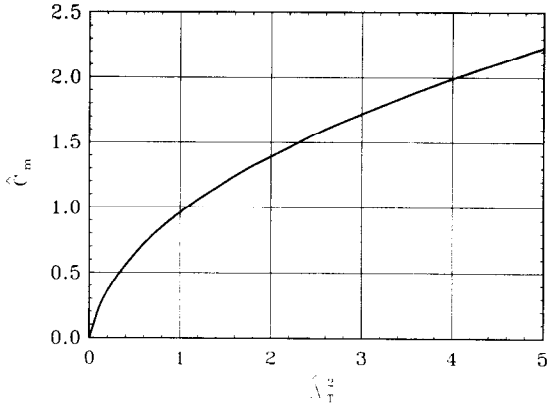

Fig. 2.11. Dependence of the maximal reduced increment $\max \mathrm{Re}(\hat{\Lambda})$ on the energy spread parameter $\hat{\Lambda}_T^2$. Here $\hat{\Lambda}_p^2 = 0$.

Fig. 2.12. Dependence of the optimal value of the detuning parameter $\hat{C}_m$ on the energy spread parameter $\hat{\Lambda}_T^2$. Here $\hat{\Lambda}_p^2 = 0$.

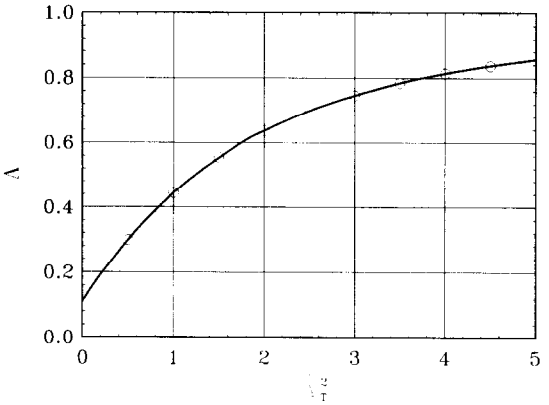

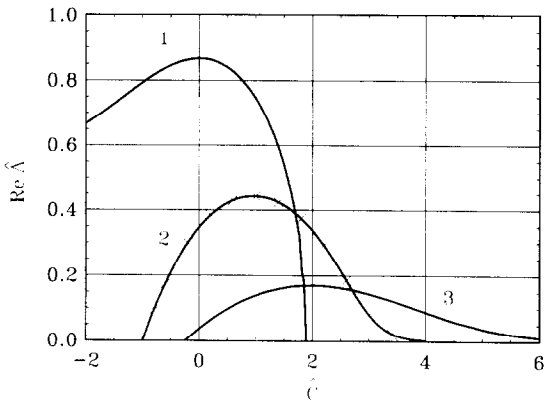

Fig. 2.13. Dependence of the preexponential factor A entering Eq. (2.27) on the energy spread parameter $\hat{\Lambda}_T^2$. Here $\hat{C} = \hat{C}_m$ and $\hat{\Lambda}_p^2 = 0$. Solid curve is calculated with analytical formula (2.37) and circles with the numerical solution of Eq. (2.14).

Fig. 2.14. Dependence of the reduced increment $\mathrm{Re}(\hat{\Lambda})$ on the detuning parameter $\hat{C}$ for several values of the energy spread parameter $\hat{\Lambda}_T^2$. Curve (1): $\hat{\Lambda}_T^2 = 0$, curve (2): $\hat{\Lambda}_T^2 = 1$ and curve (3): $\hat{\Lambda}_T^2 = 4$. Solid curves are calculated with exact solution of the eigenvalue Eq. (2.39) and crosses are results of numerical simulations with Eqs. (3.5) and (3.6). Here $\hat{\Lambda}_p^2 = 0$.

motion of the electron in the planar undulator differs from that in the helical one. The main peculiar feature of this motion is that longitudinal velocity of the electron v_z oscillates along the undulator axis. This results in some novel features of the FEL amplifier. For instance, there is a possibility to amplify electromagnetic wave with a frequency multiple to the main resonance frequency [16–18].

Theoretical problems of the FEL amplifier with the planar undulator have been studied by many authors [19–24]. The early studies have been performed without taking into account the space charge field. For the first time this problem has been studied in Refs. [21]. Not all the aspects of the problem have been considered correctly in this paper and finally they have been resolved in papers [23,24].

2.4.1. Self-consistent field equation

Magnetic field of the planar undulator is of the form:

$$\boldsymbol{H}_l(z) = \boldsymbol{e}_x H_l \cos(\kappa_w z),$$

where $\boldsymbol{e}_x$ is the unit vector directed along the x axis of the Cartesian coordinate system (x, y, z). We assume the electron to move along identical sinusoidal trajectories parallel to the z axis:

$$\boldsymbol{v}_y(z) = -\boldsymbol{e}_y c\theta_l \sin(\kappa_w z).$$

The oscillation amplitude of the transverse velocity of electrons is considered as a small value and the longitudinal velocity of electrons v_z is close to the velocity of light ($v_z \simeq c$).

In the FEL amplifier with the planar undulator only a linearly polarized plane electromagnetic wave may be amplified. In the frame of the one-dimensional model, the electric field vector of amplified wave may be represented as

$$\boldsymbol{E} = \boldsymbol{e}_y \tilde{E}_y(z) \exp[i\omega(z/c - t)] + \text{c.c.}$$

where ω is the frequency of the amplified wave. It is assumed that the field complex amplitude of the amplified wave $\tilde{E}_y$ is the slowly changing function of the coordinate z in the sense that $|\partial \tilde{E}_y/\partial z| \ll \kappa_w |\tilde{E}_y|$.

The Hamiltonian of the particle is given with the expression (2.1). In the same way as it has been done above, we choose the coordinate z as a new time and the phase

$$\psi = \kappa_w z + \omega(z/c - t)$$

as new generalized coordinate. The form of the Hamiltonian of new variables coincides with that of expression (2.3). In the first order of $\boldsymbol{A}_\perp$ and at small deviations of the electron energy $\mathcal{E}$ from nominal energy $\mathcal{E}_0$, the Hamiltonian takes the form

$$H(P, \psi, z) = \left[C + \frac{\omega\theta_l^2}{4c}\cos(2\kappa_w z)\right] P + \frac{\omega}{2c\gamma_l^2 \mathcal{E}_0} P^2 - [U e^{i\psi} + U^* e^{-i\psi}] + \int d\psi e E_z, \qquad (2.40)$$

where $P = \mathcal{E} - \mathcal{E}_0$, $C = \kappa_w - \omega/(2c\gamma_l^2)$ is the average detuning of the electron with the energy $\mathcal{E} = \mathcal{E}_0$ from the resonance (we assume here that $C \ll \kappa_w$),

$$U = -[1 - \exp(-2i\kappa_w z)] e\theta_l \tilde{E}_y(z)/2$$

is the complex amplitude of the effective potential of interaction,

$$\theta_l = eH_l/(\mathcal{E}_0 \kappa_w), \quad \gamma_l^{-2} = \gamma^{-2} + \theta_l^2/2, \quad \gamma = \mathcal{E}_0/(m_e c^2).$$

The evolution of the distribution function $f(P, \psi, z)$ is governed by the kinetic equation (2.6). We linearize variables in the following way

$$f = f_0 + \tilde{f}_1 e^{i\psi} + \tilde{f}_1^* e^{-i\psi}, \quad E_z = \tilde{E}_z e^{i\psi} + \tilde{E}_z^* e^{-i\psi}.$$

We consider the case when the beam is modulated neither in velocity nor in density at the entrance into the undulator, i.e.

$$\tilde{f}_1|_{z=0} = 0, \quad f_0|_{z=0} = n_0 F(P), \quad \int F(P) dP = 1. \qquad (2.41)$$

In the frame of the one-dimensional model, from the Maxwell's equation, E_z satisfies to the Eq. (2.7) which leads to relation $\tilde{E}_z = -i4\pi\tilde{j}_1(z)/\omega$. Complex amplitudes $\tilde{j}_1(z)$ and $\tilde{f}_1(P,z)$ are connected by the relation $\tilde{j}_1 \simeq -ec\int \tilde{f}_1 dP$.

According to Eqs. (2.6) and (2.40), the evolution of complex amplitude $\tilde{f}_1$ is described with

$$\frac{\partial}{\partial z}\tilde{f}_1 + i\left[C + \frac{\omega\theta_l^2}{4c}\cos(2\kappa_w z) + \frac{\omega}{c\gamma_l^2\mathcal{E}_0}P\right]\tilde{f}_1 + i[U + 4\pi e\tilde{j}_1(z)/\omega]\frac{\partial}{\partial P}f_0 = 0. \tag{2.42}$$

The solution of Eq. (2.42) has the form

$$\begin{aligned}\tilde{j}_1(z) = ij_0\int_0^z dz'\{&-[1-\exp(-2i\kappa_w z')]e\theta_l\tilde{E}_y(z')/2 + 4\pi e\tilde{j}_1(z')/\omega\}\\ &\times\int dP(dF(P)/dP)\exp\{i[C+\omega P/(c\gamma_l^2\mathcal{E}_0)](z'-z)\\ &+ i\nu[\sin(2\kappa_w z') - \sin(2\kappa_w z)]\},\end{aligned} \tag{2.43}$$

where $j_0 \simeq ecn_0$ and $\nu = \theta_l^2\omega/(8c\kappa_w)$.

One more relation connecting complex amplitudes $\tilde{j}_1(z)$ and $\tilde{E}_y(z)$ follows from the wave equation

$$\partial^2\boldsymbol{A}/\partial z^2 - c^{-2}\partial^2\boldsymbol{A}/\partial t^2 = -(4\pi/c)\boldsymbol{j}_\perp,$$

where $\boldsymbol{j}_\perp$ is the density of the transverse current

$$\boldsymbol{j}_\perp = -\boldsymbol{e}_y\theta_l\sin(\kappa_w z)(\tilde{j}_1 e^{i\psi} + \text{c.c.}).$$

It follows from relation $cE_y = -\partial A_y/\partial t$ that

$$\frac{d}{dz}\tilde{E}_y = -i\pi\theta_l c^{-1}[\exp(2i\kappa_w z) - 1]\tilde{j}_1(z). \tag{2.44}$$

It is convenient for the further consideration to rewrite the expression for amplitude $\tilde{j}_1(z)$ in the form

$$\tilde{j}_1(z) = \tilde{j}_a(z)\exp[-i\nu\sin(2\kappa_w z)]. \tag{2.45}$$

Using expression (2.45) and expansion

$$\exp[i\nu\sin(2\kappa_w z)] = \sum_{n=-\infty}^{n=+\infty} J_n(\nu)\exp(2in\kappa_w z),$$

we rewrite Eqs. (2.43) and (2.44) as follows

$$\begin{aligned}\tilde{j}_a(z) = ij_0\int_0^z dz'\Bigg\{&-\frac{e\theta_l}{2}\tilde{E}_y(z')\sum_{n=-\infty}^{n=+\infty}J_n(\nu)\{\exp[2in\kappa_w z'] - \exp[2i(n-1)\kappa_w z]\}\\ &+\frac{4\pi e}{\omega}\tilde{j}_a(z')\Bigg\}\end{aligned}$$

$$\times \int_{-\infty}^{\infty} dP\,(dF(P)/dP)\exp[i(\omega P/(c\gamma_l^2\mathcal{E}_0)+C)(z'-z)], \tag{2.46}$$

$$\frac{d}{dz}\tilde{E}_y = -i\pi\theta_l c^{-1}\tilde{j}_a(z)\sum_{n=-\infty}^{n=+\infty}(-1)^n J_n(\nu)\{\exp[2i(n+1)\kappa_w z] - \exp[2in\kappa_w z]\}. \tag{2.47}$$

2.4.2. Analytic treatment of the FEL amplifier with the planar undulator

The system of two coupled equations (2.46) and (2.47) can be solved with Laplace transformation techniques. The Laplace transforms of Eqs. (2.46) and (2.47) have the form:

$$\bar{j}_a(p) = \frac{ij_0\omega D(p)}{\gamma_l^2 c\mathcal{E}_0}\left\{-\frac{e\theta_l}{2}\sum_{n=-\infty}^{n=+\infty}J_n(\nu)[\bar{E}(p-2in\kappa_w)-\bar{E}(p-2i(n-1)\kappa_w)] + \frac{4\pi e}{\omega}\bar{j}_a(p)\right\}, \tag{2.48}$$

$$p\bar{E}(p) - E_{\text{ext}} = -\frac{i\pi\theta_l}{c}\sum_{n=-\infty}^{n=+\infty}(-1)^n J_n(\nu) \times [\bar{j}_a(p-2i(n+1)\kappa_w) - \bar{j}_a(p-2in\kappa_w)], \tag{2.49}$$

where notations are introduced ($\mathrm{Re}(p) > 0$): $E_{\text{ext}} = \tilde{E}_y(0)$,

$$\bar{j}_a(p) = \int_0^{\infty} dz e^{-pz}\tilde{j}_a(z), \quad \bar{E}(p) = \int_0^{\infty} dz e^{-pz}\tilde{E}_y(z),$$

$$D(p) = \int_{-\infty}^{\infty} d\xi\,(dF(\xi)/d\xi)[p+i\xi+iC]^{-1}.$$

If Eq. (2.48) is solved, we get the formula

$$\bar{j}_a(p) = -\frac{i\theta_l j_0\omega}{2\gamma_l^2\gamma I_A}\frac{D(p)}{1-i\Lambda_p^2 D(p)}\sum_{n=-\infty}^{n=+\infty}J_n(\nu)[\bar{E}(p-2in\kappa_w)-\bar{E}(p-2i(n-1)\kappa_w)],$$

where $\Lambda_p^2 = 4\pi j_0/(I_A\gamma_l^2\gamma)$ and $I_A = m_e c^3/e \simeq 17$ kA. Substituting the expression for $\bar{j}_a(p)$ into Eq. (2.49) we have

$$p\bar{E}(p) - E_{\text{ext}} = -\frac{\pi\theta_l^2 j_0\omega}{2c\gamma_l^2\gamma I_A}\sum_{n=-\infty}^{n=+\infty}(-1)^n J_n(\nu) \times\left\{\frac{D(p-2i(n+1)\kappa_w)}{1-i\Lambda_p^2 D(p-2i(n+1)\kappa_w)} \times\sum_{m=-\infty}^{m=+\infty}J_m(\nu)[\bar{E}(p-2i(m+n+1)\kappa_w)-\bar{E}(p-2i(m+n)\kappa_w)]\right.$$

$$- \frac{D(p-2in\kappa_w)}{1-i\Lambda_p^2 D(p-2in\kappa_w)}$$

$$\times \sum_{k=-\infty}^{k=+\infty} J_k(\nu)\left[\bar{E}(p-2i(k+n)\kappa_w) - \bar{E}(p-2i(k+n-1)\kappa_w)\right] \Bigg\}. \tag{2.50}$$

The inverse Laplace transform is defined with the integral

$$\tilde{E}_y(z) = \frac{1}{2\pi i}\int_{\gamma'-i\infty}^{\gamma'+i\infty} d\lambda \bar{E}(\lambda) e^{\lambda z}. \tag{2.51}$$

The constant γ' is a real positive number which is greater than real parts of all the singularities of function $\bar{E}(\lambda)$. As it is difficult to analyze Eq. (2.50) in the general form, it seems interesting to consider the important case of the high gain limit. In this case the expression for the wave field (2.51) reduces to the single residue of the integrand taken in the pole located at the point with the most positive real part

$$\tilde{E}_y(z) = \operatorname{Res} \bar{E}(\Lambda)\exp(\Lambda z), \quad \operatorname{Re}(\Lambda) > 0. \tag{2.52}$$

We consider the energy spread in the beam to be a Gaussian with the distribution function (2.29a) and the function $D(\lambda)$ given by the expression

$$D(\lambda) = i\int_0^\infty \exp[-\Lambda_T^2\tau^2/2 - (\lambda + iC)\tau]\tau d\tau, \quad \operatorname{Re}\lambda > 0 \tag{2.53}$$

where $\Lambda_T^2 = \omega^2\langle(\Delta\mathcal{E})^2\rangle/(c^2\gamma_l^4\mathcal{E}_0^2)$ is the energy spread parameter.

Within the scope of accepted limitations the typical scale of length (where the amplitude and the phase of the wave change significantly) is much more than the undulator period, i.e.

$$|\Lambda|,\ \Lambda_p,\ \Lambda_T,\ |C| \ll \kappa_w. \tag{2.54}$$

Using formula (2.53) and relation (2.54) it is easy to show that at $|n| > 0$ the following inequality takes place

$$|D(\Lambda)| \gg |D(\Lambda - 2in\kappa_w)| \propto (2n\kappa_w)^{-2}.$$

Therefore, in the right-hand part of Eq. (2.50) when $\lambda \to \Lambda$ all terms of $D(\lambda - 2in\kappa_w)$ type may be neglected with respect to term $D(\lambda)$. Besides, as Λ is the pole of function $\bar{E}(\lambda)$, all terms of $\bar{E}(\lambda - 2in\kappa_w)$ type, except of $\bar{E}(\lambda)$, may be omitted in the right-hand part of Eq. (2.50) at $\lambda \to \Lambda$. As a result, it follows from Eq. (2.50) that near the pole $\lambda \simeq \Lambda$ integrand in Eq. (2.51) takes the form

$$\bar{E}(\lambda) \simeq E_{\text{ext}}\left[\lambda - \frac{D(\lambda)\Gamma^3}{1-i\Lambda_p^2 D(\lambda)}\right]^{-1}, \tag{2.55}$$

where

$$\Gamma = \left[\frac{\pi\theta_l^2 j_0\omega}{2c\gamma_l^2\gamma I_A}\right]^{1/3}[J_0(\nu) - J_1(\nu)]^{2/3}.$$

Thus, according to expression (2.55), the eigenvalue equation of the FEL amplifier with the planar undulator is reduced to

$$\hat{\Lambda} - \frac{\hat{D}}{1 - i\hat{\Lambda}_p^2\hat{D}} = 0, \tag{2.56}$$

where $\hat{\Lambda} = \Lambda/\Gamma$, $\hat{\Lambda}_p^2 = \Lambda_p^2/\Gamma^2$, $\hat{\Lambda}_T^2 = \Lambda_T^2/\Gamma^2$, $\hat{C} = C/\Gamma$,

$$\hat{D} = i\int_0^\infty \exp[-\hat{\Lambda}_T^2\tau^2/2 - (\hat{\Lambda} + i\hat{C})\tau]\tau d\tau.$$

If $\hat{\Lambda}_T^2 \to 0$, then $\hat{D} \to i(\hat{\Lambda} + i\hat{C})^{-2}$ and the eigenvalue equation (2.56) may be rewritten as

$$[(\hat{\Lambda} + i\hat{C})^2 + \hat{\Lambda}_p^2]\hat{\Lambda} = i. \tag{2.57}$$

Let us derive now the asymptotic formula for the gain. Using Eqs. (2.52) and (2.55), the asymptotic expression for the amplitude of field $\tilde{E}_y(z)$ may be written as

$$\tilde{E}_y = E_{\text{ext}}\exp(\hat{\Lambda}\hat{z})\left\{1 - \frac{\hat{D}'}{(1 - i\hat{\Lambda}_p^2\hat{D})^2}\right\}^{-1}, \tag{2.58}$$

where $\hat{z} = \Gamma z$ and $\hat{D}' = d\hat{D}/d\hat{\Lambda}$.

It is evident from Eqs. (2.20), (2.21), (2.31), (2.53) and (2.56)–(2.58) that in all the cases the eigenvalue equations and asymptotic formula for the gain of the FEL amplifier with the planar undulator written down in the reduced form fully agrees with the corresponding reduced relations for the FEL amplifier with the helical undulator (see Section 2.3).

3. Saturation effects in the FEL amplifier

In Section 2 we have studied the linear mode of the FEL amplifier operation when an increase of the input power W_{ext} leads to proportional increase of the output power W_f. When input power is increased further, the operation of the amplifier becomes to be nonlinear: output power increases more slowly than input one, and at a certain value of W_{ext} the output power reaches a maximum. To find the FEL characteristics at saturation, it is necessary to solve the equations of the nonlinear theory of the FEL amplifier. Analytical methods are of limited usefulness in the study of the nonlinear regime, and numerical simulations must be used. The first numerical simulations of the nonlinear mode of the FEL amplifier operation have been carried out in Ref. [25], and they were developed further in the later studies of Refs. [26,27].

The similarity techniques are known to play a dominant role in numerical simulation of processes observed in the FEL. Within the scope of the one-dimensional approximation the output characteristics of the amplifier are controlled by 8 dimensional parameters of both beam and undulator

$$l_w,\ \kappa_w,\ \omega,\ \mathcal{E}_0,\ j_0,\ H_w,\ \langle(\Delta\mathcal{E})^2\rangle,\ E_{\text{ext}},$$

where l_w, κ_w and H_w are, respectively, the length, the wavenumber and the magnetic field of the undulator; ω and E_{ext} are, respectively, the input signal frequency and amplitude; $\mathcal{E}_0$, j_0 and $<$

$(\Delta\mathcal{E})^2 >$ are, respectively, the energy, the density of the beam current and the energy spread in the electron beam.

The system of self-consistent field equations describing a phenomenon of the beam-wave interaction in the undulator may be formulated as a relation between dimensionless quantities. The equations show that a family of the similar modes of operation of the FEL amplifier is controlled by the values of 5 dimensionless parameters

$$\Gamma l_w,\ \hat{C},\ \hat{\Lambda}_p^2,\ \hat{\Lambda}_T^2,\ E_{\text{ext}}/E_0,$$

where Γ is the gain parameter, $\hat{C}$ is the detuning parameter, $\hat{\Lambda}_p^2$ is the space charge parameter, $\hat{\Lambda}_T^2$ is the energy spread parameter and E_{ext}/E_0 is reduced value of the input signal (here E_0 is new normalization factor appearing in the nonlinear theory). Therefore, in the general case we can write for the value of the output signal E_f

$$E_f/E_0 = \mathcal{D}(\Gamma l_w, \hat{C}, \hat{\Lambda}_p^2, \hat{\Lambda}_T^2, E_{\text{ext}}/E_0).$$

In a high-gain mode (i.e. at $E_{\text{ext}}/E_0 \ll 1$) and when the dimensionless undulator length is rather large, the field output amplitude in a saturation mode is independent of both undulator length and input signal amplitude. In this practically prominent case the maximal amplifier efficiency is a function of only 3 dimensionless parameters: detuning $\hat{C}$, space charge $\hat{\Lambda}_p^2$ and energy spread $\hat{\Lambda}_T^2$.

In the general case the universal function $\mathcal{D}$ should be calculated numerically solving the reduced self-consistent field equations.

The authors of Ref. [28] were the first to write the working equations in the reduced form. Detailed study of application of similarity techniques in the FEL amplifier theory has been presented in Refs. [14,23,24].

3.1. Self-consistent equations

The equation describing the change of the particle energy $\mathcal{E}$ as a function of the coordinate z along the undulator axis can be obtained from the Hamiltonian $\tilde{\mathcal{H}}$ written in the variables $\mathcal{E}$ and canonically conjugate phase $\psi = \kappa_w z + \omega(z/c - t)$. In the first order in the expansion in the vector potential of the wave $A_\perp$ and neglecting the space charge field, the Hamiltonian (2.4) can be written as

$$\omega\tilde{\mathcal{H}}(\mathcal{E}, \psi, z) = H = \int^{\mathcal{E}} [\kappa_w - \omega(v_z^{-1}(\mathcal{E}) - c^{-1})]\, d\mathcal{E} - u\sin(\psi + \psi_0), \tag{3.1}$$

where $v_z(\mathcal{E})$ is the longitudinal component of the electron velocity, u and ψ_0 are, respectively, the amplitude and phase of the effective potential which are connected with the complex amplitude of the electric field $\tilde{E}$ by the relation $(u > 0)$

$$(u/2)\exp(i\psi_0) = -e^2 H_w \tilde{E}/(2\mathcal{E}\kappa_w) = -e\theta_s\tilde{E}/2 = iU.$$

The equations of motion corresponding to the Hamiltonian (3.1) are as follows:

$$\begin{aligned} d\mathcal{E}/dz &= -\partial H/\partial\psi = u\cos(\psi + \psi_0), \\ d\psi/dz &= \partial H/\partial\mathcal{E} = \kappa_w - \omega(v_z^{-1} - c^{-1}) - \partial u/\partial\mathcal{E}\sin(\psi + \psi_0). \end{aligned} \tag{3.2}$$

From Eq. (2.13) we find that the amplitude and phase of the effective potential are governed by the equations:

$$du/dz = \frac{\pi e^3 H_w^2}{c\kappa_w^2 \mathcal{E}^2} j_1 \cos(\psi_0 - \psi_1), \quad d\psi_0/dz = -\frac{\pi e^3 H_w^2}{c\kappa_w^2 \mathcal{E}^2} \frac{j_1}{u} \sin(\psi_0 - \psi_1), \tag{3.3}$$

where j_1 and ψ_1 are, respectively, the amplitude and phase of the first harmonic of the longitudinal component of the beam current density j_z

$$j_1 \cos\psi_1 = \frac{1}{\pi} \int_0^{2\pi} j_z \cos\psi d\psi, \quad j_1 \sin\psi_1 = -\frac{1}{\pi} \int_0^{2\pi} j_z \sin\psi d\psi,$$

Eqs. (3.2) and (3.3) form a system of self-consistent equations for the FEL amplifier in the one-dimensional approximation.

For small deviations of the energy from the initial value, the Hamiltonian (3.1) takes the form

$$H = CP + \omega P^2/(2\gamma_z^2 \mathcal{E}_0 c) - u\sin(\psi + \psi_0), \tag{3.4}$$

where $P = \mathcal{E} - \mathcal{E}_0$ and C is the detuning from the resonance for a particle of nominal energy $\mathcal{E}_0$

$$C = \kappa_w + \omega/c - \omega/v_z(\mathcal{E}_0) \simeq \kappa_w - \omega/(2c\gamma_z^2).$$

It is convenient to perform the normalization procedure replacing physical variables z, P, u, C and j_1 by $\hat{z} = \Gamma z$, $\hat{P} = \omega P/(c\gamma_z^2 \mathcal{E}_0 \Gamma)$, $\hat{u} = \omega u/(c\gamma_z^2 \mathcal{E}_0 \Gamma^2)$, $\hat{C} = C/\Gamma$ and $\hat{j}_1 = j_1/j_0$. As a result, eqs. (3.2) and (3.3) can be written as

$$d\hat{P}/d\hat{z} = \hat{u}\cos(\psi + \psi_0), \quad d\psi/d\hat{z} = \hat{P} + \hat{C} + \beta\hat{u}\sin(\psi + \psi_0), \tag{3.5}$$

$$d\hat{u}/d\hat{z} = \hat{j}_1 \cos(\psi_0 - \psi_1), \quad d\psi_0/d\hat{z} = -(\hat{j}_1/\hat{u})\sin(\psi_0 - \psi_1), \tag{3.6}$$

where $\beta = c\gamma_z^2 \Gamma/\omega$. The efficiency parameter β is inversly proportional to the number of the undulator periods per the gain length $1/\Gamma$ and is always small. We perform the study of the nonlinear regime of the FEL amplifier with untapered undulator neglecting the term proportional to β in the second equation of the system (3.5). Applicability region of such an approximation may be estimated on the base of the obtained solutions. Simulations show that the maximal value of the reduced amplitude of the field $\hat{u}_{\max}$ is of the order of unity, so the neglected term is always much less than unity.

3.2. Numerical simulation algorithm

We simulate the electron beam with N macroparticles per interval $(0, 2\pi)$ over phase ψ. The beam current density $\hat{j}_z = j_z/j_0$ is periodical in phase ψ and is calculated as

$$\hat{j}_z = -\frac{2\pi}{N} \sum_{j=1}^{N} \delta(\psi - \psi_{(j)}) \tag{3.7}$$

where $\psi_{(j)}$ are phases of the particles and $\delta(\psi - \psi_{(j)})$ is the delta function. It follows from Eq. (3.7) that $\hat{j}_z$ has the following normalization

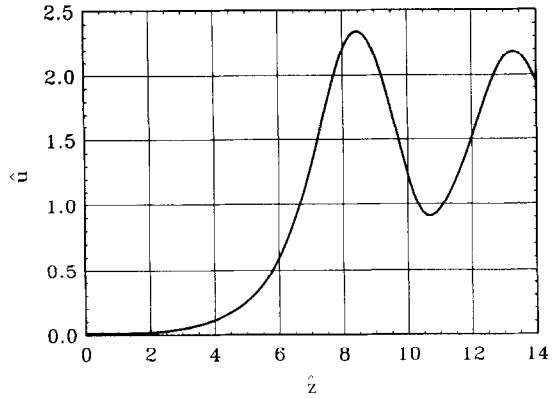

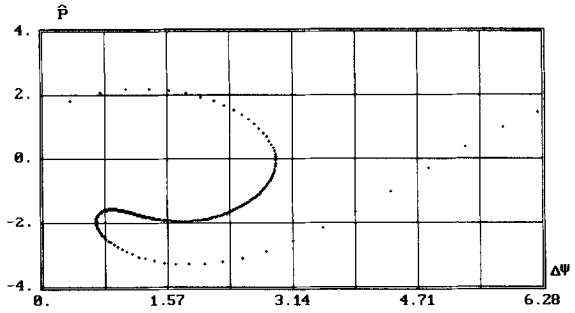

Fig. 3.1. Dependence of the reduced field amplitude $\hat{u}$ on the reduced undulator length $\hat{z}$. Here $\hat{C} = 0$, $\hat{\Lambda}_p^2 = 0$, $\hat{\Lambda}_T^2 = 0$ and $\hat{u}_{ext} = 0.01$.

Fig. 3.2. Phase space distribution of the particles at the FEL amplifier exit at saturation. Here the reduced undulator length is $\hat{z}_f = 8.4$, $\hat{C} = 0$, $\hat{\Lambda}_p^2 = 0$, $\hat{\Lambda}_T^2 = 0$ and $\hat{u}_{ext} = 0.01$.

$$\int_0^{2\pi} \hat{j}_z \, d\psi = -2\pi.$$

The amplitude $\hat{j}_1$ and phase ψ_1 of the first harmonic of the beam current density are given with the expressions

$$\hat{j}_1 \cos\psi_1 = \frac{1}{\pi}\int_0^{2\pi} \hat{j}_z \cos\psi d\psi = -\frac{2}{N}\sum_{j=1}^{N} \cos\psi_{(j)},$$

$$\hat{j}_1 \sin\psi_1 = -\frac{1}{\pi}\int_0^{2\pi} \hat{j}_z \sin\psi d\psi = \frac{2}{N}\sum_{j=1}^{N} \sin\psi_{(j)}.$$

Equations of motion (3.5) for N particles together with the field equations (3.6) compose the system of $2N + 2$ equations describing the amplification process in the FEL amplifier.

We consider the initial conditions when the electron beam is neither modulated in velocity nor in density and there is electromagnetic wave of amplitude E_{ext} at the undulator entrance at $z = 0$ $(j = 1, \ldots, N)$

$$\hat{P}_{(j)}(0) = 0, \quad \hat{j}_1(0) = 0, \quad \hat{u}(0) = \hat{u}_{ext} = E_{ext}/E_0,$$

where $E_0 = (c\gamma_z^2 \mathcal{E}_0 \Gamma^2)/(e\omega\theta_s)$.

The plot in Fig. 3.1 presents the dependence of the reduced field amplitude $\hat{u}$ on the reduced undulator length $\hat{z}$ at $\hat{C} = 0$ and $\hat{u}_{ext} = 0.01$. The field stops growing in the saturation regime when the beam is overmodulated and a significant fraction of the electrons fall into the accelerating phase of the effective potential. The maximal value of the reduced field amplitude at $\hat{C} = 0$ is

$$\hat{u}_{max} = E_{max}/E_0 = 2.34 \tag{3.8}$$

and in a high gain limit, i.e. at $E_{ext}/E_0 \ll 1$ does not depend on the field amplitude at the amplifier input.

To analyze the dynamics of the particles in the undulator, it is convenient to study their distribution on the phase plane $(\hat{P}, \Delta\psi)$, where $\Delta\psi = \psi + \psi_0$. Fig. 3.2 presents such a distribution when FEL amplifier operates in a saturation mode (it corresponds to the point $\hat{z} = 8.4$ of the plot in Fig. 3.1)

3.3. Energy conservation law

In the framework of the one-dimensional model and in the high gain limit the efficiency of the FEL amplifier is usually defined as the ratio of the output radiation power flux to the flux density of the electron beam power. The average power flux transported by the electromagnetic wave is given by

$$\Pi = cE^2/(4\pi).$$

Therefore, the efficiency of the amplifier in the limit of $G \gg 1$ is given by

$$\eta = e\Pi/(\mathcal{E}_0 j_0) = \beta\hat{u}^2/4. \tag{3.9}$$

It is convenient to normalize the value of physical efficiency by the efficiency parameter β and introduce the notion of the reduced efficiency

$$\hat{\eta} = \eta/\beta = \hat{u}^2/4.$$

The electromagnetic power radiated by the electron beam must be equal to the electron beam energy losses, i.e. $\Pi = -\langle P\rangle j_0/e$, where $\langle P\rangle$ is the mean energy losses in the beam. Therefore, using the power conservation law, we can define the amplifier efficiency as the ratio of the average energy losses $\langle P\rangle$ to the nominal energy $\mathcal{E}_0$: $\eta = -\langle P\rangle/\mathcal{E}_0$. Now we go over to the reduced energy losses $\langle\hat{P}\rangle$. Then the expression for the efficiency takes the form $\hat{\eta} = \eta/\beta = -\langle\hat{P}\rangle$. In the macroparticle model we have

$$\langle d\hat{P}/d\hat{z}\rangle = \hat{u}N^{-1}\sum_{j=1}^{N}\cos(\psi_{(j)} + \psi_0).$$

Here we have used the first canonical equation of motion (3.5). The sum in the latter expression can be expressed in the terms of the amplitude and phase of the first harmonic of the beam density:

$$N^{-1}\sum_{j=1}^{N}\cos(\psi_{(j)} + \psi_0) = -\tfrac{1}{2}\hat{j}_1\cos(\psi_1 - \psi_0).$$

Using the first equation of the system (3.6), we obtain

$$\langle d\hat{P}/d\hat{z}\rangle = -\tfrac{1}{2}\hat{u}d\hat{u}/d\hat{z}.$$

From this it follows that

$$\hat{\eta} = -\langle\hat{P}\rangle = \hat{u}^2/4.$$

Comparison of the obtained result with the expression (3.9) shows that the power conservation law takes place.

In the special case of tuning to the exact resonance ($\hat{C} = 0$), from relations (3.8) and (3.9) we obtain the value of the reduced efficiency

$$\hat{\eta}_{max} = 1.37. \tag{3.10}$$

3.4. Saturation in the high-gain FEL amplifier

When the FEL amplifier is tuned to the exact resonance, $\hat{C} = 0$, and when the reduced length of the amplifier $\hat{z} > 4$, the power gain at saturation can be calculated with the simple formula

$$G_{max} = \tfrac{1}{38} \exp(\sqrt{3}\hat{z}), \tag{3.11}$$

or, in decibels,

$$G_{max}(\mathrm{dB}) = 10 \lg G_{max} = 7.5\hat{z} - 15.8.$$

The field amplitude at the amplifier input E_{ext} at which the saturation regime is reached can be found from the expression

$$E_{ext}/E_0 = \hat{u}_{ext} = 2.34/\sqrt{G_{max}}, \tag{3.12}$$

with the value of G given by Eq. (3.11). These simple formulae provide an accuracy about of several per cent with respect to the results of the numerical simulations.

It should be noted that the graph presented in Fig. 3.1 enables one to calculate the growth of the field amplitude for any amplifier tuned to the exact resonance $\hat{C} = 0$ and having the reduced length $\hat{z} > 4$. It is seen from this plot and relations (3.11) and (3.12) that saturation point of the amplifier $\hat{z}_{max}$ is given by the relation:

$$\hat{z}_{max} = 3.1 + \frac{2}{\sqrt{3}} \ln(\hat{u}_{ext}^{-1}). \tag{3.13}$$

The field amplitude at the point $\hat{z} = \hat{z}_{max} - \Delta\hat{z}$ is equal to the field amplitude corresponding to that at $\hat{z} = 8.4 - \Delta\hat{z}$ presented by the plot in Fig. 3.1. When $\Delta\hat{z} > 4$, the linear approximation becomes applicable, and the field amplitude E can be found using expression (2.25) where E_{ext} should be calculate using expressions (3.11) and (3.12).

An important characteristic of the FEL amplifier is the amplification bandwidth at the saturation. Let us consider a specific example. Let the reduced length of the amplifier be $\hat{z} = 7.4$. Then, according to Eqs. (3.11) and (3.12), exactly on resonance the saturation regime is reached for the input amplitude $\hat{u}_{ext} = 2.34 \times 10^{-2}$ and the gain is $G = 40$ dB. The dependence of the gain on the detuning of such an amplifier is presented in Fig. 3.3. In this case the amplification bandwidth is equal to $\Delta\hat{C} = 1.54$. The graph in Fig. 3.4 can be used to find $\Delta\hat{C}$ for an amplifier operating in the saturation regime for $\hat{C} = 0$ and having a different value of the gain G (i.e. a different reduced length).

In the general case, for any value of the detuning parameter $\hat{C} < 1.89$, there exists a value of the input amplitude $\hat{u}_{ext}$ for which the output amplitude reaches a maximum. The maximal efficiency of the amplifier $\hat{\eta}_{max}$ is a universal function of the detuning parameter $\hat{C}$. A graph of this function is shown in Fig. 3.5. We see that the maximal efficiency is a growing function of the detuning parameter. This phenomenon is a simple consequence of the fact that when the detuning parameter is increased, the electrons interact with the wave for a longer distance.

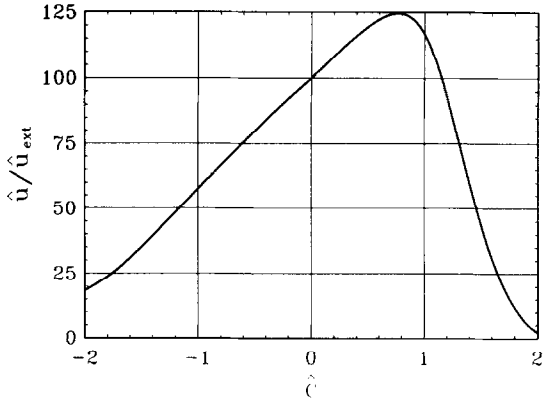

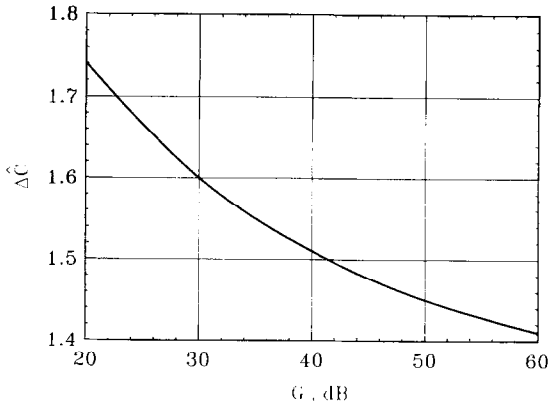

Fig. 3.3. Dependence of the field gain $\hat{u}/\hat{u}_{ext}$ on the detuning parameter $\hat{C}$. At exact resonance, $\hat{C} = 0$, the FEL amplifier operates at saturation regime. Here the reduced undulator length is $\hat{z}_f = 7.4$, $\hat{\Lambda}_p^2 = 0$, $\hat{\Lambda}_T^2 = 0$ and $\hat{u}_{ext} = 0.0234$.

Fig. 3.4. The dependence of the amplification bandwidth $\Delta\hat{C}$ on the maximum power gain. At exact resonance, $\hat{C} = 0$, the FEL amplifier operates at saturation regime. Here $\hat{\Lambda}_p^2 = 0$ and $\hat{\Lambda}_T^2 = 0$.

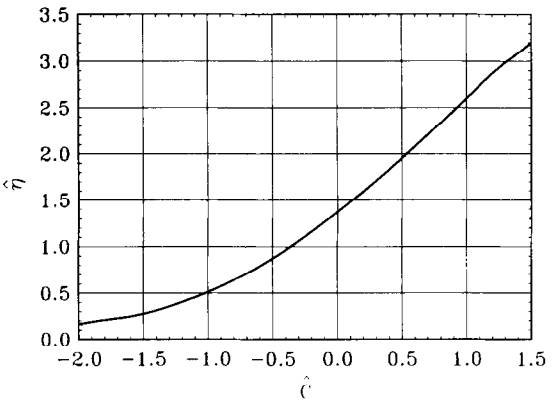

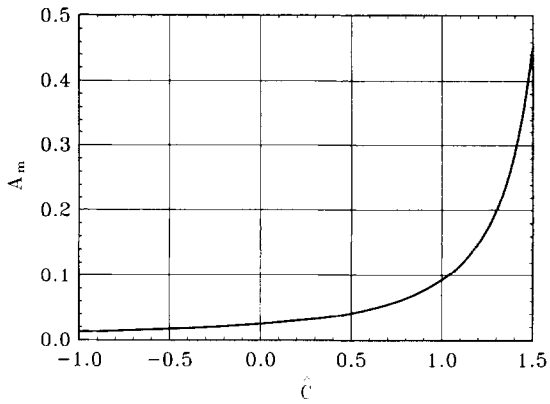

Fig. 3.5. Dependence of the maximal reduced efficiency $\hat{\eta}_{max}$ of the FEL amplifier on the detuning parameter $\hat{C}$. Here $\hat{\Lambda}_p^2 = 0$ and $\hat{\Lambda}_T^2 = 0$.

Fig. 3.6. Dependence of the preexponential factor A entering Eq. (3.14) on the detuning parameter $\hat{C}$.

The power gain in the saturation regime is also a universal function of the detuning $\hat{C}$

$$G_{max} = A_m(\hat{C}) \exp[2\,\mathrm{Re}(\hat{\Lambda})\hat{z}]. \tag{3.14}$$

A graph of the function $A_m(\hat{C})$ is shown in Fig. 3.6. The values of the reduced increment can be found with the help of the plot in Fig. 2.2. The amplitude of the input signal at which the saturation regime is reached can be determined using the graphs in Figs. 2.2, 3.5 and 3.6 and the expression

$$\hat{u}_{ext} = 2(\hat{\eta}_{max}/G_{max})^{1/2}.$$

Another important characteristic of the amplifier is amplitude characteristic describing the dependence of the output signal on input one. The dependence of $\hat{u}$ on $\hat{u}_{ext}$ for an amplifier operating in the saturation regime for $\hat{C} = 0$ is shown in Fig. 3.7. It should be noted that in the high gain limit

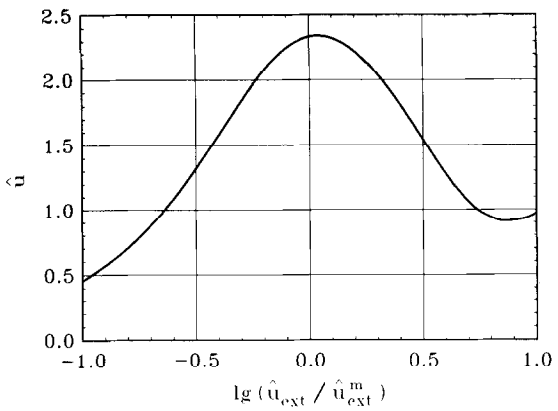

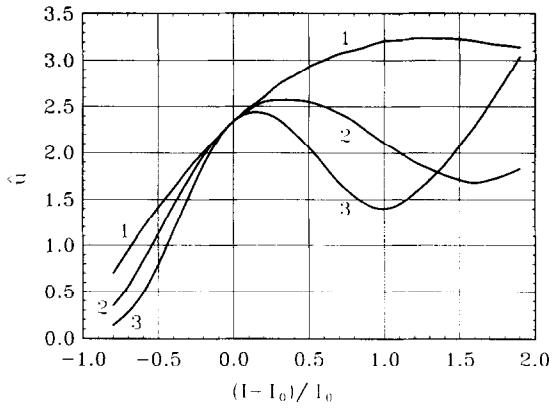

Fig. 3.7. Dependence of the output field amplitude $\hat{u}$ on the input field amplitude $\hat{u}_{ext}$. At $\hat{u}_{ext} = \hat{u}^{m}_{ext}$ the FEL amplifier operates at saturation regime. Here $\hat{C} = 0$, $\hat{\Lambda}_p^2 = 0$ and $\hat{\Lambda}_T^2 = 0$.

Fig. 3.8. Dependence of the field amplitude at the amplifier exit on the beam current for different values of the gain G. At $I = I_0$ amplifier operates in the saturation regime and reduced parameters are calculated at $I = I_0$. Curve (1): $G = 20$ dB, curve (2): $G = 40$ dB and curve (3): $G = 60$ dB. Here $\hat{C} = 0$, $\hat{\Lambda}_p^2 = 0$ and $\hat{\Lambda}_T^2 = 0$.

the amplitude characteristic of the amplifier is independent of the gain value.

The admissible deviations of the beam current from a nominal value can be determined using Fig. 3.8, where we give the graphs of the dependence of the field amplitude at the amplifier output on the beam current for different values of the gain G.

As a rule, the number of macroparticles for numerical simulations has been chosen to be $N = 100, \ldots, 200$. In this case the results of simulations are independent of the actual value of N to within the error of 0.1%. The simulation code has been tested by means of simulation of the linear mode of operation. In Fig. 2.1 we compare results of the calculations of the linear stage of the FEL amplifier operation obtained with the analytical formulae and with the numerical simulation algorithm. In Fig. 2.2 we compare the values of the increment obtained by numerical simulations with the values of the increment obtained by solving the eigenvalue equation (2.26). In Fig. 2.5 we compare the amplitude-frequency characteristics obtained by numerical simulations and by analytic solution of the initial-value problem using eq. (2.23). We see that there is good agreement between the numerical and analytical results. For $N = 200$ macroparticles the discrepancy is less than 0.1%.

3.5. *Space charge effects*

To carry out a comprehensive numerical simulations of the processes occurring in the FEL amplifiers, the equation of motion (3.5) must be supplemented by the corresponding term determining the action of the space charge field. In the framework of the one-dimensional model there is a possibility to present one visual method of calculation the space charge field which is equivalent to the use of Green's function method (not expanded in a Fourier series) [24].

In the nonlinear regime the beam current j_z is a periodical function of phase ψ and may be expanded in a Fourier series:

$$j_z = \sum_1^\infty \tilde{j}_n(z)\exp(in\psi) + \text{c.c.}$$

In the framework of the one-dimensional approximation we get from Maxwell equation

$$E_z = 4\pi\omega^{-1}\sum_1^\infty n^{-1} j_n(z)\sin(n\psi + \psi_n), \tag{3.15}$$

where j_n and ψ_n are given with the expression

$$j_n \begin{Bmatrix}\cos(\psi_n)\\ \sin(\psi_n)\end{Bmatrix} = \frac{1}{\pi}\int_0^{2\pi} j_z \begin{Bmatrix}\cos(n\psi)\\ -\sin(n\psi)\end{Bmatrix} d\psi.$$

When performing simulations, we represent the electron beam with N layers per interval $(0, 2\pi)$ of phase ψ. Then the beam current j_z may be presented in the form

$$j_z = -\frac{2\pi}{N} j_0 \sum_{j=1}^N \delta(\psi - \psi_{(j)}),$$

where $\delta(\psi - \psi_{(j)})$ is the delta function and $\psi_{(j)}$ is the phase of the j th layer. The amplitude j_n and phase ψ_n of the beam current Fourier harmonic are given with the following expression

$$j_n \begin{Bmatrix}\cos(\psi_n)\\ \sin(\psi_n)\end{Bmatrix} = \frac{2}{N} j_0 \sum_{j=1}^N \begin{Bmatrix}-\cos(n\psi_j)\\ \sin(n\psi_j)\end{Bmatrix}.$$

Substituting this expression into Eq. (3.15) for E_z and using formula

$$\sum_1^\infty n^{-1}\sin(n\xi) = (\pi - \xi)/2, \quad (0 < \xi < 2\pi),$$

we get the expression for the field acting on the ith layer:

$$E_z^{(i)} = -\frac{4\pi j_0}{N\omega}\sum_{j\neq i}[\pi\,\mathrm{sgn}(\psi_{(i)} - \psi_{(j)}) - (\psi_{(i)} - \psi_{(j)})],$$

where

$$\mathrm{sgn}(\psi_{(i)} - \psi_{(j)}) = 1, \quad \text{at } (\psi_{(i)} - \psi_{(j)}) > 0,$$
$$\mathrm{sgn}(\psi_{(i)} - \psi_{(j)}) = -1, \quad \text{at } (\psi_{(i)} - \psi_{(j)}) < 0.$$

Using the expression for the Hamiltonian (2.5), we find that the inclusion of the space charge field in this case is reduced to the addition of the term $-eE_z(\psi, z)$ to the right-hand side of Eq.(3.5). Finally, the equations of motion of the ith layer can be written in the following reduced form

$$\frac{d\hat{P}_{(i)}}{d\hat{z}} = \hat{u}\cos(\psi_{(i)} + \psi_0) + \hat{\Lambda}_p^2\left\{\frac{1}{N}\sum_{j\neq i}[\pi\,\mathrm{sgn}(\psi_{(i)} - \psi_{(j)}) - (\psi_{(i)} - \psi_{(j)})]\right\},$$

$$\frac{d\psi_{(i)}}{d\hat{z}} = \hat{P}_{(i)} + \hat{C}. \tag{3.16}$$

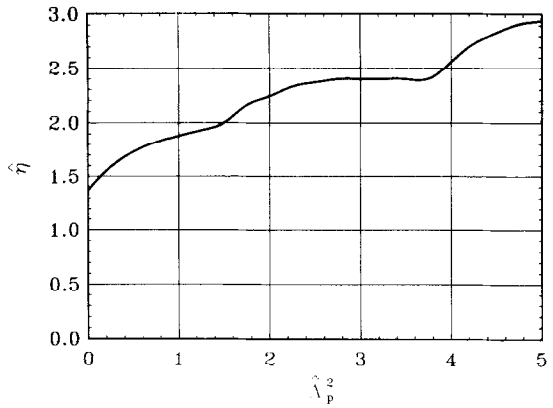

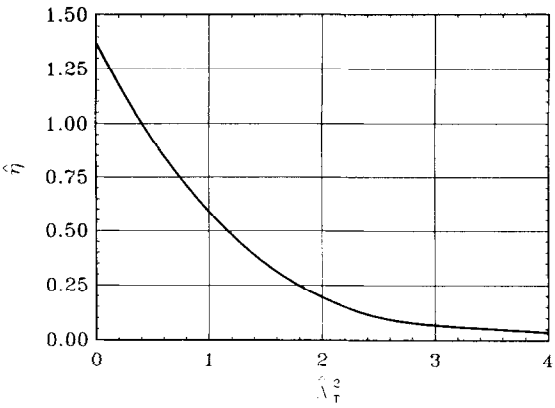

Fig. 3.9. Dependence of the maximal reduced efficiency $\hat{\eta}_{max}$ of the FEL amplifier on the space charge parameter $\hat{\Lambda}_p^2$. Here $\hat{\Lambda}_T^2 = 0$ and the value of the detuning parameter $\hat{C} = \hat{C}_m(\hat{\Lambda}_p^2)$ corresponds to the maximum gain in the linear mode of operation (see Fig. 2.7).

Fig. 3.10. Dependence of the maximal reduced efficiency $\hat{\eta}_{max}$ of the FEL amplifier on the energy spread parameter $\hat{\Lambda}_T^2$. Here $\hat{\Lambda}_p^2 = 0$ and the value of the detuning parameter $\hat{C} = \hat{C}_m(\hat{\Lambda}_T^2)$ corresponds to the maximum gain in the linear mode of operation (see Fig. 2.12).

When the space charge field is taken into account, the maximal efficiency of the amplifier in the high gain limit is a universal function of two parameters, the detuning parameter $\hat{C}$ and the space charge parameter $\hat{\Lambda}_p^2$. In the special case when the amplifier is tuned to the maximal increment in the linear mode of operation, the amplifier efficiency in the saturation regime is a universal function of the only space charge parameter $\hat{\Lambda}_p^2$. This dependence is shown in Fig. 3.9. We see from this figure that the maximal efficiency of the amplifier is a growing function of the space charge parameter. This is the consequence of the fact that the space charge fields prevent the beam overmodulation near the saturation point, so, the interaction of the modulated electron beam with the wave is prolonged. It should be noted, however, that the undulator length is increased in this case, too.

Numerical code has been tested using the results of linear theory. Fig. 2.8 presents comparative results of simulations and analytical calculations. At the number of macroparticles $N = 200$ the both results coincides with an accuracy better than 0.1%.

3.6. *Energy spread effects*

When the beam has a Gaussian energy spread, the maximal efficiency of the amplifier in the high gain limit is a universal function of three parameters, the detuning $\hat{C}$, the space charge parameter $\hat{\Lambda}_p^2$ and the energy spread parameter $\hat{\Lambda}_T^2$. In the special case when the space charge field can be neglected, at $\hat{\Lambda}_p^2 \to 0$, and when the amplifier is tuned to the maximum of increment in the linear mode of operation, the amplifier efficiency is a universal function of the only energy spread parameter $\hat{\Lambda}_T^2$. A graph of this function is presented in Fig. 3.10. From this plot we see that the energy spread leads to a sharp drop in the amplifier efficiency.

The energy spread of the beam has been included in the simulation algorithm by dividing all the macroparticles in the phase interval $0 \leq \psi \leq 2\pi$ for $\hat{z} = 0$ into a small even number N_ψ of groups. The macroparticles in each group have identical phases ψ for $\hat{z} = 0$. The initial values of the

reduced momentums $\hat{P}_{(i)}$ of the particles in each group ($i = 1, \ldots, N_p$) are described by a Gaussian distribution with the rms deviation $\langle(\Delta\hat{P})^2\rangle = \hat{\Lambda}_T^2$. The phases of the groups of particles for $\hat{z} = 0$ were distributed in the interval from 0 to 2π in such a way that the amplitude of the first harmonic of the macroparticle density was equal to zero. It should be noted that at a small number of groups N_ψ such a technique provides good results only in the case of the absence of the space charge field. In the opposite case, the presence of the even harmonics of density in the initial distribution may lead to a significant inaccuracy of simulations. To avoid this problem, we have used the following trick. After preparing the initial ensemble as it has been described above, we introduce a fictitious "drift space" of a length $\hat{l}_p$ to let the particles to distribute more homogeneously in the phase ψ. It results in a strong suppression of the parasitic harmonics of density while the energy distribution remains to be a Gaussian. Optimal value of the length of such a drift space is given with the expression:

$$\hat{l}_p = \frac{0.18}{\hat{\Lambda}_T}\frac{N_p}{N_\psi}.$$

The use of such a technique for preparation of the initial macroparticle ensemble enables one to simulate rather well an unmodulated electron beam at the number of divisions $N_\psi = 4$ and $N_p = 100$.

The simulation code has been tested at the linear stage. Figs. 2.9 and 2.12 present comparative results obtained by means of numerical simulations (the crosses) and analytical results (solid curves calculated with Eqs. (2.37) and (2.38)). The number of groups in the phase ψ was equal to $N_\psi = 4$ and the number of particles in each group was equal to $N_p = 200$. It is seen from these plots that there is good agreement between the numerical and analytical results.

4. FEL amplifier with a tapered undulator

The operation of the FEL amplifier is based on the prolonged (resonance) interaction of the electron beam with the electromagnetic wave in the undulator. Amplification process may be divided into two stages, linear and nonlinear. At the linear stage of amplification, exponential growth of the electromagnetic field amplitude and of the beam modulation amplitude takes place. Nevertheless, the beam modulation in the linear regime is much less than unity, so the most fraction of the radiation power is produced at the nonlinear stage of operation, when the beam modulation becomes to be of about unity. In the case of untapered undulator, the bunched beam effectively interacts with the electromagnetic wave along the length which is of the order of the gain length $l_g \sim \Gamma^{-1}$. At this stage of amplification electrons lose a visual fraction of their energy which results in the violation of the resonance condition. As a result, the beam is overmodulated, the most fraction of electrons fall into the accelerating phase of effective potential and the electron beam becomes to take off the power from the electromagnetic wave. Remembering that the field amplitude at the saturation is of the order of $E_0 = (c\gamma_z^2\mathcal{E}_0\Gamma^2)/(e\omega\theta_s)$, we estimate the saturation efficiency of the FEL amplifier to be of the order of $\eta \sim eE_0\theta_s/\mathcal{E}_0\Gamma = c\gamma_z^2\Gamma/\omega \simeq \Gamma/2\kappa_w$. So, we see that the efficiency of the FEL amplifier with untapered undulator is limited by the value of the efficiency parameter $\beta = \Gamma/2\kappa_w$ which is always much less than unity.

So, the next problem to be solved is that how to prolong interaction of the bunched electron beam with the electromagnetic wave. A reliable method to increase the FEL amplifier efficiency was proposed more than ten years ago in Ref. [29]. It was proposed to increase the FEL efficiency

by an adiabatic change of the undulator parameters (or, in other words, by the use of, so called, undulator tapering). Nevertheless, that paper contained only an idea, because all the calculations has been performed in the approximation of the given radiation field, while the problem requires solution of the self-consistent field equations. Later this idea has been confirmed by the results of numerical simulations with the self-consistent field equations [27,30] and finally has been verified experimentally, an efficiency $\eta \simeq 34\%$ was achieved [2].

For the first time the universal relations for finding optimal characteristics of the undulator tapering and output characteristics of the FEL amplifier with the tapered undulator have been obtained in Ref. [14] by means of application the similarity techniques.

To make our exposure more clear, we study at first the case of a low efficiency approximation, when the FEL amplifier efficiency increases significantly with respect to the case of untapered undulator but still remains much less than unity. Then we study the most complex case of the high efficiency FEL amplifier. All the results are obtained by means of similarity techniques and possess a high degree of generality.

4.1. Low efficiency approximation

4.1.1. Optimization of undulator parameters

According to the system of equations (3.5), the particle motion is determined by the detuning parameter

$$C = \kappa_w - \frac{\omega}{2c\gamma_z^2} = \kappa_w - \frac{\omega(1+K^2)}{2c\gamma^2},$$

which is a function of undulator period $\lambda_w = 2\pi/\kappa_w$ and of the undulator parameter $K = eH_w/(m_e c^2 \kappa_w)$. The change of the undulator parameters causes the detuning parameter to be a function of the coordinate z. In this section we consider one of the possible ways to change the undulator parameters (or, in other words, the way of the undulator tapering), namely that of a change of the undulator period λ_w and the undulator field H_w for constant undulator parameter K = const. It assumes the magnetic field of the undulator to be changed inversely proportional to the undulator period, $H_w \propto \lambda_w^{-1}$.

According to Refs. [14,31], in the case of a helical undulator with bifilar winding, the field at the undulator axis is

$$H_w \propto I_s R^{-1}[(\kappa_w R)^2 K_0(\kappa_w R) + (\kappa_w R) K_1(\kappa_w R)],$$

where I_s and R are, respectively, the current and radius of the winding and K_0 and K_1 are modified Bessel functions. At the constant current in the winding, the undulator parameter K for such an undulator is a universal function of the parameter $\kappa_w R$. Therefore, the undulator tapering in this case is organized in a simple way by shaping the windings radius proportionally to the undulator period, $R \propto \lambda_w$.

In this section we consider the case of a low efficiency approximation, when the FEL amplifier efficiency increases significantly with respect to the case of untapered undulator but still remains much less than unity. Such an approximation is not only of methodological interest but also of practical interest, since the amplifier length grows considerably with increasing efficiency, and under real conditions in many cases it is sufficient to increase the value of the efficiency, for instance, from

$\eta = 1\%$ to $\eta = 10\%$. The condition of the small value of the efficiency η enables one to use for the simulations the system of equations (3.5) and (3.6) which was used in Section 3 for simulations of the amplifier with untapered undulator. The only difference is that the detuning parameter $\hat{C}$ in the second equation of (3.5) becomes to be a given function of coordinate z and is expressed for $K =$ const in terms of the undulator wavenumber κ_w change as $\hat{C} = \hat{C}(0) + \Delta\kappa_w/\Gamma$.

Let us consider the case when the detuning is constant in the initial section and then, beginning at some distance, grows as a quadratic polynomial

$$C(z) = C(0) + \Delta\kappa_w(z) = \alpha_0 + \alpha_1(z - z_i) + \alpha_2(z - z_i)^2,$$

where z_i is the coordinate of the tapering beginning. The detuning parameter $\hat{C}$ in the Eqs. (3.5) can be written in the reduced form as

$$\hat{C} = k_0 + k_1(\hat{z} - \hat{z}_i) + k_2(\hat{z} - \hat{z}_i)^2,$$
$$\hat{z}_i = \Gamma z_i, \quad k_0 = \alpha_0/\Gamma, \quad k_1 = \alpha_1/\Gamma^2, \quad k_2 = \alpha_2/\Gamma^3. \tag{4.1}$$

The choice of the quadratic law of the tapering can be easily understood when analyzing a simple model situation. Let us consider the case of a completely bunched electron beam. It follows from the first equation of (3.6) that the field amplitude is growing proportionally to the undulator length. Then, it follows form the first equation of (3.5) that the change of the particle energy is proportional to the squared length of the undulator. Finally, from the second equation of (3.5) we find, that the resonance condition takes place when the detuning parameter $\hat{C}$ is changed quadratically, too. This qualitative consideration allows one to find an asymptotic behaviour of the detuning $\hat{C}(\hat{z})$.

To find optimal values of the tapering parameters k_0, k_1, k_2 and $\hat{z}_i$, we have performed a set of calculation to maximize the output amplitude at

$$(\hat{z} - \hat{z}_i) \gg 1$$

and obtained the following values:

$$k_0 = 0, \quad k_1 = 1.44, \quad k_2 = 0.36. \tag{4.2}$$

The optimal length of untapered undulator section can be found from the relation:

$$\hat{z}_i = 1.7 + \frac{2}{\sqrt{3}} \ln(\hat{u}_{\text{ext}}^{-1}). \tag{4.3}$$

Comparison of relations (3.13) and (4.3) shows that the undulator tapering must start at distance of $\Delta\hat{z} = 1.4$ before the saturation point of untapered undulator.

Phase analysis shows that at optimal parameters of the tapering (4.2) and (4.3), 65% of the particles are trapped in the regime of coherent deceleration. The trapping factor depends strongly on the value of coefficient k_2. At $k_2 > 0.4$, particles do not trap in the regime of coherent deceleration. At $k_2 < 0.36$, the trapping process is stable and the fraction of the trapped fraction is even increased. However, the equilibrium decelerating phase in this case shifts closer to 90° which results in a more slow increase of the field amplitude than in the case of $k_2 = 0.36$.

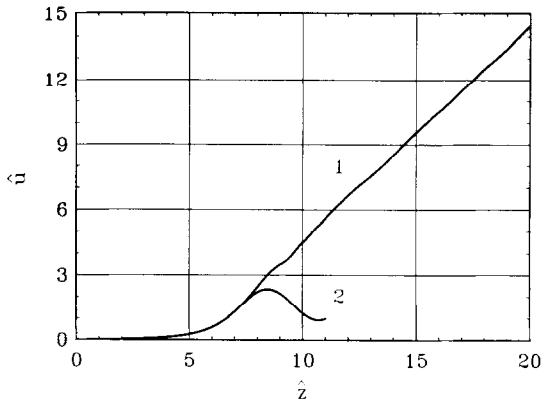

Fig. 4.1. Dependence of the reduced field amplitude $\hat{u}$ on the reduced undulator length $\hat{z}$. Here $\hat{\Lambda}_p^2 = 0$, $\hat{\Lambda}_T^2 = 0$ and $\hat{u}_{ext} = 0.01$. Curve 1 corresponds to the case of the undulator tapering according to the law $\hat{C} = 0$ at $\hat{z} < 7$ and $\hat{C} = 1.44 \times (\hat{z} - 7) + 0.36 \times (\hat{z} - 7)^2$ at $\hat{z} > 7$. Curve 2 corresponds to the case of untapered undulator at $\hat{C} = 0$.

4.1.2. Calculation technique of the optimized FEL amplifier characteristics

In Fig. 4.1 we show a graph of the reduced field amplitude $\hat{u}(\hat{z})$ for the value of the input amplitude $\hat{u}_{ext} = 0.01$. Undulator tapering begins at $\hat{z}_i = 7$ and follows the law

$$\hat{C} = 1.44(\hat{z} - 7) + 0.36(\hat{z} - 7)^2.$$

At the same figure we present the dependence of $\hat{u}(\hat{z})$ on $\hat{z}$ for untapered undulator. Fig. 4.2 presents the phase distributions of the macroparticles at different coordinates of the tapered section.

The plot in Fig. 4.1 can be used to calculate the dependence of the field amplitude on the undulator length for an arbitrary value of input signal $\hat{u}_{ext}$. Indeed, up to the value $\hat{z} = \hat{z}_i$ given by Eq. (4.3), the function $\hat{u}(\hat{z})$ can be calculated using technique described in Section 3.4. Then the point with coordinate $\hat{z}_i$ is put in the correspondence with the point in Fig. 4.1 at $\hat{z} = 7$, and the value of the reduced field amplitude at the point with coordinate $\hat{z} = \hat{z}_i + \Delta\hat{z}$ is equal to the value $\hat{u}(7 + \Delta\hat{z})$ in Fig. 4.1.

In the general case when undulator parameters are tapered according to relations (4.1)–(4.3), the field amplitude at $(\hat{z} - \hat{z}_i) > 3$ can be calculated with the following approximate formula

$$\hat{u}(\hat{z}) \simeq \hat{z} - \frac{2}{\sqrt{3}} \ln(\hat{u}_{ext}^{-1}). \tag{4.4}$$

Here it should be noted once more that this formula is valid in the low efficiency approximation only, i.e. when the output efficiency at the amplifier exit at $\hat{z} = \hat{z}_f$ is small:

$$\eta = [\hat{u}(\hat{z}_f)]^2 \frac{\beta}{4} \ll 1.$$

In Fig. 4.3 we present the plots of the dependence of the output field amplitude on the detuning $\hat{C}$ at different lengths of the undulator. The gain G in the untapered section is equal to $G = 40$ dB. Initial detuning C is equal to

$$C = \kappa_w(0) - \omega(1 + K^2)/2\gamma^2 c,$$

where $\kappa_w(0)$ is the wavenumber of the undulator at its entrance. We see from Fig. 4.3 that the bandwidth of the amplifier with the tapered undulator is close to that of the amplifier with untapered

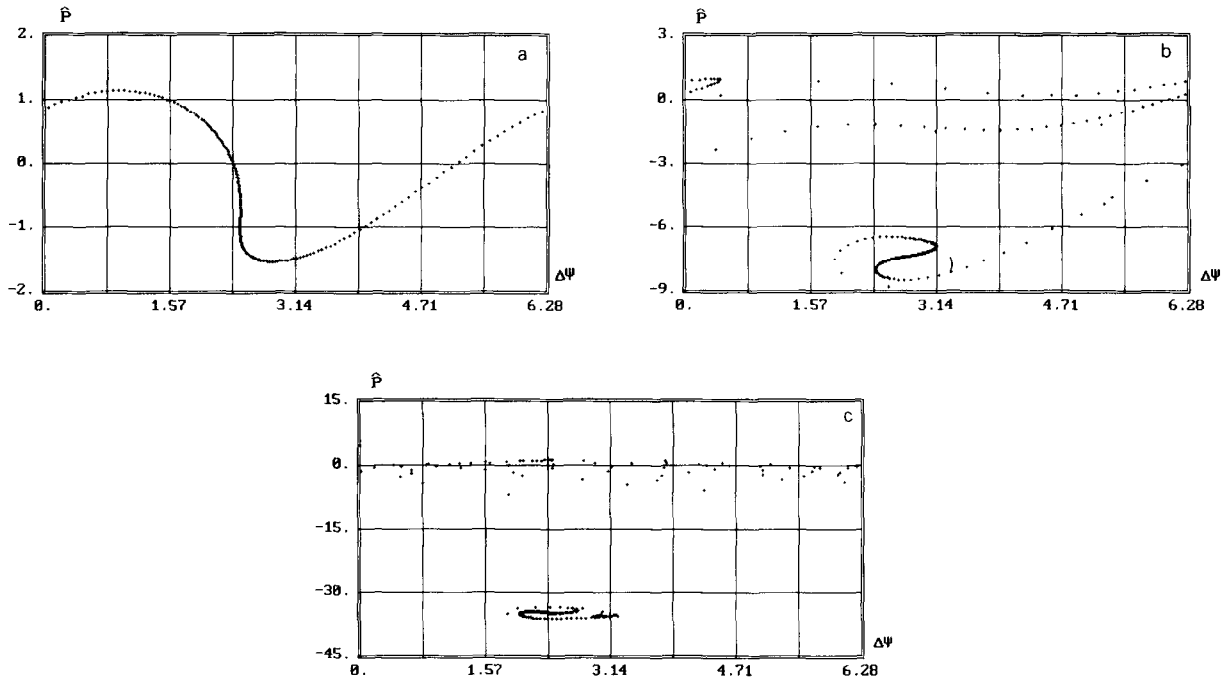

Fig. 4.2. Phase space distribution of the particles in the case of the undulator tapering according to the law $\hat{C} = 0$ at $\hat{z} < 7$ and $\hat{C} = 1.44 \times (\hat{z} - 7) + 0.36 \times (\hat{z} - 7)^2$ at $\hat{z} > 7$. (a): $\hat{z} = 7$, (b): $\hat{z} = 10$ and (c): $\hat{z} = 15$. Here $\hat{\Lambda}_p^2 = 0$, $\hat{\Lambda}_T^2 = 0$ and $\hat{u}_{ext} = 0.01$.

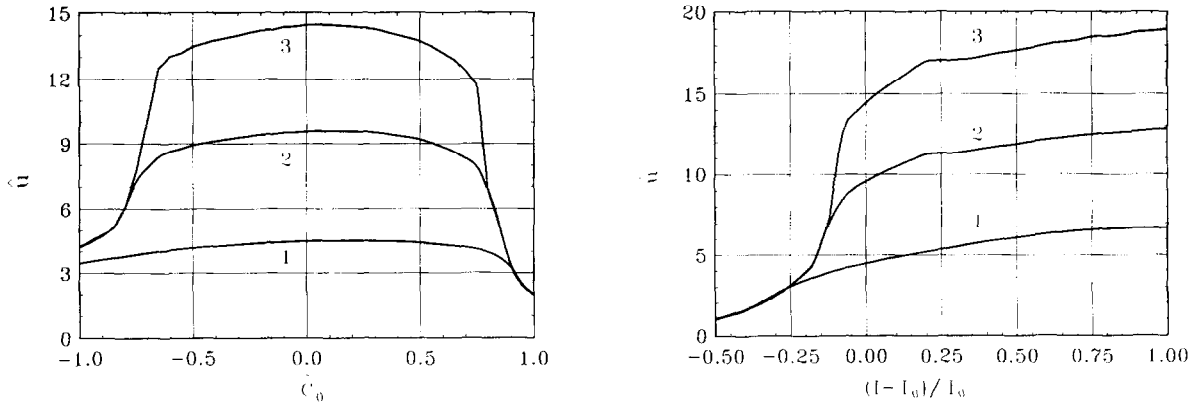

Fig. 4.3. Dependence of the field amplitude at the amplifier exit on the detuning parameter $\hat{C}$ for several values of the length of the tapered section. Here $\hat{\Lambda}_p^2 = 0$, $\hat{\Lambda}_T^2 = 0$ and $\hat{u}_{ext} = 0.01$. The detuning parameter $\hat{C}$ changes according to the law $\hat{C} = \hat{C}_0$ at $\hat{z} < \hat{z}_i$ and $\hat{C} = \hat{C}_0 + 1.44 \times (\hat{z} - \hat{z}_i) + 0.36 \times (\hat{z} - \hat{z}_i)^2$ at $\hat{z} > \hat{z}_i$. The values of the variation beginning $\hat{z}_i$ are given with Eq. (4.3). Curve (1): $\hat{z} - \hat{z}_i = 3$, curve (2): $\hat{z} - \hat{z}_i = 8$ and curve (3): $\hat{z} - \hat{z}_i = 13$.

Fig. 4.4. Dependence of the field amplitude at the amplifier exit on the beam current for different values of the tapered section length. The reduced parameters are calculated at $I = I_0$. Here $\hat{\Lambda}_p^2 = 0$, $\hat{\Lambda}_T^2 = 0$ and $\hat{u}_{ext} = 0.01$. The detuning parameter $\hat{C}$ changes according to Eq. (4.1) with coefficients given with Eqs. (4.2) and (4.3). Curve (1): $\hat{z} - \hat{z}_i = 3$, curve (2): $\hat{z} - \hat{z}_i = 8$ and curve (3): $\hat{z} - \hat{z}_i = 13$.

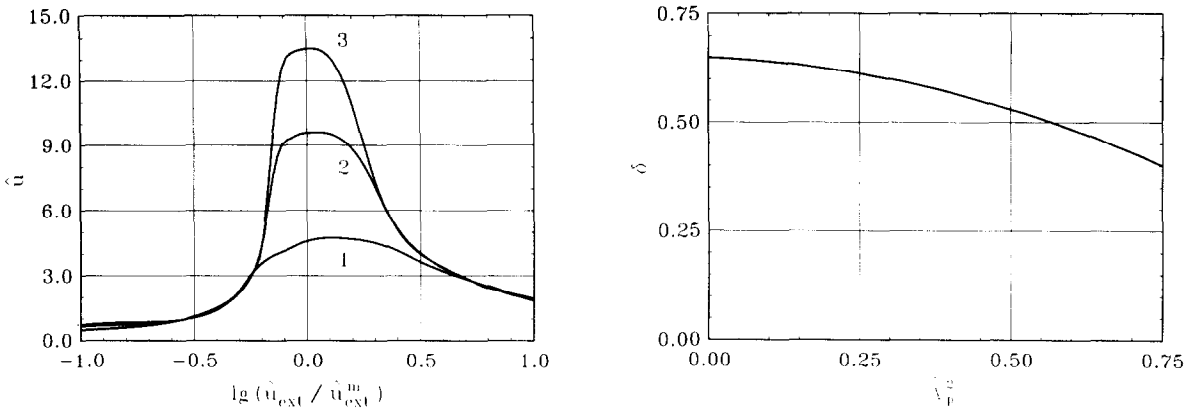

Fig. 4.5. Dependence of the output field amplitude $\hat{u}$ on the input field amplitude $\hat{u}_{ext}$ for different values of the tapered section length. Here $\hat{\Lambda}_p^2 = 0$, $\hat{\Lambda}_T^2 = 0$ and $\hat{u}_{ext} = 0.01$. The detuning parameter $\hat{C}$ changes according to Eq. (4.1) with coefficients given with Eqs. (4.2) and (4.3). The values of the variation beginning $\hat{z}_i$ are calculated with Eq. (4.3) at $\hat{u} = \hat{u}_{ext}^m$. Curve (1): $\hat{z} - \hat{z}_i = 3$, curve (2): $\hat{z} - \hat{z}_i = 8$ and curve (3): $\hat{z} - \hat{z}_i = 13$.

Fig. 4.6. Dependence of the trapping factor on the space charge parameter $\hat{\Lambda}_p^2$. The undulator tapering is performed according to Eq. (4.5). Here $\hat{\Lambda}_T^2 = 0$.

undulator. It means that the requirements on the admissible electron energy deviations remains the same.

Limitations on the deviation of the beam current from a nominal value can be obtained with the help of Fig. 4.4 presenting the plots of the dependencies of the output field amplitude on the beam current deviation $\Delta I = I - I_0$. When calculating these plots, we have performed the normalization procedure at the nominal value of the beam current I_0. It is seen from these plots that the regime of coherent deceleration remains stable with the increase of the beam current with respect to nominal value. It can be understood from relation (4.1). It follows from this relation that at the increase of the beam current at all the other parameters fixed, the actual value of the tapering coefficient k_2 is decreased which, as we discussed above, does not destroy the process of the coherent deceleration.

Amplitude characteristics of the amplifier with tapered undulator are presented in Fig. 4.5. It is seen from these plots that there is no significant dependence of the output amplitude on the value of the input signal amplitude.

Another important characteristic of the amplifier is the energy spread of the electrons at the undulator exit. When the value of the efficiency η is increased significantly with respect to untapered case, the average energy of the trapped particles is

$$\bar{\mathcal{E}} = \mathcal{E}_0(1 - 0.38\beta\hat{u}^2).$$

The rms energy spread of the trapped particles oscillates with the undulator length. It is connected with the fact that the phase density of the particles is inhomogeneous inside the separatrix. As the particles perform slow energy oscillations with respect to the equilibrium energy, these result in slow oscillations of the rms energy spread. Numerical simulations show that maximal value of the reduced rms energy spread $\langle(\Delta\hat{P})^2\rangle$ is less or of the order of unity. Remembering that

$$\langle(\Delta\mathcal{E}/\mathcal{E}_0)^2\rangle = \beta^2\langle(\Delta\hat{P})^2\rangle,$$

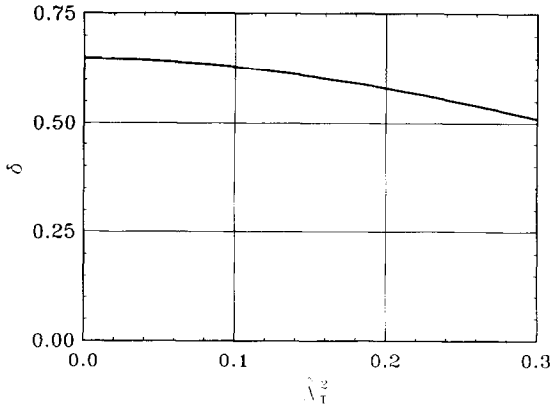

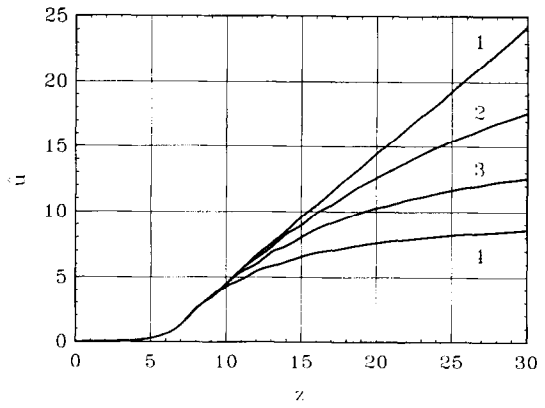

Fig. 4.7. Dependence of the trapping factor on the energy spread parameter $\hat{\Lambda}_T^2$. The undulator tapering is performed according to Eq. (4.5). Here $\hat{\Lambda}_p^2 = 0$.

Fig. 4.8. Dependence of the reduced field amplitude $\hat{u}$ on the reduced undulator length $\hat{z}$ for different values of the saturation parameter β. Here $\hat{\Lambda}_p^2 = 0$, $\hat{\Lambda}_T^2 = 0$ and $\hat{u}_{ext} = 0.01$. The detuning parameter changes according to the law $\hat{C} = 0$ at $\hat{z} < 7$ and $\hat{C} = 1.44 \times (\hat{z} - 7) + 0.36 \times (\hat{z} - 7)^2$ at $\hat{z} > 7$. Curve (1): $\beta = 0$, curve (2): $\beta = 0.003$, curve (3): $\beta = 0.01$, and curve (4): $\beta = 0.03$.

we write the following expression for the rms energy spread of the trapped particles:

$$\langle(\Delta\mathcal{E}/\mathcal{E}_0)^2\rangle^{1/2} \lesssim \beta.$$

The rms energy spread and average energy of untrapped particles are almost independent on the length of the undulator and are equal to

$$\langle(\Delta\mathcal{E}/\mathcal{E}_0)^2\rangle^{1/2} \simeq 2\beta, \quad \bar{\mathcal{E}} \simeq \mathcal{E}_0(1 - 0.6\beta).$$

4.1.3. Space charge and energy spread effects

Now we complicate our study with the inclusion of the space charge field. In this case the detuning should change as

$$\hat{C} = \begin{cases} \hat{C}_m & \text{at } \hat{z} < \hat{z}_i, \\ \hat{C} = \hat{C}_m + k_1(\hat{z} - \hat{z}_i) + k_2(\hat{z} - \hat{z}_i)^2 & \text{at } \hat{z} > \hat{z}_i, \end{cases} \tag{4.5}$$

where $\hat{C}_m$ is the detuning corresponding to the maximal value of the increment in the linear mode of operation. Optimization to the maximal field at $\hat{z} - \hat{z}_i \gg 1$ of the tapering coefficients k_1, k_2 and $\hat{z}_i$ has been performed using the systems of the self-consistent equations (3.6) and (3.16) and have obtained a set of optimal values of the tapering coefficients as functions of the space charge parameter. Fig. 4.6 illustrates the dependence of the trapping factor as the function of the space charge parameter.

Using Eqs. (3.5) and (3.6) we have performed also the similar study of the energy spread influence on the trapping efficiency. These results are presented in Fig. 4.7.

It is seen from Figs. 4.6 and 4.7 that the space charge field and energy spread limit significantly a possibility to increase the FEL amplifier efficiency by means of the undulator tapering.

4.1.4. Applicability region of the low efficiency approximation

We have described above the motion of the particles by the Hamiltonian (3.4) obtained from the Hamiltonian (3.1) by expansion in the small energy deviation $P = \mathcal{E} - \mathcal{E}_0$. This approximation may be violated in the case of a tapered undulator, so in the high efficiency case it is necessary to use Eqs. (3.2) and (3.3), obtained from the original Hamiltonian (3.1).

We normalize Eqs. (3.2) and (3.3) in the usual manner with the only refinement that all the normalization factors are calculated using the initial values of the beam and undulator parameters. We consider the case of the undulator tapering at the constant undulator parameter K = const. The electron rotation angle may be written in the form

$$\theta = \theta_s/(1 + \Delta\mathcal{E}/\mathcal{E}_0) = \theta_s/(1 + \beta\hat{P}).$$

As a result, we obtain the following equation of motion

$$\frac{d\hat{P}}{d\hat{z}} = \frac{\hat{u}}{1+\beta\hat{P}}\cos(\psi + \psi_0), \quad \frac{d\psi}{d\hat{z}} = \frac{\hat{P}(1+\beta\hat{P}/2)}{(1+\beta\hat{P})^2} + \hat{C} + \beta\hat{u}\frac{\sin(\psi+\psi_0)}{(1+\beta\hat{P})^2}. \tag{4.6}$$

Here, as before, the detuning parameter is

$$\hat{C} = \kappa_w(z)/\Gamma - \omega(1+K^2)/2\gamma^2 c\Gamma.$$

Field equations for $\hat{u}$ and ψ_0 have the form

$$\frac{d\hat{u}}{d\hat{z}} = -\frac{2}{N}\sum_{j=1}^{N}\frac{\cos(\psi_{(j)}+\psi_0)}{1+\beta\hat{P}_{(j)}}, \quad \frac{d\psi_0}{d\hat{z}} = \frac{1}{\hat{u}}\frac{2}{N}\sum_{j=1}^{N}\frac{\sin(\psi_{(j)}+\psi_0)}{1+\beta\hat{P}_{(j)}}. \tag{4.7}$$

Let us at first consider the case of quadratic law of the undulator tapering with parameters given by relations (4.1) and (4.2), i.e. at $\hat{z} > \hat{z}_i$ we have

$$\hat{C} = 1.44(\hat{z} - \hat{z}_i) + 0.36(\hat{z} - \hat{z}_i)^2.$$

The results of numerical simulations for several values of the efficiency parameter β are presented in Fig. 4.8. At a sufficiently short undulator length the energy losses of the trapped particle are small, $\Delta\mathcal{E}/\mathcal{E}_0 = \beta\hat{P} \ll 1$. In this case the system of equations (4.6) and (4.7) transits to the systems of equations (3.5) and (3.6), which is illustrated by the plots in Fig. 4.8. In this initial section the average energy of the trapped particles decreases quadratically with the undulator length, compensating for the quadratic increase of the parameter $\hat{C}$ in the equation for phase ψ of the system (4.6). The average change of the phase of the trapped particles is zero, $\langle d\psi/d\hat{z}\rangle = 0$, and their motion corresponds to phase oscillations about the equilibrium decelerating phase $\psi_e + \psi_0$ = const (according to the second equation of the system (4.7), at $\hat{u} \gg 1$ the change of the phase of effective potential ψ_0 can be neglected). As the length of the undulator is increased, the difference between the approximate system of equations (3.5) and (3.6) and the original system (4.6) and (4.7) becomes to be significant. It is seen from the equation for the phase

$$\frac{d\psi}{d\hat{z}} = \frac{\hat{P}(1+\beta\hat{P}/2)}{(1+\beta\hat{P})^2} + \hat{C}$$

that compensation of the quadratic growth of the detuning parameter $\hat{C}$ will take place at a smaller decelerating rate of the trapped particles. Numerical simulations show that at the final stage of

deceleration, the number of the trapped particles does not change and they perform phase oscillations about the equilibrium decelerating phase $\psi_e+\psi_0$, which, in turn, is decreased adiabatically approaching to the value of 90°. As a result, the growth of the field amplitude is slowed and further increase of the undulator length becomes to be ineffective. The plots in Fig. 4.8 give a notion of the validity region of the low efficiency approximation considered in the previous section. For instance, from this figure we see that in the range of the efficiency parameter $0.003 < \beta < 0.03$, the use of the results obtained with the approximate system of the self-consistent equations (3.5) and (3.6) is correct if the final amplifier efficiency does not exceed the value of 10%.

4.2. *The high efficiency FEL amplifier*

We have obtained above that the quadratic law of the undulator tapering, which is optimal in the low efficiency case, does not provide a possibility to achieve the high efficiency of the amplifier compared with the unity. To achieve this goal, the undulator parameters must be changed more faster than quadratic polynomial (4.1). Analyzing the form of Eq. (4.6) for the phase, we see that the linear law of the field amplitude change will take place also in the high efficiency case when at $\hat{z} > \hat{z}_i = \hat{z}_m - 1.4$ the detuning parameter will be changed as

$$\hat{C} = T(\hat{z})[1 - \beta T(\hat{z})/2][1 - \beta T(\hat{z})]^{-2}, \quad T(\hat{z}) = 1.44(\hat{z} - \hat{z}_i) + 0.36(\hat{z} - \hat{z}_i)^2. \tag{4.8}$$

The results of numerical simulations confirm this assumption. In fact, when the detuning parameter is changed as in Eq. (4.8), the field amplitude changes according to the linear law (4.4)

$$\hat{u}(\hat{z}, \beta) = \hat{u}(\hat{z}) \simeq \hat{z} - \hat{z}_m + 3$$

even in the region where the amplifier efficiency becomes comparable to unity. The motion of the trapped particles in the deeply decelerating regime proceeds as follows. The trapped particles execute phase oscillations about the equilibrium decelerating phase $\psi_e + \psi_0$, which nevertheless is decreased, approaching to 90°. On the other hand, the rotation angle of the trapped electrons is increased while the trapped particles lose their energy. These two effects compensate each other and effective interaction of the beam with the electromagnetic wave takes place up to the amplifier efficiency about of unity.

Using relations (3.9) and (4.4) we can calculate the total length $\hat{z}_f$ of the undulator required to attain the efficiency $\hat{\eta}$

$$\hat{z}_f = 2\sqrt{\hat{\eta}} + \frac{2}{\sqrt{3}} \ln(\hat{u}_{\text{ext}}^{-1}). \tag{4.9}$$

It is evident that efficiency η must obviously to be less than the trapping efficiency which is equal to 65%. According to Eq. (4.8), the total change of the undulator wavenumber is equal to

$$C = \Delta\kappa_w(z_f) = 2\pi\left[\lambda_w^{-1}(z_f) - \lambda_w^{-1}(z_i)\right] = \Gamma T(\hat{z}_f)[1 - \beta T(\hat{z}_f)/2][1 - \beta T(\hat{z}_f)]^{-2},$$

where $T(\hat{z}_f)$ and $\hat{z}_f$ are calculated from Eqs. (4.8) and (4.9).

The output characteristics of the amplifier with 40% efficiency are presented in Figs. 4.9 and 4.10. We see from these plots that the characteristics of the high efficiency amplifier do not differ significantly from those of the low efficiency amplifier. Analyzing the dependence of the field amplitude

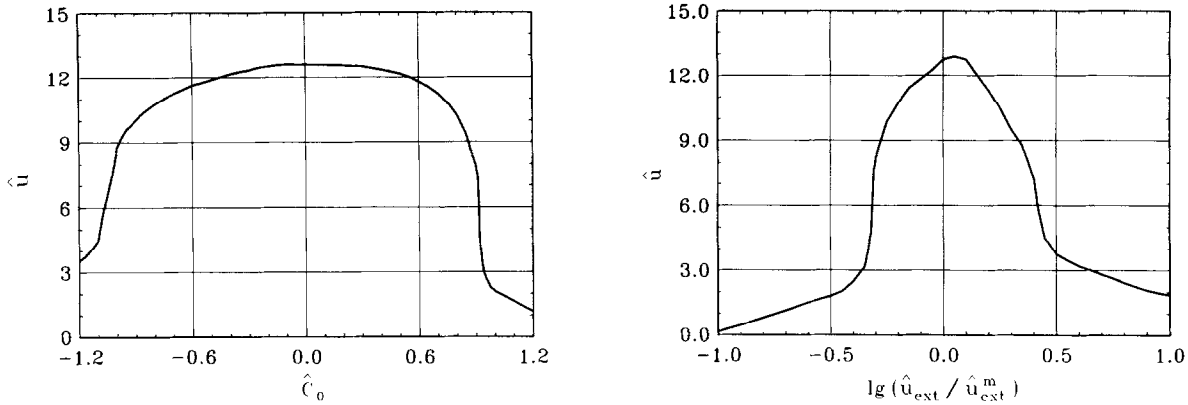

Fig. 4.9. Dependence of the field amplitude at the amplifier exit on the detuning parameter $\hat{C}$ in a high efficiency case. Here $\hat{\Lambda}_p^2 = 0$ and $\hat{\Lambda}_T^2 = 0$. The detuning parameter $\hat{C}$ changes according to the law $\hat{C} = \hat{C}_0$ at $\hat{z} < \hat{z}_i$ and $\hat{C} = \hat{C}_0 + \hat{C}_{tap}$ at $\hat{z} > \hat{z}_i$. The values of the variation beginning $\hat{z}_i$ are given with Eq. (4.3). The change of the detuning $\hat{C}_{tap}$ is given with Eq. (4.8). At $\hat{C}_0 = 0$ the FEL amplifier efficiency is equal to 40 % and the power gain at the end of untapered section (at $\hat{z} = \hat{z}_i$) is equal to 40 dB.

Fig. 4.10. Dependence of the output field amplitude $\hat{u}$ on the input field amplitude $\hat{u}_{ext}$ in a high efficiency case. Here $\hat{\Lambda}_p^2 = 0$ and $\hat{\Lambda}_T^2 = 0$. The detuning parameter $\hat{C}$ changes according to Eq. (4.8) where the beginning of the tapering $\hat{z}_i$ corresponds to the nominal value of the input signal $\hat{u}_{ext}^m$. At $\hat{u}_{ext} = \hat{u}_{ext}^m$ the FEL amplifier efficiency is equal to 40 % and the power gain at the end of untapered section (at $\hat{z} = \hat{z}_i$) is equal to 40 dB.

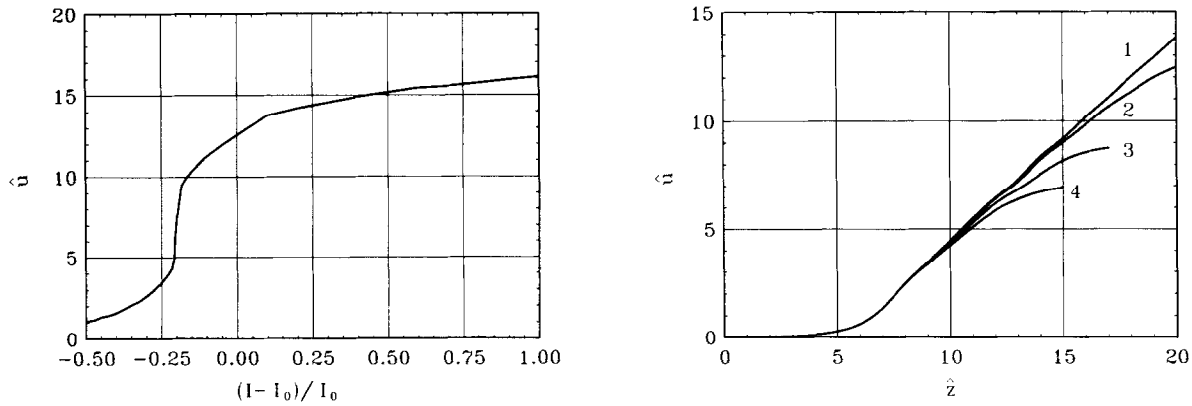

Fig. 4.11. Dependence of the field amplitude at the amplifier exit on the beam current for a high efficiency case. Here $\hat{\Lambda}_p^2 = 0$ and $\hat{\Lambda}_T^2 = 0$. The detuning parameter $\hat{C}$ changes according to Eq. (4.8). The reduced parameters are calculated at $I = I_0$. At $I = I_0$ the FEL amplifier efficiency is equal to 40 % and the power gain at the end of untapered section (at $\hat{z} = \hat{z}_i$) is equal to 40 dB.

Fig. 4.12. Dependence of the reduced field amplitude $\hat{u}$ on the reduced undulator length $\hat{z}$ for different values of the parameter s. Here $\hat{\Lambda}_p^2 = 0$, $\hat{\Lambda}_T^2 = 0$, $\beta = 0.01$ and $\hat{u}_{ext} = 0.01$. The undulator field changes according to Eqs. (4.10), (4.13) and (4.16). The length of the tapered section is given with Eq. (4.15). Curve (1): $s = \infty$, curve (2): $s = 5$, curve (3): $s = 1$ and curve (4): $s = 0.5$.

at the amplifier output on the beam current, presented in Fig. 4.11, we obtain that even for a significant increase of the current, the output field amplitude is practically unchanged, and the amplifier efficiency is decreased only due to the increase of the beam power. For example, when the beam current is increased by the factor of 1.5 with the other parameters fixed, the efficiency is decreased from 40% to 33%.

4.3. Some generalizations

4.3.1. Tapering at a fixed undulator period

We have studied above the undulator tapering at a fixed undulator parameter K = const. Another popular way of the tapering is tapering at a fixed undulator period λ_w = const. From the theoretical point of view this method seems to be more complicated, so the obtained results, as we will show below, are not so general than those obtained above for the tapering at K = const.

It follows from the definition of the detuning C that in order to preserve the synchronism, at the tapering with the fixed undulator period λ_w, the undulator field H_w must be decreased. The simplest law of the magnetic field change is a quadratic one:

$$\frac{H_w(z_i) - H_w(z)}{H_w(z_i)} = e_0 + e_1(z - z_i) + e_2(z - z_i)^2. \tag{4.10}$$

The normalization procedure is performed in a usual way. We calculate normalization factors from the initial values of the beam and the undulator parameters. In accordance with Eqs. (3.2) and (3.3) the corresponding system of the reduced self-consistent equations has the form

$$\begin{aligned}
\frac{d\hat{P}}{d\hat{z}} &= \frac{1}{1+\beta\hat{P}}\left[1 - \frac{1+s}{s}\beta T(\hat{z})\right]\hat{u}\cos(\psi+\psi_0),\\
\frac{d\psi}{d\hat{z}} &= \frac{1}{(1+\beta\hat{P})^2}\left\{\hat{P}\left[1+\frac{\beta\hat{P}}{2}\right] + T(\hat{z})\left[1 - \frac{1+s}{2s}\beta T(\hat{z})\right]\right.\\
&\quad \left. + \beta\hat{u}\left[1 - \frac{1+s}{s}\beta T(\hat{z})\right]\sin(\psi+\psi_0)\right\},
\end{aligned} \tag{4.11}$$

$$\begin{aligned}
\frac{d\hat{u}}{d\hat{z}} &= -\left[1 - \frac{1+s}{s}\beta T(\hat{z})\right]\left[\frac{2}{N}\sum_{j=1}^{N}\frac{\cos(\psi_{(j)}+\psi_0)}{1+\beta\hat{P}_{(j)}}\right],\\
\frac{d\psi_0}{d\hat{z}} &= \frac{1}{\hat{u}}\left[1 - \frac{1+s}{s}\beta T(\hat{z})\right]\left[\frac{2}{N}\sum_{j=1}^{N}\frac{\sin(\psi_{(j)}+\psi_0)}{1+\beta\hat{P}_{(j)}}\right],
\end{aligned} \tag{4.12}$$

The coefficients $s = K^2$ and $\beta = c\gamma_z^2\Gamma/\omega$ are calculated using the initial values of the beam and undulator parameters. The function $T(\hat{z})$ is

$$\begin{aligned}
&T(\hat{z}) = k_0 + k_1(\hat{z} - \hat{z}_i) + k_2(\hat{z} - \hat{z}_i)^2,\\
&k_0 = \frac{s}{1+s}\frac{e_0}{\beta}, \quad k_1 = \frac{s}{1+s}\frac{e_1}{\beta\Gamma}, \quad k_2 = \frac{s}{1+s}\frac{e_2}{\beta\Gamma^2}.
\end{aligned} \tag{4.13}$$

At the initial part of the tapered section, when the change of the energy of the trapped particles is small, we can expand Eqs. (4.11) and (4.12) in the small parameter $\beta\hat{P}$ and obtain the system of equation describing the low efficiency approximation:

$$\frac{d\hat{P}}{d\hat{z}} = \hat{u}\cos(\psi + \psi_0), \quad \frac{d\psi}{d\hat{z}} = \hat{P} + T(\hat{z}),$$

$$\frac{d\hat{u}}{d\hat{z}} = \hat{j}_1\cos(\psi_0 - \psi_1), \quad \frac{d\psi_0}{d\hat{z}} = -\frac{\hat{j}_1}{\hat{u}}\sin(\psi_0 - \psi_1).$$

This system coincides with the system of equations (3.5) and (3.6) describing the low efficiency approximation of the undulator tapering at a fixed undulator parameter K = const. The detuning parameter $\hat{C}(\hat{z})$ in this case is equal to $T(\hat{z})$. Therefore, we can conclude that in the low efficiency approximation, at $\eta \ll 1$, the both tapering methods are equivalent.

The coefficients k_0, k_1, k_2 and $\hat{z}_i$ have been optimized to the field maximum at $(\hat{z} - \hat{z}_i) \gg 1$ using the system of equations (4.11) and (4.12). It was assumed that $s \simeq 1$ and $\beta \simeq 10^{-2}$. The following values have been obtained:

$$k_0 = 0, \quad k_1 = 1.44, \quad k_2 = 0.3, \quad \hat{z}_i = 1.7 + \frac{2}{\sqrt{3}}\ln(\hat{u}_{\text{ext}}^{-1}).$$

Phase analysis has shown that 68% of the particles are trapped in the regime of coherent deceleration.

The fact that the value of the coefficient k_2 is slightly less than that of the undulator tapering at a fixed undulator parameter, requires some explanation. Numerical simulations performed with the initial equations (4.6), (4.7), (4.11) and (4.12) shows that as the undulator field is decreased, the phase motion of the particles becomes less stable with respect to that calculated with Eqs. (3.5) and (3.6). The main losses of the trapped particles occur within the first period of phase oscillation, at

$$(\hat{z} - \hat{z}_i) \simeq 3.$$

when the particles come quite close to the boundary of the stability region. For parameters of practical interest $s \simeq 1$ and $\beta \simeq 10^{-2}$, the difference in the simulation results obtained with the initial and approximate equations becomes to be visible, and for $k_2 = 0.36$ it causes the number of trapped particles to decrease visibly in passing through the critical point. Therefore, the more stable regime becomes possible at $k_2 = 0.3$.

The length of the tapering section $(z_f - z_i)$ obviously can not exceed the distance over which the undulator field H_w decreases to zero as in Eq. (4.10) and can be found from the equation

$$0.3\beta\frac{1+s}{s}(\hat{z}_f - \hat{z}_i)^2 + 1.44\beta\frac{1+s}{s}(\hat{z}_f - \hat{z}_i) - 1 = 0. \tag{4.14}$$

To be strict, the minimal value of the undulator field is limited from below not by zero but by the condition $H_w \gg E/(2\gamma_z^2)$. This is one of the basic assumptions of the theory which means that the transverse constrained motion of the electrons in the undulator is defined by magnetic field of the undulator but not the radiation field. Using Eqs. (4.10) and (4.13), this condition may be written in the following reduced form

$$\frac{1+s}{s}\beta^2\hat{u}(\hat{z}) \ll \left[\frac{1+s}{s}\beta T(\hat{z})\right]. \tag{4.15}$$

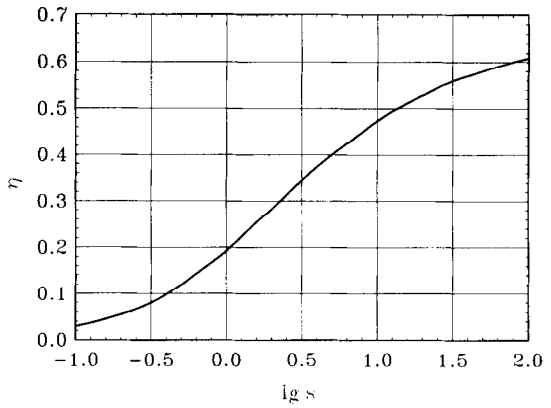

Fig. 4.13. Dependence of the efficiency of the amplifier on the parameter s. Here $\hat{\Lambda}_p^2 = 0$, $\hat{\Lambda}_T^2 = 0$, $\beta = 0.01$ and $\hat{u}_{ext} = 0.01$. The undulator field changes according to Eqs. (4.10), (4.13) and (4.16). The length of the tapered section is given with Eq. (4.15).

However, for parameters of practical interest

$$0.1 < s, \quad \beta < 0.03$$

the length of the tapered section obtained with Eq. (4.15) does not differ significantly from that obtained with Eq. (4.14).

In Fig. 4.12 we show graphs of the field amplitude $\hat{u}(\hat{z}, s, \beta)$ for $s = 0.5$, 1 and 5 and at $\beta = 0.01$. The reduced function $T(\hat{z})$ of the undulator field tapering was as follows:

$$T(\hat{z}) = 1.44(\hat{z} - \hat{z}_i) + 0.3(\hat{z} - \hat{z}_i)^2, \quad \hat{z}_i = 1.7 + \frac{2}{\sqrt{3}} \ln(\hat{u}_{ext}^{-1}). \tag{4.16}$$

For comparison, in the same figure we show the graph of the field amplitude $\hat{u}(\hat{z})$ calculated with the system of approximate equations (3.5) and (3.6). It is seen from these plots that the larger the parameter s, the less the field amplitude $\hat{u}(\hat{z}, s, \beta)$ deviates from the linear behaviour in the final part of the tapered section. The dependence of the maximal efficiency of the amplifier on the values of parameter s wfor $\beta = 0.01$ is shown in Fig. 4.13. It is seen that at $s \gg 1$ the undulator tapering at a constant undulator period gives the same results as the tapering at a constant undulator parameter, and a high efficiency can be achieved.

The results of numerical simulations show that the maximal efficiency of the amplifier does not depend significantly on the value of the efficiency parameter β when it changes in the limits $0.003 < \beta < 0.03$. So, in many practical situations the plot in Fig. 4.13 is of use to obtain the maximal efficiency of the amplifier.

4.4. FEL amplifier with a planar undulator

When performing the study of the FEL amplifier we assumed for simplicity the undulator to be a helical one and the radiation to be circularly polarized. All the results and plots obtained above refer also to the case of the linearly polarized radiation and the planar undulator with the field

$$H_y = 0, \quad H_x = H_l \cos(\kappa_w z),$$

by the following redefinition of the parameters

$$\Gamma \to \Gamma' = [\pi j_0 \theta_l^2 \omega A_{JJ}^2 \gamma^{-1} \gamma_l^{-2} I_A^{-1} (2c)^{-1}]^{1/3}, \quad E_0 \to E_0' = 2\mathcal{E}_0 \gamma_l^2 (\Gamma')^2 c/(e\theta_l^2 \omega A_{JJ}),$$
$$C \to C' = \kappa_w - \omega(2c)^{-1}\gamma_l^{-2}, \quad \beta \to \beta' = c\gamma_l^2 \Gamma' \omega^{-1},$$
$$\Lambda_p \to \Lambda_p' = [4\pi j_0 \gamma^{-1} \gamma_l^{-2} I_A^{-1}]^{1/2}, \quad \Lambda_T \to \Lambda_T' = c^{-1}\omega\gamma_l^{-2}(\langle(\Delta\mathcal{E})^2\rangle)^{1/2}\mathcal{E}_0^{-1}.$$

Here, as it was done in Section 2, we have introduced the following notations

$$\theta_l = eH_l/(\mathcal{E}_0 \kappa_w), \quad \gamma_l^{-2} = \gamma^{-2} + \theta_l^2/2.$$

Factor A_{JJ} is given by the formula

$$A_{JJ} = [J_0(\nu) - J_1(\nu)],$$

where $\nu = \theta_l^2 \omega/(8c\kappa_w)$, J_0 and J_1 are the Bessel functions. The field of the amplified wave is described by the expression

$$E_x = 0, \quad E_y = E_l(z)\cos[\omega(z/c - t) + \psi_0(z)].$$

It should be noted however that the study of the undulator tapering at a fixed undulator period can not be interpreted in this way. Indeed, in this case factor A_{JJ} is a function of coordinate z. As a result, Eqs. (4.11) and (4.12) should be written taking into account this dependence and the problem should study separately.

Let us demonstrate the way of calculation the saturation characteristics of the amplifier with a planar undulator. Using Eq. (3.13) we find that in the exact resonance $\hat{C}' = 0$ and in the absence of the space charge field and the energy spread,

$$(\Lambda_p'/\Gamma')^2 \to 0, \quad (\Lambda_T'/\Gamma')^2 \to 0,$$

the field saturation is reached at the undulator length

$$z_m = (\Gamma')^{-1}\left[3.1 + \frac{2}{\sqrt{3}}\ln(E_0'/E_l^{\text{ext}})\right]$$

where E_l^{ext} is the field amplitude at the undulator entrance. The value of the radiation field at the saturation is $(E_l)_{\max} = 2.34E_0'$.

4.5. *Applicability region of the one-dimensional theory of the FEL amplifier*

In Sections 2–4 we have presented one-dimensional theory of the FEL amplifier. Due to the simplicity of the basic approximations of this model, it provides the most clear way to understand the physical mechanism of the FEL amplifier operation, to study the influence of the space charge fields and the energy spread of the electrons in the beam on the FEL operation. It provides also a reliable way to study undulator tapering technique to increase the FEL amplifier efficiency.

The validity region of the one-dimensional model is limited with the condition that the radiation does not expand in outer space outside the electron beam. In many practical situations diffraction effects influence significantly on the process of the field formation in the FEL. For instance, at a fast growing of the optical field amplitude along the undulator axis, the radiation field eigenmode

with complicated transverse distribution of the radiation field is formed by the electron beam (in other words, the so called "optical guiding" effect takes place). In essentially three-dimensional case the analysis of the FEL amplifier must be performed by simultaneous solution of the equations of motion of the beam electrons and the field equations under corresponding boundary conditions for the electromagnetic field. In sections 9 – 11 we present such an extension of the FEL amplifier theory and present rigorous analysis of the applicability region of the one-dimensional approximation.

It should be noticed that the one-dimensional model is not only of methodological significance. For instance, calculations of the FEL amplifiers of X-ray wavelength can be performed in the framework of one-dimensional model [4]. It provides also a reliable way for calculation of a novel FEL amplifier configuration, namely of a FEL amplifier with diaphragm line. Such a FEL amplifier scheme has been proposed in Ref. [32] and can be used in perspective FEL amplifier schemes for inertial confinement fusion. In this scheme a periodic diaphragm line is used for focusing and confinement of the radiation in the amplifier. It has a form of a sequence of totally absorbing screens with holes. At a large value of the Fresnel number, eigenmodes of diaphragm line have rather small diffraction losses. For instance, in a visible wavelength range, at the radius of the hole 1 cm and the distance between the screens 1 m, diffraction losses of the ground eigenmode are about of 0.01% per one diaphragm.

At a relatively small gain of the radiation field amplitude along the undulator axis, the electron beam does not affect significantly on the transverse distribution of the radiation field and the latter is defined mainly by the diaphragm line. The transverse field distribution of the ground TEM_{00} eigenmode of the diaphragm line is of the form:

$$|\tilde{E}| \propto J_0(\nu_{01} r/R),$$

where r is transverse coordinate, R is the radius of the diaphragm line holes, J_0 is the Bessel function and ν_{01} is the first root of the Bessel function of zero order. When the transverse size of the electron beam is much less than aperture of diaphragm line (which usually takes place in practice), the radiation field change over the electron beam can be neglected which reveals a possibility to use one-dimensional approximation. In this case an "effective" beam current density can be substituted into the equations of the one-dimensional FEL amplifier theory:

$$j_0 = I\,[\,\pi R^2 J_1^2(\nu_{01})\,]^{-1} \simeq 3.7 I/(\pi R^2),$$

where I is the total beam current. In addition, the distinction between the phase velocity of TEM_{00} mode and the velocity of light c should be taken into account in the FEL resonance condition.

In some cases such an approach can provide correct description of the processes in the FEL amplifier with diaphragm line [32]. As a result, all universal formulae and plots presented in Sections 2–4 can be used directly for calculations.

5. Linear theory of the FEL oscillator

In Sections 5–8 we exposure a one-dimensional theory of a FEL oscillator. In some sense this device is a more complicated object with respect to the FEL amplifier. In the case of the FEL amplifier, the frequency, of the amplified wave is determined by a master oscillator, the amplitude and the phase of the electromagnetic wave do not depend on time and depend on the space coordinates only (in the one-dimensional approximation – on the only longitudinal coordinate z). The dependence of the

electromagnetic field on the longitudinal coordinate is obtained by self-consistent solution of Maxwell equations and equations of electron motion at definite initial conditions at the undulator entrance.

The FEL oscillator consists of a resonator with an "active medium" – electron beam in an undulator. During the lasing process several longitudinal modes with different frequencies can be excited in the resonator. A rigorous solution of the lasing problem consists in integration of the self-consistent field equations at given initial and boundary conditions and evolution of all the modes should be obtained. This problem can be solved only in a limited number of special cases. In the small signal approximation the problem can be reduced to an eigenvalue problem, i.e. to finding eigenvalues and eigenfunctions of the modes. For instance, such an approach made it possible to develop three-dimensional theory of the FEL oscillator with plane Fabry-Perot resonator (see Refs. [33,34]). Peculiar feature of these papers is application of impedance boundary conditions of resonance type, which makes it possible to reduce the problem of the open resonator to a closed one. In Appendix C we use a similar approach to exposure the linear one-dimensional theory of the FEL oscillator.

In the general case the problem of the FEL oscillator in the rigorous formulation can not be solved due to significant difficulties in the calculations. So, the most researches in the FEL oscillator theory have been performed using phenomenological approach consisting in the study of the FEL oscillator as the FEL amplifier with a feedback. In Sections 5–8 we use this approach to the analysis of the FEL oscillator. The main idea of this approach is that interaction of the electron beam with the electromagnetic wave during their pass in the undulator is treated in the same way as for the FEL amplifier. Then the losses in the mirrors are taken into account and the wave interacts with a fresh electron beam at the next undulator pass. In this way the evolution of the field amplitude in the resonator is obtained. One can imagine a visual picture of this process. Let us consider a semi-infinite sequence of plane-parallel equidistantly placed semi-transparent plates. In each second period the undulator is placed between the plates. The travelling electromagnetic wave is fed to the system input. When the wave propagates in the first undulator, the amplification process takes place. After transmission of the wave through the first pair of plates, its amplitude is multiplied by a transmission factor (which is equal to the reflection coefficient of the mirrors) and is fed to the input of the second undulator, etc.

This approach enables one to study a single-mode approximation as well as a multi-mode approximation. To simulate the latter case, several waves with different frequencies (corresponding to longitudinal modes of the resonator) are fed to the undulator entrance. Each mode modulates the electron beam at its own frequency. In the linear mode of operation all the modes grow in time independently according to the increments which are defined by the gain curve. In the nonlinear mode of operation, due to nonlinear modulation of the electron beam density, the mode competition effect becomes to play a significant role. For instance, an important effect of sideband instability can be described in this way [35,44].

In the present study we use the single-mode approximation which assume that the mode selection takes place and after the linear mode of the FEL oscillator operation, a single mode is settled corresponding to the maximum of the gain curve. Besides, we assume the field gain per one resonator pass to be small (the case of a large field gain is discussed in Section 6.6). Similarly to the study of the FEL amplifier, we do not take into account the slippage effects. Nevertheless, such a relatively simple model enables one to take into account almost all main effects influencing the FEL oscillator operation and in many cases provides adequate description of the processes in the FEL oscillator.

5.1. Basic relations

We consider a plane Fabry-Perot resonator equipped with two plane parallel mirrors placed at distance L between them. A helical undulator having length l_w is placed inside the resonator and its axis coincides with the resonator axis. Magnetic field at the undulator axis is given with the expression

$$\boldsymbol{H}_w(z) = \boldsymbol{e}_x H_w \cos(\kappa_w z) - \boldsymbol{e}_y H_w \sin(\kappa_w z),$$

where $\boldsymbol{e}_{x,y}$ are the unit vectors directed along the x and y coordinates of the Cartesian coordinate system (x, y, z). The beginning of the undulator is placed at $z = 0$. We neglect the transverse variations of the undulator field and assume the electrons to move along the constrained helical trajectories in parallel with the z axis (in average over the undulator period). The electron rotation angle θ_s is considered to be small and longitudinal electron velocity v_z is close to the velocity of light ($v_z \simeq c$).

We suppose the electromagnetic field in the resonator to be circularly polarized because of the helical magnetic system of the undulator. Using the complex representation, we can write the expression for the electrical field of the wave synchronous with the electron beam:

$$E_x + iE_y = \tilde{E}(z) \exp[i\omega(z/c - t)].$$

It is assumed that the field gain per one undulator pass is small, i.e.

$$|\tilde{E}(l_w) - \tilde{E}(0)|/|\tilde{E}(0)| \ll 1. \tag{5.1}$$

The power gain coefficient is defined as

$$G = |\tilde{E}(l_w)|^2/|\tilde{E}(0)|^2 - 1.$$

Introducing notation

$$Z = \tilde{E}(l_w)/\tilde{E}(0) - 1,$$

we rewrite condition (5.1) in the following form

$$G \simeq 2\,\mathrm{Re}(Z).$$

In the amplification process the phase of the electromagnetic wave changes, too. Taking into account that $\arg\{\tilde{E}(0)\} = \psi_0$ and $\arg\{\tilde{E}(l_w)\} = \psi_0 + \Delta\psi_0$, we may write:

$$\Delta\psi_0 \simeq \mathrm{Im}(Z).$$

In the small signal approximation, the values of G and $\Delta\psi_0$ do not depend on the value of the field $\tilde{E}(0)$ stored in the resonator. We denote the power gain coefficient for the small signal gain as G_s. It is function of the frequency and parameters of the electron beam and the undulator. After reflection from the both mirrors the radiation is fed to the undulator entrance and is amplified in the undulator, etc. The lasing condition is formulated as follows:

$$\max(G_s) > \alpha,$$

where α is the relative power losses per one resonator round-trip. If (T_1, Γ_1) and (T_2, Γ_2) are the transmission and absorption coefficients of the first and the second resonator mirror, respectively, then $\alpha = T_1 + T_2 + \Gamma_1 + \Gamma_2$.

To find the gain, we use the approach presented in Section 2. Expression for the complex amplitude of the first harmonic of the beam current density (2.11) has the form

$$\tilde{j}_1(z) = ij_0 \int_0^z dz' [U + 4\pi e \tilde{j}_1(z')/\omega] \times \int dP dF(P)/dP \exp\{i[C + \omega P/(c\gamma_z^2 \mathcal{E}_0)](z' - z)\}.$$

The change of the field amplitude in the resonator is described with expression (2.13)

$$d\tilde{E}/dz = -2\pi\theta_s \tilde{j}_1(z)/c.$$

Here is a place to remember notations introduced in Section 2: $P = \mathcal{E} - \mathcal{E}_0$ is the deviation of the electron energy $\mathcal{E}$ from the nominal value $\mathcal{E}_0$, $C = \kappa_w - \omega/2c\gamma_z^2$ is the detuning of the electron with the nominal energy $\mathcal{E}_0$, $U = -e\theta_s \tilde{E}(z)/2i$ is the complex amplitude of the particle-wave interaction,

$$\theta_s = eH_w/\mathcal{E}_0\kappa_w, \quad \gamma_z^{-2} = \gamma^{-2} + \theta_s^2, \quad \gamma = \mathcal{E}_0/m_e c^2.$$

Using these relation we can find the gain and the change of the phase of the wave in the small signal regime.

5.2. *Small-signal gain*

5.2.1. *Cold electron beam*

Let us find the gain coefficient in the absence of the space charge field and energy spread. The distribution function of a monoenergetic electron beam is given by the delta function $F(P) = \delta(P)$. From Eq. (2.11) we obtain

$$\tilde{j}_1(z) = ij_0\theta_s e\omega(2\mathcal{E}_0\gamma_z^2 c)^{-1} \int_0^z dz'(z' - z)\tilde{E}(z') \exp[iC(z' - z)].$$

Integrating Eq. (2.13) over z under condition (5.1), we obtain the expression for the function Z

$$Z = -i\pi j_0 \theta_s^2 e\omega(\mathcal{E}_0\gamma_z^2 c^2)^{-1} \int_0^{l_w} dz \int_0^z dz'(z' - z) \exp[iC(z' - z)].$$

It is convenient to rewrite this expression in the following form

$$Z = i\frac{\tau}{2} \int_0^1 d\xi \int_0^\xi d\xi' \xi' \exp(-i\hat{C}\xi'), \tag{5.2}$$

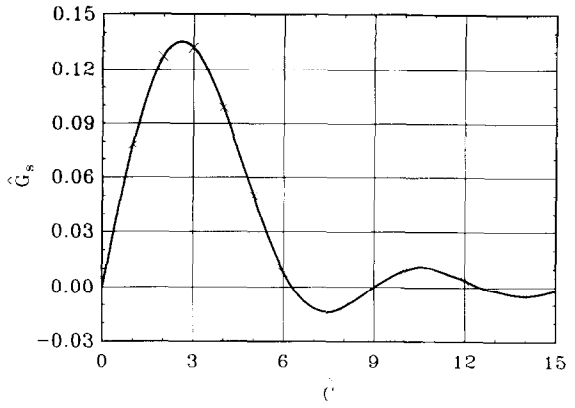

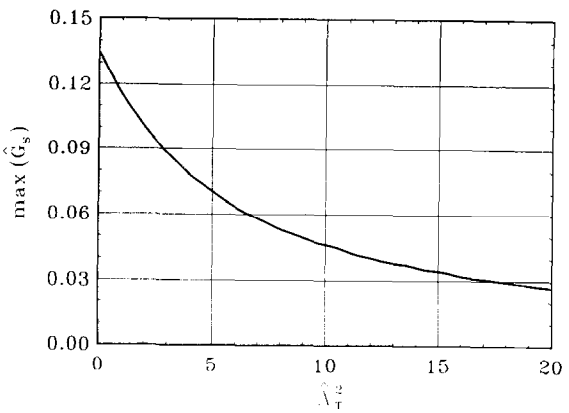

Fig. 5.1. The reduced small-signal gain $\hat{G}_s$ versus the reduced detuning $\hat{C}$ at $\hat{\Lambda}_T = 0$ and $\hat{\Lambda}_p = 0$. The full curve is calculated with the analytical formulae (5.3) and the crosses are the results of the numerical simulations with the formulae (6.1) and (6.2).

Fig. 5.2. The maximal reduced small-signal gain $\hat{G}_s$ versus the energy spread parameter $\hat{\Lambda}_T^2$ at $\hat{\Lambda}_p = 0$. The calculations have been performed with the formulae (5.3b) and (5.4).

where $\tau = 2\pi\theta_s^2\omega j_0 l_w^3 (c\gamma_z^2\gamma I_A)^{-1}$ is the gain parameter, $I_A = mc^3/e \simeq 17$ kA is Alfven's current and $\hat{C} = Cl_w$ is the detuning parameter. Introducing notations $\hat{G}_s = G_s/\tau$ and $\hat{Z} = 2Z/\tau$ and integrating Eq. (5.2), we reduce the function $\hat{Z}$ to the algebraic expression

$$\hat{Z} = 2i\hat{C}^{-2}\left[2(\hat{C})^{-1}\sin(\hat{C}/2) - \cos(\hat{C}/2)\right]\exp(-i\hat{C}/2). \tag{5.3a}$$

The gain and the field phase increment per one undulator pass are expressed in terms of the function $\hat{Z}$ as

$$\hat{G}_s = \mathrm{Re}(\hat{Z}), \quad \Delta\psi_0/\tau = \tfrac{1}{2}\,\mathrm{Im}(\hat{Z}). \tag{5.3b}$$

In the case under study (in the absence of the space charge field and energy spread), the maximal gain is the function of the only detuning parameter $\hat{C}$. The gain reaches its maximum at $\hat{C} = \hat{C}_m = 2.6$

$$\max(\hat{G}_s) = 0.135.$$

The dependence of the $\hat{G}_s$ on the detuning $\hat{C}$ is presented in Fig. 5.1 (note that the gain curve is antisymmetric with respect to $\hat{C} = 0$).

5.2.2. *Gaussian energy spread*

Let us consider the electron beam with a Gaussian energy spread with the distribution function given by Eq. (2.29a). In the case of negligibly small space charge field, we obtain

$$\hat{Z} = i\int_0^1 d\xi \int_0^\xi d\xi' \xi' \exp[-i\hat{C}\xi' - \hat{\Lambda}_T^2(\xi')^2/2], \tag{5.4}$$

where $\hat{\Lambda}_T^2 = \omega^2 l_w^2\langle(\Delta\mathcal{E})^2\rangle/(c^2\mathcal{E}_0^2\gamma_z^4) = (4\pi N_w)^2\langle(\Delta\mathcal{E})^2\rangle/\mathcal{E}_0^2$ is the energy spread parameter and N_w is the number of undulator periods. According to Eq. (5.4), maximal gain $\max(\hat{G}_s) = \max(\mathrm{Re}\,\hat{Z})$

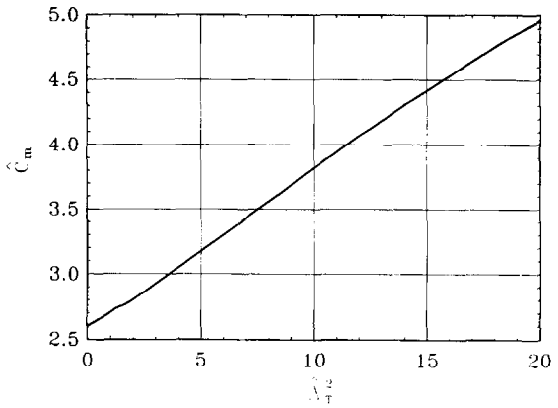

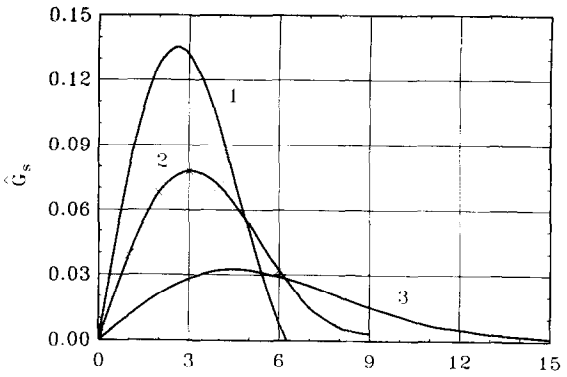

Fig. 5.3. The optimal reduced detuning $\hat{C}_m$ versus the energy spread parameter $\hat{\Lambda}_T^2$ at $\hat{\Lambda}_p = 0$. The calculations have been performed with the formulae (5.3b) and (5.4).

Fig. 5.4. The reduced small-signal gain $\hat{G}_s$ versus the reduced detuning $\hat{C}$ at $\hat{\Lambda}_p = 0$. The full curves are calculated with the analytic formulae (5.3b) and (5.4) and the crosses are the results of numerical simulations with formulae (6.1) and (6.2). Curve (1): $\hat{\Lambda}_T^2 = 0$, curve (2): $\hat{\Lambda}_T^2 = 4$, curve (3): $\hat{\Lambda}_T^2 = 16$.

and the detuning $\hat{C}$ corresponding to this maximal gain are universal functions of the energy spread parameter $\hat{\Lambda}_T^2$. The plots of these functions are presented in Figs. 5.2 and 5.3. For illustration, the gain curves for several values of $\hat{\Lambda}_T^2$ are presented in Fig. 5.4. At large values of the energy spread parameter, $\hat{\Lambda}_T^2 \gg 1$, we have asymptotically:

$$\hat{C}_m \simeq \hat{\Lambda}_T, \quad \max(\hat{G}_s) \simeq \sqrt{\pi/2e}\hat{\Lambda}_T^{-2} \simeq 0.76\hat{\Lambda}_T^{-2},$$

where $e = 2.71828$ is the base of natural logarithm.

5.2.3. *Space charge influence*

Let us study the space charge field influence on the gain for a monoenergetic electron beam which distribution function is $F(P) = \delta(P)$. Complex amplitude $\tilde{j}_1(z)$ of the first harmonic of the beam current density can be found by the Laplace transform. Multiplying Eq. (2.11) by $\exp(-pz)$ and integrating over z from 0 to ∞, we obtain

$$\bar{j}_1(p) = \int_0^\infty e^{-pz}\tilde{j}_1(z)\,dz = -\omega j_0 U\gamma_z^{-2}\mathcal{E}_0^{-1}\{p[(p+iC)^2 + \Lambda_p^2]\}^{-1},$$

where $\Lambda_p^2 = 4\pi j_0/(\gamma_z^2\gamma I_A)$. To obtain $\tilde{j}_1$, we must perform the inverse Laplace transform of the function $\bar{j}_1(p)$. The complex function $\bar{j}_1(p)$ is satisfied to the Jordan's lemma, so, using the residue theory we obtain

$$\tilde{j}_1(z) = \frac{i\tilde{E}\omega e\theta_s j_0}{2c\gamma_z^2\mathcal{E}_0}\left\{\frac{1}{C^2 - \Lambda_p^2} + \frac{\exp[-i(C+\Lambda_p)z]}{2\Lambda_p(C+\Lambda_p)} - \frac{\exp[-i(C-\Lambda_p)z]}{2\Lambda_p(C-\Lambda_p)}\right\}.$$

Substituting this expression into Eq. (2.13) and integrating over z, we find

$$\hat{Z} = i(\hat{C}^2 - \hat{\Lambda}_p^2)^{-2}\{\hat{\Lambda}_p^2 - \hat{C}^2 - 2i\hat{C}(1 - \cos(\hat{\Lambda}_p)\exp(-i\hat{C}))$$

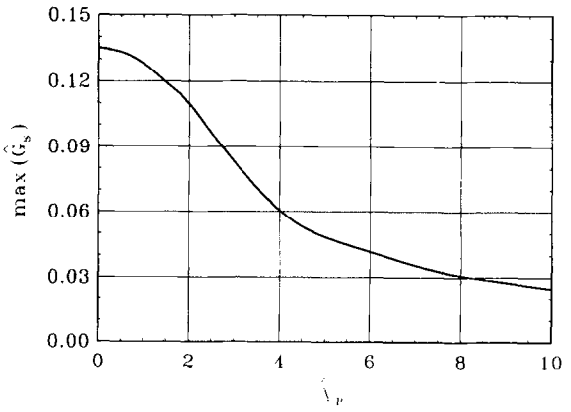

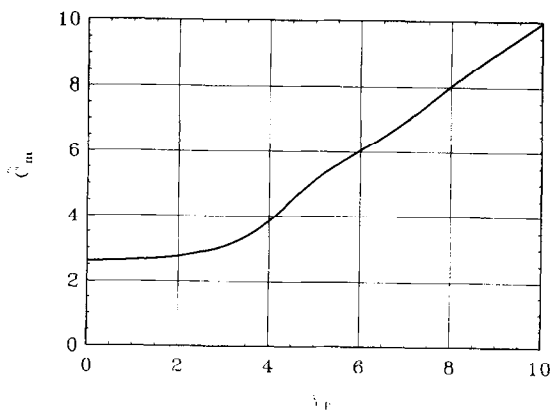

Fig. 5.5. The maximal reduced small-signal gain $\hat{G}_s$ versus the space charge parameter $\hat{\Lambda}_p$ at $\hat{\Lambda}_T^2 = 0$. The calculations have been performed with the formulae (5.3b) and (5.5).

Fig. 5.6. The optimal reduced detuning $\hat{C}_m$ versus the space charge parameter $\hat{\Lambda}_p$ at $\hat{\Lambda}_T^2 = 0$. The calculations have been performed with the formulae (5.3b) and (5.5).

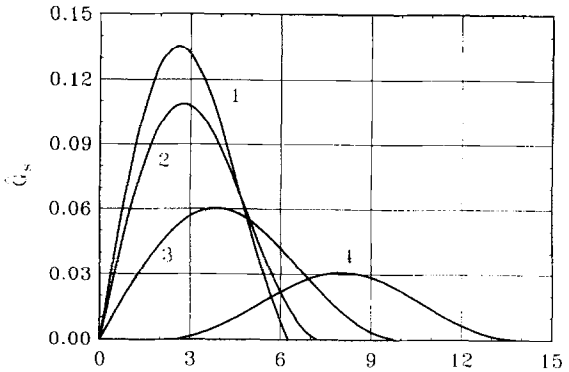

Fig. 5.7. The reduced small-signal gain $\hat{G}_s$ versus the reduced detuning $\hat{C}$ at $\hat{\Lambda}_T^2 = 0$. The full curves are calculated with the analytical formulae (5.3b) and (5.5) and the crosses are the results of numerical simulations with formulae (6.2) and (6.6) Curve (1): $\hat{\Lambda}_p = 0$, curve (2): $\hat{\Lambda}_p = 2$, curve (3): $\hat{\Lambda}_p = 4$, curve (4): $\hat{\Lambda}_p = 8$.

$$- \hat{\Lambda}_p^{-1}(\hat{C}^2 + \hat{\Lambda}_p^2)\sin(\hat{\Lambda}_p)\exp(-i\hat{C})\}, \tag{5.5}$$

where $\hat{\Lambda}_p = \Lambda_p l_w$ is the space charge parameter. It follows from Eq. (5.5) that maximal gain $\max(\hat{G}_s) = \max(\mathrm{Re}(\hat{Z}))$ and the detuning $\hat{C}_m$ corresponding to this maximum are universal functions of the space charge parameter $\hat{\Lambda}_p$. The plots of these functions for several values of $\hat{\Lambda}_p$ are presented in Figs. 5.5 and 5.6. The gain curves for several values of $\hat{\Lambda}_p$ are presented in Fig. 5.7. At large values of the space charge parameter, $\hat{\Lambda}_p \gg 1$, maximal gain is achieved at $\hat{C}_m \simeq \hat{\Lambda}_p$ and is equal

$$\max(\hat{G}_s) \simeq (4\hat{\Lambda}_p)^{-1}.$$

The lasing condition, written down for the reduced parameters, is of the form

$$\max(\hat{G}_s) > \hat{\alpha},$$

where $\hat{\alpha} = \alpha/\tau$ is the parameter of resonator losses.

In conclusion of this section we compare the results obtained above with the results obtained in Appendix C, where the problem of the FEL oscillator is formulated as an eigenvalue problem. In the latter case the field in the resonator is represented as a superposition of the oscillations with different longitudinal wavenumbers and time-dependent amplitudes:

$$E_x + iE_y = \sum_m \tilde{E}_m(t) \exp(-i\omega_m t) \sin(k_m z + \delta),$$

where $k_m = m\pi/L - 2i/n'L$, $\omega_m = m\pi c/L$, $\delta = i/n'$, n' is refractive index of material of the mirrors ($|n'| \gg 1$) and m is integer number ($m \gg 1$). In the small signal approximation, solution for the amplitudes of longitudinal modes is seeking in the form $\tilde{E}_m = \text{const} \times \exp(\epsilon t)$. The obtained eigenvalue is of the form:

$$\hat{\epsilon} = 2L\epsilon/c\tau + 4/n'\tau.$$

It was shown in Appendix C that $\hat{\epsilon} = \hat{Z}/2$, so the lasing condition should be written as

$$\max(\mathrm{Re}(\hat{\epsilon})) > \mathrm{Re}(4/n'\tau).$$

In the case of different values of refractive indexes of the mirrors, the value of $2/n'$ should be substituted by

$$2/n' \to 1/n_1' + 1/n_2'.$$

The both approaches are similar at the following interpretation

$$\hat{G}_s = 2\,\mathrm{Re}(\hat{\epsilon}), \quad \Delta\psi_0/\tau = \mathrm{Im}(\hat{\epsilon}), \quad \hat{\alpha} = \mathrm{Re}(8/n'\tau).$$

6. Saturation effects in the FEL oscillator

All the results obtained in the previous section refer to the initial stage of the FEL oscillator operation: in this case the radiation output power grows exponentially in time while the radiation field phase increases linearly in time. Near the saturation point the electrons motion becomes nonlinear, the beam is overmodulated and the radiation output power achieves asymptotically its saturation level. To find the saturation power of the FEL oscillator one should solve equations of the nonlinear FEL oscillator theory. Analytical methods have very limited possibilities in the nonlinear theory, numerical simulations algorithms are more preferable. The most convenient way to calculate the nonlinear mode of the FEL oscillator operation consists in the use of a macroparticle method when one solves the equations of particle motion simultaneously with the Maxwell's equations (see e.g. Refs. [37–39] and references therein). Another approach is based on the assumption that the FEL oscillator output characteristics at saturation may be interpreted in the same way as a conventional laser output characteristics [40]. Using approach of the bunched beam, the authors of Refs. [41,42] have obtained simple formulae describing the saturation effects in the FEL oscillator. In the presented paper we will use the conventional macroparticle method to analyze the nonlinear mode of the FEL oscillator operation.

In the framework of the one-dimensional theory the FEL oscillator output characteristics are determined with 8 parameters

$$\mathcal{E}_0, \quad j_0, \quad \langle(\Delta\mathcal{E})^2\rangle, \quad \kappa_w, \quad H_w, \quad l_w, \quad L, \quad \alpha.$$

Using the similarity techniques when writing down the FEL equations, one can find that all FEL oscillator characteristics at the saturation are determined with three reduced parameters: $\hat{\alpha} = \alpha/\tau$, $\hat{\Lambda}_p$ and $\hat{\Lambda}_T$, where α is attenuation coefficient of the radiation power at one resonator round-trip. The similarity law for the FEL oscillator efficiency η may be written as

$$\hat{\eta} = \eta/\beta = \hat{F}(\hat{\alpha}, \hat{\Lambda}_p, \hat{\Lambda}_T),$$

where $\beta = (4\pi N_w)^{-1}$ and N_w is the number of undulator periods. The universal function $\hat{F}$ is calculated in this section with the self-consistent FEL oscillator equations.

In the same way as it was described in the previous section, we find the change of the field amplitude after undulator pass and, after taking into account reflections on the mirrors, the process of amplification is calculated again, etc. As the field in the resonator is growing, the gain factor G is decreased and approaches asymptotically to the value of the resonator losses α.

In this paper we have limited the analysis of the nonlinear processes in the FEL oscillator with the following assumptions

(i) we study the case of infinitely long electron beam pulse and do not consider the effects connected with the finite pulse duration;

(ii) the lasing frequency ω corresponds to the maximum of the gain in the linear stage, i.e. the value of the detuning parameter $\hat{C}$ is assumed to be equal to $\hat{C}_m$, when increment achieves its maximum at the linear stage;

(iii) we do not consider such physical effects as the longitudinal modes competition, sideband instabilities etc. (see e.g. Refs. [43,44]).

6.1. Self-consistent equations

In the considered model of the FEL oscillator the plane electromagnetic wave reflects by turns from the resonator mirrors. This process can be illustrated with the following simple picture. Let us consider a semi-infinite sequence of plane-parallel equidistantly placed semi-transparent plates. The period of this system is equal to L, where L is the resonator base. In each second period the undulator is placed between the plates. The travelling electromagnetic wave is fed to the system input

$$E_x + iE_y = \tilde{E}\exp[i\omega(z/c - t)].$$

When the wave transmits through the pair of plates, its complex amplitude is multiplied by a factor of $(1 - \alpha/2)$ and when the wave propagates in the undulator, the amplification process takes place. Hence, we should find out the FEL amplifier self-consistent equations.

The self-consistent equations describing amplification process of the wave in the undulator are similar to Eqs. (3.2) and (3.3) describing amplification process in the FEL amplifier. Nevertheless, it is convenient to renormalize these equations to the form

$$d\hat{P}/d\hat{z} = \hat{u}\cos(\psi + \psi_0), \quad d\psi/d\hat{z} = \hat{P} + \hat{C} + \beta\hat{u}\sin(\psi + \psi_0), \tag{6.1}$$

$$d\hat{u}/d\hat{z} = (\tau\hat{j}_1/2)\cos(\psi_0 - \psi_1), \quad d\psi_0/d\hat{z} = -(\tau\hat{j}_1/2\hat{u})\sin(\psi_0 - \psi_1), \tag{6.2}$$

where $\hat{z} = z/l_w$, $\hat{u} = u\omega l_w^2/(c\gamma_z^2\mathcal{E}_0)$ is effective potential of interaction of the particle with the electromagnetic wave, $(u/2)\exp(i\psi_0) = iU = -e\theta_s\tilde{E}/2$, $\hat{P} = \omega P l_w/(c\gamma_z^2\mathcal{E}_0)$, $P = \mathcal{E} - \mathcal{E}_0$ and $\beta = c\gamma_z^2/\omega l_w = (4\pi N_w)^{-1}$ is the efficiency parameter. Definition of the detuning parameter $\hat{C}$ and the gain parameter τ have been introduced in Section 5. Parameter β is inversely proportional to the number of the undulator periods N_w and is always small. Hence, we neglect the summand proportional to β in the second equation (6.1).

When performing numerical simulations, the value of the detuning $\hat{C}$ is set to be $\hat{C}_m$ corresponding to the maximum of the small signal gain calculated in Section 5. The amplitude and phase of the first harmonic of the beam current density, j_1 and ψ_1, are calculated as in

$$j_1\cos\psi_1 = \frac{1}{\pi}\int_0^{2\pi} j_z\cos\psi d\psi, \quad j_1\sin\psi_1 = -\frac{1}{\pi}\int_0^{2\pi} j_z\sin\psi d\psi.$$

6.2. Nonlinear simulation algorithm

We simulate the electron beam with N macroparticles per interval $(0, 2\pi)$ over phase ψ. The beam current density $\hat{j}_z = j_z/j_0$ is calculated as

$$\hat{j}_z = -\frac{2\pi}{N}\sum_{k=1}^{N}\delta(\psi - \psi_{(k)}),$$

where $\psi_{(k)}$ are the phases of the particles and $\delta(\psi - \psi_{(k)})$ is the delta function. In accordance with its definition the function $\hat{j}_z$ has the following normalization

$$\int_0^{2\pi}\hat{j}_z d\psi = -2\pi.$$

The amplitude and phase of the first harmonic of the beam current density are given with the expressions

$$\hat{j}_1\cos\psi_1 = \frac{1}{\pi}\int_0^{2\pi}\hat{j}_z\cos\psi d\psi = -\frac{2}{N}\sum_{k=1}^{N}\cos\psi_{(k)},$$

$$\hat{j}_1\sin\psi_1 = -\frac{1}{\pi}\int_0^{2\pi}\hat{j}_z\sin\psi d\psi = \frac{2}{N}\sum_{k=1}^{N}\sin\psi_{(k)}.$$

The simulation is performed as follows. At the moment of time t_j we have at the undulator entrance the unmodulated electron beam and the electromagnetic field with amplitude $E^{(j)} = |\tilde{E}(t_j)|$ and phase $\psi_0^{(j)}$, i.e. at $z = 0$ we have $(k = 1, \ldots, N)$

$$\hat{P}_{(k)} = 0, \quad \hat{j}_1 = 0, \quad \hat{u} = \hat{u}^{(j)} = E^{(j)}/E_0, \quad \psi_0 = \psi_0^{(j)},$$

where $E_0 = (c\gamma_z^2\mathcal{E}_0)/(e\omega_m\theta_s l_w^2)$. The equation of motion (6.1) and the field equations (6.2) are solved numerically with the Runge-Kutta scheme. After one undulator pass we calculate the increase

of the field amplitude $\Delta\hat{u}^{(j)}$ and its phase $\Delta\psi_0^{(j)}$. Then, after the radiation round-trip in the resonator, i.e. at the moment of time $t_{j+1} = t_j + 2L/c$, we obtain the following initial conditions at the undulator entrance

$$\hat{P}_{(k)} = 0, \quad \hat{j}_1 = 0, \quad \hat{u} = \hat{u}^{(j+1)} = [1 - \alpha/2][\Delta\hat{u}^{(j)} + \hat{u}^{(j)}], \quad \psi_0 = \psi_0^{(j)} + \Delta\psi_0^{(j)}.$$

We do not take into account the phase change after the reflection from the resonator mirrors because this effect does not influence the FEL oscillator operation in the one-dimensional approximation. The multiple using of this procedure under the given initial conditions for the radiation field at the moment of time t_0 enables one to obtain the field evolution in time.

6.3. *The resonator losses and efficiency optimization*

At the linear stage of lasing, when $\hat{u} \ll 1$, the field amplitude grows in time exponentially. Near the saturation, when $\hat{u} \sim 1$, the electron beam is overmodulated which leads to the slower growing of the field amplitude. When the power gain becomes equal to the resonator losses, the field amplitude $\hat{u}$ achieves asymptotically its maximal value $\hat{u}^{(\infty)}$. So, field amplitude at saturation $\hat{u}^{(\infty)}$ depends on the value of the resonator losses and a problem of the FEL efficiency optimization is arisen.

When the field amplification per one resonator pass is small, the saturation condition may be written down as

$$\Delta\hat{u}^{(\infty)} = \alpha\hat{u}^{(\infty)}/2. \tag{6.3}$$

Let us consider now Eqs. (6.1) and (6.2) more thoroughly. First, the value of $\Delta\hat{u}^{(j)}$ is proportional to the gain parameter τ. Further, the amplitude $\hat{j}_1$ and the phase $(\psi_1 - \psi_0)$ of the first harmonic of the beam current density are the functions of the only parameter $\hat{u}$ – the field amplitude in the resonator at the given moment. As a result, at the saturation the field amplitude increase $\Delta\hat{u}^{(\infty)}$ may be represented as

$$\Delta\hat{u}^{(\infty)} = \tau f(\hat{u}^{(\infty)}). \tag{6.4}$$

Hence, it follows from Eqs. (6.3) and (6.4) that in the case of the negligibly small space charge field and energy spread the field amplitude at the saturation is the function of the only parameter, namely the reduced damping factor $\hat{\alpha} = \alpha/\tau$

$$\hat{u}^{(\infty)} = f_1(\hat{\alpha}).$$

The FEL efficiency at the saturation is defined usually as the ratio of the radiation power losses in the resonator to the electron beam power. In the case under consideration the density of the radiation power losses is given with expression

$$\Pi = cE^{(\infty)}\Delta E^{(\infty)}/(2\pi),$$

so we have for the FEL efficiency

$$\eta = e\Pi/(\mathcal{E}_0 j_0) = \beta\hat{u}^{(\infty)}\Delta\hat{u}^{(\infty)}/\tau,$$

where β is introduced above the efficiency parameter which is inversely proportional to the number of the undulator periods N_w

$$\beta = c\gamma_z^2/\omega l_w = (4\pi N_w)^{-1}.$$

It is convenient for the further consideration to introduce the reduced efficiency $\hat{\eta} = \eta/\beta$. Using relation (6.3) we get

$$\hat{\eta} = \eta/\beta = \hat{\alpha}(\hat{u}^{(\infty)})^2/2. \tag{6.5}$$

Now let us show that the conservation energy law takes place in the considered FEL oscillator model. We have introduced above the FEL efficiency in terms of the radiation power. On the other hand, the FEL efficiency may be expressed in terms of the electron energy losses: $\eta = -\langle P\rangle/\mathcal{E}_0$, where $P = (\mathcal{E} - \mathcal{E}_0)$, $\mathcal{E}_0$ is the nominal electron energy at the undulator entrance and symbol $\langle \ldots \rangle$ means the averaging over beam electrons. Using the definition of the reduced energy deviation $\hat{P}$, we find that the reduced efficiency is expressed as $\hat{\eta} = -\langle \hat{P}\rangle$. One can find from the system of canonical equations (6.1) that the energy losses of the electron beam are equal

$$\langle d\hat{P}/d\hat{z}\rangle = \hat{u}N^{-1}\sum_{k=1}^{N}\cos(\psi_{(k)} + \psi_0).$$

Remembering that

$$N^{-1}\sum_{k=1}^{N}\cos(\psi_{(k)} + \psi_0) = -\tfrac{1}{2}\hat{j}_1\cos(\psi_1 - \psi_0),$$

and using the first equation of the system (6.2) we get

$$\langle d\hat{P}/d\hat{z}\rangle = -(\hat{u}/\tau)d\hat{u}/d\hat{z}.$$

It follows from this relation that in the limit of small gain per one resonator pass, the reduced efficiency at the saturation is given by

$$\hat{\eta} = -\langle \hat{P}\rangle = \hat{u}^{(\infty)}\Delta\hat{u}^{(\infty)}/\tau = \hat{\alpha}(\hat{u}^{(\infty)})^2/2.$$

Comparing this expression with Eq. (6.5) we find that the total energy of the electron beam and radiation conserves.

Using the approach presented above we have calculated the universal characteristics of the FEL oscillator at saturation. In all cases we have assumed that the FEL lasing frequency ω corresponds to the maximum increment (i.e. to the value of the detuning parameter $\hat{C} = \hat{C}_m$).

The plot of the reduced FEL efficiency versus the reduced damping factor $\hat{\alpha}$ is presented in Fig. 6.1. It is clearly seen that there is the optimum value of $\hat{\alpha}$ when the FEL efficiency achieves its maximum. The existence of this maximum may be easily explained as follows. When the value of radiation losses in the resonator is increased (i.e. $\hat{\alpha}$ is increased), the ratio of the radiation losses to the radiation power stored in the resonator is increased, too. But at the same time the value of the radiation power stored in the resonator is decreased. When the value of $\hat{\alpha}$ is rather large, near the lasing threshold, the radiation field amplitude in the resonator becomes small which leads to the weak energy exchange between the radiation field and the electron beam. Using the plot in Fig. 6.1 one may find the universal values of the maximum reduced efficiency and the optimum value of the reduced damping factor [39]

$$\hat{\eta}_{\max} = 3.62, \quad \hat{\alpha}_{\text{opt}} = 0.028.$$

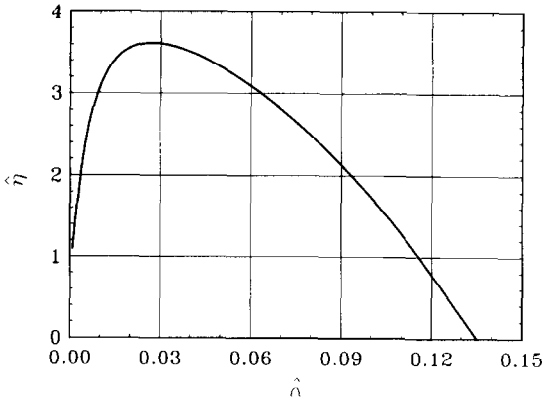

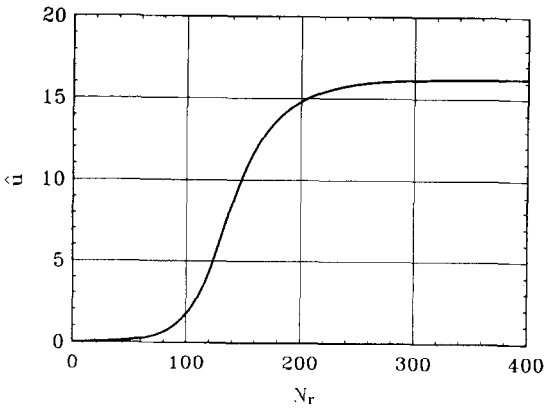

Fig. 6.1. The reduced efficiency versus the reduced damping factor. The FEL oscillator operates at the saturation. It is assumed that $\hat{\Lambda}_T = 0$ and $\hat{\Lambda}_p = 0$..

Fig. 6.2. The reduced field amplitude in the resonator versus the number of the resonator round-trips at optimal value of the reduced damping factor $\hat{\alpha} = 0.028$. Here $\hat{\Lambda}_T^2 = 0$, $\hat{\Lambda}_p = 0$, $\tau = 1$ and $\hat{u}^{(0)} = 0.01$.

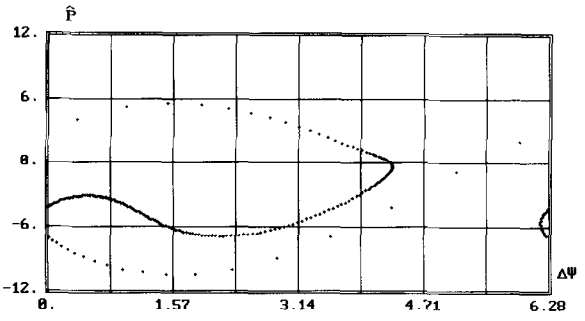

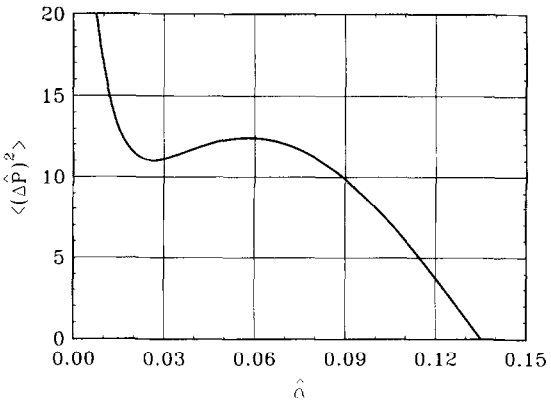

Fig. 6.3. Phase space distribution of the particles at the undulator exit. The FEL oscillator operates at the saturation. Here $\hat{\Lambda}_T^2 = 0$, $\hat{\Lambda}_p = 0$ and $\hat{\alpha}_{opt} = 0.028$.

Fig. 6.4. The reduced rms energy spread of the particles at the undulator exit versus the reduced damping factor. The FEL oscillator operates at the saturation. Here $\hat{\Lambda}_T^2 = 0$ and $\hat{\Lambda}_p = 0$..

The value of the FEL efficiency is calculated with the relation $\eta_{max} = 0.29/N_w$. The plot in Fig. 6.2 illustrates the time evolution of the field stored in the resonator at optimal value of the resonator losses α_{opt}.

Another practically important characteristic of the FEL oscillator at the saturation is the electron energy distribution at the undulator output. Fig. 6.3 presents the phase distributions of electrons at the undulator output when the FEL oscillator operates at the saturation. Fig. 6.4 illustrates the reduced energy spread of electrons at the undulator output as a function of the reduced damping factor $\hat{\alpha}$. It is seen from this plot that near the lasing threshold, when $\hat{\alpha}$ is decreasing, the energy spread is increased. Then, after achieving maximum, it begins to decrease. At the value of $\hat{\alpha} = \hat{\alpha}_{opt} = 0.028$ the energy spread $\langle(\Delta\hat{P})^2\rangle = f(\hat{\alpha})$ achieves its minimum. The energy spread $\langle(\Delta\mathcal{E})^2\rangle/\mathcal{E}_0^2$ and the

reduced energy spread $\langle(\Delta\hat{P})^2\rangle$ are connected with the following relation

$$\langle(\Delta\mathcal{E})^2\rangle/\mathcal{E}_0^2 = N^{-1}\mathcal{E}_0^{-2}\sum_{k=1}^{N}(\mathcal{E}_{(k)} - \langle\mathcal{E}\rangle)^2 = \beta^2 N^{-1}\sum_{k=1}^{N}(\hat{P}_{(k)} - \langle\hat{P}\rangle)^2 = \beta^2\langle(\Delta\hat{P})^2\rangle,$$

where the value of $\langle(\Delta\hat{P})^2\rangle$ may be found with the help of Fig. 6.4. At the optimal value of the resonator losses, at $\hat{\alpha} = \hat{\alpha}_{\rm opt} = 0.028$, the energy spread of electrons at the undulator output is given with the simple formula

$$\sqrt{\langle(\Delta\mathcal{E}/\mathcal{E}_0)^2\rangle} \simeq 0.26/N_w.$$

The number of macroparticles during the simulations has been chosen usually equal to $N = 100\ldots200$. In this case the simulation results do not depend on the value of N with an accuracy better than 10^{-3}. The testing runs have been performed at the small signal regime. In Fig. 5.1 we compare the results of the increment calculations obtained with the analytical formula (5.3) and with the numerical simulations. There is good agreement between the numerical and analytical results.

6.4. *Space charge and the FEL efficiency*

Let us now study the influence of the space charge field on the nonlinear regime of the FEL oscillator operation. This requires to include the corresponding corrections in the equation of motion (6.1) which are similar to those of the FEL amplifier equations (3.16)

$$\frac{d\hat{P}_{(k)}}{d\hat{z}} = \hat{u}\cos(\psi_{(k)} + \psi_0) + \hat{\Lambda}_p^2\left\{\frac{1}{N}\sum_{i\neq k}[\pi\,\mathrm{sgn}(\psi_{(k)} - \psi_{(i)}) - (\psi_{(k)} - \psi_{(i)})]\right\},$$

$$\frac{d\psi_{(k)}}{d\hat{z}} = \hat{P}_{(k)} + \hat{C}. \tag{6.6}$$

Here the normalization procedure has been performed in the same way as it was done in section 5: $\hat{z} = z/l_w$, $\hat{C} = Cl_w$, $\hat{P} = \omega P l_w/(c\gamma_z^2\mathcal{E}_0)$, $\hat{\Lambda}_p^2 = \Lambda_p^2 l_w^2 = 4\pi j_0 l_w^2/(\gamma_z^2\gamma I_A)$, and $\hat{u} = u\omega l_w^2/(c\gamma_z^2\mathcal{E}_0)$.

When the space charge fields are taken into account, the reduced efficiency is the universal function of two parameters: the radiation damping factor $\hat{\alpha}$ and space charge parameter $\hat{\Lambda}_p$. At each value of the space parameter $\hat{\Lambda}_p$ there is the value of the optimal value of $\hat{\alpha}_{\rm opt}$ when the FEL efficiency achieves its maximum. This maximal efficiency and $\hat{\alpha}_{\rm opt}$ are universal functions of the only parameter, namely $\hat{\Lambda}_p$. The dependence of the maximal FEL efficiency on the space charge parameter $\hat{\Lambda}_p$ is presented in Fig. 6.5. It is seen that efficiency of the FEL oscillator grows with $\hat{\Lambda}_p$. Fig. 6.6 illustrates the dependence of the optimal value of the radiation damping factor $\hat{\alpha}_{\rm opt}$ on the space charge parameter $\hat{\Lambda}_p$ and the plots in Fig. 6.7 show the dependence of the efficiency on the radiation damping factor $\hat{\alpha}$ at several values of $\hat{\Lambda}_p$.

The simulations have been tested at the linear stage of the FEL oscillator operation and Fig. 5.7 illustrates this. At the number of macroparticles $N = 200$ the divergence of the analytical and simulation results does not exceed 10^{-3}.

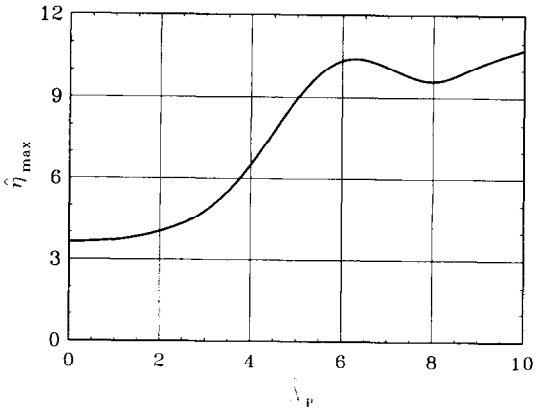

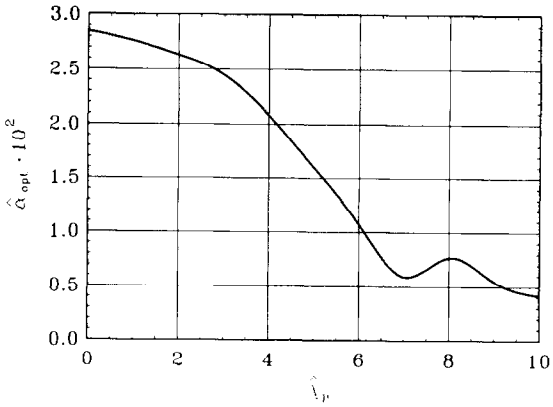

Fig. 6.5. The maximal reduced efficiency versus the space charge parameter $\hat{\Lambda}_p$. The FEL oscillator operates at the saturation. Here $\hat{\Lambda}_T^2 = 0$..

Fig. 6.6. The optimal reduced damping factor versus the space charge parameter $\hat{\Lambda}_p$. The FEL oscillator operates at the saturation. Here $\hat{\Lambda}_T^2 = 0$..

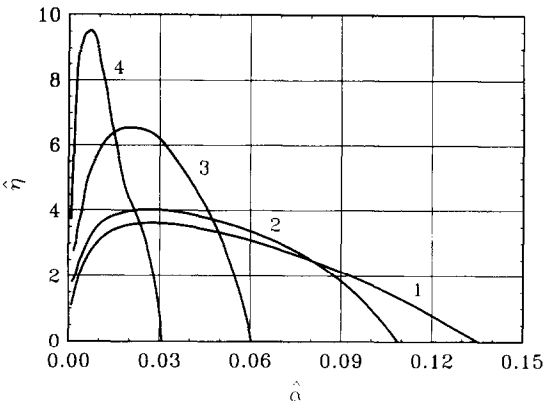

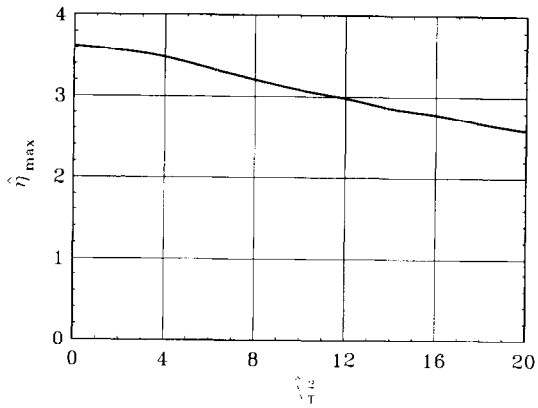

Fig. 6.7. The reduced efficiency versus the reduced damping factor for several values of the space charge parameter $\hat{\Lambda}_p$. The FEL oscillator operates at the saturation. Here $\hat{\Lambda}_T^2 = 0$. Curve (1): $\hat{\Lambda}_p = 0$, curve (2): $\hat{\Lambda}_p = 2$, curve (3): $\hat{\Lambda}_p = 4$ and curve (4): $\hat{\Lambda}_p = 8$.

Fig. 6.8. The maximal reduced efficiency versus the energy spread parameter $\hat{\Lambda}_T^2$. The FEL oscillator operates at the saturation. Here $\hat{\Lambda}_p = 0$..

6.5. *Energy spread and the FEL efficiency*

In the presence of the initial energy spread in the electron beam the FEL reduced efficiency is the universal function of three parameters: $\hat{\alpha}$, $\hat{\Lambda}_p$ and $\hat{\Lambda}_T^2$ (we assume here the energy spread to be the Gaussian). Let us consider the case of negligibly small space charge field ($\hat{\Lambda}_p^2 \to 0$). In this case the maximal reduced FEL efficiency and the optimal value of the radiation damping factor $\hat{\alpha}_{opt}$ are the universal functions of the energy spread parameter $\hat{\Lambda}_T^2$. The plots of these functions are presented in Figs. 6.8 and 6.9, and in Fig. 6.10 the dependencies of the FEL efficiency versus the radiation damping factor are plotted.

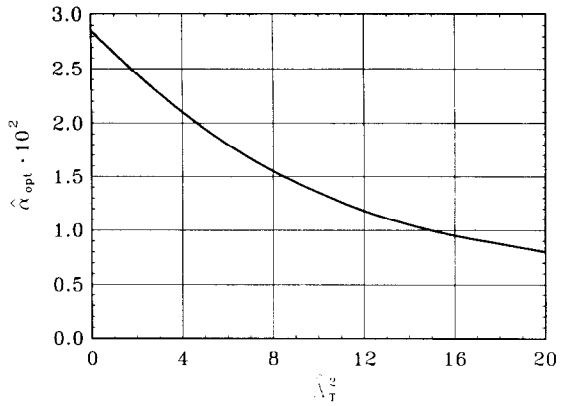

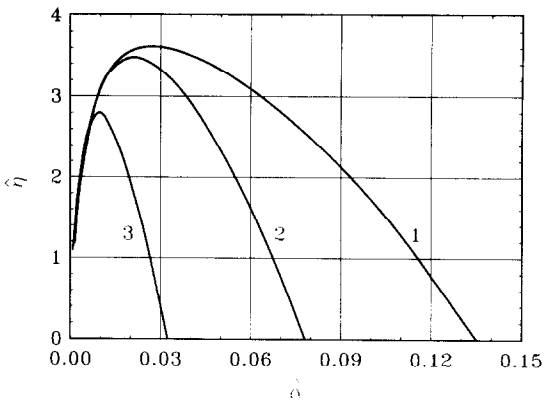

Fig. 6.9. The optimal reduced damping factor versus the energy spread parameter $\hat{\Lambda}_T^2$. The FEL oscillator operates at the saturation. Here $\hat{\Lambda}_p = 0$..

Fig. 6.10. The reduced efficiency versus reduced damping factor. The FEL oscillator operates at the saturation. Here $\hat{\Lambda}_p = 0$. Curve (1): $\hat{\Lambda}_T^2 = 0$, curve (2): $\hat{\Lambda}_T^2 = 4$ and curve (3): $\hat{\Lambda}_T^2 = 16$.

The code for simulation of the energy spread effects operates in the same way as it was described in Section 3. The testing of the code has been performed at the linear stage and Fig. 5.4 illustrates this. The macroparticle ensemble for these simulation runs has been prepared as follows. First, we have prepared the micro-ensemble of 200 particles corresponding to the Gaussian energy distribution. Then we have distributed 4 micro-ensembles evenly over phase ψ from 0 to 2π. It is seen from the plots that there is good agreement between the simulation and analytical results.

6.6. *Some generalizations*

Let us generalize the results obtained in this section. First, we show the method of finding the optimal relation between the transmission and absorption coefficients of the mirrors. The radiation damping factor α appearing in expressions (6.3) and (6.5) may be presented in the form

$$\alpha = T_1 + T_2 + \Gamma_1 + \Gamma_2,$$

where (T_1, Γ_1) and (T_2, Γ_2) are the transmission and absorption coefficients of the first and the second resonator mirror, respectively. Let us also introduce the practical FEL efficiency η_{out} given with the ratio of the output FEL radiation power to the electron beam power and the reduced practical efficiency $\hat{\eta}_{\text{out}}$

$$\hat{\eta}_{\text{out}} = \eta_{\text{out}}/\beta = T(T+\Gamma)^{-1}\hat{\eta}$$

where $T = T_1 + T_2$ and $\Gamma = \Gamma_1 + \Gamma_2$. Calculating $\hat{\alpha} = (T+\Gamma)/\tau$ one can find with the help of Fig. 6.1 the reduced efficiency $\hat{\eta}$. The practical efficiency $\hat{\eta}_{\text{out}}$ can be optimized, for example, by the appropriate choice of the transmission coefficient T of the mirror at the constant value of the absorption coefficient Γ. The plots in Figs. 6.11 and 6.12 show the dependence of this maximal practical efficiency $\max(\hat{\eta}_{\text{out}})$ and the corresponding optimal value of the transmission coefficient $\hat{T}_{\text{opt}} = T/\tau$ on the absorption coefficient $\hat{\Gamma} = \Gamma/\tau$. Fig. 6.13 illustrates the practical efficiency dependence on the transmission coefficient for several values of the absorption coefficient $\hat{\Gamma}$.

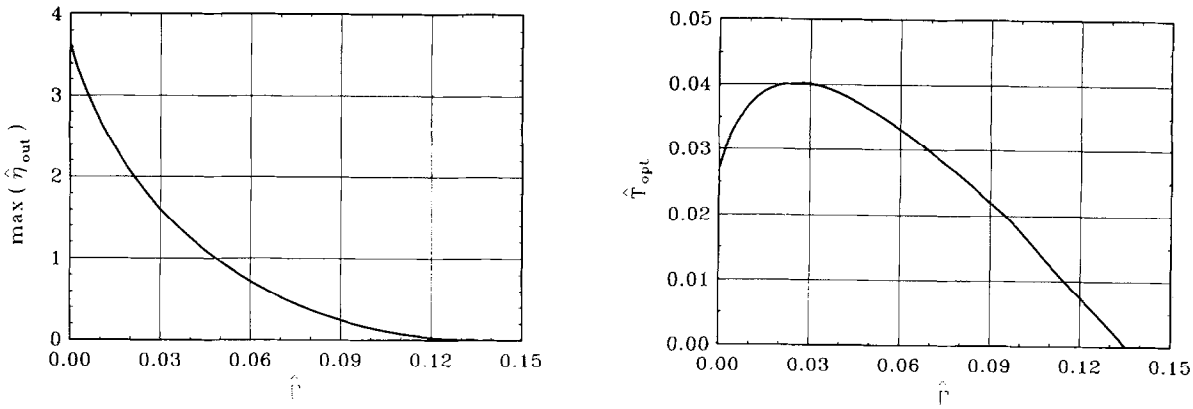

Fig. 6.11. The maximal reduced practical efficiency versus the reduced absorption coefficient $\hat{\Gamma}$. The FEL oscillator operates at the saturation. Here $\hat{\Lambda}_T^2 = 0$ and $\hat{\Lambda}_p = 0$..

Fig. 6.12. The optimal reduced transmission coefficient $\hat{T}$ versus the reduced absorption coefficient $\hat{\Gamma}$. The FEL oscillator operates at the saturation. Here $\hat{\Lambda}_T^2 = 0$ and $\hat{\Lambda}_p = 0$..

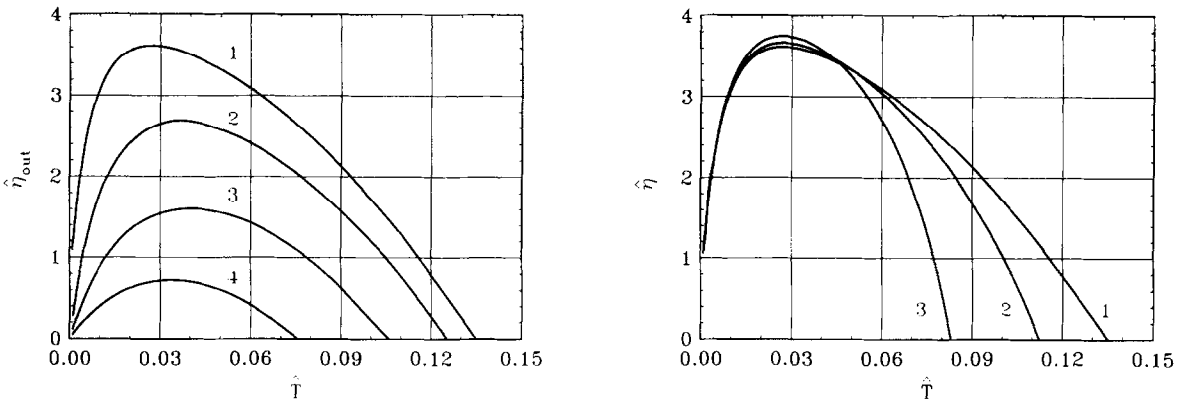

Fig. 6.13. The reduced practical efficiency versus the reduced transmission coefficient $\hat{T}$ at several values of the absorption coefficient $\hat{\Gamma}$. The FEL oscillator operates at the saturation. Here $\hat{\Lambda}_T^2 = 0$ and $\hat{\Lambda}_p = 0$. Curve (1): $\hat{\Gamma} = 0$, curve (2): $\hat{\Gamma} = 0.01$, curve (3): $\hat{\Gamma} = 0.03$ and curve (4): $\hat{\Gamma} = 0.06$.

Fig. 6.14. The reduced efficiency versus the reduced transmission coefficient $\hat{T}$ for several values of the gain parameter τ. The FEL oscillator operates in the saturation. Here $\hat{\Lambda}_T^2 = 0, \hat{\Lambda}_p = 0$ and $\hat{\Gamma} = 0$. Curve (1): $\tau \to 0$, curve (2): $\tau = 2$ and curve (3): $\tau = 6$,.

All the results presented above refer to the case of the small radiation field amplification per one resonator pass. Let us consider now the FEL oscillator with the field gain per one resonator pass about of unity. The analysis of the obtained results will allow us to obtain the validity region of the approximation of the small amplification.

For simplicity we consider the resonator equipped with two mirrors: one perfectly reflecting and another with the transmission coefficient T and absorption coefficient $\Gamma \simeq 0$.

According to the self-consistent equations (6.1) and (6.2), the approximate criterion of the small field amplification is given with the small value of the gain parameter τ, while the equations itself

are valid in the case of the high field gain. Formula (6.4) remains to be valid in the case of the high amplification, while the condition (6.3) should be changed to

$$T(\hat{u}^{(\infty)} + \Delta\hat{u}^{(\infty)})^2 = 2\hat{u}^{(\infty)}\Delta\hat{u}^{(\infty)} + (\Delta\hat{u}^{(\infty)})^2. \tag{6.7}$$

The FEL reduced efficiency at the arbitrary value of the gain parameter τ is given with the following expression

$$\hat{\eta} = \eta/\beta = T(\hat{u}^{(\infty)} + \Delta\hat{u}^{(\infty)})^2/(2\tau). \tag{6.8}$$

Substituting (6.4) into (6.7), we obtain that the field amplitude $\hat{u}^{(\infty)}$ at the saturation and the reduced efficiency (in accordance with Eq. (6.8)) are functions of two parameters, namely T and τ:

$$\hat{u}^{(\infty)} = f_1(T,\tau), \quad \hat{\eta} = f_2(T,\tau).$$

The comparative results of the strict and asymptotical calculations are presented in Fig. 6.14. The dependence of the optimal value of the reduced detuning $\hat{C}_m$ on parameter τ has been taken into account in this calculations. The curves 2 and 3 are simulation results with the formulae (6.4) and (6.8). The curve 1 is calculated with the approximation of the small amplification (see Fig. 6.1). It is seen that in the region of practical interest, at $\hat{T} = T/\tau \simeq 0.03$, the values of the reduced efficiency $\hat{\eta}$ is close to the asymptotical ones even when parameter $\tau \sim 5$. Therefore, all the plots presented in this section for the case of the small signal amplification can be used in practice, even when the field amplification per one resonator pass has an order of several tens of percents.

All the results presented above in Sections 5 and 6 refer to the case of circularly polarized radiation and helical undulator. They may be simply transferred to the case of the linearly polarized radiation and a planar undulator with magnetic field

$$H_y = 0, \quad H_x = H_l\cos(\kappa_w z),$$

by the following redetermination of the parameters

$$\tau \to \tau' = \pi\omega\theta_l^2 j_0 l_w^3 A_{JJ}^2 (c\gamma_l^2\gamma I_A)^{-1}, \quad E_0 \to E_0' = 2\mathcal{E}_0\gamma_l^2 c(e\theta_l\omega l_w^2 A_{JJ})^{-1},$$
$$\hat{C} \to \hat{C}' = (\kappa_w - \omega(2c)^{-1}\gamma_l^{-2})l_w, \quad \beta \to \beta' = c\gamma_l^2(\omega l_w)^{-1} = (4\pi N_w)^{-1},$$
$$\hat{\Lambda}_p \to \hat{\Lambda}_p' = l_w[4\pi j_0\gamma^{-1}\gamma_l^{-2}I_A^{-1}]^{1/2},$$
$$\hat{\Lambda}_T \to \hat{\Lambda}_T' = l_w\omega\gamma_l^{-2}\mathcal{E}_0^{-1}c^{-1}\sqrt{\langle(\Delta\mathcal{E})^2\rangle} = 4\pi N_w\sqrt{\langle(\Delta\mathcal{E})^2\rangle/\mathcal{E}_0^2}.$$

Here the following notations have been introduced: $\theta_l = eH_l/(\mathcal{E}_0\kappa_w)$, $\gamma_l^{-2} = \gamma^{-2} + \theta_l^2/2$, $A_{JJ} = [J_0(\nu) - J_1(\nu)]$, $\nu = \theta_l^2\omega/(8c\kappa_w)$ and J_0 and J_1 are Bessel functions.

To illustrate the calculation of the output characteristics of the FEL oscillator with the planar undulator let us consider, for example, the saturation regime. With the plot in Fig. 6.1 we find, that in the case of negligibly small space charge fields and energy spread

$$\hat{\Lambda}_p' = \Lambda_p' l_w \to 0, \quad \hat{\Lambda}_T' = \Lambda_T' l_w \to 0,$$

the FEL oscillator efficiency achieves its maximum $\eta_{\max} = 3.62 \times \beta'$ when the field damping factor is equal to: $\alpha = 0.028 \times \tau'$.

In conclusion of this section it should be noted that the one-dimensional theory is widely used for calculations of practical devices. The main reason for this is that it provides the most simple way for taking into account diffraction effects. As a rule, optical resonators with spherical mirrors are used in the real systems. At small field gain, the electron beam does not affect significantly the field eigenmode in the resonator and it remains to be close to that of the empty resonator. As a result, the motion of electrons can be calculated in the approximation of the given field. To take into account the field distribution in the resonator, the notion of the filling factor is introduced. For instance, when the field eigenmode in the resonator is a Gaussian TEM_{00} one, the field distribution in the waist is of the form

$$|\tilde{E}| \propto \exp(-r^2/w_0^2),$$

where r is the transverse coordinate and w_0 is the size of the waist. When transverse size of the electron beam is much less than w_0 and when we can neglect the change of the Gaussian mode along the undulator, we substitute in the one-dimensional equations the value of the beam current density j_0 by effective value

$$(j_0)_{eff} = 2I_0/\pi w_0^2,$$

where I_0 is the total beam current. In many practical situation such an approach provides adequate way for calculation the FEL oscillator parameters.

7. FEL oscillator with a tapered undulator

Tapering of the undulator parameters, for the first time proposed in Ref. [29], is widely used now to increase the efficiency of a free electron laser. In Section 4 we have performed detailed analysis of application of the undulator tapering to increase the FEL amplifier efficiency and have shown that the efficiency increase is achieved by the adiabatic change of the resonant energy, for instance, with the undulator field decrease at a fixed undulator period.

In the case of the FEL amplifier all the parameters influencing the resonance condition (the undulator field and period, the frequency of the amplified wave and the initial electron energy), are defined by experimenters. In comparison with the FEL amplifier, the situation with the FEL oscillator is more complicated because the lasing frequency is defined by the condition of the maximum amplification in the small-signal regime (it takes place when one can neglect the longitudinal mode competition and the sideband instabilities). The position of the amplification maximum depends on the depth of the tapering (see e.g. Ref. [45]). Detailed analysis of this effect has been performed in Ref. [46]. It was shown that the lasing frequency shift due to the tapering may lead to the situation when the particles are far from the exact resonance at the undulator entrance. At some values of the depth of the tapering this effect leads to the significant decrease of the FEL oscillator efficiency when the undulator parameters are tapered in the same way as in the FEL amplifier (for instance, by decreasing the undulator field at fixed period). It was shown in Ref. [46] that in some cases quite a different way of tapering is more preferable, for instance, with the undulator field increase at the fixed period (so called "negative tapering").

In this section we consider the one-dimensional theory of the FEL oscillator with a linear law of undulator tapering. The simplest case is under study: we do not take into account the space charge

fields and energy spread in the beam. The field amplification per one resonator pass is assumed to be small, the electron pulse length is infinitely long and we do not take into account the longitudinal mode competition.

7.1. Small-signal mode of operation

To calculate small signal mode of the FEL oscillator operation, we use the approach similar to that used in Section 5.

The electron beam moves along the axis of the helical undulator with the length l_w (the case of a planar undulator is discussed in the end of this section). The magnetic field at the undulator axis is of the form

$$H_x + iH_y = H_w(z)\exp\left[-i\int \kappa_w(z)dz\right].$$

The electric field of the synchronous with the electron beam wave is presented in the complex form

$$E_x + iE_y = \tilde{E}\exp[i\omega(z/c - t)].$$

To describe the electron motion we use the Hamiltonian formalism with the "energy-phase" variables. In this representation the electron energy $\mathcal{E}$ is canonical momentum conjugated with the phase

$$\psi = \int \kappa_w(z)dz + \omega(z/c - t)$$

as canonical coordinate. When the electron energy deviation from the nominal value $\mathcal{E}_0$ is small, we can write the following expression for Hamiltonian (we neglect the space charge fields here)

$$H(P,\psi,z) = C(z)P + \omega P^2/2c\gamma_z^2\mathcal{E}_0 - [Ue^{i\psi} + C.C.](1 - P/\mathcal{E}_0), \tag{7.1}$$

where $C(z) = \kappa_w(z) - [1 + K^2(z)]\omega/2c\gamma^2$ is the detuning of the particle with the nominal energy $\mathcal{E}_0$, $\gamma = \mathcal{E}_0/mc^2$, $\gamma_z^{-2} = \gamma^{-2} + \theta_s^2$, $K(z) = eH_w(z)/\kappa_w(z)mc^2$ is the undulator parameter, m and $-e$ are, respectively the mass and charge of the electron, $U = -e\theta_s\tilde{E}/2i$ is the complex amplitude of effective potential and $\theta_s = K(0)/\gamma$ is the electron rotation angle at the undulator entrance. We assume relative change of the undulator parameters to be a small value, $|\Delta H_w/H_w(0)|$, $|\Delta\kappa_w/\kappa_w(0)| \ll 1)$, so we neglect these changes in the amplitude factors and keep them only in the detuning.

The evolution of the electron beam distribution function f is described by the kinetic equation

$$\frac{\partial f}{\partial z} + \frac{\partial H}{\partial P}\frac{\partial f}{\partial \psi} - \frac{\partial H}{\partial \psi}\frac{\partial f}{\partial P} = 0.$$

In the linear approximation we shall seek the solution for f in the form

$$f = f_0 + \tilde{f}_1(P,z)e^{i\psi} + \text{c.c.}$$

and then we have for the complex amplitude $\tilde{f}_1$ the following equation

$$\partial\tilde{f}_1/\partial z + i[C(z) + P\omega/c\gamma_z^2\mathcal{E}_0]\tilde{f}_1 + iU\partial f_0/\partial P = 0. \tag{7.2}$$

When one has an unmodulated electron beam at the undulator entrance, the solution for $\tilde{f}_1$ has the form

$$\tilde{f}_1 = -\exp[-iF(z)]\int_0^z dz' iU df_0/dP \exp[iF(z')], \tag{7.3}$$

where $F(z) = \int_0^z [C(s) + P\omega/c\gamma_z^2\mathcal{E}_0]ds$. Further on we shall consider only the case of the linear tapering when the detuning changes according to the law: $C(z) = C_0 + bz$. The longitudinal component of the beam current is equal to

$$j_z = -j_0 + \tilde{j}_1 e^{i\psi} + \text{c.c.}, \quad j_0 \simeq ecn_0, \quad \tilde{j}_1 \simeq -ec\int \tilde{f}_1 dP,$$

where n_0 is the beam density at $z = 0$. In the framework of the one-dimensional model, from Maxwell's equations we get the following equation for the slowly changing amplitudes $\tilde{E}(z)$ and $\tilde{j}_1(z)$

$$d\tilde{E}/dz = -2\pi\theta_s c^{-1}\tilde{j}_1(z). \tag{7.4}$$

In this paper we consider the case of the "cold" electron beam when the initial distribution function of the electron beam is $f_0 = n_0\delta(P)$, where $\delta(\ldots)$ is the delta-function. Substituting this expression into Eq. (7.3) and after integrating over P we get the expression for $\tilde{j}_1(z)$. Then we substitute the obtained result into Eq. (7.4) and after integration over z we get the following expression for the field amplification per one undulator pass (we assume here a small change of field $\tilde{E}$ per one pass)

$$\tilde{E}(l_w)/\tilde{E}(0) - 1 = Z = -i\pi\theta_s^2 e j_0 \omega (c^2\gamma_z^2\mathcal{E}_0)^{-1}\int_0^{l_w} dz \int_0^z d\zeta(\zeta - z)\Phi(\zeta, z),$$

where $\Phi(\zeta, z) = \exp[iC_0(\zeta - z) + ib(\zeta^2 - z^2)/2]$. After performing the normalization procedure, we obtain the expression for the function $\hat{Z} = 2Z/\tau$

$$\hat{Z} = i\int_0^1 d\xi \int_0^\xi d\xi' \xi' \exp\{-i[\hat{C}_0\xi' + \hat{b}\xi\xi' - \hat{b}(\xi')^2/2]\}. \tag{7.5}$$

In the same way as it was done in the previous sections, we define the reduced gain coefficient as $\hat{G}_s = G_s/\tau = \text{Re}\,(\hat{Z})$. Then, from Eq. (7.5) we have:

$$\hat{G}_s = \int_0^1 d\xi \int_0^\xi d\xi' \xi' \sin[\hat{C}_0\xi' + \hat{b}\xi\xi' - \hat{b}(\xi')^2/2], \tag{7.6}$$

where $\hat{C}_0 = C_0 l_w$, $\hat{b} = bl_w^2$ and $\tau = 2\pi\theta_s^2 j_0 \omega l_w^3/I_A\gamma_z^2\gamma c$ is the gain parameter introduced in Section 5.

Let us express the tapering parameter $\hat{b}$ in terms of the undulator parameters. At the linear change of the undulator period $\lambda_w = 2\pi/\kappa_w$ and fixed undulator parameter K, we get

$$\hat{b} \simeq -2\pi N_w[\lambda_w(l_w) - \lambda_w(0)]/\lambda_w(0),$$

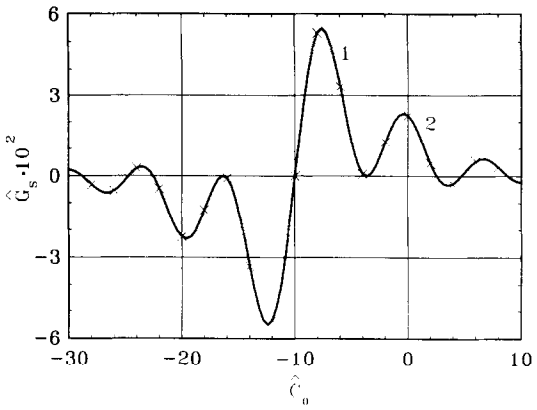

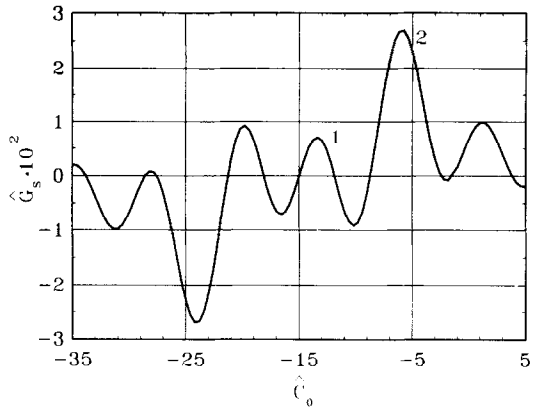

Fig. 7.1. The reduced small-signal gain $\hat{G}_s$ versus the reduced detuning $\hat{C}_0$ at the undulator entrance. Here $\hat{b} = 20$, (1) is the first maximum and (2) is the second maximum. The full curve is calculated with formula (7.6) and the crosses are the results of numerical calculations with formulae (6.1) and (6.2).

Fig. 7.2. The reduced small-signal gain $\hat{G}_s$ versus the reduced detuning $\hat{C}_0$ at the undulator entrance. Here $\hat{b} = 30$, (1) is the first maximum and (2) is the second maximum.

where N_w is the number of undulator periods. At the linear change of the undulator field and fixed period we get

$$\hat{b} \simeq \{-4\pi N_w K^2(0)/[1 + K^2(0)]\}[H_w(l_w) - H_w(0)]/H_w(0).$$

It should be noted that these expressions for $\hat{b}$ are valid for the both: positive and negative signs of $\hat{b}$.

In the case of untapered undulator, integration of expression (7.6) is performed analytically and we get the well known result of Eq. (5.3).

Figs. 7.1 and 7.2 show the gain profiles for two different positive values of the tapering parameter $\hat{b}$. It is clearly seen that the curves are antisymmetric with respect to the line $\hat{C}_0 = -\hat{b}/2$. The value of $\hat{G}_s$ at the first maximum (dominating at $\hat{b} = 0$) is decreasing rapidly when parameter $\hat{b}$ is increasing and at $\hat{b} \simeq 26$ the first maximum becomes less than the second one. Further, the second maximum dominates till $\hat{b} \simeq 38$, and so on. We limit our consideration only with these two maxima, i.e. with the region $0 < |\hat{b}| < 38$. The position of the maxima is given approximately with the formula $\hat{C}_0^m \simeq \hat{C}_0^m|_{\hat{b}=0} - \hat{b}/2$ which is valid for the both positive and negative values of parameter $\hat{b}$. For instance, at the positive values of $\hat{b}$, maxima shift in the direction of the smaller values of the detuning parameter $\hat{C}_0$ (i.e. the lasing frequency increases with respect to the case $\hat{b} = 0$). A more precise formula for the first maximum has the form: $\hat{C}_0^m = 2.6 - \hat{b}/2 - y_1(|\hat{b}|)$, and for the second maximum: $\hat{C}_0^m = 10.6 - \hat{b}/2 - y_2(|\hat{b}|)$, where y_1 and y_2 are the positively valued functions of the absolute value of $\hat{b}$ giving a small contribution to the change of $\hat{C}_0^m$ (i.e. $y_{1,2} \ll |\hat{b}|$). The values of the maximal gain $\hat{G}_s^m$ do not depend on the sign of $\hat{b}$ and are universal functions of the absolute value of $\hat{b}$. The plots of these functions for two maxima under consideration are presented in Fig. 7.3.

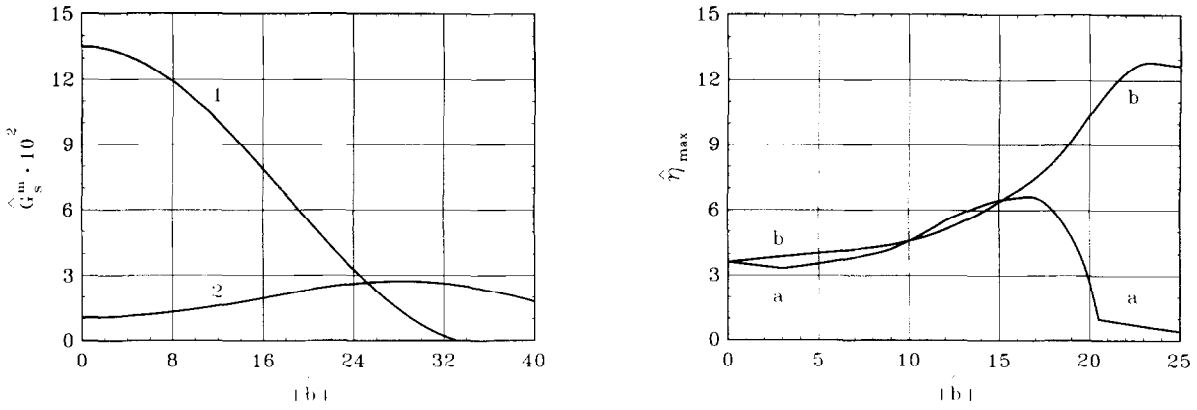

Fig. 7.3. The maximal reduced small-signal gain $\hat{G}_s$ as a function of the tapering parameter. Here (1) is the first maximum and (2) is the second maximum.

Fig. 7.4. The maximal reduced efficiency at the saturation as a function of the tapering parameter for the first maximum. Curve (a): $\hat{b} > 0$, and curve (b): $\hat{b} < 0$.

7.2. *Efficiency optimization*

We use Eqs. (6.1) and (6.2) for numerical simulation of the nonlinear mode of operation of the FEL oscillator with tapered undulator. The only distinction is that now the detuning parameter is the function of the longitudinal coordinate, $\hat{C}(\hat{z}) = \hat{C}_0 + \hat{b}\hat{z}$, where $\hat{C}_0$ corresponds to the maximum of the small signal gain, $\hat{C}_0 = \hat{C}_0^m$.

In the stationary regime of the FEL oscillator operation, the reduced efficiency $\hat{\eta} = \eta/\beta$ is given by the relation $\hat{\eta} = \hat{\alpha}(u^{(\infty)})^2/2$, where $\hat{\alpha} = \alpha/\tau$ is the parameter of resonator losses. In the case of untapered undulator, the field amplitude $\hat{u}^{(\infty)}$ at the saturation depends only on $\hat{\alpha}$, so the FEL efficiency $\hat{\eta}$ at the saturation is the universal function of the only parameter $\hat{\alpha}$ and achieves its maximum $\hat{\eta}_{max} = 3.62$ at $\hat{\alpha}_{opt} = 0.028$ (see Section 6).

In the case of the linear law of the undulator parameter tapering, the FEL efficiency $\hat{\eta}$ at the saturation is universal function of two parameters: $\hat{\eta} = F(\hat{\alpha}, \hat{b})$. At each value of the tapering parameter $\hat{b}$ there is always the optimal value $\hat{\alpha}_{opt}(\hat{b})$ when efficiency achieves its maximum $\hat{\eta}_{max}(\hat{b})$. In Figs. 7.4 and 7.5 we present the plots of the maximal FEL efficiency $\hat{\eta}_{max}(\hat{b})$ and $\hat{\alpha}_{opt}(\hat{b})$ in the range $0 < |\hat{b}| < 25$ when the lasing takes place at the first maximum of the gain curve. The complicated behaviour of these plots at the positive values of parameter $\hat{b}$ needs some explanations. The rapid decrease of the efficiency at $\hat{b} \simeq 20$ is explained as follows. Let us consider the field amplification coefficient $\hat{G}$ as the function of the field amplitude $\hat{u}$ in the resonator. When the field amplitude is increasing, coefficient $\hat{G}$ achieves its minimum at first, and at large values of $\hat{u}$ it achieves the maximal value. The dependencies of $\hat{G}(\hat{u})$ and $\hat{\eta}(\hat{u})$ at the value of $\hat{b} = 15$ are presented in Fig. 7.6. It is seen from the plot of $\hat{G}(\hat{u})$ that the transition from the range of the small field to the range of the strong field (where efficiency achieves its maximum) is possible only at $\hat{\alpha} < \hat{G}_{min}$. At $\hat{b} = 15$ the maximal FEL efficiency is achieved at $\hat{u}_{opt} = 58$ and conditions $\hat{\alpha} < \hat{G}_{min}$ and $\hat{\alpha} = \hat{G}(\hat{u}_{opt})$ are fulfilled simultaneously at $\hat{\alpha} = \hat{\alpha}_{opt} = 3.8 \times 10^{-3}$. Thus, at the given value of the undulator tapering parameter $\hat{b}$, there is always the optimal value of the field damping factor $\hat{\alpha}$ when the FEL efficiency achieves its absolute maximum. Then, if parameter $\hat{b}$ is increasing, the value of $\hat{G}_{min}$ is decreasing

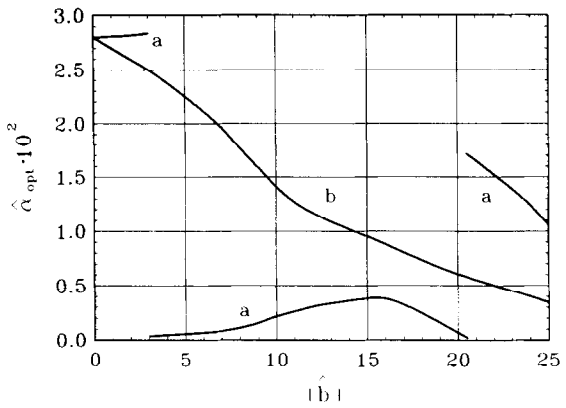

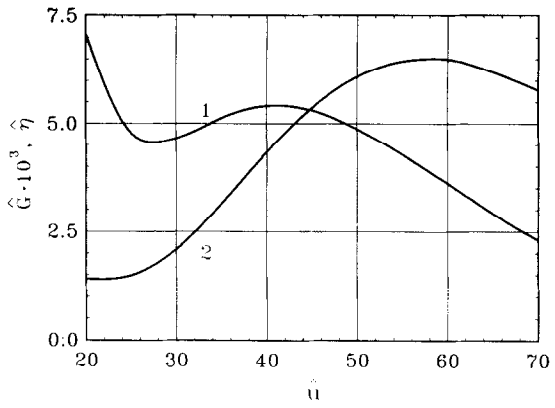

Fig. 7.5. The optimal reduced damping factor as a function of the tapering parameter for the first maximum. Curve (a): $\hat{b} > 0$ and curve (b): $\hat{b} < 0$.

Fig. 7.6. The reduced gain $\hat{G}$ (curve 1) and the reduced efficiency (curve 2) versus the reduced field amplitude for $\hat{b} = 15$..

and at $\hat{b} > 17$ the equilibrium state in the region of the strong field is possible only at $\hat{u} > \hat{u}_{opt}$ and the FEL efficiency is decreasing rapidly. At $\hat{b} \simeq 21$ the decrease of $\hat{G}_{min}$ leads to the leap of the function $\hat{\alpha}_{opt}(\hat{b})$ and the break of the function $\hat{\eta}_{max}(\hat{b})$. The further increase of parameter $\hat{b}$ leads to the situation when the FEL saturation is achieved at the small field and low efficiency. Thus, in the region $0 < |\hat{b}| < 25$, the tapering with the positive value of $\hat{b}$ (i.e., for instance, at the decreasing of the undulator field and fixed undulator period) becomes ineffective. This is explained by the shift of the lasing detuning $\hat{C}_0^m$ to the region of negative values. As a result, at the initial part of the undulator the particles are bunched at the accelerating phase of the effective potential and take away the energy from the radiation field, and only then the field amplification process takes place. So, in this case the undulator tapering with $\hat{b} < 0$, when the field amplification is performed from the very beginning of the undulator, has an advantage against the tapering with $\hat{b} > 0$.

Figs. 7.7 and 7.8 show the dependencies of $\hat{\eta}_{max}(\hat{b})$ and $\hat{\alpha}_{opt}(\hat{b})$ in the range $26 < |\hat{b}| < 38$ when the lasing takes place at the second maximum of the gain curve. In this case the maximal FEL efficiency increases significantly but is achieved at small values of the parameter $\hat{\alpha}$ (which corresponds to very strong fields).

With the help of the plots in Figs. 7.4, 7.5, 7.7 and 7.8 one can find the optimal value of the resonator Q-quality and maximal FEL efficiency corresponding to the given value of the tapering parameter $\hat{b}$. In many practical situations, the problem arises how to find the optimal value of the tapering parameter and maximal FEL efficiency at the given value of the resonator losses. In Figs. 7.9 an 7.10 we show the dependencies of the efficiency $\hat{\eta}$ on the value of the tapering parameter $\hat{b}$ for the value of $\hat{\alpha} = 5 \times 10^{-3}$ and in Figs. 7.11 and 7.12 we present the phase distributions of the particles at the undulator exit when the FEL oscillator operates in the saturation regime.

Table 7.1 presents optimal values of $\hat{b}$ and the corresponding values of the efficiency for different values of $\hat{\alpha}$. It is seen from Table 7.1 that in the wide region of the reduced damping factor values, good results may be achieved using the tapering within $\hat{b} = 26$–30. In this region of the tapering parameter $\hat{b}$, the lasing happens at the second maximum of the gain curve which is only slightly shifted to the negative values of the detuning parameter. Almost the same results (the increase of the efficiency by the factor of 2–3.5 with respect to the case of untapered undulator) can be achieved

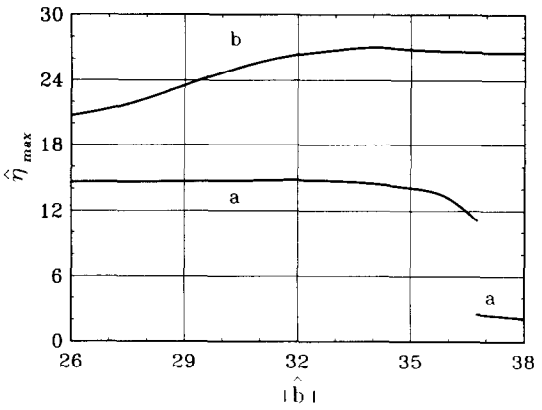

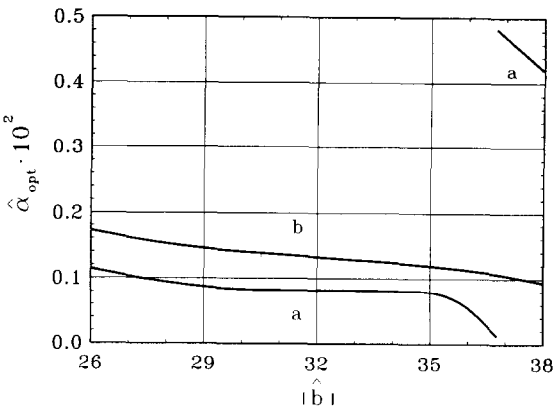

Fig. 7.7. The maximal reduced efficiency at the saturation as a function of the tapering parameter for the second maximum. Curve (a): $\hat{b} > 0$ and curve (b): $\hat{b} < 0$.

Fig. 7.8. The optimal reduced dumping factor as a function of the tapering parameter for the second maximum. Curve (a): $\hat{b} > 0$ and curve (b): $\hat{b} < 0$.

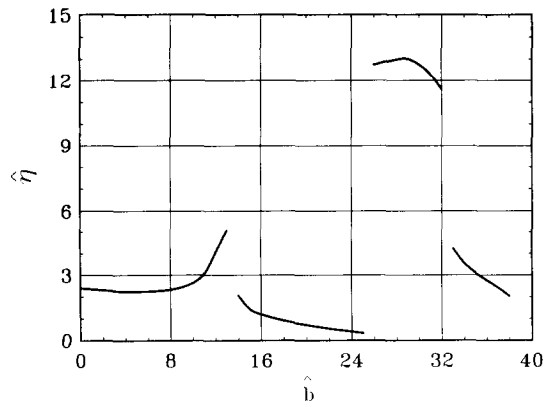

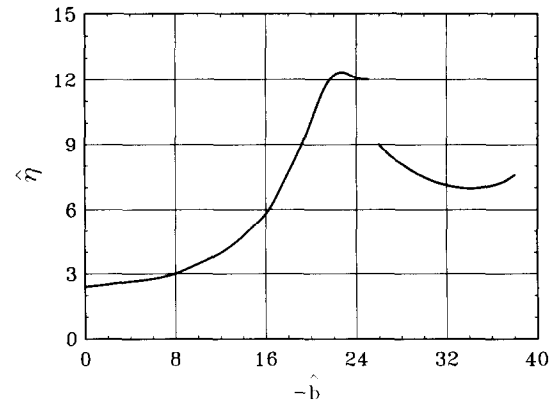

Fig. 7.9. The reduced efficiency at the saturation as a function of the tapering parameter. Here $\hat{\alpha} = 0.005$ and $\hat{b} > 0$.

Fig. 7.10. The reduced efficiency at the saturation as a function of the tapering parameter. Here $\hat{\alpha} = 0.005$ and $\hat{b} < 0$.

using the "negative tapering" in the region of the tapering parameter $\hat{b} = -20$ to -25.

All the results obtained above may be generalized to the case of a linearly polarized radiation and a planar undulator having magnetic field

$$H_y = 0, H_x = H_l(z)\cos\left(\int \kappa_w(z)dz\right)$$

by the following redetermination of the problem parameters

$$\tau \to \tau' = \pi\theta_l^2 j_0 \omega l_w^3 A_{JJ}^2 (c\gamma_l^2 \gamma I_A)^{-1}, \quad E_0 \to E_0' = 2c\mathcal{E}_0\gamma_l^2 (e\theta_l \omega l_w^2 A_{JJ})^{-1},$$
$$\beta \to \beta' = c\gamma_l^2 (\omega l_w)^{-1} = (4\pi N_w)^{-1}, \quad C(z) \to C'(z) = \kappa_w(z) - \omega[1 + K_l^2(z)/2]/2c\gamma^2,$$

where $K_l(z) = eH_l(z)/[\kappa_w(z)mc^2]$, $\theta_l = K_l(0)/\gamma$, $\gamma_l^{-2} = \gamma^{-2} + \theta_l^2/2$, $A_{JJ} = [J_0(\nu) - J_1(\nu)]$ and $\nu = \theta_l^2\omega/(8c\kappa_w)$. When the undulator period is tapered by a linear law at the constant undulator

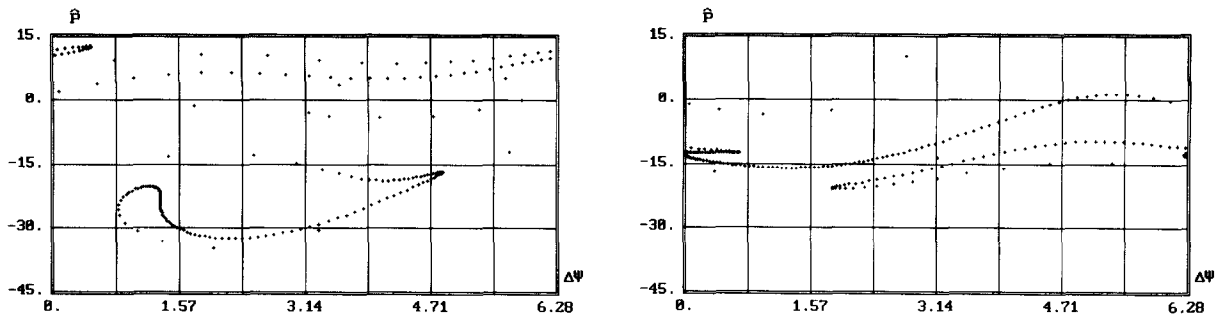

Fig. 7.11. Phase space distribution of the particles at the undulator exit. The FEL oscillator operates at the saturation. Here $\hat{\alpha} = 0.005$ and $\hat{b} = 29$.

Fig. 7.12. Phase space distribution of the particles at the undulator exit. The FEL oscillator operates at the saturation. Here $\hat{\alpha} = 0.005$ and $\hat{b} = -23$.

Table 7.1
Optimal parameters of the FEL oscillator with tapered undulator.

$10^2 \times \hat{\alpha}$	$\hat{b}/\lvert\hat{b}\rvert$	$\lvert\hat{b}\rvert$	$\hat{\eta}$
0.1–0.15	−1	26–38	20–27
0.15–0.2	−1	26–29	17–23
0.2–0.3	+1	26–32	9–12
0.3–0.5	+1	26–32	10–13
0.3–0.5	−1	23–25	10–13
0.5–0.7	+1	26–30	12–13
0.5–0.7	−1	20–25	10–12.5
0.7–−1.0	+1	26–28	8–12.5
0.7–−1.0	−1	18–25	8–10.5
1.0–−1.3	+1	26–28	6–10
1.0–−1.3	−1	18–25	7–8.5

parameter K_l, the tapering parameter $\hat{b}$ is equal to:

$$\hat{b} \simeq -2\pi N_w [\lambda_w(l_w) - \lambda_w(0)]/\lambda_w(0),$$

where $\lambda_w = 2\pi/\kappa_w$. At the linear tapering of the undulator field and fixed undulator period we have

$$\hat{b} \simeq \{-2\pi N_w K_l^2(0)/[1 + K_l^2(0)/2]\}[H_l(l_w) - H_l(0)]/H_l(0).$$

8. FEL oscillator with multicomponent undulator

We assume a multicomponent undulator to be composed of two undulators separated by drift space or dispersion section. There are two popular configurations of the multicomponent undulator. The first one uses two identical (or almost identical) sections. The first undulator modulates electron beam in the energy. After passing the dispersion section, the energy modulation transforms into the density modulation and bunched electron beam radiates electromagnetic radiation in the second undulator.

Such a FEL oscillator configuration provides the small signal gain which is much more than that of the homogeneous undulator of the same total length. This device has been proposed in Refs. [47,48] and was named "optical klystron". Application of this scheme is necessary when the gain parameter is small and there is a need to reach the lasing threshold.

Another popular scheme of the multicomponent undulator is named as undulator with a prebuncher [49]. The length of the prebuncher is much less than the length of the main undulator section. As a rule, the main undulator is a tapered one. The length of the drift space is much less than that of the optical klystron and does not influence significantly on the beam bunching at the linear mode of operation. On the other hand, its parameters are chosen in such a way, that it optimally enhanced the beam bunching when operating at the nonlinear mode of operation. As a result, the bunched beam is fed to the input of the main undulator with tapered parameters, and the FEL oscillator efficiency can be increased significantly with respect to the case considered in Section 7.

As a rule, the main emphasis in the theory of the optical klystron is put on the small signal analysis (see Refs. [47,48,50–55]). The small signal gain is usually obtained either via derivation of spontaneous spectrum (Madey theorem [56]), or by using kinetic equation. In this paper we present a universal study of the small signal gain of the FEL oscillator with multicomponent undulator taking into account energy spread in the beam, the difference of the undulator section lengths, tapering of the second undulator section and phase shift of the wave in the drift space. As for nonlinear analysis, using similarity techniques we present for the first time simple analytical relations for the maximal FEL efficiency and optimal value of the resonator losses.

We should note that the presented results of the nonlinear theory cannot be used directly for calculation of the optical klystron installed in the storage ring. In this case the radiation in the resonator interacts with the single electron beam circulating in the storage ring which complicates considerations because the beam dynamics in the storage ring should be taken into account. Special studies of this problem have shown that these effects significantly reduce the output power of the optical klystron [57–60]. In this section we consider the simplest formulation of the problem when the driving electron beam of the FEL oscillator is modulated neither in velocity nor in density at the undulator entrance and its parameters do not depend on time.

8.1. Small-signal mode of operation

The multicomponent undulator consists of two undulators of length l_1 and l_2, respectively, and the drift space of length d. To find the small signal gain, we use the approach developed in the previous sections using the Hamiltonian (7.1), kinetic equation (7.2) and electrodynamic equation (7.4).

We begin with the case of untapered undulators. Evolution of the complex amplitude $\tilde{f}_1$ of the first harmonic of the distribution function is described by the equation

$$\partial \tilde{f}_1/\partial z + i(C + \omega P/c\gamma_z^2\mathcal{E}_0)\tilde{f}_1 + iU\partial f_0/\partial P = 0, \tag{8.1}$$

where $f_0 = n_0 F(P)$. The general form of the solution for $\tilde{f}_1$ is

$$f_1 = -in_0 \int_0^z dz' U\partial F/\partial P \exp[i(C + \omega P/c\gamma_z^2\mathcal{E}_0)(z' - z)] + \tilde{f}_1(0)\exp[-i(C + \omega P/c\gamma_z^2\mathcal{E}_0)z]. \tag{8.2}$$

We study the case of the electron beam which is modulated neither in velocity nor in density at the entrance into the undulator, so we let $\tilde{f}_1(0) = 0$ at $z = 0$.

There is no beam-wave interaction in the drift space and longitudinal relativistic factor γ_z is equal to the total one γ. The evolution of the function $\tilde{f}_1$ in the drift space results in the multiplying by the phase factor $\exp[-i\omega(z/c - t)]$. We denote the value of the function $\tilde{f}_1$ (see Eq. (8.1)) at $z = l_1$ as $\tilde{f}_1^{(\Leftarrow)}$, and the value of this function at the end of the drift space as $\tilde{f}_1^{(\Rightarrow)}$. These values are related with each other as

$$\tilde{f}_1^{(\Rightarrow)} = \tilde{f}_1^{(\Leftarrow)} \exp(i\psi_f),$$

where $\psi_f \simeq (\omega d/c)[1 - v(\mathcal{E})/c]$. In the same way as it was done in the previous sections, we denote γ as the relativistic factor, γ_z as the longitudinal relativistic factor in the undulators, C as detuning of the particle in the undulators and $P = \mathcal{E} - \mathcal{E}_0$ as the deviation of the electron energy from nominal value. The values of γ, γ_z and C refer to the particle with the nominal energy $\mathcal{E}_0$. So, the latter expressions can be written as

$$\psi_f = -(\gamma_z^2/\gamma^2) d(C + \omega P/c\gamma_z^2\mathcal{E}_0 - \kappa_w)$$

and

$$\tilde{f}_1^{(\Rightarrow)} = -in_0 \exp[i(\gamma_z^2/\gamma^2)\kappa_w d] \int_0^{l_1} dz' U \partial F/\partial P \times \exp[i(C + \omega P/c\gamma_z^2\mathcal{E}_0)(z' - l_1 - (\gamma_z^2/\gamma^2)d)]. \tag{8.3}$$

As there is no beam-wave interaction in the drift space, it is convenient for calculations to let the total length of the system to be equal to $l_w = l_1 + l_2$. The change of the distribution function $\tilde{f}_1$ in the drift space is introduced as a leap at $z = l_1$. The solution of Eq. (8.1) in the interval $l_1 < z < l_w$ with the initial condition (8.3) is

$$\tilde{f}_1 = -in_0 \left\{ \exp(i\delta\psi) \int_0^{l_1} dz' U \partial F/\partial P \exp[i(C + \omega P/c\gamma_z^2\mathcal{E}_0)[z' - z - (\gamma_z^2/\gamma^2)d]] + \int_{l_1}^{z} dz' U \partial F/\partial P \exp[i(C + \omega P/c\gamma_z^2\mathcal{E}_0)(z' - z)] \right\}, \tag{8.4}$$

where $\delta\psi = (\gamma_z^2/\gamma^2)\kappa_w d$.

Let us consider the case of "cold" electron beam with $F(P) = \delta(P)$. Using relation

$$\tilde{j}_1 = -ec \int \tilde{f}_1 dP,$$

we find expressions for the first harmonic of the beam current density

$$\tilde{j}_1 = (j_0\omega/\mathcal{E}_0\gamma_z^2 c) \int_0^z dz'(z' - z) U \exp[iC(z' - z)] \quad \text{at } 0 < z < l_1,$$

$$\tilde{j}_1 = (j_0\omega/\mathcal{E}_0\gamma_z^2 c)\left\{\exp(i\delta\psi)\int_0^{l_1} dz'[z'-z-(\gamma_z^2/\gamma^2)d]U\exp[iC[z'-z-(\gamma_z^2/\gamma^2)d]]\right.$$
$$\left.+\int_{l_1}^{z} dz'(z'-z)U\exp[iC(z'-z)]\right\} \quad \text{at } l_1 < z < l_w.$$

To find the function $\hat{Z} = 2Z/\tau$, where Z is defined as $Z = \tilde{E}(l_w)/\tilde{E}(0) - 1$ and τ is the gain parameter, we integrate Eq. (7.4) in the limits from 0 to l_w and perform the normalization to the total undulator length l_w:

$$\hat{Z} = i\int_0^{\hat{l}_1} d\xi \int_0^{\xi} d\xi'\xi'\exp(-i\hat{C}\xi') + i\int_0^{1-\hat{l}_1} d\xi \int_0^{\xi} d\xi'\xi'\exp(-i\hat{C}\xi')$$
$$+ i\exp(i\delta\psi)\int_0^{1-\hat{l}_1} d\xi \int_{\xi+\hat{d}}^{\xi+\hat{l}_1+\hat{d}} d\xi'\xi'\exp(-i\hat{C}\xi'), \tag{8.5}$$

where $\hat{C} = Cl_w$, $\hat{l}_1 = l_1/l_w$ and $\hat{d} = (\gamma_z^2/\gamma^2)(d/l_w)$. In a special case of a helical undulator $\hat{d} = d/(1+K^2)l_w$, and for a planar undulator $\hat{d} = d/(1+K^2/2)l_w$. Expression of the phase shift of the wave in the drift space with respect to the electron beam is written in the form: $\delta\psi = 2\pi N_w\hat{d}$, where N_w is the total number of the undulator periods in the both sections.

8.1.1. Optical klystron

Integrating Eq. (8.5) for the case of $\hat{l}_1 = 1/2$ and $\delta\psi = 2\pi k$ $(k = 1, 2, \ldots)$, we obtain

$$\hat{Z} = \frac{1}{\hat{C}^3}[\hat{C} + 4i + 2F(\hat{C}/2) + F(\hat{C}\hat{d}) + F(\hat{C}(\hat{d}+1)) - 2F(\hat{C}(\hat{d}+1/2))], \tag{8.6}$$

where $F(\zeta) = (2i-\zeta)\exp(-i\zeta)$. One can easy find that at $\hat{d} \to 0$ expression (8.6) transforms to the corresponding expression (5.3) for untapered undulator. The reduced small signal gain $\hat{G}_s = G_s/\tau$ is written as

$$\hat{G}_s = \mathrm{Re}(\hat{Z}) = -\frac{1}{\hat{C}^3}[2f(\zeta)|_0^{\hat{C}/2} + f(\zeta)|_{\hat{C}(\hat{d}+1/2)}^{\hat{C}(\hat{d}+1)} - f(\zeta)|_{\hat{C}\hat{d}}^{\hat{C}(\hat{d}+1/2)}], \tag{8.7}$$

where $f(\zeta) = 2\cos(\zeta) + \zeta\sin(\zeta)$ and

$$f(\zeta)|_a^b = f(b) - f(a).$$

Fig. 8.1 presents the gain curve for specific value of parameter $\hat{d}$. At large values of the parameter $\hat{d}$, maxima of the gain curve are separated approximately by $2\pi/\hat{d}$. It is explained as follows. The maximum of the gain curve corresponds to an optimal value of the beam-wave phase shift at the entrance of the second undulator. At the exact resonance $(\hat{C} = 0)$, the beam-wave phase shift in the drift space is equal to some value $\delta\psi$. At a finite value of the detuning, an additional phase shift appears equal to $\hat{C}\hat{d}$. Maximum of the gain curve corresponds to the optimal beam-phase shift at the entrance to the second section. Additional beam-wave phase shift equal to 2π caused by the change

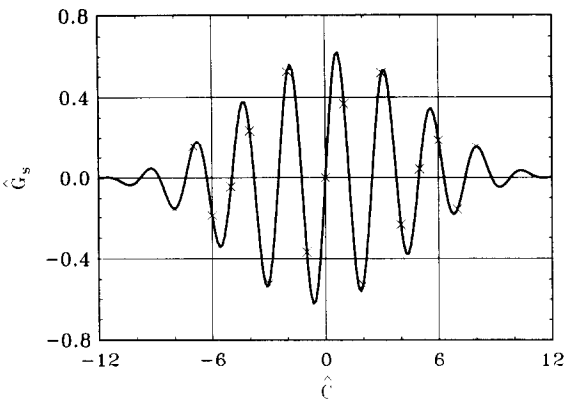

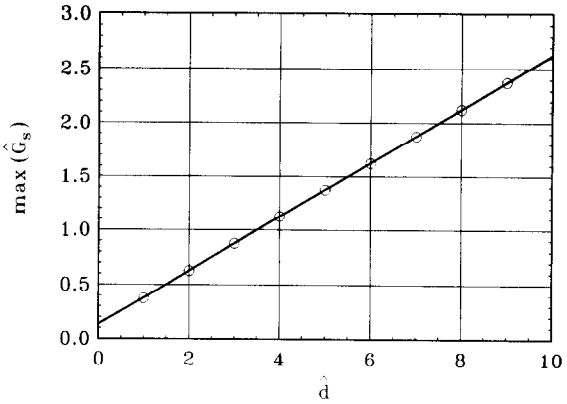

Fig. 8.1. The reduced small-signal gain$\hat{G}_s$ versus the reduced detuning $\hat{C}$. Here $\overline{\delta\psi} = 0$, $\hat{d} = 2$ and $\hat{l}_1 = 1/2$. The solid curve is calculated with analytical formula (8.7) and the crosses are the results of calculations with nonlinear simulation code.

Fig. 8.2. The maximal reduced small-signal gain $\hat{G}_s$ versus the reduced length of the drift section. Here $\overline{\delta\psi} = 0$ and $\hat{l}_1 = 1/2$. The full curve is the result of calculations with formula (8.7) and the circles are the result of calculations with asymptotic formula (8.8).

of the detuning by the value $2\pi/\hat{d}$ corresponds to the next maximum. When $\delta\psi = 2\pi k$ $(k = 1, 2, \ldots)$, the gain curve is antisymmetric with respect to $\hat{C} = 0$. When $\delta\psi$ is changed smoothly, the maximums are shifted inside the envelope of the gain curve and the picture is repeated each time when $\delta\psi$ changes by 2π.

Though $\delta\psi$ depends on $\hat{d}$, its change by the value of unity is achieved at a small relative change of parameter $\hat{d}$ when the latter is greater or of an order of unity. For instance, $\delta\psi$ changes by 2π at $\Delta\hat{d}/\hat{d} = 1/N_w\hat{d} \ll 1$ because $N_w \gg 1$. It means, that when $\hat{d} \gtrsim 1$, $\delta\psi$ and $\hat{d}$ can be considered as independent parameters.

It is convenient to introduce nonmultiple beam-wave phase shift

$$\overline{\delta\psi} = 2\pi\{N_w\hat{d} - [N_w\hat{d}]\},$$

where $[\ldots]$ denotes integer fraction of the number.

Let us consider the case $\overline{\delta\psi} = 0$ and $\hat{l}_1 = 1/2$ which corresponds to that of the optical klystron. Maximum of the small signal gain $\max(\hat{G}_s)$ and the detuning $\hat{C}_m$ corresponding to this maximum are universal functions of parameter $\hat{d}$. In Figs. 8.2 and 8.3 we presents these functions calculated with Eq. (8.7). The circles in these figures correspond to the values calculated with the asymptotical formulae

$$\hat{C}_m = \frac{\pi}{2(\hat{d} + 1/2)}, \quad \max(\hat{G}_s) = \frac{\hat{d} + 1/2}{4} \tag{8.8}$$

which are valid in the limit $\hat{d} \gg 1$. It is seen that even at $\hat{d} \simeq 1$, asymptotical formulae (8.8) provide a good approximation.

Let us now consider a more general case when the second undulator is tapered by a linear law

$$C(z) = \begin{cases} C_0 & \text{at } 0 < z < l_1 \\ C_0 + b(z - l_1) & \text{at } l_1 < z < l_w. \end{cases}$$

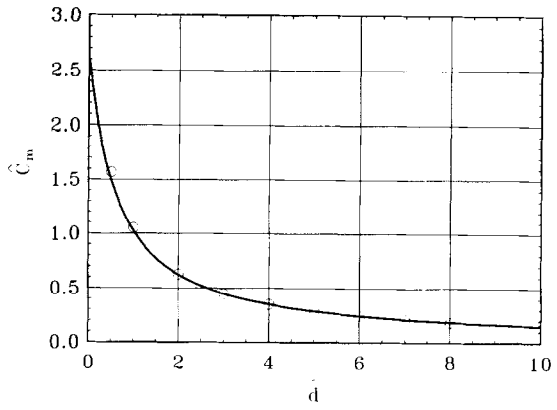

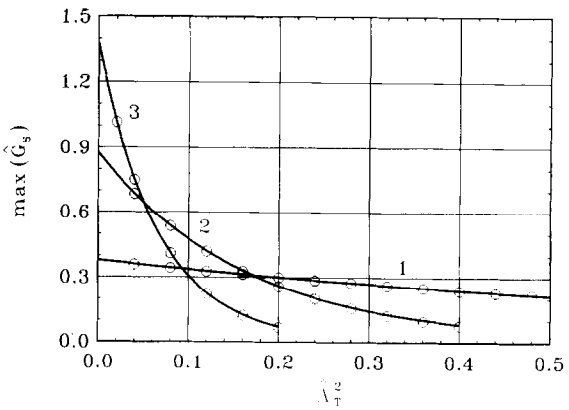

Fig. 8.3. The optimal reduced detuning $\hat{C}_m$ versus the reduced length of the drift section. Here $\overline{\delta\psi} = 0$ and $\hat{l}_1 = 1/2$. The full curve is the result of calculations with formula (8.7) and the circles are the result of calculations with asymptotic formula (8.8).

Fig. 8.4. The maximal reduced small-signal gain $\hat{G}_s$ versus the energy spread parameter $\hat{\Lambda}_T^2$ for several values of the reduced length of the drift section. Here $\overline{\delta\psi} = 0$, $\hat{l}_1 = 1/2$ and $\hat{b} = 0$. The full curves are the result of calculations with formula (8.9) and the circles are the result of calculations with asymptotic formula (8.10). Curve (1): $\hat{d} = 1$, curve (2): $\hat{d} = 3$ and curve (3): $\hat{d} = 5$.

Besides, we take into account the energy spread in the beam assuming it to be a Gaussian with the distribution function $F(P)$ given by Eq. (2.29a). In this case we obtain

$$\hat{Z} = i\int_0^{\hat{l}_1} d\xi \int_0^{\xi} d\xi' \xi' \exp[-i\hat{C}_0\xi' - \hat{\Lambda}_T^2(\xi')^2/2]$$
$$+ i\int_0^{1-\hat{l}_1} d\xi \int_0^{\xi} d\xi' \xi' \exp[-i\hat{C}_0\xi' + i\hat{b}\xi'(\xi'/2 - \xi) - \hat{\Lambda}_T^2(\xi')^2/2]$$
$$+ i\exp(i\delta\psi)\int_0^{1-\hat{l}_1} d\xi \exp(-i\hat{b}\xi^2/2) \int_{\xi+\hat{d}}^{\xi+\hat{l}_1+\hat{d}} d\xi' \xi' \exp[-iC_0\xi' - \hat{\Lambda}_T^2(\xi')^2/2], \tag{8.9}$$

where $\hat{C}_0 = C_0 l_w$, $\hat{b} = b l_w^2$ and $\hat{\Lambda}_T = 4\pi N_w \sqrt{\langle(\Delta\mathcal{E}/\mathcal{E}_0)^2\rangle}$ is the energy spread parameter.

First, we study the influence of the energy spread on the operation of the optical klystron (in this case the second undulator is untapered and $\hat{b} = 0$). We assume also that $\delta\psi = 0$. The maximal small signal gain $\max(\hat{G}_s)$ is a function of two parameters, $\hat{d}$ and $\hat{\Lambda}_T^2$. In Fig. 8.4 we present the plots of this function for several fixed values of $\hat{d}$. The circles in these plots are calculated with asymptotical formula

$$\max(\hat{G}_s) = \frac{\hat{d} + 1/2}{4} \exp[-\tfrac{1}{2}\hat{\Lambda}_T^2(\hat{d} + 1/2)^2] \tag{8.10}$$

which is valid for $\hat{d} \gg 1$. It follows from this formula that at each value of the energy spread parameter there is an optimal value of the parameter $\hat{d}$

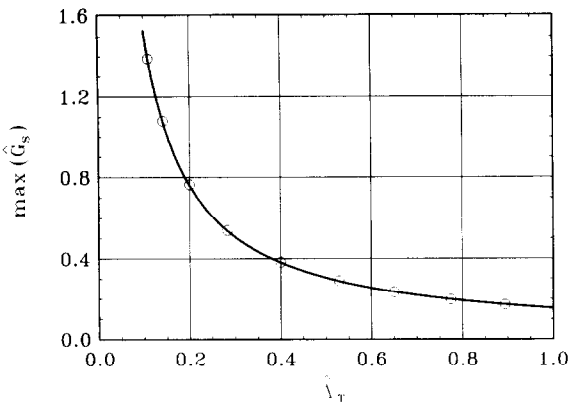

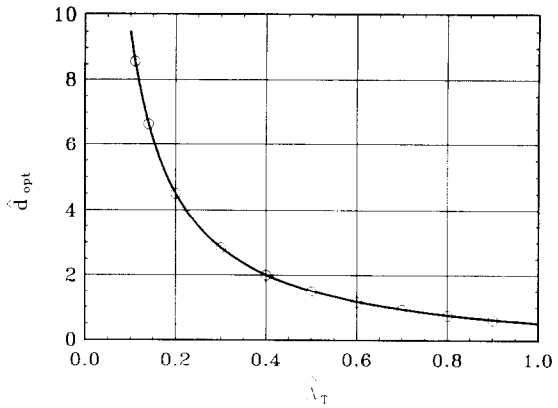

Fig. 8.5. The maximal reduced small-signal gain $\hat{G}_s$ versus the $\hat{\Lambda}_T$ parameter. Here $\overline{\delta\psi} = 0$, $\hat{l}_1 = 1/2$ and $\hat{b} = 0$. The full curves is the result of calculations with formula (8.9) and the circles are the result of calculations with asymptotic formula (8.11b).

Fig. 8.6. The optimal reduced length of the drift section $\hat{d}_{\rm opt}$ versus the $\hat{\Lambda}_T$ parameter. Here $\overline{\delta\psi} = 0$, $\hat{l}_1 = 1/2$ and $\hat{b} = 0$. The full curves is the result of calculations with formula (8.9) and the circles are the result of calculations with asymptotic formula (8.11a).

$$\hat{d}_{\rm opt} = \frac{1}{\hat{\Lambda}_T} - \frac{1}{2}, \tag{8.11a}$$

when the maximal value of the gain

$$\max(\hat{G}_s) = \frac{0.152}{\hat{\Lambda}_T} \tag{8.11b}$$

is achieved.

Figs. 8.5 and 8.6 present the corresponding dependencies (solid curves are calculated with exact formula (8.9) and circles – with the asymptotic formulae (8.11). Analyzing the obtained relations and plots we can conclude that the optical klystron has a benefit in the small signal gain with respect to the conventional FEL oscillator scheme (see Section 5) only in the case of small energy spread, $\hat{\Lambda}_T \ll 1$.

8.1.2. FEL oscillator with a prebuncher

Let us now consider another popular configuration of the FEL oscillator with multicomponent undulator, namely that of the FEL oscillator with a prebuncher. In this case the first undulator (prebuncher) is short, $\hat{l}_1 \ll 1$, and the second undulator (main undulator) is tapered by a linear law ($\hat{b} \neq 0$). As a rule, in this case parameter $\hat{d}$ is small, $\hat{d} \ll 1$. In Figs. 8.7 and 8.8 we present the curves of the small signal gain for $\hat{l}_1 = 0.05$, $\hat{d} = 0.3$, $\hat{b} = 30$ and $\hat{\Lambda}_T^2 = 0$ calculated with Eq. (8.9). It is seen from these plots that the shape of the gain curves and positions of maximums depend strongly on the value of the beam-wave phase shift parameter $\overline{\delta\psi}$ (in the presented plots its values are equal to 0 and π). It reveals a possibility to optimize the position of the main maximum in order to achieve maximal efficiency at saturation. Fig. 8.9 presents the dependence on the beam-wave phase shift $\overline{\delta\psi}$ of the detuning parameter $\hat{C}_0^m$ corresponding to position of the main maximum of the small signal gain. To be strict, at small values of $\hat{d} \lesssim 1$, parameters $\overline{\delta\psi}$ and $\hat{d}$ are not independent. Nevertheless,

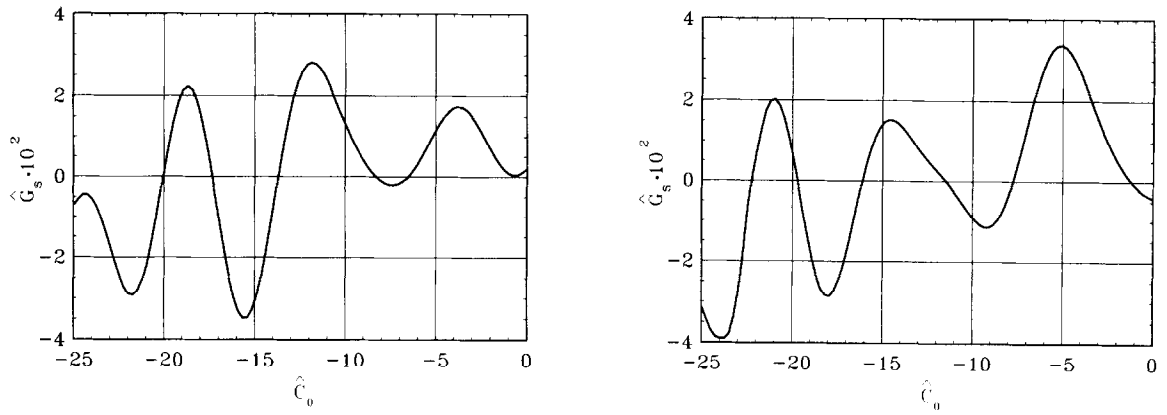

Fig. 8.7. The reduced small-signal gain $\hat{G}_s$ versus the reduced detuning $\hat{C}_0$ at the undulator entrance. Here $\overline{\delta\psi} = 0$, $\hat{d} = 0.3$, $\hat{l}_1 = 0.05$, $\hat{b} = 30$ and $\hat{A}_T^2 = 0$. The calculations have been performed with formula (8.9).

Fig. 8.8. The reduced small-signal gain $\hat{G}_s$ versus the reduced detuning $\hat{C}_0$ at the undulator entrance. Here $\overline{\delta\psi} = \pi$, $\hat{d} = 0.3$, $\hat{l}_1 = 0.05$, $\hat{b} = 30$ and $\hat{A}_T^2 = 0$. The calculations have been performed with formula (8.9).

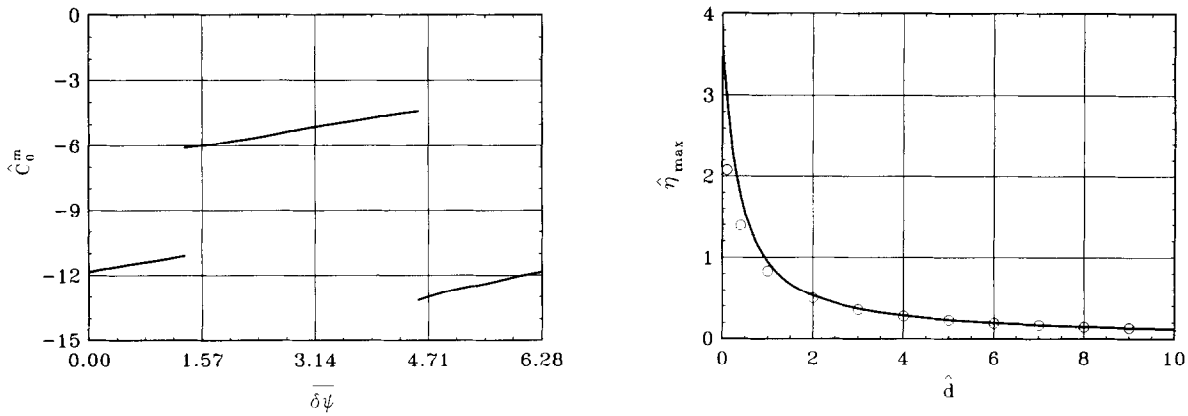

Fig. 8.9. Optimal reduced detuning $\hat{C}_0^m$ versus the $\overline{\delta\psi}$ parameter. Here $\hat{d} = 0.3$, $\hat{l}_1 = 0.05$, $\hat{b} = 30$ and $\hat{A}_T^2 = 0$. The calculations have been performed with formula (8.9).

Fig. 8.10. Maximal reduced efficiency at the saturation versus the reduced length of the drift section $\hat{d}$. Here $\overline{\delta\psi} = 0$, $\hat{l}_1 = 1/2$, $\hat{b} = 0$ and $\hat{A}_T^2 = 0$. The full curve is the result of calculations with formulae (8.12) and (8.13) and the circles are the result of calculations with asymptotic formula (8.19).

at the number of the undulator periods of about several tens (which usually takes place in practice), relative change of the parameter $\hat{d}$ is small when $\overline{\delta\psi}$ changes from 0 to 2π.

For simplicity, we have assumed above that undulators are separated with the drift space. When the length of the drift space $\hat{d}$ becomes to be too large, it is replaced by equivalent dispersion section. Let, for instance, the magnetic field in the dispersion section to be $\boldsymbol{H} = \boldsymbol{e}_x H(z)$ and the length to be d. Then parameter $\hat{d}$ is calculated as follows

$$\hat{d} = \hat{d}_0 \left[1 + e^2 (m^2 c^4 d)^{-1} \int_0^d \left(\int_0^z H(\xi) d\xi \right)^2 dz \right],$$

where $\hat{d}_0$ is calculated in the same way as $\hat{d}$ for the drift space. When the main undulator is a planar one with the undulator parameter equal to K and the dispersion section has a form of nonresonant plane undulator of length d and undulator parameter K_d, then

$$\hat{d} = \left[\frac{1 + K_d^2/2}{1 + K^2/2}\right] \frac{d}{l_w}.$$

8.2. Saturation effects

Nonlinear simulations of the FEL oscillator with multicomponent undulator are performed in the same way as it was described in Section 6. For convenience, we rewrite the system of the self-consistent equations

$$d\hat{P}/d\hat{z} = \hat{u}\cos(\psi + \psi_0), \quad d\psi/d\hat{z} = \hat{P} + \hat{C}; \tag{8.12}$$

$$d\hat{u}/d\hat{z} = (\tau\hat{j}_1/2)\cos(\psi_0 - \psi_1), \quad d\psi_0/d\hat{z} = -(\tau\hat{j}_1/2\hat{u})\sin(\psi_0 - \psi_1). \tag{8.13}$$

Notations and simulation algorithm are almost identical to those described in Section 6 with the following exceptions. Integration of Eqs. (8.12) and (8.13) is performed in the limits from $\hat{z} = 0$ to $\hat{z} = 1$. To take into account the action of the drift space, we change the phases of the particles by a leap at $\hat{z} = \hat{l}_1$

$$\psi^{(\Rightarrow)} = \psi^{(\Leftarrow)} + [\hat{P} + \hat{C}]\hat{d} - \overline{\delta\psi}. \tag{8.14}$$

Parameter $\overline{\delta\psi}$ has been defined above, the detuning parameter corresponds to the maximum of the small signal gain and $\hat{P}$ is the reduced energy deviation at the prebuncher exit. When the case of the tapered main undulator is simulated, the detuning changes linearly at $\hat{z} > \hat{l}_1$.

In Fig. 8.1 we present the testing results of the simulation code (crosses) at the linear stage.

8.2.1. Optical klystron

Numerical simulations show that the nonlinear stage in the optical klystron differs significantly from that of the conventional FEL oscillator. In the latter case nonlinear processes becomes to be significant when the value of the reduced field amplitude in the resonator becomes to be $\hat{u} \simeq 1$. At the optimal choice of the FEL oscillator parameters, rather high value of the field can be achieved, $\hat{u} \gg 1$. Contrary to this, in the optical klystron with a large value of parameter $\hat{d}$ (or, in other words, with a high value of the small signal gain), the decrease of the gain occurs at small value of the radiation field, at $\hat{u} \ll 1$. In this case there is almost no phase motion of the particles in the undulators and saturation effects are defined by nonlinear dynamics of the particles in the dispersion section. This process can be well described using analytical techniques developed for calculation of microwave klystrons. First, we consider a situation when process of the beam bunching in the undulators can be neglected. In the first undulator the beam is modulated in the energy, in the dispersion section the beam is modulated in density and in the second undulator the bunched beam amplifies the wave. The detuning parameter in this case should be chosen to be close to zero. Amplitude of the energy modulation after the first undulator is $\Delta\hat{P} = \hat{u}\hat{l}_1$. In the same way as in the theory of microwave klystron, we introduce the bunching parameter X

$$X = \hat{u}\hat{l}_1\hat{d}.$$

It follows from the theory of klystron that the first harmonic of the beam current, appearing in Eqs. (8.13), is

$$\hat{j}_1 = 2J_1(X),$$

where J_1 is Bessel function.

The increment of the field in the second undulator is equal to

$$\Delta\hat{u} = \hat{l}_2\tau J_1(X),$$

where $\hat{l}_2 = 1 - \hat{l}_1$. The power gain coefficient is

$$G = 2\Delta\hat{u}/\hat{u} = 2(1 - \hat{l}_1)\tau J_1(X)/\hat{u}. \tag{8.15}$$

In the saturation regime the gain must be equal to the resonator losses, $G = \alpha$. The reduced efficiency (see Section 6) is $\hat{\eta} = \hat{\alpha}\hat{u}^2/2$, where $\hat{\alpha} = \alpha/\tau$. Using these relations, we obtain

$$\hat{\eta} = (1 - \hat{l}_1)\hat{u}J_1(\hat{u}\hat{l}_1\hat{d}). \tag{8.16}$$

Thus, using Eq. (8.15) and the saturation condition $G = \alpha$, we can find the value of the resonator field at saturation, and then, using Eq. (8.16), obtain the maximal efficiency at the saturation. However, to find the saturation efficiency and the optimal value of the parameter of resonator losses $\hat{\alpha}$, there is no need to solve a transcendental equation. Indeed, we can find maximum of the efficiency in $\hat{u}$ by setting its derivative with respect to $\hat{u}$ to be zero, $J_0(\hat{u}\hat{l}_1\hat{d}) = 0$, where J_0 is Bessel function. We see that the optimal value of the bunching parameter X is equal to the root of the Bessel function J_0

$$X_{\text{opt}} = \hat{u}_{\text{opt}}\hat{l}_1\hat{d} = 2.405. \tag{8.17}$$

Using Eqs. (8.15)–(8.17) and remembering that $J_1(2.405) = 0.519$, we find

$$\hat{\eta}_{\max} = 1.25(1 - \hat{l}_1)/(\hat{d}\hat{l}_1), \quad \hat{\alpha}_{\text{opt}} = 0.432\hat{d}\hat{l}_1(1 - \hat{l}_1). \tag{8.18}$$

We see that the dependence of the maximal efficiency $\hat{\eta}_{\max}$ on the length of the first undulator $\hat{l}_1$ is more strong that the corresponding dependency of $\hat{\alpha}_{\text{opt}}$. For instance, when $\hat{l}_1$ is decreased from 0.5 to 0.2, the efficiency is increased by a factor of four while parameter $\hat{\alpha}_{\text{opt}}$ is decreased by 30%. So, we may conclude that if there is a possibility to reduce the parameter of resonator losses, the first undulator should be done shorter than the second undulator and a significant benefit in the efficiency can be achieved at the same total length of the undulators.

More precise formulae, valid even when $\hat{d} \simeq 1$, can be obtained taking into account the beam bunching not only in the dispersion section but also in the undulators. Let us consider a special case of $\hat{l}_1 = 1/2$. One can obtain that in this case the bunching parameter is

$$X = \begin{cases} \hat{u}\hat{z}^2/2, & \text{at } \hat{z} < 1/2, \\ \hat{u}/8 + \hat{u}\hat{d}/2, & \text{at the entrance into the second section,} \\ (\hat{u}/2)(\hat{d} + \hat{z} - 1/4), & \text{at } \hat{z} > 1/2. \end{cases}$$

The first harmonic of the current $\hat{j}_1$ as well as the bunching parameter are now functions of $\hat{z}$. So, for the field increment we have

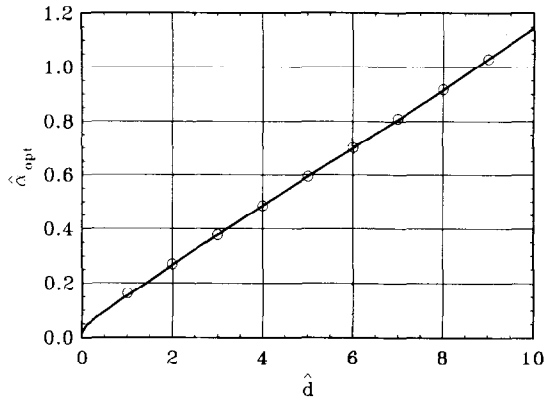

Fig. 8.11. Optimal value of the reduced damping factor versus the reduced length of the drift section $\hat{d}$. Here $\overline{\delta\psi} = 0$, $\hat{l}_1 = 1/2$, $\hat{b} = 0$ and $\hat{\Lambda}_T^2 = 0$. The full curve is the result of calculations with formulae (8.12) and (8.13) and the circles are the result of calculations with asymptotic formula (8.19).

$$\Delta\hat{u} = \tau \int_{1/2}^{1} d\hat{z}\, J_1(X).$$

Integration of this expression can be performed analytically which allows us to write analytical formula for the efficiency

$$\hat{\eta} = 2[J_0((\hat{u}/2)(\hat{d}+1/4)) - J_0((\hat{u}/2)(\hat{d}+3/4))].$$

We perform the optimization procedure and obtain

$$\hat{\eta}_{max} = 1.25/(\hat{d}+1/2), \quad \hat{\alpha}_{opt} = 0.108(\hat{d}+1/2). \tag{8.19}$$

In Figs. 8.10 and 8.11 we present the corresponding dependencies calculated as with approximate formulae (8.19) as with numerical simulations with Eqs. (8.12)–(8.14). We see that approximate formulae (8.19) provide a high accuracy of calculations even at $\hat{d} \simeq 1$. For illustration, in Fig. 8.12 we present the phase distribution of the particles at the exit of magnetic system when the optical klystron operates in the saturation.

Let us now study the influence of the energy spread on the characteristics of the optical klystron at saturation. When $\hat{l}_1 = 1/2$ and $\overline{\delta\psi} = 0$, the values of the maximal efficiency $\hat{\eta}_{max}$ and parameter of resonator losses $\hat{\alpha}_{opt}$ are functions of two parameters, $\hat{d}$ and $\hat{\Lambda}_T$. When the length of the drift space is chosen to provide maximum of the small signal gain (it can be obtained from Fig. 8.6), then $\hat{\eta}_{max}$ and $\hat{\alpha}_{opt}$ are functions of the only energy spread parameter $\hat{\Lambda}_T$. The plots of these functions are presented in Figs. 8.13 and 8.14.

8.2.2. *FEL oscillator with a prebuncher*

Let us present some results of numerical simulations of the FEL oscillator with a prebuncher and tapered main undulator. Parameters of the oscillator are the same as those used for numerical example for the linear mode of operation (see Figs. 8.7–8.9). The parameter of resonator losses is chosen to be $\hat{\alpha} = 5 \times 10^{-3}$ and initial detuning corresponds to the maximum of the small signal gain in Fig. 8.9. The dependence of the reduced efficiency on the beam-wave phase shift parameter $\overline{\delta\psi}$ is presented

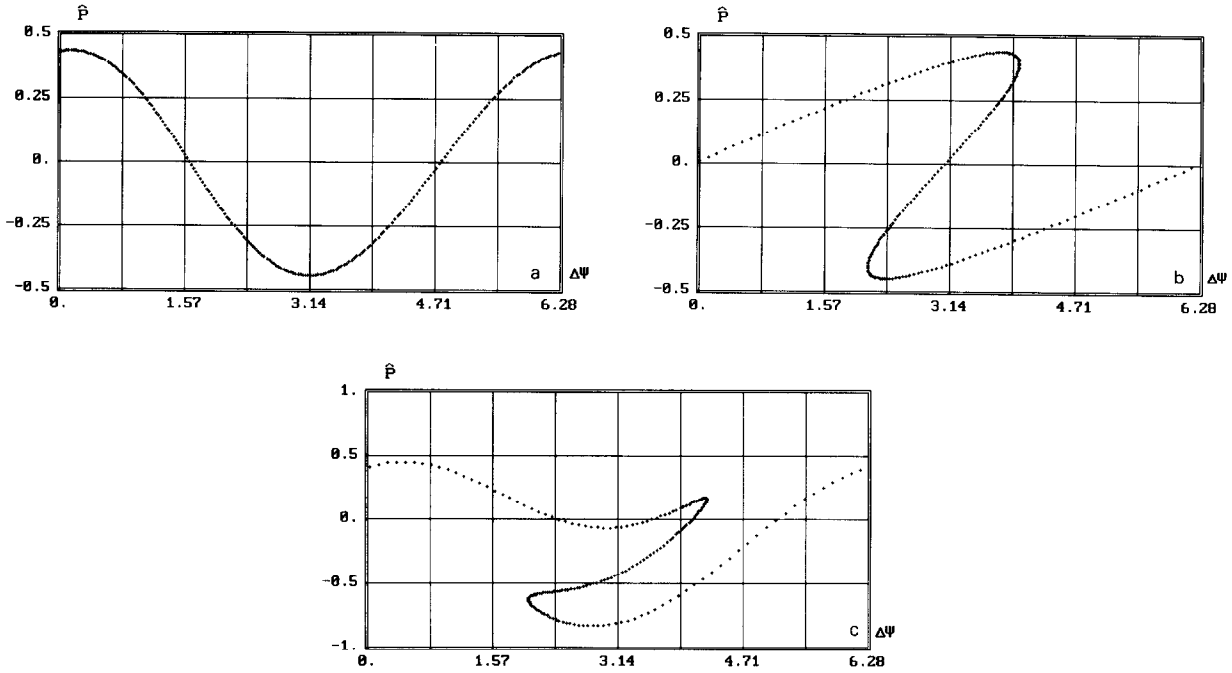

Fig. 8.12. Phase space distribution of the particles in the optical klystron operating at the saturation. Here $\hat{\alpha} = 0.594$, $\overline{\delta\psi} = 0$, $\hat{d} = 5$, $\hat{l}_1 = 1/2$, $\hat{b} = 0$ and $\hat{\Lambda}_T^2 = 0$. (a): distribution after the first undulator section, (b): distribution after the drift section and (c): distribution after the second undulator section.

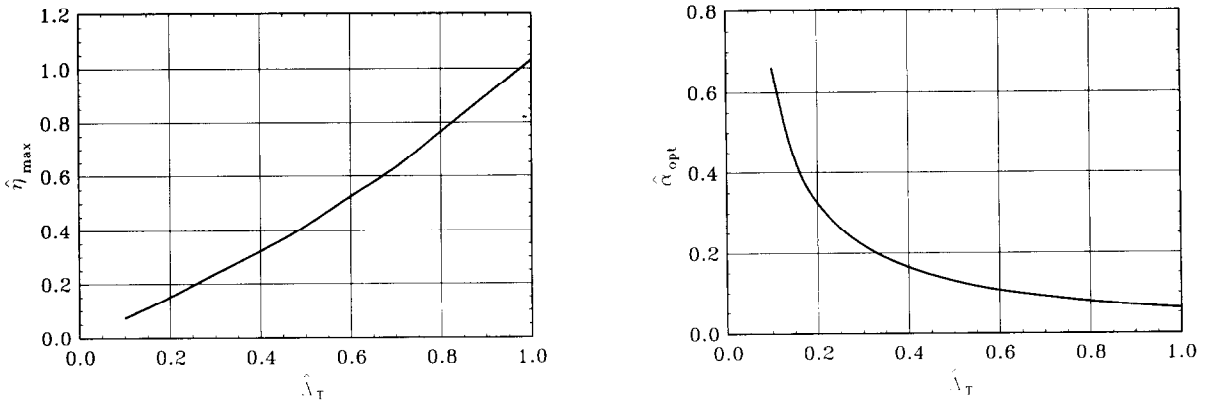

Fig. 8.13. The maximal reduced efficiency of the optical klystron at saturation versus the $\hat{\Lambda}_T$ parameter. Here $\overline{\delta\psi} = 0$, $\hat{d} = \hat{d}_{\mathrm{opt}}$, $\hat{l}_1 = 1/2$, $\hat{b} = 0$. The value of $\hat{d} = \hat{d}_{\mathrm{opt}}(\hat{\Lambda}_T)$ corresponds to the maximum of the small-signal gain $\hat{G}_s$.

Fig. 8.14. The optimal value of the reduced damping factor versus the $\hat{\Lambda}_T$ parameter. Here $\overline{\delta\psi} = 0$, $\hat{d} = \hat{d}_{\mathrm{opt}}$, $\hat{l}_1 = 1/2$, $\hat{b} = 0$. The value of $\hat{d} = \hat{d}_{\mathrm{opt}}(\hat{\Lambda}_T)$ corresponds to the maximum of the small-signal gain $\hat{G}_s$.

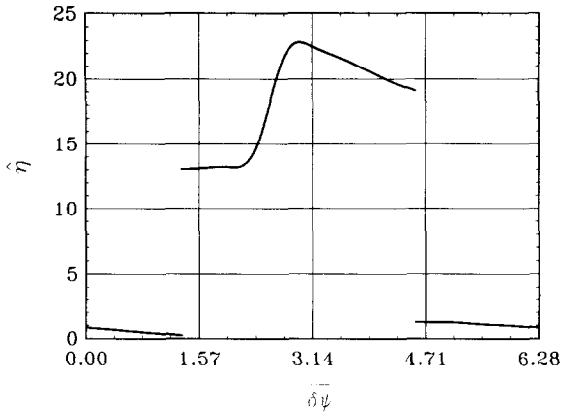

Fig. 8.15. The reduced efficiency at the saturation versus the $\overline{\delta\psi}$ parameter. Here $\hat{d} = 0.3$, $\hat{l}_1 = 0.05$, $\hat{b} = 30$, $\hat{\Lambda}_T^2 = 0$ and $\hat{\alpha} = 0.005$.

in Fig. 8.15. It is seen that there is a strong dependence of the efficiency on the value of the phase shift in the drift space. Comparing these results with those presented in Fig. 7.10 we conclude that the use of the prebuncher increases the efficiency by a factor of two with respect to the scheme with the tapered undulator without prebuncher (see Section 7).

8.3. *Perspectives of the efficiency increase*

In conclusion of this section we should make some remarks on the problem of the FEL oscillator efficiency. The efficiency of the FEL oscillator with a homogeneous undulator is rather small, $\eta \simeq 0.29/N_w$, where N_w is the number of the undulator periods (see Section 6). Usually N_w is about several tens which results in the FEL efficiency η less than one percent. Second, undulator tapering does not give such excellent results with respect to the FEL amplifier, it enables one to increase the FEL oscillator efficiency by a factor of 2 or 3. Using additional possibilities, such as a prebuncher, one increases the efficiency additionally by a factor of two. In any case the maximal FEL oscillator efficiency does not exceed a value of several per cent.

On the other hand, the efficiency of the FEL amplifier with tapered undulator can be done about of unity (see Section 4). Such a significant difference in the efficiency between the FEL amplifier and FEL oscillator configurations is connected with principal difference between these two FEL configurations when undulator tapering is used. In the case of the FEL amplifier, the frequency of the amplified wave is determined by a master oscillator, the initial conditions at the undulator entrance are fixed, the process of the field amplification develops in space, and, as a result, spatial tapering of the undulator parameters enables one to trap a significant fraction of the electrons in the regime of coherent deceleration. Contrary to this, the lasing frequency of the FEL oscillator depends on the value of the undulator tapering depth and is defined by the condition of the maximum of the small-signal gain in the linear mode of operation. Another difference is that the initial conditions at the undulator entrance depend on time due to the dependence on time of the field stored in the resonator. As a result, the dependence of the FEL oscillator efficiency on the tapering depth is nonmonotonous and breaking and the final FEL oscillator efficiency does not increase significantly with respect to the case of homogeneous undulator (see Section 7).

So, it seems impossible to achieve a high efficiency in the FEL oscillator using the conventional approach of undulator tapering. On the other hand, one should remember the history of the acceleration technique development. In the mid 1940s it was an idea by McMillan and Veksler to use the principle of phase stability of the particle motion in time-dependent electromagnetic fields, which has led to the invention of synchrotron and opened a way to attain superhigh energies [61,62]. It is evident now that only an approach similar to that proposed by McMillan and Veksler may solve the problem to construct the high-efficiency FEL oscillators. For the first time such an approach to increase the FEL oscillator efficiency was proposed in Ref. [63]. It is based on a natural feature of the FEL oscillator, namely the dependence on time of the radiation field stored in the resonator. It was proposed to introduce time-dependent accelerating fields into the interaction region (which is equivalent in its action to the undulator tapering). As a result, this makes it possible to trap electrons into the ponderomotive well and perform conversion of the microwave energy to the optical one. To increase number of trapped electrons (which results in higher efficiency), the authors of Ref. [63] proposed to use a prebuncher together with a homogeneous undulator. Numerical estimations, presented in Refs. [63,64] have shown that an efficiency of about several tens per cent can be achieved in such modification of the FEL oscillator. Later this idea has been developed in Ref. [65] where several alternative technical solutions have been proposed totally based on a well developed conventional RF structure and undulator technology.

There is another way to realize the idea of time-dependent variation of the FEL oscillator parameters to increase the efficiency. It was proposed to change in time the magnetic field of the undulator rather than to introduce the accelerating field into the interaction region [66,67]. The feasibility of this method has been confirmed by the results of numerical simulations. It was shown that the high efficiency ($\eta \sim 20\%$) FEL oscillator operating in the continuous or quasi-continuous mode may be constructed at the present level of accelerator technique R & D [67].

9. An introduction to analysis of diffraction effects

In the preceding sections we have studied the processes in the FEL in the framework of one-dimensional model. Due to the simplicity of the basic approximations of this model, it provides the most clear way to understand the physical mechanism of the FEL operation, the influence of the space charge fields and the energy spread of the electrons in the beam on the FEL operation. It provides also a reliable way to study undulator tapering technique to increase the FEL efficiency.

The validity region of the one-dimensional model is limited with the condition that the radiation does not expand in outer space outside the electron beam. In many practical situations diffraction effects influence significantly on the process of the field formation in the FEL, so the problem is arisen of the FEL description taking into account diffraction effects. A theoretical analysis of the processes in the FEL boils down to a simultaneous solution of field equations and equations of motion of beam electrons under corresponding boundary conditions for the electromagnetic field. It should be noticed that in such a general formulation, this problem can not be solved and usually the FEL models are constructed which in some way simplify the processes occurring in the FEL. However, with the simple calculated relations given these models allow to reveal main factors influencing the operation of practical systems. Therefore, in a number of cases solutions of model problems may be suitable for FEL designers, especially at the design stage of an experiment.

Nowadays there is a perceptible progress in the development of analytical techniques in the linear theory of the FEL amplifier. In particular, during last years almost all the rigorous results of the FEL amplifier mode theory were obtained. The first rigorous results of the eigenvalue problem solution, taking into account diffraction effects, were obtained in Ref. [68] in the framework of the FEL amplifier with "open" axisymmetric electron beam with a stepped profile of the beam current density. It has been shown that in the linear high-gain limit the radiation of the electron beam in the undulator can be represented as a set of modes. When amplification takes place, the mode configuration in the transverse plane remains unchanged while the amplitude grows with the undulator length exponentially. Each mode is characterized with the increment eigenvalue and the field distribution eigenfunction in terms of transverse coordinates. The mode with the highest increment has the advantage over all other modes. Following the gain process along the undulator axis one can find that the field distribution is settled corresponding to the mode with the maximal increment. This effect has been named "optical guiding".

Mode consideration of Ref. [68] was restricted with the ground symmetrical TEM_{00} mode. In Ref. [69] this approach was generalized to the case of the higher order TEM_{mn} modes. Besides, in Ref. [69] the influence on the FEL amplifier operation of the energy spread of electrons in the beam and space charge fields, were taken into account. The complete analytical description of the FEL amplifier with the "open" sheet electron beam was presented in Ref. [70]. First rigorous results of the mode theory of the FEL amplifier with gradient profile of electron beam were presented in Ref. [71] for the case of sheet electron beam with Epstein profile of current density. Another gradient profile allowing rigorous solutions, is the bounded parabolic one. Solutions for this profile were obtained in Ref. [72]. When considering axially symmetric geometry, there exists the only profile allowing analytical solutions, namely the bounded parabolic profile. Mode theory of the FEL amplifier describing this case was developed in Ref. [69].

There are many different approaches to description of the linear mode of operation of the FEL amplifier with the "open" electron beam. For example, the method based on the operational techniques and expansion of the radiation fields in terms of Hermite-gaussian modes is used to solve the initial problem for electron beams with an arbitrary gradient profile of current density [73]. Some different approaches are used to take into account betatron oscillation effects, namely the variational method [74] and method of orthogonal expansion of the electron distribution function [75].

Physical approximations of the FEL amplifier model with the "open" electron beam assume the waveguide or vacuum chamber walls to be placed far enough from the electron beam, formally at infinity. Such a model gives a possibility to simplify significantly the FEL amplifier description. The approximation of the "open" beam describes rather well the operation of the FEL amplifiers of short-wave infrared, visible and VUV wavelength ranges, but it is not appropriate enough for describing the FEL amplifiers of microwave and millimeter wavelength ranges. To obtain a correct description of the latter case it is necessary to take into account the influence of the waveguide walls on the FEL amplifier operation. Besides, the analysis of the general case makes it possible to obtain the applicability region of the FEL amplifier model with the "open" beam.

It should be noted that the generalized approach does not help someone very much in the construction of the theory of the FEL amplifier with a waveguide: there are some peculiarities in each specific situation. In particular, the structure of self-consistent field equations strongly depends on the type of undulator. Recently some analytical results of the FEL amplifier theory with planar waveguide were obtained [72]. These investigations were stimulated by the proposal to design perspective microwave

FEL amplifier with a planar geometry [76]. Paper [72] is devoted to the quasi-optical theory of the FEL amplifier with the sheet electron beam, planar undulator and planar waveguide. Rigorous solutions were obtained for electron beams with the stepped and bounded parabolic profiles. This model may be considered as a limitary transition of the FEL amplifier model with the rectangular waveguide. The analytical solutions obtained for the planar geometry may serve as a reliable test base for simulation codes (as far as we know, it is impossible to obtain analytical solutions for rectangular geometry).

The first results of the mode theory of the FEL amplifier with axisymmetric electron beam, overmoded circular waveguide and helical undulator has been presented in Ref. [77]. It should be noted that this case is more complicated than the case of the planar geometry. In particular, it was found that azimuthal symmetry of the electron beam current density modulation does not lead to the azimuthal symmetry of the radiation fields and vice versa. Physically it means that azimuthal symmetry is violated by the helicity of the undulator. Indeed, the electron beam moving in the helical magnetic field may be considered as a gyrothrope active medium. In the case of the open beam it results in the circular polarization of the radiation field. The presence of the walls of the circular waveguide significantly complicates the situation because boundary conditions on the waveguide walls are different for radial and azimuthal components of the electric field of the amplified wave. As a result, double degeneration of azimuthal modes is eliminated and it leads to the mentioned above difference between the azimuthal dependencies of the electron beam density modulation and radiation field.

As far as we know, there are no other beam profiles except the above mentioned profiles (stepped, bounded parabolic, Epstein and annular) which admit analytical solutions. To find the radiation modes for electron beam with an arbitrary gradient profile, one should use approximate methods and the multilayer approximation method is one of them [71]. It may be used when one can perform the separation of variables.

Unfortunately, due a complexity of the problem, there are no significant achievements in the development of analytical techniques for the FEL oscillators. As far as we know, there exists only two papers [33,34] where a novel analytical method to solve the eigenvalue problem for active open plane Fabry-Perot resonator has been developed. The base concept of this approach is the application of rigorous impedance boundary conditions of resonance-type (proposed by L.A. Veinstein in Ref. [78]) at the open resonator ends. This makes it possible to reduce the problem of the open resonator to a closed one. As a result the equations are obtained which may be resolved analytically by means of standard methods. The method is applicable as in the FEL theory as in semiclassical theory of laser [79–82].

One of the important aspects of the FEL theory is the analysis of the nonlinear processes. The analytical methods are limited in the description of the saturation effects and numerical simulation codes are being used. The main problems of the nonlinear simulations are connected with the calculation of the radiation and space charge fields. Several different methods are used to calculate the radiation fields: various modifications of the transverse mode spectral method (see e.g. Ref. [83]), the finite difference method [84–86] and the Green's function method [87]. The developed nonlinear codes provide a possibility to perform rather rigorous calculations of the FEL amplifiers. On the other hand, situations with the codes for calculations of the FEL oscillators is not so excellent which is connected with the problem of the rigorous calculations of the radiation fields (a similar problem takes place in the theory of quantum lasers, too).

So, we see that incorporation into consideration of the effects of radiation diffraction, waveguide walls, etc., would lead to a substantial increase in the review's volume. To be acquainted with such generalizations the reader should refer to original publications. In this paper we limit our consideration of the diffraction effects with the case of the FEL amplifier with the "open" electron beam when the influence of the waveguide walls (or vacuum chamber walls etc.) on the process in the FEL may be neglected. Such a model is well suitable for FEL amplifiers of short-wave infrared, visible, VUV and soft X-ray wavelength ranges.

9.1. Self-consistent field equations

The analyzed model is based on the Maxwell's wave equations taken in the paraxial approximation and the description of the electron beam with the kinetic equation expressed in "energy-phase" variables. It is anticipated that electrons move (on the average over constrained motion) only along the trajectories parallel to the undulator axis. Such a model has proved to be very fruitful to describe the physical phenomena in the FEL amplifiers and allows one to take into consideration such effects as diffraction of radiation, space charge fields and energy spread of electrons in the beam. Moreover, using the results obtained with this model, the reader can define the applicability region of the one-dimensional theory described in the previous sections.

Let us consider relativistic electron beam moving along the z axis in the field of the helical undulator. The undulator magnetic field at the axis has the form

$$H_x + iH_y = H_w \exp(-i\kappa_w z),$$

where $\kappa_w = 2\pi/\lambda_w$ is the undulator wavenumber. We neglect the transverse variation of the undulator field and assume the electrons to move along the constrained helical trajectories in parallel with the z axis. The electron rotation angle is considered to be small and the longitudinal electron velocity v_z is close to the velocity of light c ($v_z \simeq c$). The electric field of the amplified wave may be represented in the complex form

$$E_x + iE_y = \tilde{E}(z, \boldsymbol{r}_\perp) \exp[i\omega(z/c - t)]. \tag{9.1}$$

As it was done in the previous sections, we describe the electron motion using "energy-phase" variables $\mathcal{E}$ and $\psi = \kappa_w z + \omega(z/c - t)$. Using the approximation that electrons move only in the z direction, the evolution of the distribution function $f(\psi, \mathcal{E}, z, \boldsymbol{r}_\perp)$ is given by the kinetic equation

$$\frac{\partial f}{\partial z} + \frac{d\psi}{dz}\frac{\partial f}{\partial \psi} + \frac{d\mathcal{E}}{dz}\frac{\partial f}{\partial \mathcal{E}} = 0.$$

In the linear approximation we shall seek the solutions for f in the form

$$f = f_0 + \tilde{f}_1 e^{i\psi} + \tilde{f}_1^* e^{-i\psi}.$$

In the linear approximation, the energy $\mathcal{E}$ of the particle does not differ significantly from the nominal value $\mathcal{E}_0$, so the electron motion can be described with the Hamiltonian (2.5):

$$H = CP + \frac{\omega}{2c\gamma_z^2 \mathcal{E}_0} P^2 - (Ue^{i\psi} + U^* e^{-i\psi}) + \int d\psi e E_z.$$

Derivatives $d\psi/dz$ and $d\mathcal{E}/dz$ are defined with the corresponding canonical equations of motion. As a result, we obtain the following equations for the amplitude $\tilde{f}_1$

$$\frac{\partial}{\partial z}\tilde{f}_1 + i[C + \omega P/(c\gamma_z^2\mathcal{E}_0)]\tilde{f}_1 + (iU - e\tilde{E}_z)\frac{\partial}{\partial P}f_0 = 0. \tag{9.2}$$

Here notations are similar to those of section 2: $P = \mathcal{E} - \mathcal{E}_0$, $C = [\kappa_w - \omega/(2c\gamma_z^2)]$ is the detuning of the particle having nominal energy $\mathcal{E}_0$, $U = -e\theta_s\tilde{E}(z, \boldsymbol{r}_\perp)/2i$ is the complex amplitude of the particle-wave effective potential of interaction and $\tilde{E}_z(z, \boldsymbol{r}_\perp)$ is the complex amplitude of the longitudinal space charge field.

In the further consideration we use the following approximations

(a) complex amplitude of the electric field $\tilde{E}$ is the slowly changing function, i.e. $|\partial\tilde{E}/\partial z| \ll \kappa_w|\tilde{E}|$;

(b) the transverse electron beam dimension is rather large, i.e. $r_b^2 \gg \gamma_z^2 c^2/\omega^2$;

(c) The electron beam at the undulator entrance is modulated neither in velocity nor density, i.e.

$$\tilde{f}_1|_{z=0} = 0, \quad f_0|_{z=0} = n_0(\boldsymbol{r}_\perp)F(P), \tag{9.3}$$

where the function $F(P)$ describing the energy distribution is normalized to the unity. The beam current density is connected with the distribution function as follows (we assume here $v_z \simeq c$):

$$j_z = -j_0(\boldsymbol{r}_\perp) + \tilde{j}_1 \exp^{i\psi} + C.C., \quad \tilde{j}_1 \simeq -ec\int \tilde{f}_1 dP,$$

where $-j_0(\boldsymbol{r}_\perp) \simeq -ecn_0(\boldsymbol{r}_\perp)$ is the longitudinal component of the beam current density at the undulator entrance at $z = 0$.

In the frame of accepted limitation on the electron beam transverse size, we can write the following expression for $\tilde{E}_z$

$$\tilde{E}_z = -4\pi i\tilde{j}_1/\omega. \tag{9.4}$$

Complex amplitude $\tilde{j}_1$ can be obtained with the integration of kinetic equation (9.2). Using initial conditions (9.3) and expression (9.4) we have

$$\tilde{j}_1(z, \boldsymbol{r}_\perp) = ij_0(\boldsymbol{r}_\perp)\int_0^z dz'[U(z', \boldsymbol{r}_\perp) + 4\pi e\tilde{j}_1(z', \boldsymbol{r}_\perp)/\omega]$$

$$\times \int_{-\infty}^{\infty} dP\frac{dF(P)}{dP}\exp[i\,(C + \omega P/(c\gamma_z^2\mathcal{E}_0))\,(z' - z)]. \tag{9.5}$$

Now we should consider electrodynamic problem. The electromagnetic field in the amplifier is subjected to the wave equation

$$c^2\nabla^2\boldsymbol{E} - \partial^2\boldsymbol{E}/\partial t^2 = c^2\nabla(\nabla\cdot\boldsymbol{E}) + 4\pi\partial\boldsymbol{j}/\partial t, \tag{9.6}$$

which can be obtained from Maxwell equations. In the frame of accepted limitation, we can neglect the term $\nabla(\nabla\cdot\boldsymbol{E})$ in the right-hand side of Eq. (9.6). When the transverse electron motion in

the undulator is defined by the undulator field but not radiation field and in the ultrarelativistic approximation we can write the following expression for the transverse beam current density

$$\boldsymbol{j}_\perp = \theta_s[\boldsymbol{e}_x \cos(\kappa_w z) - \boldsymbol{e}_y \sin(\kappa_w z)](\tilde{j}_1 e^{i\psi} + \text{c.c.}) \tag{9.7}$$

We seek the solution for $\boldsymbol{E}$ in the form of Eq. (9.1). Substituting Eqs. (9.1) and (9.7) into Eq. (9.6) and neglecting the fast oscillating terms, we obtain equation for the slowly changing amplitudes $\tilde{j}_1$ and $\tilde{E}$

$$c^2[\nabla_\perp^2 + 2i(\omega/c)\partial/\partial z]\tilde{E} = -4\pi i\theta_s\omega\tilde{j}_1, \tag{9.8}$$

where $\nabla_\perp^2$ is the Laplace operator over transverse coordinates. When writing down this equation we have assumed the characteristic scale of the radiation field $\tilde{E}$ change along the z axis to be much more than the radiation wavelength, so the second derivative of $\tilde{E}$ with respect to z has been omitted. One can see that at the right-hand side equal to zero, Eq. (9.8) coincides with the well known wave equation written down in paraxial approximation (see e.g. Ref. [88]).

So, we have obtained the system of self-consistent field equations (9.5) and (9.8). This system can be solved by two methods. First, we can substitute Eq. (9.5) into the right-hand side of Eq. (9.8). Then expressing the function $\tilde{j}_1(z', \boldsymbol{r}_\perp)$ in terms of Eq. (9.8), we obtain integro-differential equation for the field amplitude $\tilde{E}$

$$\nabla_\perp^2\tilde{E} + 2i\frac{\omega}{c}\frac{\partial\tilde{E}}{\partial z} = ij_0(\boldsymbol{r}_\perp)\int_0^z dz'\left[\frac{2\pi e}{c^2}\theta_s^2\omega\tilde{E}(z', \boldsymbol{r}_\perp) + \frac{4\pi e}{\omega}\left[\nabla_\perp^2\tilde{E} + 2i\frac{\omega}{c}\frac{\partial\tilde{E}}{\partial z'}\right]\right]$$
$$\times\int_{-\infty}^{\infty} dP\frac{dF}{dP}\exp\left[i\left(C + \frac{\omega}{\gamma_z^2\mathcal{E}_0 c}P\right)(z'-z)\right]. \tag{9.9}$$

Another method consists in obtaining a single integral equation for the first harmonic $\tilde{j}_1(z, \boldsymbol{r}_\perp)$. In this case we solve Eq. (9.8) with respect to $\tilde{E}(z', \boldsymbol{r}_\perp)$, then substitute this solution into Eq. (9.5), and obtain the only integral equation for the first harmonic of the beam current density $\tilde{j}_1(z, \boldsymbol{r}_\perp)$.

Let us represent the radiation field as a sum of external and radiated waves: $\tilde{E} = \tilde{E}_{\text{ext}} + \tilde{E}_i$. Solving Eq. (9.8), we find the field of the radiated wave $\tilde{E}_i$:

$$\tilde{E}_i(z, \boldsymbol{r}_\perp) = i\theta_s\frac{\omega}{c^2}\int_0^z\frac{dz'}{z-z'}\int d\boldsymbol{r}_\perp\tilde{j}_1(z', \boldsymbol{r}'_\perp)\exp\left[\frac{i\omega|\boldsymbol{r}_\perp - \boldsymbol{r}'_\perp|^2}{2c(z-z')}\right]. \tag{9.10}$$

Substituting Eq. (9.10) into Eq. (9.5), we obtain the single integral equation for the first harmonic of the beam current density $\tilde{j}_1$

$$\tilde{j}_1(z, \boldsymbol{r}_\perp) = ij_0(\boldsymbol{r}_\perp)\int_0^z dz'\left\{-\frac{e\theta_s}{2i}\tilde{E}_{\text{ext}}(z', \boldsymbol{r}_\perp) + \frac{4\pi e}{\omega}\tilde{j}_1(z', \boldsymbol{r}_\perp)\right.$$
$$\left. - \frac{e\theta_s^2\omega}{2c^2}\int_0^{z'}\frac{dz''}{z'-z''}\int d\boldsymbol{r}'_\perp\tilde{j}_1(z'', \boldsymbol{r}'_\perp)\exp\left[\frac{i\omega|\boldsymbol{r}_\perp - \boldsymbol{r}'_\perp|^2}{2c(z'-z'')}\right]\right\}$$

$$\times \int_{-\infty}^{\infty} dP \frac{dF}{dP} \exp\left[i \left(C + \frac{\omega}{\gamma_z^2 \mathcal{E}_0 c} P \right) (z' - z) \right]. \tag{9.11}$$

When the energy spread is negligibly small ($F(P) \to \delta(P)$, where $\delta(P)$ is the delta function), this equation is reduced to:

$$\frac{d^2 \tilde{j}_1}{dz^2} + 2iC \frac{d\tilde{j}_1}{dz} + \left[\frac{4\pi e}{c\gamma_z^2 \mathcal{E}_0} j_0(\boldsymbol{r}_\perp) - C^2 \right] \tilde{j}_1$$

$$= \frac{\omega}{c\gamma_z^2 \mathcal{E}_0} j_0(\boldsymbol{r}_\perp) \left\{ \frac{e\theta_s}{2i} \tilde{E}_{\text{ext}}(z, \boldsymbol{r}_\perp) + \frac{e\theta_s^2 \omega}{2c^2} \int_0^z \frac{dz'}{z - z'} \int d\boldsymbol{r}'_\perp \tilde{j}_1(z', \boldsymbol{r}'_\perp) \right.$$

$$\left. \times \exp\left[\frac{i\omega |\boldsymbol{r}_\perp - \boldsymbol{r}'_\perp|^2}{2c(z - z')} \right] \right\}. \tag{9.12}$$

So, the self-consistent field method in the linear approximation enables one to get from the kinetic equation and Maxwell's equations the only equation either for the field amplitude of amplified wave (9.9) or for the modulation amplitude of the beam current density (9.11). Both of the ways lead to the same results but for the analytical calculations it is preferable to use the equation for the wave field: in this case the mathematical apparatus is always connected with more conventional differential equations. At the same time the situations with the computer simulations is proved to be reversed and the method using the equation for the modulation amplitude of the beam current density is more convenient.

9.2. Conservation energy law

Let us show that the energy conservation law takes place, i.e. the output radiation power of the FEL amplifier is equal to the power losses of the electron beam. To find radiation power W, we consider the Fresnel diffraction approximation. So as diffraction angles are small, the vectors of electric and magnetic field are equal in the absolute value and are perpendicular to each other. Thus, the expression for the radiation power can be written in the form:

$$W = \frac{c}{4\pi} \int \overline{|\boldsymbol{E}|^2} d\boldsymbol{r}_\perp,$$

where the line denotes the averaging in time. Total electromagnetic field in the undulator is the sum of external and radiated waves, so the total radiation power W consists of three summands: $W = W_1 + W_2 + W_3$. The summand W_1 refers to the radiated wave

$$W_1 = \frac{c}{4\pi} \int \overline{|\boldsymbol{E}_i|^2} d\boldsymbol{r}_\perp, \tag{9.13a}$$

the summand W_2 refers to the external wave and is equal to the external signal power

$$W_2 = \frac{c}{4\pi} \int \overline{|\boldsymbol{E}_{\text{ext}}|^2} d\boldsymbol{r}_\perp = W_{\text{ext}}. \tag{9.13b}$$

The interference summand W_3 is equal to:

$$W_3 = \frac{c}{2\pi}\int \overline{(\boldsymbol{E}_i \cdot \boldsymbol{E}_{\rm ext})}\, d\boldsymbol{r}_\perp . \tag{9.13c}$$

Let us consider the summand W_1. So as the radiation field in the Fresnel diffraction zone has the form (9.10), then W_1 is given with:

$$\begin{aligned} W_1 &= \frac{c}{4\pi}\int \overline{|\boldsymbol{E}_i|^2}\, d\boldsymbol{r}_\perp \\ &= \frac{\omega^2\theta_s^2}{4\pi c^3}\int d\boldsymbol{r}_\perp \left\{ \int_0^z \frac{dz'}{z-z'} \int d\boldsymbol{r}'_\perp \tilde{j}_1(z', \boldsymbol{r}'_\perp) \exp\left[\frac{i\omega|\boldsymbol{r}_\perp - \boldsymbol{r}'_\perp|^2}{2c(z-z')}\right]\right\} \\ &\times \left\{ \int_0^z \frac{dz''}{z-z''} \int d\boldsymbol{r}''_\perp \tilde{j}_1^*(z'', \boldsymbol{r}''_\perp) \exp\left[-\frac{i\omega|\boldsymbol{r}_\perp - \boldsymbol{r}''_\perp|^2}{2c(z-z'')}\right]\right\}. \end{aligned} \tag{9.14}$$

The products of integrals over z' and z'' can be represented as

$$\int_0^z \Phi(z')dz' \int_0^z \Phi^*(z'')dz'' = \int_0^z \Phi(z')dz' \int_0^{z'} \Phi^*(z'')dz'' + \text{c.c.} \tag{9.15}$$

The integral over transverse coordinate $\boldsymbol{r}_\perp$ is equal to:

$$\begin{aligned} &\int d\boldsymbol{r}_\perp \exp\left\{\frac{i\omega|\boldsymbol{r}_\perp - \boldsymbol{r}'_\perp|^2}{2c(z-z')} - \frac{i\omega|\boldsymbol{r}_\perp - \boldsymbol{r}''_\perp|^2}{2c(z-z'')}\right\} \\ &= \int_{-\infty}^{\infty} dx \int_{-\infty}^{\infty} dy \exp\left\{\frac{i\omega}{2c}\frac{(x-x')^2 + (y-y')^2}{z-z'} - \frac{i\omega}{2c}\frac{(x-x'')^2 + (y-y'')^2}{z-z''}\right\} \\ &= \frac{2\pi i c}{\omega}\frac{(z-z')(z-z'')}{z'-z''} \exp\left\{\frac{-i\omega|\boldsymbol{r}'_\perp - \boldsymbol{r}''_\perp|^2}{2c(z'-z'')}\right\}. \end{aligned}$$

As a result, expression (9.14) can be written in the form

$$\begin{aligned} W_1 = \frac{i\omega^2\theta_s^2}{2c^2}\int_0^z dz' \int_0^{z'} \frac{dz''}{z'-z''} \int d\boldsymbol{r}'_\perp \int d\boldsymbol{r}''_\perp \tilde{j}_1^*(z'', \boldsymbol{r}''_\perp)\tilde{j}_1(z', \boldsymbol{r}'_\perp) \\ \times \exp\left\{\frac{-i\omega|\boldsymbol{r}'_\perp - \boldsymbol{r}''_\perp|^2}{2c(z'-z'')}\right\} + \text{c.c.} \end{aligned} \tag{9.16}$$

To calculate the interference summand W_3, we represent the field of the external wave at $z = 0$ in a Fourier series:

$$\left[(\boldsymbol{E}_{\rm ext})_x + i(\boldsymbol{E}_{\rm ext})_y\right]_{z=0} = \tilde{E}_{\rm ext}(0, \boldsymbol{r}_\perp)\exp(-i\omega t) = \exp(-i\omega t)\int A(\boldsymbol{k}_\perp)\exp(i\boldsymbol{k}_\perp \cdot \boldsymbol{r}_\perp)d\boldsymbol{k}_\perp .$$

Each Fourier component is a plane wave:

$$\tilde{E}_{\rm ext}(z,\boldsymbol{r}_\perp)\exp(i\omega(z/c-t))=\exp(-i\omega t)\int d\boldsymbol{k}_\perp A(\boldsymbol{k}_\perp)\exp(i\boldsymbol{k}_\perp\cdot\boldsymbol{r}_\perp+ik_z z),$$

where

$$k_z=\frac{1}{c}\sqrt{\omega^2-k_\perp^2c^2}\simeq\frac{\omega}{c}-\frac{c|k_\perp|^2}{2\omega}.$$

Therefore, the complex amplitude $\tilde{E}_{\rm ext}(z,\boldsymbol{r}_\perp)$ of the external field is given by

$$\tilde{E}_{\rm ext}(z,\boldsymbol{r}_\perp)=\int d\boldsymbol{k}_\perp A(\boldsymbol{k}_\perp)\exp\left\{i\boldsymbol{k}_\perp\cdot\boldsymbol{r}_\perp-\frac{ik_\perp^2c}{2\omega}z\right\}. \tag{9.17}$$

Substituting this expression for $\tilde{E}_{\rm ext}(z,\boldsymbol{r}_\perp)$ into Eq. (9.13c), we obtain:

$$\begin{aligned}W_3&=\frac{c}{4\pi}\int(\tilde{E}_{\rm ext}\tilde{E}_i^*+\tilde{E}_{\rm ext}^*\tilde{E}_i)d\boldsymbol{r}_\perp\\&=-i\frac{\theta_s\omega}{4\pi c}\int d\boldsymbol{r}_\perp\int d\boldsymbol{k}_\perp A(\boldsymbol{k}_\perp)\exp\left\{i\boldsymbol{k}_\perp\cdot\boldsymbol{r}_\perp-\frac{ik_\perp^2c}{2\omega}z\right\}\\&\times\int_0^z\frac{dz'}{z-z'}\int d\boldsymbol{r}'_\perp\tilde{j}_1^*(z',\boldsymbol{r}'_\perp)\exp\left\{-\frac{i\omega|\boldsymbol{r}_\perp-\boldsymbol{r}'_\perp|^2}{2c(z-z')}\right\}+\text{c.c.}\end{aligned}$$

Integral over transverse coordinate $\boldsymbol{r}_\perp$ can be calculated as:

$$\begin{aligned}&\int d\boldsymbol{r}_\perp\exp\left\{i\boldsymbol{k}_\perp\cdot\boldsymbol{r}_\perp-\frac{i\omega|\boldsymbol{r}_\perp-\boldsymbol{r}'_\perp|^2}{2c(z-z')}\right\}\\&=\int_{-\infty}^{\infty}d\zeta\exp\left\{ik_x\zeta-\frac{i\omega(\zeta-x')^2}{2c(z-z')}\right\}\int_{-\infty}^{\infty}d\xi\exp\left\{ik_y\xi-\frac{i\omega(\xi-y')^2}{2c(z-z')}\right\}\\&=-\frac{2\pi ic}{\omega}(z-z')\exp\left\{i\boldsymbol{k}_\perp\cdot\boldsymbol{r}'_\perp+\frac{ik_\perp^2c}{2\omega}(z-z')\right\}.\end{aligned}$$

As a result, we obtain:

$$\begin{aligned}W_3&=-\tfrac{1}{2}\theta_s\int_0^z dz'\int d\boldsymbol{r}'_\perp\tilde{j}_1^*(z',\boldsymbol{r}'_\perp)\int d\boldsymbol{k}_\perp A(\boldsymbol{k}_\perp)\exp\left\{i\boldsymbol{k}_\perp\cdot\boldsymbol{r}'_\perp-\frac{ik_\perp^2c}{2\omega}z'\right\}+\text{c.c.}\\&=-\tfrac{1}{2}\theta_s\int_0^z dz'\int d\boldsymbol{r}'_\perp\tilde{j}_1^*(z',\boldsymbol{r}'_\perp)\tilde{E}_{\rm ext}(z',\boldsymbol{r}'_\perp)+\text{c.c.}\end{aligned} \tag{9.18}$$

The expressions for W_1 and W_3 can be written in terms of effective potentials of the radiated field U_i and external field $U_{\rm ext}$

$$U_i=-\frac{e\theta_s\tilde{E}_i(z,\boldsymbol{r}_\perp)}{2i},\quad U_{\rm ext}=-\frac{e\theta_s\tilde{E}_{\rm ext}(z,\boldsymbol{r}_\perp)}{2i}.$$

Using Eqs. (9.16) and (9.18) we write for the sum $W_1 + W_3$:

$$W_1 + W_3 = \frac{1}{e}\int_0^z dz'\{i\int dr'_\perp [U_i(z', r'_\perp) + U_{ext}(z', r'_\perp)]\tilde{j}_1^*(z', r'_\perp) + \text{c.c.}\}. \tag{9.19}$$

On the other hand, the radiated power $W_1 + W_3$ must be equal to the difference of the electron beam powers at the exit and the entrance of the undulator. First, we find the energy change of the single electron

$$\frac{d\mathcal{E}}{dz} = -\frac{\partial H}{\partial \psi} = i(U_i + U_{ext} + 4\pi e\tilde{j}_1/\omega)\exp(i\psi) + \text{c.c.}$$

To find averaged power losses in the beam, we must multiply $d\mathcal{E}/dz$ by the beam current density $-j_z(\psi, z, r_\perp)/e$, average over phase ψ and integrate over transverse coordinate and the z coordinate:

$$\begin{aligned}\Delta W_e &= -\frac{1}{2\pi e}\int_0^{2\pi} d\psi \int dr'_\perp \int_0^z j_z(\psi, z, r'_\perp)\frac{d\mathcal{E}}{dz}\\ &= -\frac{1}{e}\int_0^z dz'\left\{\frac{i}{2\pi}\int_0^{2\pi} d\psi \int dr'_\perp (U_i + U_{ext} + 4\pi e\tilde{j}_1/\omega) j_z \exp(i\psi) + \text{c.c.}\right\}\\ &= -\frac{1}{e}\int_0^z dz'\left\{i\int dr'_\perp (U_i + U_{ext})\tilde{j}_1^* + \text{c.c.}\right\}.\end{aligned}$$

Comparing this expression with Eq. (9.19), we see that the radiation power and the change in the electron beam power have equal absolute values and are opposite in signs, i.e. $\Delta W_e + W_1 + W_3 = 0$. So, the conservation energy law takes place.

10. Linear quasi-optical theory of the FEL amplifier with an axisymmetric electron beam

In this section we present theoretical analysis of the FEL amplifier with an axisymmetric electron beam. An FEL model is discussed wherein diffraction effects, space charge fields and energy spread of electrons in the beam are taken into account.

We have shown in Section 9 that in the linear approximation the self-consistent field method makes possible to get from the kinetic and Maxwell's equations the only integro-differential equation for the radiation field amplitude. In this section this equation is used to solve the eigenvalue problem. To find the eigenvalues and eigenfunctions we use the condition of the quadratic integrability of the eigenfunction and the continuity conditions of the eigenfunction and its derivative at the beam boundary. The obtained solutions allow one to calculate increments of the eigenmodes, find the field distributions in the Fresnel and Fraunhofer diffraction zones. Asymptotical behaviour of the obtained solutions is discussed, too.

The next problem of the linear theory is the initial-value problem consisting in the finding of the evolution of the amplified wave under given conditions at the undulator entrance. The first analytical solutions of the initial problem of the FEL amplifier with axisymmetric electron beam have been

obtained in Ref. [89]. In the present paper we follow by Ref. [69] where the initial problem has been solved for the practically important case with the unmodulated electron beam and electromagnetic radiation from the master oscillator at the entrance into the undulator. When the electron beam profile is stepped, the initial problem was solved analytically with the Laplace transform technique. The asymptotic formulae for the high gain limit were derived taking into account diffraction of radiation, space charge fields and energy spread of the electrons in the beam. When the electron beam has the arbitrary gradient profile there is no possibility to obtain the rigorous analytical solution of the initial problem. For this case we have developed the algorithm of numerical integration of the self-consistent field equations.

At the design stage of an experiment the problem of optimal focusing of the external radiation beam on the electron beam is usually arisen. We have performed the optimization of the external radiation focusing for the case practically important when external radiation has the form of the Gaussian laser beam.

10.1. Solution of the eigenvalue problem

Let us consider the homogeneous axisymmetric electron beam with radius r_0. Using polar coordinates (r, φ, z), in the high-gain limit we shall seek the solution of Eq. (9.9) in the form

$$\tilde{E}(z, r, \varphi) = \Phi_n(r) e^{\Lambda z} \begin{pmatrix} \cos(n\varphi) \\ \sin(n\varphi) \end{pmatrix}, \tag{10.1}$$

where n is integer, $n \geq 0$. Substituting expressions (10.1) into Eq. (9.9) we get the Bessel equations

$$\hat{r}^2 d^2\Phi_n/d\hat{r}^2 + \hat{r} d\Phi_n/d\hat{r} + (\mu^2\hat{r}^2 - n^2)\Phi_n = 0, \quad \text{at } \hat{r} < 1, \tag{10.2a}$$

$$\hat{r}^2 d^2\Phi_n/d\hat{r}^2 + \hat{r} d\Phi_n/d\hat{r} - (g^2\hat{r}^2 + n^2)\Phi_n = 0, \quad \text{at } \hat{r} > 1, \tag{10.2b}$$

where the following notations are introduced: $\hat{r} = r/r_0$, $\hat{C} = C/\Gamma$ is the detuning parameter, $\hat{\Lambda} = \Lambda/\Gamma$ is the reduced eigenvalue, $g^2 = -2iB\hat{\Lambda}$,

$$\mu^2 = \frac{-2i\hat{D}}{1 - i\hat{\Lambda}_p^2\hat{D}} - g^2, \quad \hat{D} = \int_{-\infty}^{\infty} d\xi \frac{d\hat{F}(\xi)/d\xi}{\hat{\Lambda} + i\hat{C} + i\xi}.$$

The reduced energy distribution function $\hat{F}(\xi)$ is normalized to the unity: $\int \hat{F}(\xi) d\xi = 1$, where $\xi = \omega(\mathcal{E} - \mathcal{E}_0)/(c\gamma_z^2\Gamma\mathcal{E}_0)$ is the reduced energy deviation. The gain parameter Γ, diffraction parameter B and space charge parameter $\hat{\Lambda}_p^2$ are defined with formulae

$$\Gamma = \left[\frac{I\omega^2\theta_s^2}{I_A c^2\gamma_z^2\gamma}\right]^{1/2}, \quad B = \Gamma r_0^2\omega/c, \quad \hat{\Lambda}_p^2 = 4c^2/(\omega^2 r_0^2\theta_s^2),$$

where $I = \pi r_0^2 j_0$ is the beam current and $I_A = mc^3/e \simeq 17$ kA is Alfven's current. Function $\hat{D}$ is given with the following expression for the Gaussian energy spread

$$\hat{D} = i\int_0^{\infty} \xi \exp[-\hat{\Lambda}_T^2\xi^2/2 - (\hat{\Lambda} + i\hat{C})\xi] d\xi,$$

where $\hat{\Lambda}_T^2 = \Lambda_T^2/\Gamma^2 = \langle(\Delta\mathcal{E})^2\rangle > \omega^2/(c^2\gamma_z^4\mathcal{E}_0^2\Gamma^2)$ is the energy spread parameter. When the energy spread is negligibly small, i.e. $\hat{\Lambda}_T^2 \to 0$, we have: $\hat{D} = i(\hat{\Lambda} + i\hat{C})^{-2}$.

To avoid the singularity at $\hat{r} = 0$ the solution for $\Phi_n(\hat{r})$ inside the beam should be chosen in the form

$$\Phi_n(\hat{r}) = C_1 J_n(\mu\hat{r}), \quad \text{at } \hat{r} < 1,$$

where J_n is the Bessel function of the first kind of order n. As the field must vanish at $r \to \infty$, we should choose the solution for $\Phi_n(\hat{r})$ outside the beam in the form (we assume here that $\mathrm{Re}(g) > 0$)

$$\Phi_n(\hat{r}) = C_2 K_n(g\hat{r}), \quad \text{at } \hat{r} > 1,$$

where K_n is the modified Bessel function. The continuity conditions of Φ_n and $d\Phi_n/d\hat{r}$ at the beam boundary give us the system of two linear equations

$$C_1 J_n(\mu) = C_2 K_n(g), \quad \mu C_1 J_n'(\mu) = g C_2 K_n'(g).$$

Satisfying the compatibility condition of this system and using the relations

$$K_n'(\zeta) = nK_n(\zeta)/\zeta - K_{n+1}(\zeta), \quad J_n'(\zeta) = nJ_n(\zeta)/\zeta - J_{n+1}(\zeta),$$

we get the eigenvalue equation for the FEL amplifier with the homogeneous axisymmetric electron beam

$$\mu J_{n+1}(\mu) K_n(g) = g J_n(\mu) K_{n+1}(g). \tag{10.3}$$

The field mode eigenfunction (i.e. transverse field distribution inside the undulator) is given with the expressions

$$\Phi_n(\hat{r}) = \begin{cases} J_n(\mu\hat{r}), & \text{at } \hat{r} < 1 \\ J_n(\mu) K_n(g\hat{r})/K_n(g), & \text{at } \hat{r} > 1. \end{cases} \tag{10.4}$$

The directivity diagram of the radiation intensity is one of the important characteristics of FEL amplifier. At large distance from the amplifier exit, at $z \gg l_w$, the output radiation has the form of a spherical wave. In the axisymmetric case the radiation field amplitude depends on the observation angle $\theta = r/z$ according to the expression (we assume here the Fraunhofer diffraction approximation)

$$\Xi(\hat{\theta}) = \int_0^\infty \Phi_0(\hat{r}) J_0(\hat{\theta}\hat{r}) \hat{r} d\hat{r}, \tag{10.5}$$

where $\hat{\theta} = \theta r_0 \omega/c$ is the reduced observation angle, $\Phi_0(\hat{r})$ is the complex amplitude of axisymmetric radiation mode at the amplifier output and J_0 is the Bessel function of the first kind. When the FEL amplifier operates at the ground TEM_{00} mode, using Eq. (10.4) we can write the following expression for $\Xi(\theta)$

$$\Xi(\hat{\theta}) = \int_0^1 \zeta J_0(\hat{\theta}\zeta) J_0(\mu\zeta) d\zeta + \int_1^\infty d\zeta J_0(\mu) J_0(\hat{\theta}\zeta) K_0(g\zeta)/K_0(g)$$

$$= \frac{1}{\hat{\theta}^2 - \mu^2}[\hat{\theta} J_0(\mu) J_1(\hat{\theta}) - \mu J_1(\mu) J_0(\hat{\theta})]$$
$$- \frac{1}{g^2 + \hat{\theta}^2}[\hat{\theta} J_1(\hat{\theta}) J_0(\mu) - g J_0(\hat{\theta}) J_0(\mu) K_1(g)/K_0(g)].$$

Taking into account equation (10.3) we get the following expression for the radiation power directivity diagram

$$\frac{I(\hat{\theta})}{I(0)} = \left|\frac{\Xi(\hat{\theta})}{\Xi(0)}\right|^2 = \left|\frac{J_0(\hat{\theta}) - \hat{\theta} J_1(\hat{\theta}) J_0(\mu) K_1(g)/K_0(g)}{(1 + \hat{\theta}^2/g^2)(1 - \hat{\theta}^2/\mu^2)}\right|^2 . \tag{10.6}$$

At large values of the diffraction parameter B the Fraunhofer diffraction approximation may be used when $cR_i/(r_0^2\omega) \gg 1$, where R_i is the distance between the observation point and the amplifier exit. When $B \lesssim 1$ the above condition changes to: $|\Lambda| R_i \simeq \Gamma R_i \gg 1$.

In conclusion to this section we should notice that the presented approach to solve the eigenvalue problem can be easily extended to the case of the electron beam with an arbitrary gradient profile of current density. It can be performed by means of multilayer approximation method. The similar method is used, for example, in the optical waveguide theory (see Ref. [90]). This method consists in replacing the electron beam profile with a set of layers and in each of them the current density is supposed to be constant. The fulfillment of the continuity conditions of the eigenfunction and its derivative at all boundaries between the layers leads to the eigenvalue equation (see Ref. [69] for more details).

10.2. The analysis of the solutions

10.2.1. The field distribution

The field distribution of the ground symmetric TEM_{00} mode is presented in Fig. 10.1. One can see that at large values of diffraction parameter B the radiation field is concentrated inside and near the electron beam. When parameter B is decreasing, the radiation field redistributes in the space outside the electron beam. Figs. 10.2 and 10.3 illustrate the field distribution of the higher radiation modes TEM_{01}, TEM_{02}, TEM_{10} and TEM_{11}.

10.2.2. The directivity diagram

Fig. 10.4 illustrates the directivity diagrams of the ground TEM_{00} mode. One can see that all radiation power is concentrated in the small angle near the z axis. At large values of diffraction parameter B the width of the distribution is approximately equal to $\Delta\theta \simeq 1.8c/(r_0\omega)$. At small values of parameter B the width of the distribution is much less than $c/(r_0\omega)$. This is due to the fact that in this case the transverse dimension of the beam radiation mode at the amplifier output is much more than the electron beam size (see Fig. 10.1).

10.2.3. Increments of the eigenmodes

Let us define the increment as the real part of the eigenvalue. According to Eq. (10.3) the increment is the function of four reduced parameters (we let here the energy spread to be the Gaussian)

$$\mathrm{Re}\,\hat{\Lambda} = F(\hat{C}, \hat{\Lambda}_p^2, \hat{\Lambda}_T^2, B).$$

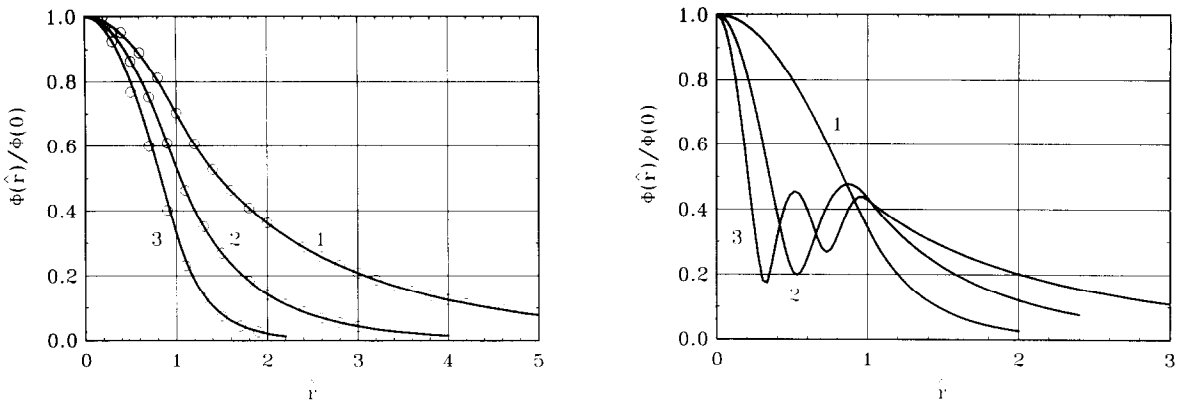

Fig. 10.1. The field distribution of TEM_{00} mode versus the reduced radius $\hat{r}$. Here $\hat{C} = 0$, $\hat{\Lambda}_p^2 = 0$, $\hat{\Lambda}_T^2 = 0$. Curve (1): $B = 0.1$, curve (2): $B = 1$ and curve (3): $B = 10$. The curves show analytical results (TEM_{00} mode) and the circles are calculated with nonlinear simulation code at the linear stage.

Fig. 10.2. The field distribution of TEM_{00}, TEM_{01} and TEM_{02} modes versus the reduced radius $\hat{r}$. Here $B = 10$, $\hat{\Lambda}_p^2 = 0$ and $\hat{\Lambda}_T^2 = 0$. Curve (1): TEM_{00} mode ($\hat{C} = 0.1$), curve (2): TEM_{01} mode ($\hat{C} = 0.7$) and curve (3): TEM_{02} mode ($\hat{C} = 2.0$).

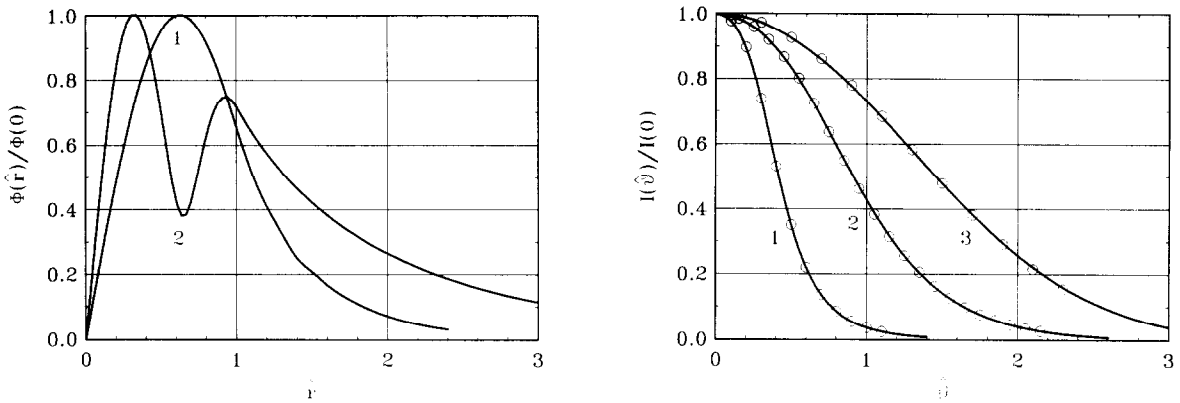

Fig. 10.3. The field distribution of TEM_{10} and TEM_{11} modes versus the reduced radius $\hat{r}$. Here $B = 10$, $\hat{\Lambda}_p^2 = 0$, $\hat{\Lambda}_T^2 = 0$. Curve (1): TEM_{10} mode ($\hat{C} = 0.2$) and curve (2): TEM_{11} mode ($\hat{C} = 1.1$).

Fig. 10.4. The directivity diagram of TEM_{00} mode. Here $\hat{C} = 0$, $\hat{\Lambda}_p^2 = 0$ and $\hat{\Lambda}_T^2 = 0$. Curve (1): $B = 0.1$, curve (2): $B = 1$ and curve (3): $B = 10$. The curves show analytical results (TEM_{00} mode) and the circles are calculated with nonlinear simulation code at the linear stage.

First, we consider the case of negligibly small space charge field and energy spread, $\hat{\Lambda}_p^2 \to 0$ and $\hat{\Lambda}_T^2 \to 0$. Some results of numerical solution of the eigenvalue equation (10.3) are presented in Figs. 10.5 and 10.6.

One-dimensional approximation corresponds to the case when diffraction effects can be neglected. This region is determined with large values of the diffraction parameter B, $B \gg 1$. In this case we let $|g| \gg 1$ and $K_n(g) \simeq K_{n+1}(g)$. Hence, we get from equation (10.3) that $J_n(\mu) \simeq 0$ which is possible only when $\mu \simeq \nu_{ni}$, where ν_{ni} is the ith root of the Bessel function of order n. As a result, we get asymptotically at $B \to \infty$, $\hat{\Lambda}_p^2 \to 0$ and $\hat{\Lambda}_T^2 \to 0$

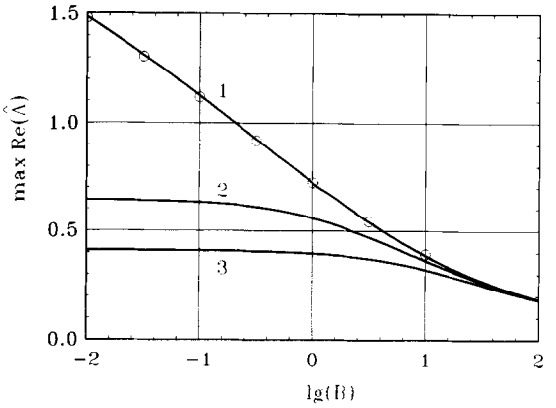

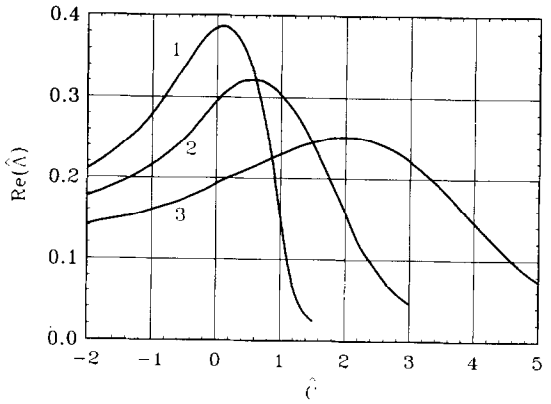

Fig. 10.5. The dependence of the maximal reduced increment $\max \mathrm{Re}(\hat{\Lambda})$ on the diffraction parameter B. Here $\hat{\Lambda}_p^2 = 0$, $\hat{\Lambda}_T^2 = 0$. Curve (1): TEM_{00} mode, curve (2): TEM_{10} mode and curve (3): TEM_{01} mode. The curves show analytical results and the circles are calculated with nonlinear simulation code at the linear stage.

Fig. 10.6. The reduced increment $\mathrm{Re}(\hat{\Lambda})$ versus the reduced detuning $\hat{C}$. Here $B = 10$, $\hat{\Lambda}_p^2 = 0$, $\hat{\Lambda}_T^2 = 0$. Curve (1): TEM_{00} mode, curve (2): TEM_{01} mode and curve (3): TEM_{02} mode.

$$2/(\hat{\Lambda} + i\hat{C})^2 \simeq g^2 = -2iB\hat{\Lambda}. \tag{10.7}$$

If we redetermine the gain parameter

$$\Gamma B^{-1/3} = \left[\frac{I\omega\theta_s^2}{I_A c\gamma\gamma_z^2 r_0^2}\right]^{1/3} \Rightarrow \Gamma \quad \text{(one-dimensional)}, \tag{10.8}$$

which corresponds to the definition of the gain parameter in the one dimensional approximation, we see that Eq. (10.7) becomes to be identical to the eigenvalue equation (2.26) of the one-dimensional theory. The accuracy of this approximation at the value of diffraction parameter $B = 8$ is illustrated in Fig. 10.7. For comparison in this plot we present also the rigorous solutions for TEM_{00} and TEM_{10} modes.

The approximation of a thin beam is defined with the condition $B \to 0$. As soon as the argument of the modified Bessel function tends to null, we should use the expansion at small arguments. For the ground TEM_{00} mode we have

$$K_0(g) \simeq -\ln(g/2) - \gamma_e, \quad K_1(g) \simeq 1/g,$$

where $\gamma_e = 0.577$ is the Euler's constant. Substituting this approximation into Eq. (10.3) we get

$$\mu J_1(\mu)/J_0(\mu) \simeq -[\ln(g/2) + \gamma_e]^{-1}.$$

Assuming the value of $|\ln(B)|$ to be large, we find with the double logarithmic accuracy the following eigenvalue equation for the ground TEM_{00} mode of the thin beam

$$2(\hat{\Lambda} + i\hat{C})^2 = -\ln(-iB\hat{\Lambda}) + (\ln 2 - 2\gamma_e + 1/2). \tag{10.9}$$

The sum of the last three members in the right-hand side of equation (9) is equal to 0.03 and may be neglected. The accuracy of this asymptotic is illustrated in Fig. 10.8.

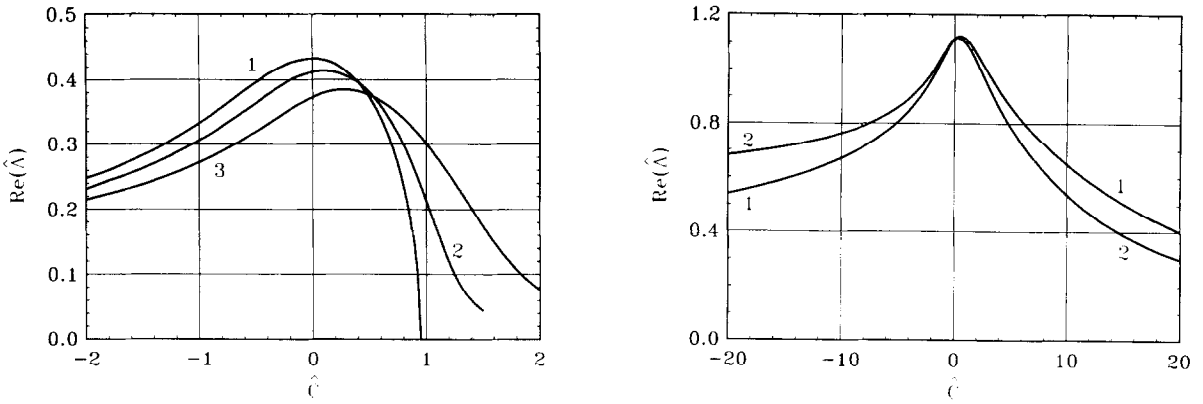

Fig. 10.7. The reduced increment $\mathrm{Re}(\hat{\Lambda})$ versus the reduced detuning $\hat{C}$. Here $B = 8$, $\hat{\Lambda}_p^2 = 0$ and $\hat{\Lambda}_T^2 = 0$. Curve (1) is the solution of asymptotic equation (2.26). Curve (2) – (TEM_{00} mode) and curve (3) – (TEM_{10} mode) are the solutions of accurate equation (10.3).

Fig. 10.8. The reduced increment $\mathrm{Re}(\hat{\Lambda})$ versus the reduced detuning $\hat{C}$. Here $B = 0.1$, $\hat{\Lambda}_p^2 = 0$, $\hat{\Lambda}_T^2 = 0$. Curve (1) is the solution of accurate equation (10.3) and curve (2) is the solution of asymptotic equation (10.9).

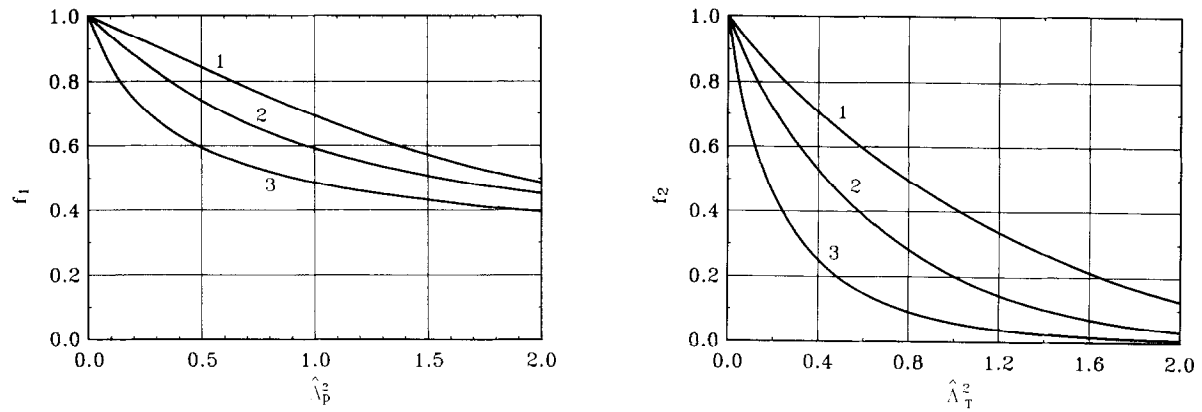

Fig. 10.9. The dependence of function f_1 for TEM_{00} mode on the space charge parameter $\hat{\Lambda}_p^2$. Curve (1): $B = 0.1$, curve (2): $B = 1$ and curve (3): $B = 10$.

Fig. 10.10. The dependence of function f_2 for TEM_{00} mode on the energy spread parameter $\hat{\Lambda}_T^2$. Curve (1): $B = 0.1$, curve (2): $B = 1$ and curve (3): $B = 10$.

Let us now study the influence of the space charge field. In the limit of $\hat{\Lambda}_T^2 \to 0$ and at fixed parameters $\hat{\Lambda}_p^2$ and B, there is always the value of the detuning $\hat{C}_m$ at which increment achieves its maximal value. This maximal increment is the function of two parameters, the space charge parameter $\hat{\Lambda}_p^2$ and the diffraction parameter B, and may be represented in the form

$$\max(\mathrm{Re}(\hat{\Lambda})) = \max(\mathrm{Re}(\hat{\Lambda})|_{\hat{\Lambda}_p^2 \to 0} \times f_1(\hat{\Lambda}_p^2, B).$$

The plots of function f_1 for the ground TEM_{00} mode are presented in Fig. 10.9.

In the limit of $B \to \infty$ and $\hat{\Lambda}_T^2 \to 0$, Eq. (10.3) transforms to the eigenvalue equation of the one-dimensional approximation

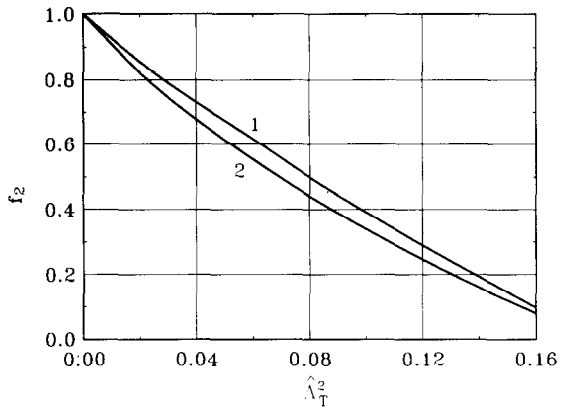

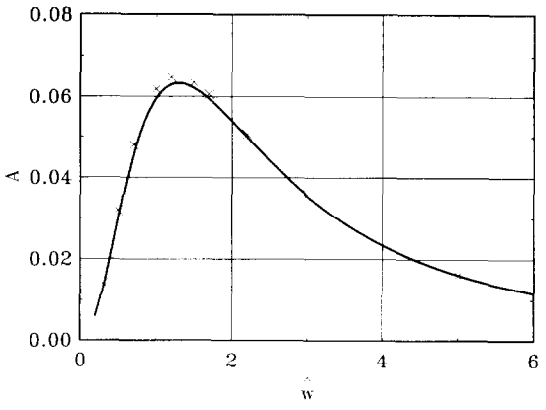

Fig. 10.11. The dependence of function f_2 for TEM_{01} mode on the energy spread parameter $\hat{\Lambda}_T^2$. Curve (1): $B = 0.1$ and curve (2): $B = 10$.

Fig. 10.12. The dependence of preexponential factor A on the reduced Gaussian laser beam waist $\hat{w}$. Here $B = 1$, $\hat{C} = 0$, $\hat{z}_0 = 0$, $\hat{\Lambda}_p^2 = 0$, $\hat{\Lambda}_T^2 = 0$. Curve is calculated with formulae (10.3), (10.22) and (10.23) and crosses are the numerical solution of the initial problem.

$$[(\hat{\Lambda} + i\hat{C})^2 + \hat{\Lambda}_p^2]\hat{\Lambda} = i/B.$$

Taking into account the redetermination procedure (10.8) for the gain parameter, we obtain that this equation is identical to the corresponding eigenvalue equation (2.22) of the one-dimensional model.

In the limit of $\hat{\Lambda}_T^2 \to 0$ and $B \to 0$, the eigenvalue equation (10.3) for the ground mode TEM_{00} takes the form

$$2[(\hat{\Lambda} + i\hat{C})^2 + \hat{\Lambda}_p^2] = -\ln(-iB\hat{\Lambda}).$$

Let us now study the influence of the energy spread on the FEL amplifier operation. In the limit of $\hat{\Lambda}_p^2 \to 0$ and at fixed parameters $\hat{\Lambda}_T^2$ and B there is always the value of the detuning parameter $\hat{C}_m$ when the increment achieves its maximum. This maximal increment is the function of only two parameters, the energy spread parameter $\hat{\Lambda}_T^2$ and the diffraction parameter B which may be expressed as

$$\max(\mathrm{Re}(\hat{\Lambda})) = \max(\mathrm{Re}(\hat{\Lambda}))|_{\hat{\Lambda}_T^2 \to 0} \times f_2(\hat{\Lambda}_T^2, B).$$

The plots of function f_2 for the first two axisymmetric modes are presented in Figs. 10.10 and 10.11. One can find from these plots that the energy spread acts as the strong radiation mode selector. Even at comparatively small values of the energy spread parameter, at $\hat{\Lambda}_T^2 \simeq 0.1$, the maximal increment of TEM_{01} mode is decreased drastically with respect to the ground TEM_{00} mode.

In the limit of $B \to \infty$ and $\hat{\Lambda}_p^2 \to 0$, the eigenvalue equation (10.3) transforms to

$$\int_0^\infty \xi \exp\{-\hat{\Lambda}_T^2\xi^2/2 - (\hat{\Lambda} + i\hat{C})\xi\}d\xi = -iB\hat{\Lambda}.$$

After redetermination procedure (10.8) of the gain parameter, this equation is reduced to the eigenvalue equation (2.39) of the one-dimensional model.

At $B \to 0$ and $\hat{\Lambda}_p^2 \to 0$, the eigenvalue equation (10.3) for TEM_{00} mode transforms to

$$\int_0^\infty \xi \exp\{-\hat{\Lambda}_T^2 \xi^2/2 - (\hat{\Lambda} + i\hat{C})\xi\} d\xi = -2/\ln(-iB\hat{\Lambda}).$$

10.3. Solution of the initial-value problem by Laplace technique

To find the evolution of the electric field of the amplified wave $\tilde{E}(z, r, \varphi)$ one should solve the self-consistent field equations under the given conditions at the undulator entrance. In this paper we consider a specific, but practically important case of the following initial conditions

(a) the electron beam is modulated neither in velocity nor density at the undulator entrance;

(b) the electric field amplitude $\tilde{E}$ takes the value $\tilde{E}_{ext}(r, \varphi)$ at the undulator entrance.

In this case evolution of the complex amplitude $\tilde{E}(z, r, \varphi)$ of the amplified wave is defined with Eq. (9.9). In this paper we consider the case of axisymmetric electron beam with stepped profile of current density. Introducing the following notations

$$\hat{z} = \Gamma z, \quad \hat{r} = r/r_0, \quad B = \Gamma r_0^2 \omega/c, \quad \hat{\Lambda}_p^2 = 4c^2/(\omega^2 \theta_s^2 r_0^2),$$

we write Eq. (9.9) in the following reduced form Region 1 ($\hat{r} < 1$):

$$\left[\frac{\partial^2}{\partial \hat{r}^2} + \frac{1}{\hat{r}}\frac{\partial}{\partial \hat{r}} + \frac{1}{\hat{r}^2}\frac{\partial^2}{\partial \varphi^2} + 2iB\frac{\partial}{\partial \hat{z}}\right] \tilde{E}(\hat{z}, \hat{r}, \varphi)$$

$$= i\int_0^{\hat{z}} d\hat{z}' \left[2\tilde{E}(\hat{z}', \hat{r}, \varphi) + \hat{\Lambda}_p^2 \left[\frac{\partial^2}{\partial \hat{r}^2} + \frac{1}{\hat{r}}\frac{\partial}{\partial \hat{r}} + \frac{1}{\hat{r}^2}\frac{\partial^2}{\partial \varphi^2} + 2iB\frac{\partial}{\partial \hat{z}'}\right] \tilde{E}(\hat{z}', \hat{r}, \varphi)\right]$$

$$\times \int_{-\infty}^{\infty} d\xi d\hat{F}(\xi)/d\xi \exp[i(\xi + \hat{C})(\hat{z}' - \hat{z})]. \tag{10.10a}$$

Region 2 ($1 < \hat{r}$):

$$\left[\frac{\partial^2}{\partial \hat{r}^2} + \frac{1}{\hat{r}}\frac{\partial}{\partial \hat{r}} + \frac{1}{\hat{r}^2}\frac{\partial^2}{\partial \varphi^2} + 2iB\frac{\partial}{\partial \hat{z}}\right] \tilde{E}(\hat{z}, \hat{r}, \varphi) = 0. \tag{10.10b}$$

Then we represent $\tilde{E}$ as a Fourier series in the angle φ

$$\tilde{E}(\hat{z}, \hat{r}, \varphi) = \sum_{n=-\infty}^{n=+\infty} \tilde{E}^{(n)}(\hat{z}, \hat{r}) e^{-in\varphi}.$$

The Laplace transforms of the Fourier coefficients $\tilde{E}^{(n)}$

$$\bar{E}^{(n)}(p, \hat{r}) = \int_0^\infty e^{-p\hat{z}} \tilde{E}^{(n)}(\hat{z}, \hat{r}) d\hat{z}$$

are submitted to the following equations

$$\left[\frac{d^2}{d\hat{r}^2}+\frac{1}{\hat{r}}\frac{d}{d\hat{r}}-\frac{n^2}{\hat{r}^2}+\bar{\mu}^2\right]\bar{E}^{(n)}(p,\hat{r})=\hat{f}^{(n)}(\hat{r}),\quad \hat{r}<1, \tag{10.11a}$$

$$\left[\frac{d^2}{d\hat{r}^2}+\frac{1}{\hat{r}}\frac{d}{d\hat{r}}-\frac{n^2}{\hat{r}^2}-\bar{g}^2\right]\bar{E}^{(n)}(p,\hat{r})=\hat{f}^{(n)}(\hat{r}),\quad \hat{r}>1 \tag{10.11b}$$

where notations are introduced

$$\bar{\mu}^2=-2i\hat{D}[1-i\hat{\Lambda}_p^2\hat{D}]^{-1}-\bar{g}^2,\quad \bar{g}^2=-2iBp,$$

$$\hat{D}=\int_{-\infty}^{\infty}d\xi\frac{d\hat{F}(\xi)/d\xi}{p+i(\xi+\hat{C})},\quad \hat{f}^{(n)}(\hat{r})=2iB\tilde{E}^{(n)}_{\text{ext}}(\hat{r}).$$

To find $\bar{E}^{(n)}$ one must solve Eqs. (10.11) with the following boundary conditions

$$\bar{E}^{(n)}(p,\hat{r})\to 0\quad \text{at } \hat{r}\to\infty,$$

$$\bar{E}^{(n)}|_{\hat{r}=1+0}=\bar{E}^{(n)}|_{\hat{r}=1-0},\quad d\bar{E}^{(n)}/d\hat{r}|_{\hat{r}=1+0}=d\bar{E}^{(n)}/d\hat{r}|_{\hat{r}=1-0}.$$

We use the Green's function method to solve inhomogeneous Eqs. (10.11). First, we consider the region inside the beam. We seek the Green's function $\hat{G}(\hat{r},\hat{r}')$ satisfying to the homogeneous equation

$$\hat{r}\frac{d}{d\hat{r}}\left[\hat{r}\frac{d\hat{G}}{d\hat{r}}\right]+(\bar{\mu}^2\hat{r}^2-n^2)\hat{G}=0 \tag{10.12}$$

at all $\hat{r}$ except of $\hat{r}=\hat{r}'$ and at the latter point the following conditions must take place

$$\hat{G}|_{\hat{r}=\hat{r}'+0}-\hat{G}|_{\hat{r}=\hat{r}'-0}=0,\quad d\hat{G}/d\hat{r}|_{\hat{r}=\hat{r}'+0}-d\hat{G}/d\hat{r}|_{\hat{r}=\hat{r}'-0}=1/\hat{r}. \tag{10.13}$$

The Green's function must be finite at $\hat{r}=0$. If two linearly independent solutions of Eq.(10.11a) $\chi(\hat{r})$ and $\psi(\hat{r})$ are normalized as

$$\psi d\chi/d\hat{r}-\chi d\psi/d\hat{r}=1/\hat{r}, \tag{10.14}$$

then the Green's function is

$$\hat{G}(\hat{r},\hat{r}')=\begin{cases}\psi(\hat{r})\chi(\hat{r}'), & \hat{r}<\hat{r}'\\ \psi(\hat{r}')\chi(\hat{r}), & \hat{r}>\hat{r}'\end{cases}$$

It satisfies to Eq. (10.12) and conditions (10.13). Moreover, if function $\psi(\hat{r})$ is finite at $\hat{r}=0$, then the requirement for the Green's function to be finite is fulfilled. The following solution of the homogeneous equations satisfy to all the mentioned above conditions

$$\psi=(\pi/2)^{1/2}J_n(\bar{\mu}\hat{r}),\quad \chi=(\pi/2)^{1/2}N_n(\bar{\mu}\hat{r}).$$

Thus, we obtain

$$\hat{G}=\begin{cases}(\pi/2)J_n(\bar{\mu}\hat{r})N_n(\bar{\mu}\hat{r}'), & \hat{r}<\hat{r}',\\ (\pi/2)J_n(\bar{\mu}\hat{r}')N_n(\bar{\mu}\hat{r}), & \hat{r}>\hat{r}'.\end{cases}$$

Finally, we find in the general form the solution of inhomogeneous Eq. (10.11a)

$$\bar{E}^{(n)} = C_1 J_n(\bar{\mu}\hat{r}) + \frac{\pi}{2} N_n(\bar{\mu}\hat{r}) \int_0^{\hat{r}} d\zeta J_n(\bar{\mu}\zeta)\zeta \hat{f}^{(n)}(\zeta)$$

$$+ \frac{\pi}{2} J_n(\bar{\mu}\hat{r}) \int_{\hat{r}}^{1} d\zeta N_n(\bar{\mu}\zeta)\zeta \hat{f}^{(n)}(\zeta). \tag{10.15}$$

To find the solution in the region outside the beam, at $\hat{r} > 1$, we also seek the Green's function $\hat{G}(\hat{r}, \hat{r}')$ of the homogeneous equation corresponding to inhomogeneous equation (10.11b). To provide boundedness of the solution at $\hat{r} \to \infty$, the following condition must be fulfilled

$$\hat{G} \to 0 \quad \text{at } \hat{r} \to \infty. \tag{10.16}$$

We choose the following solutions of the homogeneous equation satisfying the normalization conditions (10.14):

$$\psi = iI_n(\bar{g}\hat{r}), \quad \chi = iK_n(\bar{g}\hat{r})$$

and obtain the following Green's function

$$\hat{G} = \begin{cases} -I_n(\bar{g}\hat{r})K_n(\bar{g}\hat{r}'), & \hat{r} < \hat{r}', \\ -I_n(\bar{g}\hat{r}')K_n(\bar{g}\hat{r}), & \hat{r} > \hat{r}'. \end{cases} \tag{10.17}$$

So as $K_n(\bar{g}\hat{r})$ tends to zero at $\hat{r} \to \infty$, then the boundary condition (10.16) for the Green's function is fulfilled. Thus, the general solution of inhomogeneous equation (10.11b) has the form

$$\bar{E}^{(n)} = C_2 K_n(\bar{g}\hat{r}) - K_n(\bar{g}\hat{r}) \int_1^{\hat{r}} d\zeta I_n(\bar{g}\zeta)\zeta \hat{f}^{(n)}(\zeta) - I_n(\bar{g}\hat{r}) \int_{\hat{r}}^{\infty} d\zeta K_n(\bar{g}\zeta)\zeta \hat{f}^{(n)}(\zeta). \tag{10.18}$$

The continuity conditions of $\bar{E}^{(n)}(p, \hat{r})$ and $d\bar{E}^{(n)}(p, \hat{r})/d\hat{r}$ at the beam boundary $\hat{r} = 1$ give us the following equations

$$C_1 J_n(\bar{\mu}) + \frac{\pi}{2} N_n(\bar{\mu}) \int_0^1 d\zeta J_n(\bar{\mu}\zeta)\zeta \hat{f}^{(n)}(\zeta) = C_2 K_n(\bar{g}) - I_n(\bar{g}) \int_1^{\infty} d\zeta K_n(\bar{g}\zeta)\zeta \hat{f}^{(n)}(\zeta),$$

$$C_1 \bar{\mu} J_{n+1}(\bar{\mu}) + \frac{\pi}{2} N_{n+1}(\bar{\mu}) \int_0^1 d\zeta J_n(\bar{\mu}\zeta)\zeta \hat{f}^{(n)}(\zeta)$$

$$= C_2 \bar{g} K_{n+1}(\bar{g}) + \bar{g} I_{n+1}(\bar{g}) \int_1^{\infty} d\zeta K_n(\bar{g}\zeta)\zeta \hat{f}^{(n)}(\zeta).$$

The solution of this system is given with

$$C_1 = \frac{1}{\bar{\mu}J_{n+1}(\bar{\mu})K_n(\bar{g}) - \bar{g}K_{n+1}(\bar{g})J_n(\bar{\mu})} \int_1^\infty d\zeta K_n(\bar{g}\zeta)\zeta \hat{f}^{(n)}(\zeta)$$

$$+ \frac{\pi}{2}\frac{\bar{g}K_{n+1}(\bar{g})N_n(\bar{\mu}) - \bar{\mu}K_n(\bar{g})N_{n+1}(\bar{\mu})}{\bar{\mu}J_{n+1}(\bar{\mu})K_n(\bar{g}) - \bar{g}K_{n+1}(\bar{g})J_n(\bar{\mu})} \int_0^1 d\zeta J_n(\bar{\mu}\zeta)\zeta \hat{f}^{(n)}(\zeta),$$

$$C_2 = \frac{1}{\bar{\mu}J_{n+1}(\bar{\mu})K_n(\bar{g}) - \bar{g}K_{n+1}(\bar{g})J_n(\bar{\mu})} \int_0^1 d\zeta J_n(\bar{\mu}\zeta)\zeta \hat{f}^{(n)}(\zeta)$$

$$+ \frac{\bar{g}J_n(\bar{\mu})I_{n+1}(\bar{g}) + \bar{\mu}J_{n+1}(\bar{\mu})I_n(\bar{g})}{\bar{\mu}J_{n+1}(\bar{\mu})K_n(\bar{g}) - \bar{g}K_{n+1}(\bar{g})J_n(\bar{\mu})} \int_1^\infty d\zeta K_n(\bar{g}\zeta)\zeta \hat{f}^{(n)}(\zeta). \tag{10.19}$$

Substituting C_1 and C_2 into expressions (10.15) and (10.18) we get the solution for $\bar{E}^{(n)}$.

To find $\tilde{E}^{(n)}(\hat{z}, \hat{r})$ we use the inverse Laplace transformation

$$\tilde{E}^{(n)}(\hat{z}, \hat{r}) = \frac{1}{2\pi i} \int_{\gamma'-i\infty}^{\gamma'+i\infty} d\lambda \bar{E}^{(n)}(\lambda, \hat{r}) e^{\lambda z} \tag{10.20}$$

where the integration path in the complex plane λ is parallel with the imaginary axis. The real constant γ' is greater than the real parts of all the singularities of $\bar{E}^{(n)}(\lambda, \hat{r})$. We shall consider only the high-gain limit. In this case the solutions growing exponentially are given with the residues of the integrand in (10.20) lying in the right half of the complex plane λ. Using Eqs. (10.15), (10.18) and (10.19) we may write

$$\tilde{E}^{(n)} = \sum_j u_j J_n(\mu_j \hat{r}) \exp(\lambda_j \hat{z}), \quad \hat{r} < 1, \tag{10.21a}$$

$$\tilde{E}^{(n)} = \sum_j u_j \frac{J_n(\mu_j)}{K_n(g_j)} K_n(g_j \hat{r}) \exp(\lambda_j \hat{z}), \quad \hat{r} > 1. \tag{10.21b}$$

Here λ_j is the jth root of the equation ($\mathrm{Re}(\lambda_j) > 0$)

$$\bar{\mu}(\lambda_j)J_{n+1}(\bar{\mu}(\lambda_j))K_n(\bar{g}(\lambda_j)) - \bar{g}(\lambda_j)K_{n+1}(\bar{g}(\lambda_j))J_n(\bar{\mu}(\lambda_j)) = 0$$

where notations have been introduced

$$u_j = \frac{\left[\frac{K_n(g_j)}{J_n(\mu_j)}\right] \int_0^1 d\zeta J_n(\mu_j\zeta)\zeta \hat{f}^{(n)}(\zeta) + \int_1^\infty d\zeta K_n(g_j\zeta)\zeta \hat{f}^{(n)}(\zeta)}{\frac{d}{d\lambda}\left[\bar{\mu}J_{n+1}(\bar{\mu})K_n(\bar{g}) - \bar{g}K_{n+1}(\bar{g})J_n(\bar{\mu})\right]|_{\lambda=\lambda_j}},$$

$$\mu_j^2 = \frac{-2i\hat{D}_j}{1 - i\hat{\lambda}_p^2\hat{D}_j} - g_j^2, \quad g_j^2 = -2iB\lambda_j, \quad \hat{D}_j = \int_0^\infty d\xi \frac{d\hat{F}(\xi)/d\xi}{\lambda_j + i(\xi + \hat{C})}.$$

Each term in the right-hand sides of expressions (10.21) corresponds to the separate radiation mode and is characterized with the unique amplitude factor, increment and the dependence on the transverse coordinate.

In the paraxial approximation the power gain coefficient G of the radiation mode with the azimuthal index n is given with the expression

$$G = \int_0^\infty r|\tilde{E}^{(n)}(z,r)|^2 dr \left[\int_0^\infty r|\tilde{E}^{(n)}_{\rm ext}(r)|^2 dr\right]^{-1}.$$

When diffraction parameter B is not very large ($B \lesssim 10$)), one can find from Figs. 10.5 and 10.6 that the increment of TEM_{00} mode is visibly greater than the increments of higher TEM_{nk} modes ($n, k = 1, 2, 3, \ldots$). Hence, when the undulator is sufficiently long, the contribution of TEM_{00} mode in expression (10.21) is much more than the contributions of all other modes. In this case we may use the single mode approximation and write

$$\begin{aligned} G = {} & 4B^2 \exp(2\,\mathrm{Re}(\lambda_1)\hat{z}) \left|\frac{d}{d\lambda}[\bar{\mu}J_1(\bar{\mu})K_0(\bar{g}) - \bar{g}K_1(\bar{g})J_0(\bar{\mu})]|_{\lambda=\lambda_1}\right|^{-2} \\ & \times \left\{\int_0^\infty \hat{r}|\tilde{E}_{\rm ext}(\hat{r})|^2 d\hat{r}\right\}^{-1} \left\{\int_0^1 \hat{r}\left|\frac{K_0(g_1)J_0(\mu_1\hat{r})}{J_0(\mu_1)}\right|^2 d\hat{r} + \int_1^\infty \hat{r}|K_0(g_1\hat{r})|^2 d\hat{r}\right\} \\ & \times \left|\int_0^1 \hat{r}J_0(\mu_1\hat{r})\tilde{E}_{\rm ext}(\hat{r})d\hat{r} + [J_0(\mu_1)/K_0(g_1)]\int_1^\infty \hat{r}K_0(g_1\hat{r})\tilde{E}_{\rm ext}(\hat{r})d\hat{r}\right|^2, \end{aligned} \tag{10.22}$$

where λ_1 is the reduced eigenvalue of TEM_{00} mode.

10.3.1. Optimal focusing of master oscillator radiation

Let us now study the problem of the external radiation optimal focusing on the electron beam. We shall consider the case when the radiation of master oscillator has the form of the Gaussian laser beam

$$\begin{aligned} E_x + iE_y = {} & \tilde{E}_{\rm ext}(z,r)\exp[i\omega(z/c - t)] = \frac{-iE_g w^2(\omega/c)e^{-i\omega t}}{2(z - z_0) - iw^2\omega/c} \\ & \times \exp\left\{i\frac{\omega}{c}(z - z_0) + \frac{2i(\omega/c)(z - z_0)r^2 - (rw\omega/c)^2}{4(z - z_0)^2 + (w^2\omega/c)^2}\right\}. \end{aligned} \tag{10.23}$$

Here z_0 and w are the position of the focus and the waist size in the focus of the Gaussian laser beam, respectively. At $z = z_0$ the Gaussian laser beam has plane phase front and Gaussian distribution of the amplitude

$$\tilde{E}_{\rm ext}(z_0,r)\exp[i\omega(z/c - t)] = E_g e^{-i\omega t}\exp(-r^2/w^2).$$

One can easily obtain that the complex amplitude $\tilde{E}_{\rm ext}(z,r)$ of expression (10.23) is an exact solution of paraxial wave equation

$$[\partial^2/\partial r^2 + r^{-1}\partial/\partial r + 2ic^{-1}\omega\partial/\partial z]\,\tilde{E}_{\rm ext}(z,r) = 0.$$

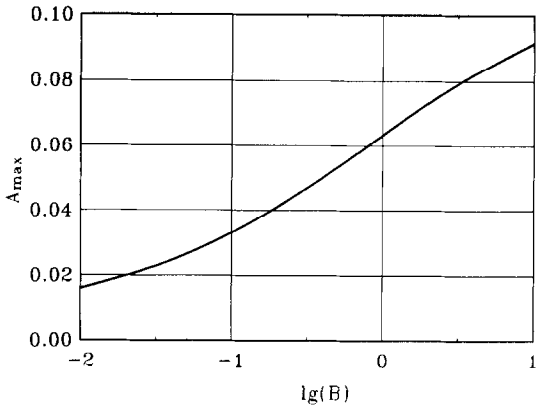

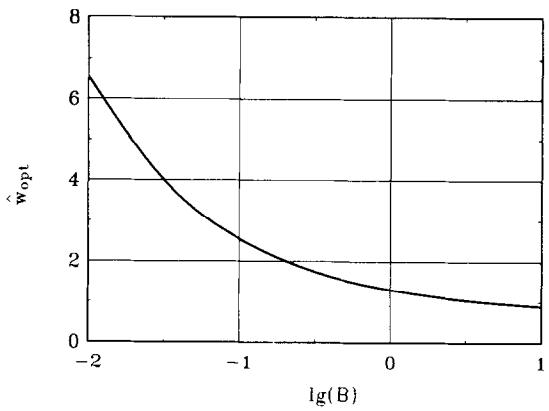

Fig. 10.13. Maximal preexponential factor A versus the diffraction parameter B. Here $\hat{C} = 0$, $\hat{z}_0 = 0$, $\hat{\Lambda}_p^2 = 0$, $\hat{\Lambda}_T^2 = 0$.

Fig. 10.14. Optimum of the reduced Gaussian laser beam waist $\hat{w}$ versus the diffraction parameter B. Here $\hat{C} = 0$, $\hat{z}_0 = 0$, $\hat{\Lambda}_p^2 = 0$, $\hat{\Lambda}_T^2 = 0$.

When the undulator is sufficiently long, the power gain is submitted to the exponential dependence

$$G = A \exp[2\,\mathrm{Re}(\hat{\Lambda})\hat{z}],$$

where factor A is the function of six reduced parameters: $B, \hat{C}, \hat{\Lambda}_p^2, \hat{\Lambda}_T^2, \hat{w} = w/r_0$ and $\hat{z}_0 = \Gamma z_0$.

Let us consider the case of negligibly small the space charge field and energy spread ($\hat{\Lambda}_p^2 \to 0$ and $\hat{\Lambda}_T^2 \to 0$) and accurate resonance ($\hat{C} = 0$). Then at the fixed value of diffraction parameter B there are always the optimal values of the laser Gaussian beam parameters $\hat{w}$ and $\hat{z}_0$ when factor A achieves its maximum. To simplify the optimization problem we will not perform the variation of $\hat{z}_0$ and set it equal to zero. We will show below that such a choice of $\hat{z}_0$ is close to the optimum. Fig. 10.12 presents the dependence of factor A on the reduced laser beam waist $\hat{w}$ at fixed value of parameter B. The maximal value of factor A and the laser beam waist $\hat{w}$ corresponding to this maximum are the universal functions of the only parameter B. The plots of these functions are presented in Figs. 10.13 and 10.14. Fig. 10.15 presents the dependence of factor A on the reduced laser beam focus coordinate $\hat{z}_0$. It is clearly seen that the value of A at $\hat{z}_0 = 0$ does not differ significantly from its maximal value.

In conclusion we present in Fig. 10.16 the resonance curve of the power gain G and in Fig. 10.17 the dependence of the reduced bandwidth of the amplifier $\Delta\hat{C}$ on the power gain G (we calculate the bandwidth at the half of the nominal power).

10.4. Integration of the self-consistent field equations on a computer

We have shown above that in the case of the stepped profile of the beam current density, the initial-value problem can be solved analytically using Eq. (9.9). When the electron beam has an arbitrary gradient profile of current density one should use the numerical methods to solve the initial problem. The self-consistent field method in the linear approximation enables one to get from the kinetic equation and Maxwell's equations the only equation either for the field amplitude of amplified wave or for the modulation amplitude of the beam current density. Both of the ways lead to the

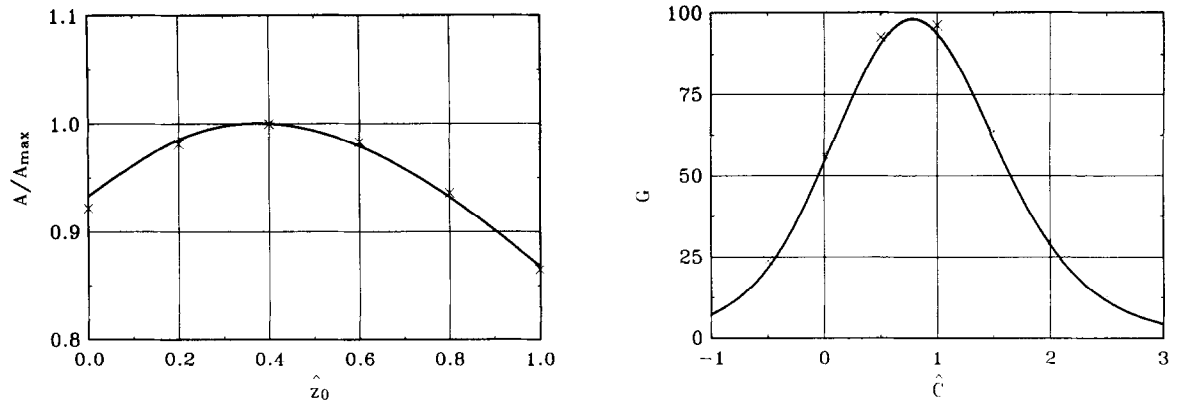

Fig. 10.15. The dependence of the preexponential factor A on the position of the Gaussian laser beam focus. Here $B = 1$, $\hat{C} = 0$, $\hat{\Lambda}_p^2 = 0$, $\hat{\Lambda}_T^2 = 0$. Curve is calculated with formulae (10.3), (10.22) and (10.23) and crosses are the numerical solution of the initial problem.

Fig. 10.16. The power gain G dependence on the reduced detuning $\hat{C}$. Here $B = 1$, $\hat{w} = 1.3$, $\hat{z} = 4.7$, $\hat{\Lambda}_p^2 = 0$, $\hat{\Lambda}_T^2 = 0$. Curve is calculated with formulae (10.3), (10.22) and (10.23) and crosses are the numerical solution of the initial problem.

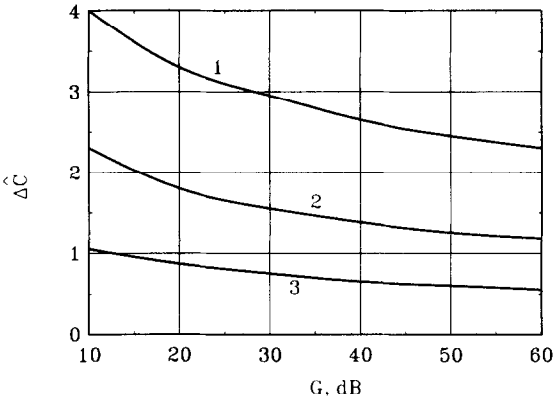

Fig. 10.17. The amplifier reduced bandwidth $\Delta\hat{C}$ versus the power gain G. Here $\hat{\Lambda}_p^2 = 0$, $\hat{\Lambda}_T^2 = 0$. The reduced laser beam waist is optimized at $\hat{C} = 0$. Curve (1): $B = 0.1$ and $\hat{w} = 2.55$, curve (2): $B = 1$ and $\hat{w} = 1.3$ and curve (3): $B = 10$ and $\hat{w} = 0.89$.

same results but for the analytical calculations it is preferable to use the equation for the wave field (9.9): in this case the mathematical apparatus is always connected with more conventional differential equations. At the same time the situations with the computer simulations is proved to be reversed and the method using the equation for the modulation amplitude of the beam current density (9.12) is more convenient.

In this section we present the algorithm of the initial problem numerical solution using Eq. (9.12). The case of axially symmetric radiation field modes is under study. Let us consider the case of negligibly small energy spread. The field of master oscillator has the form of the Gaussian laser beam (10.23) with amplitude

$$E_g = [8W_{ext}/(w^2 c)]^{1/2},$$

where W_{ext} is the total power of the master oscillator. Using standard normalization procedure, we rewrite Eq. (9.12) in the form

$$\frac{d^2\hat{j}_1}{d\hat{z}^2} + 2i\hat{C}\frac{d\hat{j}_1}{d\hat{z}} + [\hat{\Lambda}_p^2 - \hat{C}^2]\hat{j}_1 = \int_0^{\hat{z}} \frac{d\hat{z}'}{\hat{z}-\hat{z}'} \int_0^1 \hat{r}' d\hat{r}' \hat{j}_1(\hat{z}', \hat{r}') J_0\left[\frac{B\hat{r}\hat{r}'}{\hat{z}-\hat{z}'}\right] \exp\left\{\frac{iB(\hat{r}^2+\hat{r}'^2)}{2(\hat{z}-\hat{z}')}\right\} + \frac{1}{2i}\hat{U}_{ext}(\hat{z}, \hat{r}), \tag{10.24}$$

where the following notations are introduced

$$\hat{j}_1(z,r) = \tilde{j}_1(z,r)\pi r_0^2/I, \quad \hat{W}_{ext} = W_{ext}/W_0,$$
$$\hat{E}_g = [8\hat{W}_{ext}/(B\hat{w}^2)]^{1/2}, \quad W_0 = I\mathcal{E}_0\Gamma\gamma_z^2 c/(e\omega),$$
$$\hat{U}_{ext}(\hat{z}, \hat{r}) = -\frac{iB\hat{w}^2\hat{E}_g}{2(\hat{z}-\hat{z}_0) - iBw^2} \exp\left\{\frac{2iB(\hat{z}-\hat{z}_0)\hat{r}^2 - (B\hat{w}\hat{r})^2}{4(\hat{z}-\hat{z}_0)^2 + (B\hat{w}^2)^2}\right\}. \tag{10.25}$$

Integro-differential equation was solved using computer code FS2RL [69]. Computed value of the beam modulation $\tilde{j}_1$ are used to calculate the power gain G:

$$G = 1 + \left\{ \frac{2i}{\hat{W}_{ext}} \int_0^{\hat{z}} d\hat{z}' \int_0^{\hat{z}'} d\hat{z}'' \int_0^1 d\hat{r}' \int_0^1 d\hat{r}'' \hat{j}_1(z', \hat{r}') \frac{\hat{r}'\hat{r}''}{\hat{z}'-\hat{z}''} \times \hat{j}_1^*(\hat{z}'', \hat{r}'') J_0\left[\frac{B\hat{r}'\hat{r}''}{\hat{z}'-\hat{z}''}\right] \exp\left\{-\frac{iB(\hat{r}'^2+\hat{r}''^2)}{2(\hat{z}'-\hat{z}'')}\right\} + \text{c.c.} \right\}$$
$$- \left\{ \frac{1}{\hat{W}_{ext}} \int_0^{\hat{z}} d\hat{z}' \int_0^1 d\hat{r}' \hat{U}_{ext}^*(\hat{z}', \hat{r}') \hat{j}_1(\hat{z}', \hat{r}') \hat{r}' + \text{c.c.} \right\}. \tag{10.26}$$

Figs. 10.12, 10.15 and 10.16 present the results of the numerical solution of equation (10.24) (the crosses). The solid curves are calculated with analytical formulae. It is clearly seen that in the high gain limit there is good agreement of numerical and analytical results.

All the results of the linear theory obtained above refer to the case of the helical undulator and circularly polarized radiation. These results can be used also for the case of a planar undulator and linearly polarized radiation at the following redetermination of the parameters

$$\Gamma = [A_{JJ}^2 I\omega^2\theta_l^2(2I_A c^2\gamma_l^2\gamma)^{-1}]^{1/2}, \quad B = r_0^2\Gamma\omega/c,$$
$$C = \kappa_w - \omega/(2c\gamma_l^2), \quad \hat{\Lambda}_p^2 = 8c^2(\omega^2 r_0^2\theta_l^2 A_{JJ}^2)^{-1},$$
$$\hat{\Lambda}_T^2 = \omega^2\langle(\Delta\mathcal{E})^2\rangle/(c^2\gamma_l^4\Gamma^2\mathcal{E}_0^2), \quad W_0 = I\mathcal{E}_0\Gamma\gamma_l^2 c/(e\omega).$$

Here, as it was done in Sections 2–4, we have introduced the following notations

$$\theta_l = eH_l/(\mathcal{E}_0\kappa_w), \quad \gamma_l^{-2} = \gamma^{-2} + \theta_l^2/2.$$

Factor A_{JJ} is given by the formula

$$A_{JJ} = [J_0(\nu) - J_1(\nu)],$$

where $\nu = \theta_l^2\omega/(8c\kappa_w)$, J_0 and J_1 are the Bessel functions.

11. Nonlinear simulations of the FEL amplifier with an axisymmetric electron beam

The nature of the saturation mechanism of the FEL amplifier is the same as that described in Section 3 where we have studied saturation effects in the frame of the one-dimensional model. In the linear mode of the FEL amplifier operation, at sufficiently low input radiation power W_{ext}, an increase of W_{ext} leads to the proportional increase of the output power W_f. When the input power is increased further, the operation of the amplifier becomes to be nonlinear: output power increases more slowly than that input one, and at a certain value of W_{ext} the output power reaches a maximum. To find the FEL characteristics at saturation, it is necessary to solve the equations of the nonlinear theory of the FEL amplifier. The analytical methods are limited in the description of the saturation effects and numerical simulation codes are being used.

The main problems of the nonlinear simulations are connected with the calculation of the radiation and space charge fields. Several different methods are used to calculate the radiation fields: various modifications of the transverse mode spectral method (see e.g. Ref. [83]), the finite difference method [84–86] and the Green's function method [87]. In this paper, following Ref. [87], we present an approach to constructing numerical simulation code using Green's function method for the radiation field calculations.

When using the numerical simulation codes the problems are usually arisen of the reliability and the clear physical interpretation of the obtained results. The presented approach satisfies these requirements. First, the model approximations allow one to check the linear stage of amplification with the rigorous solutions of the linear theory (see Section 10). Second, when writing down the final equations we use the similarity techniques. This enables one not only to reduce the number of the problem parameters but also to go over to the variables possessing the clear physical sense. Each physical factor influencing the FEL operation (diffraction, space charge, energy spread etc.) is matched with its own reduced parameter. For the effect under study this reduced parameter is a measure of the corresponding physical effect. When some effect becomes less important for the FEL amplifier operation, this is reflected by the corresponding reduced parameter taking on small values and falling out of the number of the problem parameters.

The presented FEL amplifier model allows one to take into account such effects as the radiation diffraction, space charge fields, energy spread of the electrons in the beam. The initial conditions are considered when one has the radiation from master oscillator (the Gaussian laser beam) and unmodulated electron beam at the undulator entrance. The presented code enables one to calculate the frequency, amplitude and current characteristics of the FEL amplifier. The field distributions in the Fresnel and Fraunhofer zones and various electron beam characteristics could be computed, too. The code allows one to calculate all these characteristics at the constant undulator parameters as well as at the tapering ones.

11.1. The working equations

In this section we describe briefly nonlinear simulation code FS2RN for the FEL amplifier with an axisymmetric electron beam [87]. The electron beam moves along the axis of the helical undulator.

The electron motion is described in the "energy-phase" variables with the phase

$$\psi = \int \kappa_w dz - \omega(t - z/c)$$

as canonical coordinate and energy $\mathcal{E}$ as canonical momentum. The Hamiltonian has the form

$$H(\mathcal{E}, \psi, z) = \int (\kappa_w + \omega/c - \omega/v_z) d\mathcal{E} - u \sin(\psi + \psi_0) + e \int E_z d\psi,$$

where u and ψ_0 are, respectively, the amplitude and phase of effective potential

$$u \exp(i\psi_0) = -e\theta_s E \exp(i\psi_0) = -e\theta_s \tilde{E}(\boldsymbol{r}_\perp, z)$$

and E_z is the longitudinal component of the space charge electric field. The corresponding equations of motion are as follows

$$\begin{aligned} d\mathcal{E}/dz &= -\partial H/\partial\psi = u\cos(\psi + \psi_0) - eE_z, \\ d\psi/dz &= \partial H/\partial\mathcal{E} = \kappa_w + \omega/c - \omega/v_z(\mathcal{E}). \end{aligned} \tag{11.1}$$

Then we perform usual normalization procedure. The diffraction parameter B, the gain parameter Γ, the space charge parameter $\hat{\Lambda}_p^2$ and the energy spread parameter $\hat{\Lambda}_T^2$ are defined the same way as in Section 10.1 and are calculated using initial parameters of the electron beam and the undulator. So, the equation of motion (11.1) can be written in the following reduced form

$$\frac{d\hat{P}}{d\hat{z}} = \mathrm{Re}[e^{i\psi}\hat{\vartheta}\hat{U}_r - i\hat{\Lambda}_p^2\hat{U}_c], \quad \frac{d\psi}{d\hat{z}} = \hat{C} + \hat{P}\frac{1 + \beta\hat{P}/2}{(1 + \beta\hat{P})^2}. \tag{11.2}$$

Here $\hat{z} = \Gamma z$, $\hat{C} = C/\Gamma$, $\hat{P} = \omega P/(c\gamma_z^2\mathcal{E}_0\Gamma)$, $P = \mathcal{E} - \mathcal{E}_0$, $\beta = c\gamma_z^2\Gamma/\omega$ is the efficiency parameter and $\hat{\vartheta} = \theta_s/\theta_0 = (1 + \beta\hat{P})^{-1}$ is the reduced rotation angle.

The expression for the effective potential of the radiation field $\hat{U}_r$ is given with

$$\hat{U}_r = \hat{U}_{\mathrm{ext}} + 2i \int_0^{\hat{z}} \frac{d\hat{z}'}{\hat{z} - \hat{z}'} \int_0^1 d\hat{r}'\hat{r}'\hat{j}_1(\hat{z}', \hat{r}') \exp\left[\frac{iB(\hat{r}^2 + \hat{r}'^2)}{2(\hat{z} - \hat{z}')}\right] J_0\left(\frac{B\hat{r}\hat{r}'}{\hat{z} - \hat{z}'}\right), \tag{11.3}$$

where $\hat{U}_{\mathrm{ext}}$ is given with Eq. (10.25).

The complex amplitude $\hat{j}_1 = |\hat{j}_1| \exp(i\psi_1)$ entering Eq. (11.3) is calculated with the local macroparticle ensemble

$$|\hat{j}_1| = \frac{1}{N}\left[\left[\sum_{k=1}^{N} \hat{\vartheta}_{(k)} \cos(\psi_{(k)})\right]^2 + \left[\sum_{k=1}^{N} \hat{\vartheta}_{(k)} \sin(\psi_{(k)})\right]^2\right]^{1/2}$$

$$\psi_1 = -\arctan\left[\frac{\sum_{k=1}^{N} \hat{\vartheta}_{(k)} \sin(\psi_{(k)})}{\sum_{k=1}^{N} \hat{\vartheta}_{(k)} \cos(\psi_{(k)})}\right].$$

The expression for the effective potential of the space charge fields $\hat{U}_c$ is of the form

$$\hat{U}_c = \frac{B}{\beta}\sum_{n=1}^{\infty} n e^{in\psi}\left[K_0(n\hat{r}\sqrt{B/\beta})\int_0^{\hat{r}} r'd\hat{r}'\hat{a}_n(\hat{r}',\hat{z})I_0(n\hat{r}'\sqrt{B/\beta})\right.$$
$$\left. + I_0(n\hat{r}\sqrt{B/\beta})\int_{\hat{r}}^{1} r'd\hat{r}'\hat{a}_n(\hat{r}',\hat{z})K_0(n\hat{r}'\sqrt{B/\beta})\right]. \tag{11.4}$$

When $B/\beta \gg 1$ (which corresponds to the one-dimensional approximation for the space charge field, $r_0^2 \gg \gamma_z^2 c^2/\omega^2$) the expression for $\hat{U}_c$ takes the following simple form

$$\hat{U}_c = \sum_{n=1}^{\infty} e^{in\psi}\frac{\hat{a}_n(\hat{r},\hat{z})}{n}. \tag{11.5}$$

The beam density modulation harmonics $\hat{a}_n = |\hat{a}_n|\exp(i\psi_n)$ are calculated as follows:

$$|\hat{a}_n| = \frac{1}{N}\left[\left[\sum_{k=1}^{N}\cos(n\psi_{(k)})\right]^2 + \left[\sum_{k=1}^{N}\sin(n\psi_{(k)})\right]^2\right]^{1/2}$$

$$\psi_n = -\arctan\left[\frac{\sum_{k=1}^{N}\sin(n\psi_{(k)})}{\sum_{k=1}^{N}\cos(n\psi_{(k)})}\right].$$

The power gain coefficient G is calculated using Eq. (10.26).

The field distribution in the Fresnel diffraction zone (i.e. inside the undulator) is given with expression (11.3) At the large distance of z from the undulator exit, the radiation has the form of a spherical wave with the amplitude $\Xi(\theta)$ depending on an observation angle $\theta = r/z$ (we assume here the Fraunhofer diffraction approximation)

$$\Xi(\hat{\theta}) = \int_0^{\hat{l}_w} d\hat{z}\int_0^1 d\hat{r}\hat{r}\hat{j}_1(\hat{z},\hat{r})\exp(i\hat{\theta}^2\hat{z}/B)J_0(\hat{\theta}\hat{r}) - i\frac{\hat{E}_g\hat{w}^2B}{4}\exp\left[-\frac{i\hat{\theta}^2\hat{z}_0}{2B} - \frac{\hat{w}^2\hat{\theta}^2}{4}\right],$$

where $\hat{\theta}$, $\hat{E}_g$, $\hat{w}$ and $\hat{z}_0$ have been defined in Section 10.

It should be emphasized that the system of working equations (11.2) has been derived without using severe restrictions on the electron energy deviation from the initial value: we have only omitted the terms of the order of $1/\gamma^2$ in the right-hand sides of Eqs. (11.2). Hence, this algorithm allows one to simulate the FEL amplifiers with high efficiency η up to the unity (of course, the final electron energy must be sufficiently large, i.e. $\gamma_f \gg 1$).

The simulation is performed with the macroparticle method. The macroparticle ensemble is prepared as follows: the electron beam is divided into M layers over the radius and in each layer we distribute

uniformly N macroparticles over phase ψ from 0 to 2π. The initial energy spread is simulated with the additional distribution of the particles according to the Gaussian law

$$dw = \frac{1}{\sqrt{2\pi\hat{\Lambda}_T^2}} \exp\left[-\frac{\hat{P}^2}{2\hat{\Lambda}_T^2}\right] d\hat{P}.$$

As a result, we get the system of $2 \times N \times M$ ordinary differential equations (11.2) which is integrated with the Runge-Kutta scheme. It should be noted that the standard numerical quadratures are not effective for the calculation of the integral over $\hat{z}'$ in expression (11.3) as the integrand has a singularity at $\hat{z}' \to \hat{z}$. To calculate this integral, we have developed a special algorithm [87]. The integration interval $(0, \hat{z})$ is divided into some number of subintervals and $\hat{j}_1$ is approximated with the polynomials in each of them. The Bessel function $J_0(t)$, where $t = B\hat{r}\hat{r}'/(\hat{z}-\hat{z}')$, is approximated with the polynomials at small values of t and at large values of t we use the asymptotic expansion. As a result the calculation of integral (11.3) over $\hat{z}'$ is reduced to the sum of special functions: Fresnel integrals, integral sine and cosine. The definite integral over the transverse coordinate is calculated with the standard quadrature formulae.

11.2. Some results of numerical simulations

In this section we present some results of the numerical simulation of the FEL amplifier with axisymmetric electron beam with the stepped profile of the current density.

First, we present some testing results of the code at the linear stage of operation. Fig. 10.5 illustrates the results of the increment calculations with the simulation code and the analytical ones obtained in section 10. One can see that even at the number of radial mesh divisions $N = 5$ the divergence of the simulation and analytical results is less than 1% in the wide range of the diffraction parameter B. Figs. 10.1 and 10.4 present the comparative results of the field distributions and directivity diagrams. Fig. 11.1 shows the power gain at the initial stage of amplification. The thorough testing of the simulation code has shown that the code is stable and provides the required accuracy of the calculations with the corresponding choice of the simulation parameters (number of radial mesh divisions, number of macroparticles, step of integration etc.).

Let us now present some results of the numerical simulation of the FEL amplifier. First of all, we consider the FEL amplifier with untapered undulator. In this case the maximal output radiation power is achieved at the saturation point when the most part of electrons fall into the accelerating phase of the ponderomotive potential. When the external input signal power is rather small, i.e. $W_{ext} \ll W_0$, the FEL amplifier output characteristics at the saturation depend on neither the input signal power nor the interaction length and are the functions of four reduced parameters $\hat{C}, B, \hat{\Lambda}_p^2$ and $\hat{\Lambda}_T^2$. Let us now illustrate the characteristic features of the FEL amplifier operating at the saturation.

Within the above accepted limitations the FEL amplifier reduced efficiency $\hat{\eta} = \eta/\beta$ at the saturation is a universal function of the detuning parameter $\hat{C}$, diffraction parameter B, space charge parameter $\hat{\Lambda}_p^2$ and the energy spread parameter $\hat{\Lambda}_T^2$: $\hat{\eta} = f(\hat{C}, B, \hat{\Lambda}_p^2, \hat{\Lambda}_T^2)$. Fig. 11.2 illustrates the simulation results of the reduced FEL amplifier efficiency $\hat{\eta}$ versus the interaction length at the value of diffraction parameter $B = 1$. It is clearly seen from this plot that the growth of the output power is ceased at the saturation point when the most part of electrons fall into the accelerating phase of the ponderomotive potential.

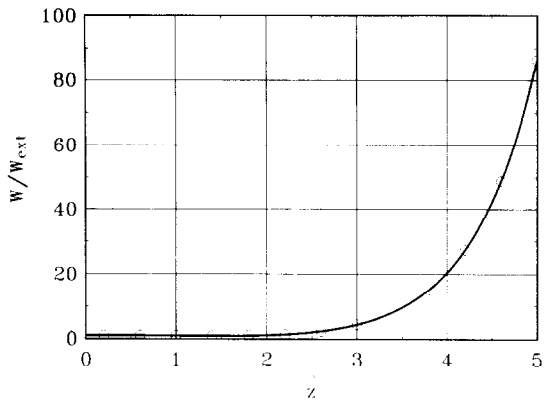

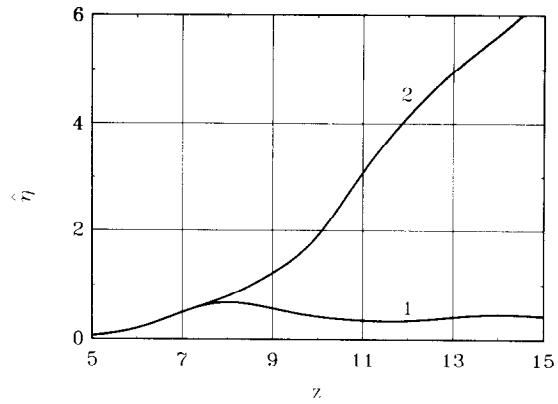

Fig. 11.1. The power gain at the linear stage of amplification. The curve is calculated with the initial problem solution code and the circles are calculated with the nonlinear simulation code. Here $B = 1$, $\hat{C} = 0$, $\hat{\Lambda}_p^2 = 0$, $\hat{\Lambda}_T^2 = 0$, $N = 5$, $M = 100$, $\hat{w} = 1.2$.

Fig. 11.2. The reduced efficiency $\hat{\eta}$ versus the interaction length. Here $B = 1$, $\hat{C} = 0$, $\hat{\Lambda}_p^2 = 0$, $\hat{\Lambda}_T^2 = 0$, $N = 5$, $M = 100$, $\hat{w} = 1.2$ and $\hat{W}_{ext} = 10^{-3}$. Curve (1): without tapering and curve (2): the tapering according to formula (11.6).

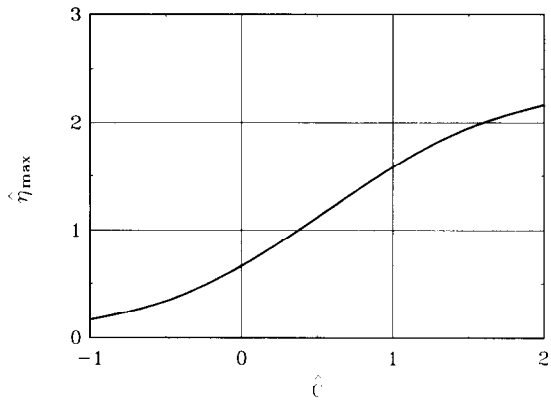

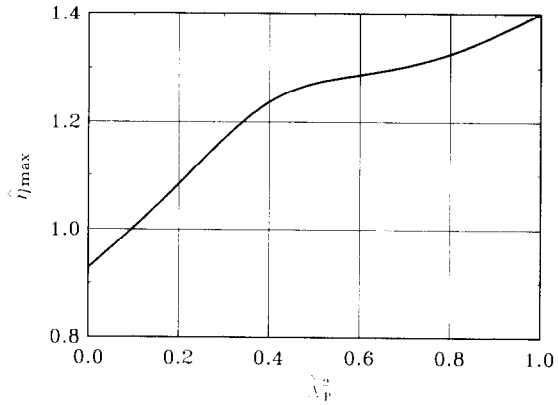

Fig. 11.3. The reduced efficiency $\hat{\eta}$ at the saturation versus the detuning parameter $\hat{C}$. Here $B = 1$, $\hat{\Lambda}_p^2 = 0$ and $\hat{\Lambda}_T^2 = 0$.

Fig. 11.4. The reduced efficiency $\hat{\eta}$ at the saturation versus the space charge parameter $\hat{\Lambda}_p^2$. Here $B = 1$ and $\hat{\Lambda}_T^2 = 0$. (The detuning parameter corresponds to the maximal increment at the linear high-gain limit).

Fig. 11.3 presents the dependence of the maximal reduced efficiency $\hat{\eta}$ on the detuning parameter $\hat{C}$. One can see from this plot that the amplifier efficiency is the increasing function of the detuning parameter $\hat{C}$. This is explained with the fact that when the detuning parameter is increased, the electrons interact with the wave for a longer distance (one should remember that this takes place only when the detuning is inside the amplification bandwidth).

Fig. 11.4 presents the dependence of the maximal reduced efficiency on the space charge parameter $\hat{\Lambda}_p^2$. It is clearly seen that the efficiency of the FEL amplifier is an increasing function of the space charge parameter. This is the consequence of the fact that the space charge fields prevent the beam overmodulation near the saturation point and the interaction of the modulated electron beam with the wave is prolonged.

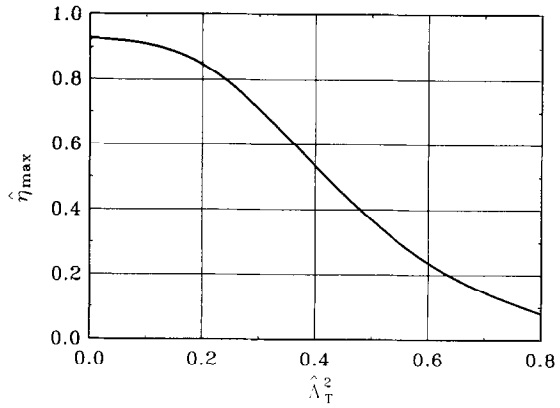

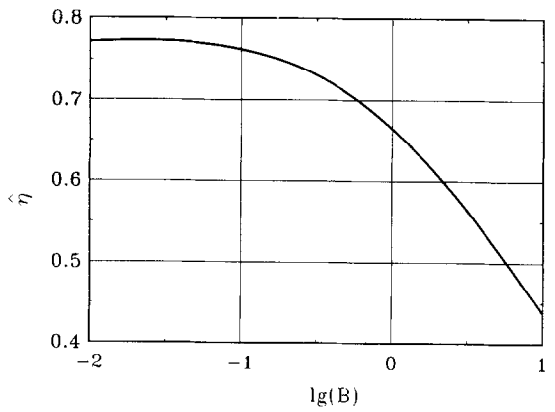

Fig. 11.5. The reduced efficiency $\hat{\eta}$ at the saturation versus the energy spread parameter $\hat{\Lambda}_T^2$. Here $B = 1$ and $\hat{\Lambda}_p^2 = 0$. (The detuning parameter corresponds to the maximum gain at the linear high-gain limit).

Fig. 11.6. The reduced efficiency $\hat{\eta}$ at the saturation versus the diffraction parameter B. Here $\hat{C} = 0$, $\hat{\Lambda}_p^2 = 0$ and $\hat{\Lambda}_T^2 = 0$.

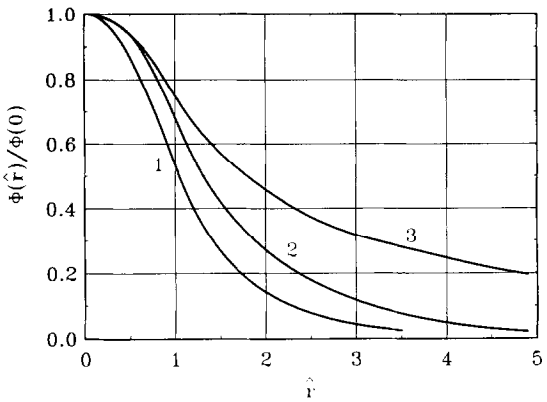

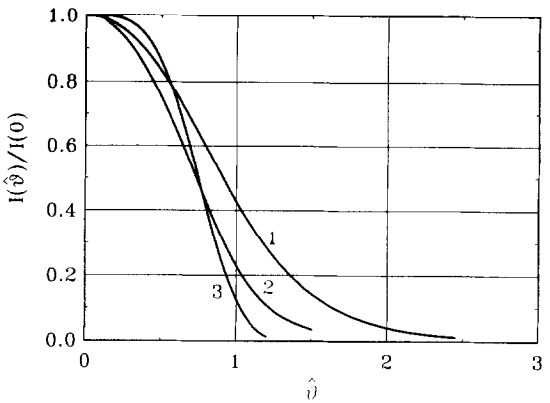

Fig. 11.7. The field distribution in the undulator versus radius: (1): at the linear stage (analytical results), (2): at the saturation, (3): at $\hat{z} = 15$ with the tapering according to formula (11.6). Here $B = 1$, $\hat{C} = 0$, $\hat{\Lambda}_p^2 = 0$, $\hat{\Lambda}_T^2 = 0$, $N = 5$, $M = 100$, $\hat{w} = 1.2$ and $\hat{W}_{ext} = 10^{-3}$.

Fig. 11.8. The directivity diagram versus the reduced observation angle: (1): at the linear stage (analytical results), (2): at the saturation, (3): at $\hat{z} = 15$ with the tapering according to formula (11.6). Here $B = 1$, $\hat{C} = 0$, $\hat{\Lambda}_p^2 = 0$, $\hat{\Lambda}_T^2 = 0$, $N = 5$, $M = 100$, $\hat{w} = 1.2$ and $\hat{W}_{ext} = 10^{-3}$.

Fig. 11.5 shows the dependence of the maximal reduced efficiency on the energy spread parameter. One can see that the amplifier efficiency is decreased drastically with the energy spread.

All the numerical simulations, presented above, have illustrated the main features of the FEL amplifier at the fixed value of diffraction parameter B. It would be interesting to trace with Fig. 11.6 the dependence of the reduced efficiency on the diffraction parameter B.

Fig. 11.7 shows the field distribution over the radius when the FEL amplifier operates at the saturation. The field distribution of the ground symmetric TEM_{00} mode (linear stage) is presented in this figure, too. One can see that the field distribution at the saturation is wider than at the linear stage and the radiation field redistributes in the space out of the electron beam.

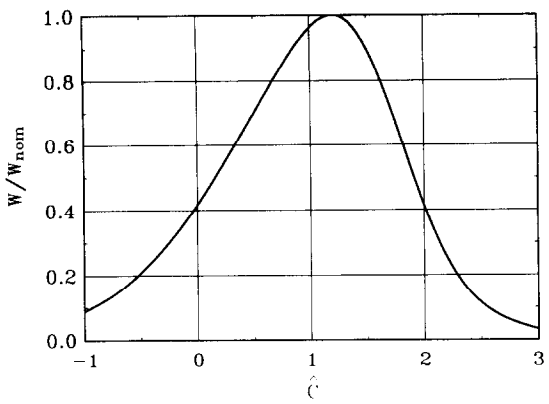

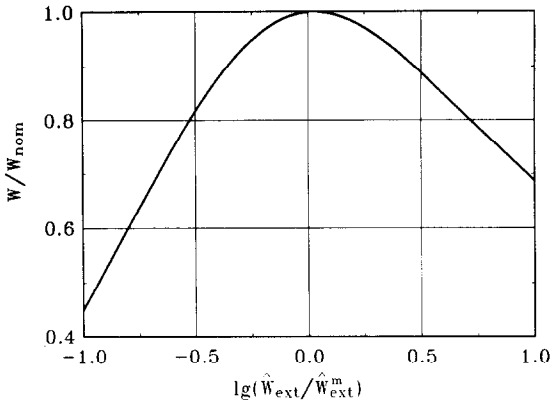

Fig. 11.9. The output power deviation W/W_{nom} from the nominal value versus the detuning parameter. FEL amplifier operates at the saturation, Here $B = 1$, $\hat{A}_p^2 = 0$, $\hat{A}_T^2 = 0$.

Fig. 11.10. The output power deviation W/W_m from the maximal value versus the deviation of the input radiation power $\hat{W}_{\text{ext}}$ from the nominal value $\hat{W}_{\text{ext}}^{\text{m}}$. FEL amplifier operates at the the saturation. Here $B = 1$, $\hat{C} = 0$, $\hat{A}_p^2 = 0$, $\hat{A}_T^2 = 0$, $N = 5$, $M = 100$, $\hat{w} = 1.2$, and $\hat{W}_{\text{ext}}^{\text{m}} = 10^{-3}$.

Fig. 11.8 illustrates the directivity diagram of the FEL amplifier at the saturation and the corresponding diagram for the ground TEM_{00} mode. It is clearly seen from these plots that the width of the radiation field distribution at the saturation is less than at the linear stage. This is the consequence of the fact that the effective size of the radiation spot at the amplifier output is greater at the saturation with respect to the linear stage (see Fig. 11.7)

In Figs. 11.9 and 11.10 one can see the basic output characteristics of the FEL amplifier at the saturation: the reduced resonance characteristic (the dependence of the efficiency on the detuning parameter) and the amplitude characteristic (the dependence of the efficiency versus the input power deviation from the nominal value). Using the reduced resonance characteristic and the definitions of the reduced parameters one can easily show that the reduced bandwidth $\Delta\hat{C}$ is connected with the physical parameters by the simple relations: frequency bandwidth is $\Delta\omega/\omega = 2\beta \cdot \Delta\hat{C}$; the electron beam energy deviation is $\Delta\mathcal{E}/\mathcal{E} = \beta \cdot \Delta\hat{C}$; the undulator field deviation is $\Delta H_w/H_w = \beta(1 + K^2) \cdot \Delta\hat{C}/K^2$.

The method of the FEL amplifier efficiency increase with the undulator parameters tapering is a well known one (see section 4). Here we shall only compare some output characteristics of the FEL amplifier with tapered undulator with output characteristics at the saturation of the FEL amplifier with untapered undulator. In Figs. 11.2, 11.7 and 11.8 we present the simulation results of the FEL amplifier with the tapered undulator. The tapering has been performed at the fixed value of undulator parameter K according to the law

$$T(\hat{z}) = \begin{cases} 0 & \text{at } \hat{z} < 7 \\ \hat{z} - 7 & \text{at } \hat{z} > 7. \end{cases} \tag{11.6}$$

One can see from the plots in Fig. 11.7 that the radiation spot size at the amplifier output is larger when the FEL amplifier operates with the tapering parameters and, as a result, the width of the radiation power directivity diagram becomes narrower (see Fig. 11.8).

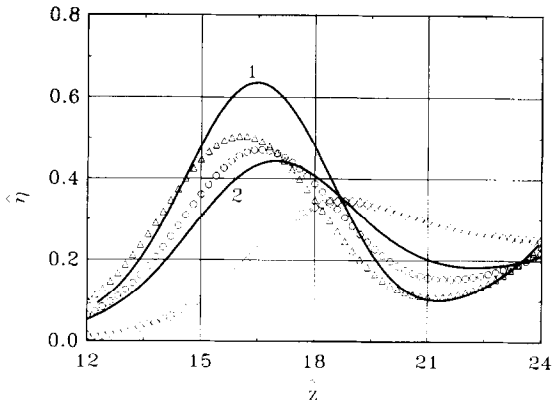

Fig. 11.11. The reduced efficiency $\hat{\eta}$ versus interaction length. The power gain coefficient at the saturation is $G = 40$ dB. (1) – one-dimensional simulations. Two-dimensional simulation with the FS2RN code at the value of diffraction parameter $B = 10$: (2) – the total efficiency, (△) – the efficiency at $\hat{r} = 0$, (o) – the efficiency at $\hat{r} = 0.5$ and (◇) – the efficiency at $\hat{r} = 1$. Here $\hat{C} = 0$, $\hat{\Lambda}_p^2 = 0$ and $\hat{\Lambda}_T^2 = 0$.

Now let us discuss the validity region of the one-dimensional FEL amplifier theory (see Sections 2–4). The linear analysis of the FEL amplifier shows that at the value of diffraction parameter $B \sim 10$ the divergence between the TEM_{00} mode increment and one-dimensional model increment does not exceed few percents (see Fig. 10.7). It is naturally to suppose that the same relations may be obtained at the nonlinear stage, too.

However, one can see from the plots in Fig. 11.11 that there is the significant difference in the efficiency calculations with these two models at the value of diffraction parameter $B = 10$. The efficiency calculated with the two-dimensional simulation code is visibly less. To explain this phenomenon, we should analyze the distribution of the electron energy losses over the radial coordinate. One can see from Fig. 11.11 that the electron energy losses are smaller for the particles located closer to the beam boundary. This asymmetry is connected with the nonuniform distribution of the radiation field over the beam due to the diffraction effects. Though at $B \simeq 10$ the value of TEM_{00} mode increment is close to the one-dimensional asymptote, the increments of the higher modes: TEM_{01}, TEM_{02}, etc. are visibly less. When the FEL amplifier power gain coefficient is sufficiently large, the only TEM_{00} radiation mode is forming. From Fig. 10.1 one can see that the nonuniformity of the TEM_{00} mode field distribution is increased with the value of the diffraction parameter. Coming to the conclusion of our discussion on this topic we should emphasize that the results of the one-dimensional nonlinear theory should be used carefully because even at the large values of the diffraction parameter the diffraction effects could play a significant role.

11.3. Applicability region

In Sections 10 and 11 we have presented analysis of the FEL amplifier operation wherein diffraction effects have been taken into account. The basic peculiarities of our approach are the three-dimensional representation of the radiation and space charge fields, and the electron motion description with the one-dimensional approximation. This model, to some extent, tends to simplify real processes occurring in the FEL amplifiers. However, within the scope of such a model we take into account almost all the main effects influencing the FEL amplifier operation: diffraction of radiation, space charge fields

and energy spread of electrons in the beam. It should be noted that in the framework of the presented model the beam emittance influence on the FEL amplifier operation has been fallen out of the consideration. To be strict, this effect should be taken into account in the framework of the fully three-dimensional theory and the results, obtained with this model, should be considered as a reliable test basis for the more complicated models. As for upgrading the numerical simulation algorithm, it is not a physical problem but computational one and can be easily resolved. Situation with upgrading the linear theory is much more complicated and there is no possibility to obtain rigorous analytical results (see, e.g. Ref. [74]).

When deriving self-consistent equation (9.9) of the linear mode of operation and constructing the numerical simulation algorithm we have neglected betatron oscillations of the particles. On the other hand, when moving in the undulator field, particles perform betatron oscillations. The wavelength of betatron oscillations is

$$\lambda_b = 2^{1/2}\lambda_w\theta_s^{-1}. \tag{11.7}$$

So, the reasonable question is arisen when this model describes correctly the real processes in the FEL amplifier. Simple physical considerations show that it takes place in two cases. First, this model is valid when the betatron oscillation wavelength is much more than characteristic length of the radiation field growth. In the linear mode of operation this length is of the order of the gain length. Second situation corresponds to such a choice of the FEL amplifier parameters which provide the characteristic transverse size of the radiation field eigenmode to be much more than the transverse size of the electron beam. In this cases the emittance effects can be taken into account as follows. As a rule, the electron beam should be matched with the focusing system of the undulator which results in the following values of the beam radius r_0 and angle spread $(\langle(\Delta\theta)^2\rangle)^{1/2}$ of the electrons in the beam

$$r_0 = (\beta_w\epsilon_n/\gamma\pi)^{1/2}, \quad (\langle(\Delta\theta)^2\rangle)^{1/2} = (\epsilon_n/\pi\beta_w\gamma)^{1/2} \tag{11.8}$$

where $\beta_w = \sqrt{2}\,\lambda_w/2\pi\theta_s$ is the beta-function of the electron beam in the undulator and ϵ_n is the normalized emittance of the beam. The presence of the angle spread in the beam results in additional spread in the longitudinal velocities which may be interpreted with introducing of additional energy spread. So, the inclusion of the emittance effects is performed by substituting the real energy spread $\sigma_E = [\langle(\Delta\mathcal{E}/\mathcal{E})^2\rangle]^{1/2}$ in the energy spread parameter

$$\hat{\Lambda}_T^2 = \sigma_E^2\omega^2/(c^2\gamma_z^4\mathcal{E}_0^2\Gamma^2)$$

by "effective" energy spread

$$\sigma_E = [\langle(\Delta\mathcal{E}/\mathcal{E})^2\rangle + \gamma_z^4\langle(\Delta\theta)^2\rangle^2/4]^{1/2}.$$

Another limitation of the model is that the radius of the electron rotation r_w in the undulator must be much less than the radius of electron beam r_0 which results in the following limitation on the electron beam emittance:

$$r_w^2 = (\theta_s\lambda_w/2\pi)^2 \ll \epsilon_n\lambda_b/2\pi\gamma. \tag{11.9}$$

One more approximation of the model refers to the linear mode of the FEL amplifier operation. When deriving Eq. (9.9) we have neglected the reduction of the plasma frequency due to finite transverse

size of electron beam. This condition assumes the transverse electron beam size to be rather large, $r_0^2 \gg \gamma_z^2 c^2/\omega^2$ which corresponds to the following limitation on the emittance value:

$$(\gamma_{z0}\lambda/2\pi)^2 \ll \epsilon_n \lambda_b/2\pi\gamma. \tag{11.10}$$

It is interesting to notice that conditions (11.9) and (11.10) are almost identical at a large value of the undulator parameter $K = eH_w\lambda_w/2\pi mc^2$.

When the FEL amplifier parameters satisfy the above mentioned conditions, the presented model provide reliable results when the emittance effects are taken into account in the way described above. For instance, this model has been used for calculations of the FEL amplifier for photon linear collider [6].

Acknowledgments

We wish to acknowledge Professor V.P. Sarantsev for invaluable collaboration and support in our work. We express special thanks to Dr. Yu.N. Ulyanov of the Automatic Systems Corporation (Samara), Professor A.N. Lebedev and Dr. A.V. Agafonov of the Lebedev Physical Institute (Moscow) for their permanent interest in our work and many useful discussions and recommendations.

Appendix A. The extended Hamiltonian formalism

In the framework of Hamiltonian formalism a system of material points is described with n pairs of canonical variables

$$x_1, x_2, \ldots, x_n, \quad p_1, p_2, \ldots, p_n$$

and with the Hamilton function

$$\mathcal{H}(x_1, x_2, \ldots, x_n, p_1, p_2, \ldots, p_n, t).$$

The canonical equations of motion have the form

$$dx_j/dt = \partial\mathcal{H}/\partial p_j, \quad dp_j/dt = -\partial\mathcal{H}/\partial x_j, \quad j = 1, \ldots, n.$$

In some cases it is convenient to generalize the Hamiltonian formalism by introducing the $(n+1)$th coordinate x_0 coinciding with the independent variable t (see e.g. Ref. [91]). In this case the Hamiltonian may be written in the form

$$\mathcal{H} = \mathcal{H}(x_0, x_1, \ldots, x_n, p_1, p_2, \ldots, p_n).$$

To provide the symmetry, new $(n+1)$th canonical variable p_0, canonically conjugated with x_0 is introduced. New Hamiltonian H of $(2n+2)$ variables is of the form

$$H(x_0, x_1, \ldots, x_n, p_0, p_1, \ldots, p_n) = \mathcal{H}(x_0, x_1, \ldots, x_n, p_1, p_2, \ldots, p_n) + p_0$$

which leads to the extended system of the canonical equations

$$dx_j/dt = \partial H/\partial p_j, \quad dp_j/dt = -\partial H/\partial x_j, \quad j = 0, 1, \ldots, n.$$

At $j = 0$ we have

$$dx_0/dt = 1, \quad dp_0/dt = -\partial H/\partial x_0 = -\partial \mathcal{H}/\partial x_0 = -\partial \mathcal{H}/\partial t.$$

Let us assume that variables x_0 and p_0 satisfy the following initial conditions at $t = 0$

$$x_0(0) = 0, \quad p_0(0) = -\mathcal{H}(x_0(0), \ldots, p_0(0), \ldots, 0).$$

In this case we get the solutions: $x_0(t) = t$ and $p_0(t) = -\mathcal{H}(t)$. Hence, Hamiltonian H at any time t is equal to zero, $H(t) = 0$, i.e. it is the integral of motion.

Let us now consider a transformation of variables given with the following expressions

$$\begin{aligned} x_0 &= x_0(\bar{x}_0, \bar{x}_1, \ldots, \bar{x}_n, \bar{p}_0, \bar{p}_1, \ldots, \bar{p}_n), \ldots \quad x_n = x_n(\bar{x}_0, \bar{x}_1, \ldots, \bar{x}_n, \bar{p}_0, \bar{p}_1, \ldots, \bar{p}_n), \\ p_0 &= p_0(\bar{x}_0, \bar{x}_1, \ldots, \bar{x}_n, \bar{p}_0, \bar{p}_1, \ldots, \bar{p}_n), \ldots \quad p_n = p_n(\bar{x}_0, \bar{x}_1, \ldots, \bar{x}_n, \bar{p}_0, \bar{p}_1, \ldots, \bar{p}_n) \end{aligned} \tag{A.1}$$

which leads to the following Hamiltonian $\bar{H}$

$$\begin{aligned} &\bar{H}(\bar{x}_0, \bar{x}_1, \ldots, \bar{x}_n, \bar{p}_0, \bar{p}_1, \ldots, \bar{p}_n) \\ &\quad = H(x_0(\bar{x}_0, \bar{x}_1, \ldots, \bar{x}_n, \bar{p}_0, \bar{p}_1, \ldots, \bar{p}_n), \ldots, p_n(\bar{x}_0, \bar{x}_1, \ldots, \bar{x}_n, \bar{p}_0, \bar{p}_1, \ldots, \bar{p}_n)). \end{aligned}$$

The derivatives of new variables with respect to time are of the form

$$\begin{aligned} d\bar{x}_j/dt &= \sum_{l=0}^{n} [(\partial \bar{x}_j/\partial x_l)(dx_l/dt) + (\partial \bar{x}_j/\partial p_l)(dp_l/dt)] \\ &= \sum_{l=0}^{n} [(\partial \bar{x}_j/\partial x_l)(\partial H/dp_l) - (\partial \bar{x}_j/\partial p_l)(\partial H/dx_l)] \\ &= \sum_{l=0}^{n} \Bigg\{ (\partial \bar{x}_j/\partial x_l) \sum_{k=0}^{n} [(\partial \bar{H}/\partial \bar{x}_k)(\partial \bar{x}_k/\partial p_l) + (\partial \bar{H}/\partial \bar{p}_k)(\partial \bar{p}_k/\partial p_l)] \\ &\quad - (\partial \bar{x}_j/\partial p_l) \sum_{k=0}^{n} [(\partial \bar{H}/\partial \bar{x}_k)(\partial \bar{x}_k/\partial x_l) + (\partial \bar{H}/\partial \bar{p}_k)(\partial \bar{p}_k/\partial x_l)] \Bigg\} \\ &= \sum_{k=0}^{n} \Bigg\{ (\partial \bar{H}/\partial x_k) \sum_{l=0}^{n} [(\partial \bar{x}_k/\partial p_l)(\partial \bar{x}_j/\partial x_l) - (\partial \bar{x}_j/\partial p_l)(\partial \bar{x}_k/\partial x_l)] \\ &\quad + (\partial \bar{H}/\partial p_k) \sum_{l=0}^{n} [(\partial \bar{p}_k/\partial p_l)(\partial \bar{x}_j/\partial x_l) - (\partial \bar{x}_j/\partial p_l)(\partial \bar{p}_k/\partial x_l)] \Bigg\}. \end{aligned} \tag{A.2}$$

and

$$d\bar{p}_j/dt = -\sum_{k=0}^{n}\Bigg\{(\partial\bar{H}/\partial p_k)\sum_{l=0}^{n}[(\partial\bar{p}_j/\partial p_l)(\partial\bar{p}_k/\partial x_l) - (\partial\bar{p}_j/\partial x_l)(\partial\bar{p}_k/\partial p_l)]$$

$$+ (\partial\bar{H}/\partial x_k)\sum_{l=0}^{n}[(\partial\bar{p}_j/\partial p_l)(\partial\bar{x}_k/\partial x_l) - (\partial\bar{x}_k/\partial p_l)(\partial\bar{p}_j/\partial x_l)]\Bigg\}. \tag{A.3}$$

To reduce the expressions (A.2) and (A.3) we introduce the Poisson brackets $[f, g]$

$$[f, g] = \sum_{l=0}^{n}[(\partial f/\partial p_l)(\partial g/\partial x_l) - (\partial g/\partial p_l)(\partial f/\partial x_l)],$$

where

$$f(x_0, x_1, \ldots, x_n, p_0, p_1, \ldots, p_n), \quad g(x_0, x_1, \ldots, x_n, p_0, p_1, \ldots, p_n).$$

As a result, the expressions (A.2) and (A.3) get the form:

$$d\bar{x}_j/dt = \sum_{k=0}^{n}\{(\partial\bar{H}/\partial\bar{x}_k)[\bar{x}_k, \bar{x}_j] + (\partial\bar{H}/\partial\bar{p}_k)[\bar{p}_k, \bar{x}_j]\},$$

$$d\bar{p}_j/dt = -\sum_{k=0}^{n}\{(\partial\bar{H}/\partial\bar{p}_k)[\bar{p}_j, \bar{p}_k] + (\partial\bar{H}/\partial\bar{x}_k)[\bar{p}_j, \bar{x}_k]\}. \tag{A.4}$$

Using these expressions one can find out that the conditions

$$[\bar{x}_k, \bar{x}_j] = 0, \quad [\bar{p}_k, \bar{x}_j] = \delta_{kj}, \quad [\bar{p}_k, \bar{p}_j] = 0 \tag{A.5}$$

are the necessary and sufficient for the transformation (A.1) to be canonical, and variables $\bar{x}_j$ and $\bar{p}_j$ satisfy the canonical equations with Hamiltonian $\bar{H}$

$$d\bar{x}_j/dt = \partial\bar{H}/\partial\bar{p}_j, \quad d\bar{p}_j/dt = -\partial\bar{H}/\partial\bar{x}_j, \quad j = 0, 1, \ldots, n. \tag{A.6}$$

Let us consider, for illustration, the point transformation [92]

$$x_j = F_j(\bar{x}_0, \ldots, \bar{x}_n), \quad j = 0, \ldots, n. \tag{A.7}$$

We wish to go over to the new system of $(2n+2)$ variables $(\bar{p}_j, \bar{x}_j)$ which are independent functions p_j and x_j and satisfy the condition

$$\sum_{j=0}^{n}\bar{p}_j d\bar{x}_j = \sum_{j=0}^{n} p_j dx_j. \tag{A.8}$$

One can easily find the formulae of this transformation

$$\bar{p}_j = \sum_{l=0}^{n} p_l \partial F_l/\partial\bar{x}_j. \tag{A.9}$$

Calculating the Poisson brackets (A.5) one can easily find that expressions (A.7) and (A.9) determine the canonical transformation.

Let us now go over to a new independent variable $\bar{x}_0$ in place of t. The expressions (A.6) lead to the following equations

$$d\bar{x}_j/d\bar{x}_0 = (d\bar{x}_j/dt)(dt/d\bar{x}_0) = (\partial\bar{H}/\partial\bar{p}_j)(\partial\bar{H}/\partial\bar{p}_0)^{-1} = -[\partial\bar{p}_0/\partial\bar{p}_j]_{\bar{H}},$$
$$d\bar{p}_j/d\bar{x}_0 = (d\bar{p}_j/dt)(dt/d\bar{x}_0) = -(\partial\bar{H}/\partial\bar{x}_j)(\partial\bar{H}/\partial\bar{p}_0)^{-1} = [\partial\bar{p}_0/\partial\bar{x}_j]_{\bar{H}}.$$

Here the symbol $(\ldots)_{\bar{H}}$ means that the corresponding derivative is calculated at the constant value of $\bar{H}(\bar{x}_0, \ldots, \bar{x}_n, \bar{p}_0, \ldots, \bar{p}_n)$. From the condition $\bar{H} = 0$ we get:

$$p_0(\bar{x}_0, \ldots, \bar{x}_n, \bar{p}_0, \ldots, \bar{p}_n) = -\mathcal{H}(\bar{x}_0, \ldots, \bar{x}_n, \bar{p}_0, \ldots, \bar{p}_n).$$

Resolving the latter equation with respect to $\bar{p}_0$ we obtain

$$\bar{p}_0 = \tilde{\mathcal{H}}(\bar{x}_0, \ldots, \bar{x}_n, \bar{p}_1, \ldots, \bar{p}_n).$$

As a result, the equation of motion may be written in the canonical form

$$d\bar{x}_j/d\bar{x}_0 = \partial\tilde{\mathcal{H}}/\partial\bar{p}_j, \quad d\bar{p}_j/d\bar{x}_0 = -\partial\tilde{\mathcal{H}}/\partial\bar{x}_j, \quad j = 1, \ldots, n.$$

Appendix B. The general form of the solution of the initial-value problem for the FEL amplifier with a "cold" electron beam

In Section 2 we solved the initial-value problem using the Laplace method. In this section we present completely different method of solving this problem. When we can neglect the energy spread (i.e. in the case of "cold" electron beam), the kinetic equation (2.7) and the wave equation (2.13) can be reduced to a single differential equation for the field amplitude of the amplified wave $\tilde{E}$

$$\tilde{E}''' + 2i\hat{C}\tilde{E}'' + (\hat{\Lambda}_p^2 - \hat{C}^2)\tilde{E}' = i\tilde{E}, \tag{B.1}$$

where the prime denotes differentiation with respect to $\hat{z}$. Since Eq. (B.1) is a linear ordinary differential equation with constant coefficients, its solution could be seek in the form:

$$\tilde{E}(\hat{z}) = A\exp(\lambda\hat{z}).$$

According to Eq. (B.1), the factor λ in the argument of the exponential satisfies the algebraic equation

$$\lambda[(\lambda + i\hat{C})^2 + \hat{\Lambda}_p^2] = i, \tag{B.2}$$

which gives three values of λ determining three linearly independent solutions for the field amplitude:

$$\tilde{E}_1 = \exp(\lambda_1\hat{z}), \quad \tilde{E}_2 = \exp(\lambda_2\hat{z}), \quad \tilde{E}_3 = \exp(\lambda_3\hat{z}).$$

To solve the initial-value problem, we should set the initial conditions for

$$\tilde{E}(0), \quad \tilde{E}'(0), \quad \tilde{E}''(0),$$

which correspond to the field amplitude and its first and second derivatives with respect to $\hat{z}$ at the undulator entrance at $\hat{z} = 0$. Then

$$\begin{bmatrix} \tilde{E} \\ \tilde{E}' \\ \tilde{E}'' \end{bmatrix}_{\hat{z}} = M(\hat{z} \mid 0) \begin{bmatrix} \tilde{E} \\ \tilde{E}' \\ \tilde{E}'' \end{bmatrix}_0, \tag{B.3}$$

where the transition matrix $M(\hat{z}|0)$ is equal to

$$M = \begin{bmatrix} \tilde{E}_1 & \tilde{E}_2 & \tilde{E}_3 \\ \tilde{E}_1' & \tilde{E}_2' & \tilde{E}_3' \\ \tilde{E}_1'' & \tilde{E}_2'' & \tilde{E}_3'' \end{bmatrix}_z \times \begin{bmatrix} \tilde{E}_1 & \tilde{E}_2 & \tilde{E}_3 \\ \tilde{E}_1' & \tilde{E}_2' & \tilde{E}_3' \\ \tilde{E}_1'' & \tilde{E}_2'' & \tilde{E}_3'' \end{bmatrix}_0^{-1}.$$

The explicit expressions for the matrix elements M_{ij} are as follows:

$$M_{11} = \lambda_2\lambda_3 B_1 + \lambda_1\lambda_3 B_2 + \lambda_1\lambda_2 B_3,$$
$$M_{12} = -(\lambda_2 + \lambda_3)B_1 - (\lambda_1 + \lambda_3)B_2 - (\lambda_1 + \lambda_2)B_3,$$
$$M_{13} = B_1 + B_2 + B_3, \quad M_{21} = \lambda_1\lambda_2\lambda_3 M_{13},$$
$$M_{22} = -\lambda_1(\lambda_2 + \lambda_3)B_1 - \lambda_2(\lambda_1 + \lambda_3)B_2 - \lambda_3(\lambda_1 + \lambda_2)B_3,$$
$$M_{23} = \lambda_1 B_1 + \lambda_2 B_2 + \lambda_3 B_3, \quad M_{31} = \lambda_1\lambda_2\lambda_3 M_{23},$$
$$M_{32} = -\lambda_1^2(\lambda_2 + \lambda_3)B_1 - \lambda_2^2(\lambda_1 + \lambda_3)B_2 - \lambda_3^2(\lambda_1 + \lambda_2)B_3,$$
$$M_{33} = \lambda_1^2 B_1 + \lambda_2^2 B_2 + \lambda_3^2 B_3,$$

where to abbreviate the notations we have introduced

$$B_1 = \frac{\exp(\lambda_1\hat{z})}{(\lambda_1 - \lambda_2)(\lambda_1 - \lambda_3)}, \quad B_2 = \frac{\exp(\lambda_2\hat{z})}{(\lambda_2 - \lambda_1)(\lambda_2 - \lambda_3)}, \quad B_3 = \frac{\exp(\lambda_3\hat{z})}{(\lambda_3 - \lambda_1)(\lambda_3 - \lambda_2)}.$$

The values of $\tilde{E}'$ and $\tilde{E}''$ at the undulator entrance can be expressed in terms of the complex amplitude of the first harmonic of the particle density in the phase space f_1. Using kinetic equation (2.7) and the wave equation (2.13), we have

$$\tilde{E}'(0)/E_0 = -2\tilde{j}_1(0)/j_0, \quad \tilde{E}''/E_0 = -2\tilde{j}_1'/j_0 = -2i\left[\hat{C}\tilde{j}_1(0)/j_0 + \int \hat{P}\hat{f}_1(0,\hat{P})d\hat{P}\right],$$

$$\tilde{j}_1/j_0 = -\int \hat{f}_1(0,\hat{P})d\hat{P}$$

As an example, let us consider the case when unmodulated electron beam and an electromagnetic wave of amplitude E_{ext} are fed to the amplifier input. The initial conditions at $\hat{z} = 0$ are as follows:

$$\tilde{E}(0) = E_{ext}, \quad \tilde{E}'(0) = 0, \quad \tilde{E}''(0) = 0.$$

According to Eq. (B.3), we obtain

$$\tilde{E}(\hat{z}) = M_{11}(\hat{z}|0)E_{ext}.$$

This expression is identical to expression (2.23).

Appendix C. Treatment of the linear mode of the FEL oscillator operation as an eigenvalue problem

We consider a plane Fabry-Perot resonator of the base L equipped with two plane parallel mirrors. A helical undulator having length l_w is placed between the mirrors and its axis coincides with the resonator axis. Magnetic field at the undulator axis is given with the expression

$$\boldsymbol{H}_w(z) = \boldsymbol{e}_x H_w \cos(\kappa_w z) - \boldsymbol{e}_y H_w \sin(\kappa_w z),$$

where $\boldsymbol{e}_x$ and $\boldsymbol{e}_y$ are the unit vectors. We neglect the transverse variations of the undulator field and assume the electrons to move along the constrained helical trajectories in parallel with the z axis (averaged over the undulator period). The electron rotation angle θ_s is considered to be small and longitudinal electron velocity v_z is close to the velocity of light ($v_z \simeq c$).

We suppose the electromagnetic field in the resonator to be circularly polarized because of the helical magnetic system of the undulator. Using the complex representation, in the one-dimensional approximation the radiation field in the resonator may be presented as a superposition of the oscillations with different longitudinal wavenumbers. In the case of ideal mirrors, we have

$$E_x + iE_y = \sum_m \tilde{E}_m(t) \exp(-i\omega_m t) \sin(k_m z), \tag{C.1}$$

where $k_m = m\pi/L$, $\omega_m = cm\pi/L$ and m is integer number, $m \gg 1$. The physical meaning of expression (C.1) is that an integer number of half-waves must fit the resonator base. This expression may be generalized to the case when the resonator mirrors are made of material with refractive index n'. We suppose the value of n' to be the large complex number, i.e. $|n'| \gg 1$. For example, the refractive index of the metallic mirrors with the conductivity σ' is given with the expression $n'(\omega) = \sqrt{4\pi i\sigma'/\omega}$, where ω is the frequency of electromagnetic wave. The electromagnetic field must satisfy Leontovich's boundary conditions on the mirror surface (see e.g. Refs. [93,94]):

$$[\boldsymbol{n} \times \boldsymbol{E}_\omega]|_s = \frac{1}{n'}[\boldsymbol{n} \times [\boldsymbol{n} \times \boldsymbol{H}_\omega]]|_s,$$

where $\boldsymbol{n}$ is the unit vector perpendicular to the mirror surface, E_ω and H_ω are Fourier harmonic of the electric and magnetic field

$$\boldsymbol{E} = \boldsymbol{E}_\omega e^{-i\omega t} + \text{c.c.}, \quad \boldsymbol{H} = \boldsymbol{H}_\omega e^{-i\omega t} + \text{c.c.},$$

$n' = n'(\omega)$ is the refractive index. Using Maxwell's equation $c\nabla \times \boldsymbol{E} = -\partial \boldsymbol{H}/\partial t$, the Leontovich boundary conditions may be written in the form

$$[[E_x + iE_y] \pm \frac{ic}{n'\omega}\frac{\partial}{\partial z}[E_x + iE_y]]\Big|_{z=\{\substack{L\\0}\}} = 0. \tag{C.2}$$

Assuming the refractive index to be constant in the operating wavelength range of the FEL, we may generalize the expression (C.1) for the radiation field in the resonator for finite value of the refraction index n'

$$E_x + iE_y = \sum_m \tilde{E}_m(t) \exp(-i\omega_m t) \sin(k_m z + \delta), \tag{C.3}$$

where $k_m = m\pi/L - 2i/(n'L)$ and $\delta = i/n'$. One can obtain that this field satisfies Leontovich's boundary conditions (C.2).

It should be noted that boundary conditions (C.2) may be used in the frame of three-dimensional FEL oscillator theory, too [33,34].

In this section we let the complex amplitudes $\tilde{E}_m$ to be the slowly changing functions of time, i.e. $|\partial \tilde{E}_m/\partial t|L/c \ll |\tilde{E}_m|$. The small field amplification per one resonator pass means that the lasing frequency ω is close to one of the passive resonator frequency ω_m.

In the framework of the one-dimensional theory the electric field $\boldsymbol{E}(z,t)$ in the resonator is subjected to the wave equation

$$c^2\partial^2\boldsymbol{E}/\partial z^2 - \partial^2\boldsymbol{E}/\partial t^2 = 4\pi\partial\boldsymbol{j}/\partial t, \tag{C.4}$$

which may be obtained from Maxwell's equations. Let us now consider the problem of obtaining the vector of the induced beam current density $\boldsymbol{j}(z,t)$ appearing in Eq. (C.4). The standing wave field in the resonator may be represented as a superposition of two travelling waves. In the linear approximation vector $\boldsymbol{j}$ is proportional to the electric field strength of the wave synchronous with the electron beam. Hence, using (C.3) we may write

$$j_x + ij_y = \chi\tilde{E}_m(t)\exp[i\omega_m(z/c - t)]. \tag{C.5}$$

To find susceptibility χ, the equations of electron motion in the given electromagnetic field should be solved.

In the same way as it was done in Sections 5–8, we describe the electron motion using "energy-phase" variables $\mathcal{E}$ and $\psi = \kappa_w z - \omega_m(z/c - t)$. In the case when the space charge field can be neglected, the corresponding Hamiltonian H has the form (see Eq.(2.5):

$$H(P,\psi,z) = C_m P + \frac{\omega_m}{2c\gamma_z^2\mathcal{E}_0}P^2 - [U_m e^{i\psi} + U_m^* e^{-i\psi}][1 - P/\mathcal{E}_0],$$

where $P = \mathcal{E} - \mathcal{E}_0$, $C_m = \kappa_w - \omega_m/(2c\gamma_z^2)$ is the detuning of the mth mode with the particle having nominal energy $\mathcal{E}_0$, $U_m = e\theta_s\tilde{E}_m/4$ is the complex amplitude of the effective potential of the particle interaction with the synchronous electromagnetic wave, $\theta_s = eH_w/(\mathcal{E}_0\kappa_w)$, $\gamma_z^{-2} = \gamma^{-2} + \theta_s^2$ and $\gamma = \mathcal{E}_0/(m_e c^2)$.

The evolution of electron beam distribution function f is determined with the kinetic equation

$$\frac{\partial f}{\partial z} + \frac{\partial H}{\partial P}\frac{\partial f}{\partial \psi} - \frac{\partial H}{\partial \psi}\frac{\partial f}{\partial P} = 0.$$

In the linear approximation we shall seek the solution for f in the form

$$f = f_0 + \tilde{f}_1 e^{i\psi} + \tilde{f}_1^* e^{-i\psi}.$$

Evolution of $\tilde{f}_1$ is described by the equation

$$\frac{\partial\tilde{f}_1}{\partial z} + i(C_m + \omega_m P/(c\gamma_z^2\mathcal{E}_0))\tilde{f}_1 + iU_m\frac{\partial f_0}{\partial P} = 0. \tag{C.6}$$

We assume that the electron beam at the entrance into undulator is modulated neither in velocity nor in density, i.e.

$$\tilde{f}_1|_{z=z_i} = 0, \quad f_0|_{z=z_i} = n_0 F(P), \quad \int F dP = 1,$$

where z_i is the coordinate of the undulator entrance and n_0 is the beam density. The beam current density is connected with the distribution function $\tilde{f}_1$ as follows (we assume here $v_z \simeq c$)

$$j_z = -j_0 + \tilde{j}_1 e^{i\psi} + \text{c.c.}, \quad \tilde{j}_1 \simeq -ec\int\tilde{f}_1 dP, \quad j_x + ij_y = \theta_s\tilde{j}_1\exp[i\omega_m(z/c - t)], \tag{C.7}$$

where $-j_0 \simeq -ecn_0$ is the longitudinal component of the beam current density at the undulator entrance. Complex amplitudes $\tilde{j}_1$ and $\tilde{f}_1$ are connected with j_1 and ψ_1 as follows

$$(1/2)j_1 \exp(\psi_1) = |\tilde{j}_1| \exp(\psi_1) = \tilde{j}_1 \simeq -ec \int \tilde{f}_1 dP.$$

Substituting (C.7) into the kinetic equation and integrating over z and P we get the following equation for $\tilde{j}_1$

$$\tilde{j}_1 = ij_0 U_m \int_{z_i}^{z} dz' \int_{-\infty}^{\infty} dP \frac{dF}{dP} \exp[i(C_m + \omega_m P/(\gamma_z^2 \mathcal{E}_0 c))(z' - z)]. \tag{C.8}$$

Let us consider the case of the "cold" electron beam, i.e. the monoenergetic electron beam with the distribution function $F(P) = \delta(P)$. One can easily find that the function χ entering Eq. (C.5) is given by

$$\chi = j_0 \omega_m e \theta_s^2 (4c\gamma_z^2 \mathcal{E}_0)^{-1} \int_{z_i}^{z} dz'(z' - z) \exp[iC_m(z' - z)].$$

We shall seek the solution for the complex amplitude $\tilde{E}_m$ in the form

$$\tilde{E}_m = \text{const} \times \exp(\epsilon_m t). \tag{C.9}$$

Then we substitute Eqs. (C.3), (C.5) and (C.9) into Eq. (C.4). After multiplying the obtained equation by $\sin(k_m z)$ and integrating over z, we get

$$\hat{\epsilon}_m = \tfrac{1}{2}\hat{Z}(\hat{C}_m), \tag{C.10}$$

where

$$\hat{\epsilon}_m = 2\epsilon_m L/(c\tau) + 4/(n'\tau), \quad \tau = 2\pi\omega_m \theta_s^2 l_w^3 j_0 (c\gamma_z^2 \gamma I_A)^{-1}, \quad \hat{C}_m = C_m l_w.$$

The function $\hat{Z}$ has the form

$$\hat{Z} = i \int_0^1 d\xi \int_0^{\xi} d\xi' \xi' \exp(-i\hat{C}_m \xi'). \tag{C.11}$$

After integrating we obtain

$$\hat{Z} = 2i\hat{C}_m^{-2}[2(\hat{C}_m)^{-1} \sin(\hat{C}_m/2) - \cos(\hat{C}_m/2)] \exp(-i\hat{C}_m/2). \tag{C.12}$$

Only the modes which eigenvalues satisfy the condition

$$\mathrm{Re}(\hat{\epsilon}_m) > \mathrm{Re}(4/(n'\tau))$$

will grow exponentially in time. The lasing condition may be written as

$$\max \mathrm{Re}(\hat{\epsilon}_m) > \mathrm{Re}(4/(n'\tau)). \tag{C.13}$$

We have considered above the case of the resonator equipped with two identical mirrors. When the mirrors are made of materials with different refractive indexes n_1' and n_2', the expression for $\hat{\epsilon}_m$ is written in the form

$$\hat{\epsilon}_m = 2\epsilon_m L/(c\tau) + 4/(n'\tau) \rightarrow 2\epsilon_m L/(c\tau) + 2/(n_1'\tau) + 2/(n_2'\tau).$$

Appendix D. List of basic notations

In this section we present the list of basic notations used in our review. All notations refer to the case of helical undulator and circularly polarized radiation.[4]

D.1. General notations

c – velocity of light,
$-e$ – the charge of the electron,
m_e – the mass of the electron,
ω – the frequency of radiation ,
λ – radiation wavelength,
λ_w – undulator period,
$\kappa_w = 2\pi/\lambda_w$ – undulator wavenumber,
H_w – undulator field ,
N_w – number of undulator periods,
l_w – undulator length,
$K = \lambda_w e H_w/2\pi m_e c^2$ – undulator parameter,
$\mathcal{E}$ – electron energy,
$\mathcal{E}_0$ – nominal energy of the electron,
$\gamma = \mathcal{E}_0/m_e c^2$ – relativistic factor,
$\theta_s = K/\gamma$ – rotation angle of electron in the undulator,
$\gamma_z = (1 - v_z^2/c^2)^{-1/2} \simeq (\gamma^{-2} + \theta_s^2)^{-1/2} = \gamma/\sqrt{1+K^2}$ – longitudinal relativistic factor,
$C = \kappa_w - \omega/(2c\gamma_z^2)$ – detuning of the electron ,
j_0 – beam current density,
I – total beam current,
r_0 – radius of the electron beam,
$I_A = m_e c^3/e \simeq 17$ kA – Alfven's current.

D.2. One-dimensional model of the FEL amplifier

$\Gamma = [\pi j_0 \theta_s^2 \omega/(c\gamma_z^2 \gamma I_A)]^{1/3}$ – the gain parameter,
Λ – the eigenvalue of a partial wave,
$\hat{\Lambda} = \Lambda/\Gamma$ – the reduced eigenvalue of a partial wave,
$\hat{C} = C/\Gamma = [\kappa_w - \omega/(2c\gamma_z^2)]/\Gamma$ – the detuning parameter,
$\Lambda_p = [4\pi j_0/(\gamma_z^2 \gamma I_A)]^{1/2}$ – the longitudinal plasma wavenumber,

[4] The case of planar undulator and linearly polarized radiation is discussed in the corresponding parts of the text.

$\hat{\Lambda}_p^2 = \Lambda_p^2/\Gamma^2$ – the space charge parameter,
$\hat{\Lambda}_T^2 = \omega^2\langle(\Delta\mathcal{E}/\mathcal{E}_0)^2\rangle/(\gamma_z^4 c^2\Gamma^2)$ – the energy spread parameter,
$\beta = c\gamma_z^2\Gamma/\omega \simeq \Gamma/2\kappa_w$ – the efficiency parameter,
$E_0 = (c\gamma_z^2\mathcal{E}_0\Gamma^2)/(e\omega\theta_s)$ – saturation field amplitude parameter.

D.3. One-dimensional model of the FEL oscillator

$\tau = 2\pi\theta_s^2\omega j_0 l_w^3(c\gamma_z^2\gamma I_A)^{-1}$ – the gain parameter,
G – radiation power gain per one undulator pass,
α – the relative power losses per one resonator round-trip,
$\hat{\alpha} = \alpha/\tau$ – the parameter of resonator losses,
$\hat{C} = Cl_w$ – the detuning parameter,
$\hat{\Lambda}_T^2 = \omega^2 l_w^2\langle(\Delta\mathcal{E}/\mathcal{E}_0)^2\rangle/(c^2\gamma_z^4) = (4\pi N_w)^2\langle(\Delta\mathcal{E}/\mathcal{E}_0)^2\rangle$ – the energy spread parameter,
$\Lambda_p = [4\pi j_0/(\gamma_z^2\gamma I_A)]^{1/2}$ – the longitudinal plasma wavenumber,
$\hat{\Lambda}_p = \Lambda_p l_w$ – the space charge parameter,
$\beta = c\gamma_z^2/\omega l_w = (4\pi N_w)^{-1}$ – the efficiency parameter,
$E_0 = (c\gamma_z^2\mathcal{E}_0)/(e\omega\theta_s l_w^2)$ – saturation field amplitude parameter.

D.4. Three-dimensional model of the FEL amplifier

$\Gamma = [I\omega^2\theta_s^2/(I_A c^2\gamma_z^2\gamma)]^{1/2}$ – the gain parameter,
$\hat{C} = C/\Gamma = [\kappa_w - \omega/(2c\gamma_z^2)]/\Gamma$ – the detuning parameter,
$\hat{\Lambda}_p^2 = \Lambda_p^2/\Gamma^2 = 4c^2/(\omega^2 r_0^2\theta_s^2)$ – the space charge parameter,
$B = \Gamma r_0^2\omega/c$ – the diffraction parameter,
$\hat{\Lambda}_T^2 = \Lambda_T^2/\Gamma^2 = \langle(\Delta\mathcal{E}/\mathcal{E}_0)^2\rangle\omega^2/(c^2\gamma_z^4\Gamma^2)$ – the energy spread parameter,
Λ – the eigenvalue of an eigenmode,
$\hat{\Lambda} = \Lambda/\Gamma$ – the reduced eigenvalue of an eigenmode,
$\beta = c\gamma_z^2\Gamma/\omega$ – the efficiency parameter.
$W_0 = I\mathcal{E}_0\Gamma\gamma_z^2 c/(e\omega)$ – saturation power parameter.

References

[1] D.A.G. Deacon et al., Phys. Rev. Lett. 38 (1977) 892.
[2] T.J. Orzechowski et al., Phys. Rev. Lett. 57 (1986) 2172.
[3] Ya.S. Derbenev, A.M. Kondratenko and E.L. Saldin, Nucl. Instrum. and Methods A 193 (1982) 415.
[4] Proceedings of the workshop "Prospects for a 1 Å free-electron laser", BNL 52273, 1990.
[5] A.M. Kondratenko, E.V. Pakhtusova and E.L. Saldin, Sov. J. Dokl. Akad. Nauk 264 (1982) 849, in Russian.
[6] E.L. Saldin, V.P. Sarantsev, E.A. Schneidmiller and M.V. Yurkov, Nucl. Instrum. and Methods A 339 (1994) 583.
[7] R.A. Jong, E.T. Scharlemann and W.M. Fawley, Nucl. Instrum. and Methods A 272 (1988) 99.
[8] D. Prosnitz, ed., Free-electron lasers and applications, Vol. 1227, SPIE (1990).
[9] C. Yamanaka, Nucl. Instrum. and Methods A 318 (1993) 1.
[10] G. Dattoli and A. Renieri, Review in: Laser Handbook, Vol. 6, Free Electron Lasers (edited by W.B. Colson et al, North Holland, Amsterdam, 1990), p. 221.
[11] N.M. Kroll and W.A. McMullin, Phys. Rev. A 17 (1978) 300.
[12] D.B. McDermott and T.C. Marshall, Phys. Quantum Electron. 7 (1980) 509.

[13] E. Jerby and A. Gover, IEEE J. Quantum Electron. QE-21 (1985) 1041.
[14] E.L. Saldin, E.A. Schneidmiller and M.V. Yurkov, Sov. J. Part. Nucl. 23 (1992) 104.
[15] L.D. Landau, Zh. Eksp. Teor. Fiz. 16 (1946) 574, in Russian.
[16] W.B. Colson, Phys. Rev. A 24 (1981) 639.
[17] W.B. Colson, G. Dattoli an F. Ciocci, Phys. Rev. A 31 (1985) 828.
[18] G.A. Kornyukhin et al., Nucl. Instrum. and Methods A 237 (1985) 281.
[19] W.B. Colson, IEEE J. Quantum Electron. QE-17 (1981) 1417.
[20] M.J Schmidt and C.J. Elliott, IEEE J. Quantum Electron. QE-23 (1987) 1552.
[21] E. Jerby and A. Gover, Nucl. Instrum. and Methods A 250 (1986) 192.
[22] E.T. Scharlemann et al., Nucl. Instrum. and Methods A 250 (1986) 150.
[23] E.L. Saldin, E.A. Schneidmiller and M.V. Yurkov, Nucl. Instrum. and Methods A 313 (1992) 555.
[24] E.L. Saldin, E.A. Schneidmiller and M.V. Yurkov, Opt. Commun. 103 (1993) 205.
[25] P. Sprangle, C.M. Tang and W.M. Manheimer, Phys. Rev. A 21 (1980) 302.
[26] C.M. Tang and P. Sprangle, J. Appl. Phys. 52 (1981) 3148.
[27] C.M. Tang and P. Sprangle, Phys. Quantum Electron. 9 (1982) 627.
[28] R. Bonifacio, C. Pellegrini and L. Narducci, Opt. Commun. 50 (1984) 373.
[29] N. Kroll, P. Morton and M. Rosenbluth, SRI Rep. JSR-79-01; IEEE J. Quantum Electron. QE-17 (1981) 1436.
[30] D. Prosnitz, A. Szoke and V.K. Neile, Phys. Rev. A 24 (1981) 1436.
[31] H. Buchholz, Elektrische und magnetische Potetialfelder (Springer, Berlin, 1957).
[32] E.L. Saldin et al., "Free Electron Laser as Energy Driver for Inertial Confinement Fusion", Preprint JINR E9-94-237, Dubna, 1994; Nucl. Instrum. and Methods A, in press.
[33] E.L. Saldin, E.A. Schneidmiller and M.V. Yurkov, Nucl. Instrum. and Methods A 307 (1991) 526.
[34] E.L. Saldin, E.A. Schneidmiller and M.V. Yurkov, Nucl. Instrum. and Methods A 322 (1992) 293.
[35] B.D. McVey, Nucl. Instrum. and Methods A 250 (1986) 449.
[36] J.C. Goldstein, B.E. Newnam, R.W. Warren and R.L. Sheffield, Nucl. Instrum. and Methods A 250 (1986) 4.
[37] W.B. Colson and R.A. Freedman, Phys. Rev. A 27 (1983) 1399.
[38] W.P. Marable, C.M. Tang and P. Sprangle, Nucl. Instrum. and Methods, A 259 (1987) 210.
[39] B.W.J. McNeil, Nucl.Instrum. and Methods A 296 (1990) 388.
[40] W.W. Rigrod, IEEE J. Quantum Electron. QE-14 (1978) 377.
[41] G. Dattoli, S. Cabrini and L. Giannessi, Phys. Rev. A 44 (1991) 8433.
[42] G. Dattoli, L. Giannessi, S. Cabrini and V. Loreto, Phys. Rev. A 45 (1992) 8842.
[43] B.D. McVey, Nucl. Instrum. and Methods A 250 (1986) 449.
[44] J.C. Goldstein, B.E. Newnam, R.W. Warren and R.L. Sheffield, Nucl. Instrum. and Methods A 250 (1986) 4.
[45] W.B. Colson, Review in: Laser Handbook, Vol. 6, Free Electron Lasers (edited by W.B. Colson et al, North Holland, Amsterdam, 1990), p. 115.
[46] E.L. Saldin, E.A. Schneidmiller and M.V. Yurkov, Opt. Commun. 103 (1993) 297.
[47] N.A. Vinokurov and A.N. Skrinsky, Preprint 77-59, Nuclear Physics Institute, Novosibirsk, 1977.
[48] N.A. Vinokurov, Proc. 10th Int. Conf. on High Energy Charged Particle Accelerators, Vol. 2 (Serpukhov), 1977, p. 454.
[49] D.W. Feldman et al., Nucl. Instrum. and Methods A 85 (1989) 11.
[50] N.A. Vinokurov and A.N. Skrinsky, Preprint 78-88, Nuclear Physics Institute, Novosibirsk, 1978.
[51] R. Coisson, Part. Accel. 11 (1981) 245.
[52] I. Boscolo and V. Stagno, Nuovo Cimento B 58 (1980) 267.
[53] P. Elleaume, Physics of Quantum Electronics, Vol. 8 (Addison-Wesley, Reading, MA, 1980), p. 119.
[54] P. Elleaume, J. Phys. Colloq. 44, C1 (1983) 333.
[55] P. Elleaume, Review in: Laser Handbook, Vol. 6, Free Electron Lasers (edited by W.B. Colson et al, North Holland, Amsterdam, 1990), p. 91 (see also references therein).
[56] J.M.J. Madey, Nuovo Cimento B 50 (1979) 64.
[57] N.A. Vinokurov, Proc. 6th All-Union Conf. on Charged Particle Accelerators, Vol. 2 (Dubna), 1977, p. 233.
[58] N.A. Vinokurov, "Relativistic Microwave Electronics", 6th Issue (Proceedings of the VI Seminar on Relativistic Microwave Electronics, May 16–18, 1989, Sverdlovsk, USSR), Gorky, 1989, p. 162 (in Russian).
[59] A. Renieri, Nuovo Cimento B 53 (1979) 160.

[60] G. Dattoli and A. Renieri, Nuovo Cimento B 59 (1980) 1.
[61] E.M. McMillan, Phys. Rev. 68 (1945) 143.
[62] V.I. Veksler, J. of Phys. USSR 9 (1945) 153.
[63] A.H. Ho, R.H. Pantell and J. Feinstein, IEEE J. Quantum Electron. QE-23 (1987) 1545.
[64] A.H. Ho, R.H. Pantell and J. Feinstein, Nucl. Instrum. and Methods A 318 (1991) 758.
[65] E.L. Saldin, E.A. Schneidmiller and M.V. Yurkov, Opt. Commun. 107 (1994) 507.
[66] H. Leboutet, Proceedings of the 1991 IEEE Particle Accelerator Conference (May 6–9, 1991, San Francisco, USA), Vol. 5, p. 2763.
[67] E.L. Saldin, E.A. Schneidmiller and M.V. Yurkov, Phys. Lett. A 185 (1994) 469.
[68] G.T. Moore, Opt. Commun. 52 (1984) 46.
[69] E.L. Saldin, E.A. Schneidmiller and M.V. Yurkov, Opt. Commun. 97 (1993) 272.
[70] E.L. Saldin, E.A. Schneidmiller and M.V. Yurkov, Nucl. Instrum. and Methods A 307 (1991) 531.
[71] E.L. Saldin, E.A. Schneidmiller and M.V. Yurkov, Opt. Commun. 87 (1992) 69.
[72] E.L. Saldin, E.A. Schneidmiller and M.V. Yurkov, Nucl. Instrum. and Methods A 317 (1992) 581.
[73] G. Dattoli et al., IEEE J. Quantum Electron. QE-28 (1992) 901.
[74] L.H. Yu, S. Krinsky and R.L. Glukstern, Nucl. Instrum. and Methods A 304 (1991) 516.
[75] Y.H. Chin, K.-J. Kim and M. Xie, Nucl. Instrum. and Methods A 318 (1992) 481.
[76] V.L. Granatstein et al., Nucl. Instrum. and Methods A 272 (1988) 110.
[77] E.L. Saldin, E.A. Schneidmiller and M.V. Yurkov, Opt. Commun. 85 (1991) 117.
[78] L.A. Veinstein, Open resonators and waveguides (Sovetskoye Radio, Moscow, 1966).
[79] E.L. Saldin, E.A. Schneidmiller and M.V. Yurkov, Phys. Lett. A 161 (1992) 448.
[80] E.L. Saldin, E.A. Schneidmiller and M.V. Yurkov, Opt. Commun. 90 (1992) 381
[81] E.L. Saldin, E.A. Schneidmiller and M.V. Yurkov, Opt. Commun. 93 (1992) 378.
[82] E.L. Saldin, E.A. Schneidmiller and M.V. Yurkov, Laser Physics 2 (1992) 672.
[83] C.-M. Tang and P. Sprangle, IEEE J. Quantum Electron. QE-21 (1985) 970.
[84] E.T. Scharlemann and W.M. Fawley, Proc. SPIE 642 (1986) 2.
[85] T.M. Tran and J.S. Wurtele, Comput. Phys. Commun. 54 (1989) 263.
[86] J.C. Goldstein, T.F. Wang, B.E. Newnam, and B.D. McVey, Proc. 1987 Particle Accelerators Conf., Washington, DC, USA, p. 202.
[87] E.L. Saldin, E.A. Schneidmiller and M.V. Yurkov, Opt. Commun. 95 (1993) 141.
[88] M. Born and E. Wolf, Principles of optics (Pergamon Press, London, 1959).
[89] G.T. Moore, Nucl. Instrum. and Methods A 250 (1986) 381.
[90] M.I. Adams, An introduction to optical waveguides (Wiley, New York, 1981).
[91] E.L. Stiefel and G. Scheifele, Linear and regular celestial mechanics (Springer, Berlin, 1971).
[92] L.A. Pars, A treatise on analytical dynamics (Heinemann, London, 1964).
[93] H. Haken, Laser light dynamics, Vol. 2 (North-Holland, Amsterdam, 1985).
[94] S. Solimeno, B. Crosignani and P. DiPorto, Guiding, diffraction, and confinement of optical radiation (Academic Press Inc. New York, 1986).